ALKYLATION REACTIONS OVER SYNTHETIC ZEOLITES

A THESIS
SUBMITTED TO THE
SHIVAJI UNIVERSITY, KOLHAPUR
FOR THE DEGREE OF
DOCTOR OF PHILOSOPHY
(IN CHEMISTRY)

BY

VILAS RAMDAS CHUMBHALE

M.Sc.

UNDER THE GUIDANCE OF

DR. PAUL RATNASAMY

M.Sc., Ph. D.

INORGANIC CHEMISTRY DIVISION
NATIONAL CHEMICAL LABORATORY
PUNE - 411 008, INDIA

JULY 1992

CONTENTS

Page

CHAPTER-3 STUDIES ON PROPYLATION OF BENZENE

LIST OF TABLES

LIST OF FIGURES

****

CHAPTER - 1

INTRODUCTION

****

A: ALKYLATION OF AROMATIC HYDROCARBONS

The catalytic alkylation of aromatic hydrocarbons is a substitution reaction wherein one or more of the hydrogen atoms in the ring or in the side chain are replaced by an alkyl group. Both, substituted and unsubstituted aromataic structures, can be alkylated. In general the following overall reaction occurs

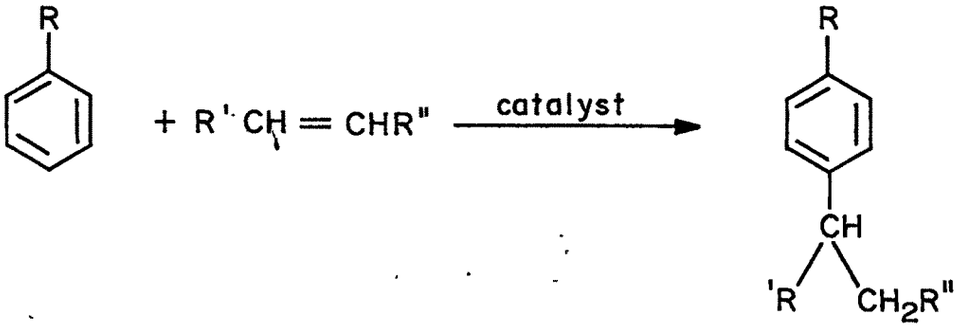

These reactions occur through electrophilic (acid catalysed), nucleophilic (base catalysed) or free radical mechanisms. Commercial alkylation of aromatic hydrocarbons is exclusively carried out via electrophilic substitution. Aluminium chloride and boron trifluoride based catalysts have been most widely investigated and commercially used. Strong mineral acids such as HF, H_2SO_4 and H_3PO_4 alone or supported on a substrate have also been used as catalysts for these reactions. More recently, synthetic zeolites have been studied. The mechanism for all the reactions is similar and in general follow the classical Friedel-Crafts path[1]

$$RCl + AlCl_3 \longrightarrow AlCl_4^- + R^+$$

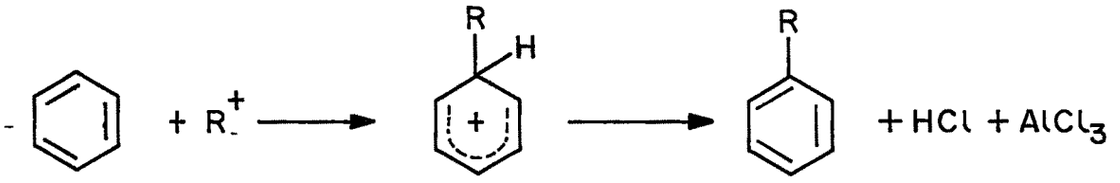

Anhydrous metal halides alone are inactive as catalysts for the alkylation of aromatic hydrocarbons. They require a co-catalyst. HCl and water are used industrially to promote the formation of intermediate carbonium ions[2]. Strong acids such as HF, H_2SO_4 and H_3PO_4 also interact with olefins to form carbonium ions[2,3]. The mechanism for zeolite catalysed alkylation reactions involve proton addition to the olefin at active acid sites on the surface of the zeolite to form the carbonium ion. Later reaction proceeds as per the alkyl halide derived ions.

The alkylation of benzene with various olefins rarely produces only the monoalkylated compound. Rather,mixtures of di-, tri- and higher substituted structures are also formed. In fact, once one alkyl group is added, its nucleophilic nature tends to make the resulting aromatic structure even more reactive by increasing the availability of π -electrons. A brief review of literature on the catalysts used in the synthesis of alkylbenzenes both in liquid and vapour phase is presented in the following discussion.

B: SYNTHESIS OF ISOPROPYLBENZENE (CUMENE)

(B1) : Liquid Phase Process

In 1895, Rodziewanowski[4] prepared cumene in a similar manner as Balsohn prepared ethylbenzene, using $AlCl_3$ catalyst[5]. Brochet pointed out that mineral acids were also effective catalysts for preparation of cumene[6]. Benzene-propylene alkyaltion has been studied extensively by Nieuland[7] and Topchiev[8] in the presence of promoted and unpromoted metal halide type catalysts. In the liquid phase process for alkylation of benzene with propylene a lower strength of sulfuric acid is employed at somewhat higher temperature[9].

(B2) : Supported Catalysts

Phosphoric acid-Kieselguhr type catalysts developed by UOP[10,11] are used in the vapour phase process using refinery propane-propylene fraction and excess benzene containing less than 0.15% thiophene. Isopropanol and diisopropyl ether which decomposed under the influence of the phosphoric acid catalyst to give propylene and water have also been used as feedstock.

(B3) : Isopropylation of Benzene over Synthetic Zeolites

Zeolites, X, Y and mordenite have been extensively studied for this reaction. The sodium and other alkali metal cation forms of the zeolite were inactive. The propylation of benzene occurs on X zeolites exchanged with Ca^{2+} or Nd^{3+}. The degree of exchange necessary to obtain measurable catalytic activity was 65 and 40%

respectively. The Y type zeolites exchanged with Ce(III), Pr, Sm and Nd had similar alkylation activity provided that the specimen had similar degree of exchange[13]. The samples with degree of calcium exchange below 40-45% were less active. Above this level a marked increase in activity was observed. A similar effect on activity for propylene alkylation was observed with ammonium exchange followed by calcination at 500°C[14].

According to Pickert et al[15] benzene-propylene alkylation activity was enhanced with increasing calcination temperature and reached a maximum when all active hydroxyl groups were removed. They suggested that carbonium ion like species were formed via polarization of reactant hydrocarbon by cation fields. Most workers agree that alkylation reactions are Brönsted acid catalysed and that maximum alkylation activity is observed at maximum OH concentration in the zeolite. Thus the calcination temperature has to be such as to produce maximum of active OH groups. Beyond this temperature the OH concentration and activity are seen to decrease. The alkylation of benzene with propylene is Brönsted acid catalysed on H-mordenite[16]. Maximum alkylation activity was observed when the hydroxyl content was at maximum at 450°C.

The catalytic activity of zeolite NaY, HX and CaX in benzene alkylation by propylene increased appreciably when propylchloride was added[17,18]. It was proposed that the addition of alkyl-halogen compounds to zeolites formed the corresponding sodium halides in the zeolite cages and by secondary reactions of the organic part of the molecule, H^+ was left in the zeolite as

hydroxyl groups. The action of chlorine and CCl_4 with residual water of the zeolite also involves the formation of more protons[19].

(B4): Isopropylation of benzene over high-silica zeolites

Only a few patents describe[20] the use of high silica zeolites like ZSM-35 and ZSM-38 in the synthesis of cumene. Benzene was alkylated with propene at 200°C/300 psig and at WHSV = 6[21,22], over HZSM-12 zeolite with silica-alumina ratio of > 12:1 and C.I. of 1-12 to give > 95% conversion. Catalysts with an inert support and strongly adherent outer coating were used for this reaction[23]. The formation of undesired, cracked and rearranged, products was almost eliminated by the use of coated catalysts.

C: ALKYLATION OF PHENOL

Alkylphenols of commercial importance are manufactured almost exclusively by the reaction of an olefin with phenol, cresols or xylenols but aliphatic alcohols and chlorides also figure extensively as the alkylating agent[24]. The use of liquid hydrogen fluoride as solvent provided a method to avoid byproducts like phenolic ethers. The use of chlorides results in processing complications stemming from the elimination of hydrogen chloride. The alkylation reaction takes place at or near atmospheric pressure in the presence of a catalyst. Traditionally, protonated acids (such as sulfuric acid, phosphoric acid, especially supported on a siliceous material

such as Fuller's earth), or Lewis acids (such as aluminium chloride or boron trifluoride) have been used.

Studies on alkylation of phenol have been mostly in the liquid phase with metal oxides[25,26] and wide pore zeolites as catalysts[27]. Yashima et al[28] have shown alkylation at the carbon atom and oxygen in phenol being competitive. Balsama et al[29] observed alkylated products being formed even in the absence of methanol. Chantal et al[30] proposed formation of an intermediate of the diphenyl ether type analogous to the oxonium ion in the methanol conversion to hydrocarbons[31]. Marczewski et al[32] studied alkylation of phenol with methanol on a series of dealuminated HY, dealuminated mordenite and HZSM-5 zeolites and on alumina. Dealumination of HY zeolite decreased both deactivation rate and catalytic activity.

D: INDUSTRIAL IMPORTANCE OF ALKYLATION

Alkylation of benzene with various olefins is one of the major petrochemical processes and is the primary use of benzene. Ethylbenzene, cumene, isobutylbenzene, p-ethyltoluene, p-diethylbenzene and p-xylene are some of the important compounds obtained by alklylation.

(D1) : Cumene (Isopropylbenzene)

Cumene can be prepared conventionally by alkylation of benzene with propylene. Cumene is further used for the manufacture of phenol and acetone by first oxidizing to cumenehydroperoxide, which in turn is cleaved to products.

Commercially 90% of phenol is produced by this route. A number of acid-type catalysts can be used, but commercially the reaction is carried out with aluminium chloride or a solid phosphoric acid on Kieselguhr. Alkylation with Kieselguhr catalyst is run at a temperature of 175-225^{o}C and at a pressure of 400-600 psig.

(D2) : Isobutylbenzene

Isobutylbenzene is mainly used as starting material for the synthesis of Ibuprofen, a anti-inflammatory drug which can be used for the treatment of rheumatism. Isobutyl benzene is produced by the alkylation of toluene with propylene in the presence of basic catalysts like Na-K/carbon.

(D3) : p-Xylene

Commercially p-xylene is the most important isomer among o, m and p-xylenes. Almost all p-xylene is converted to terephthalic acid or dimethylterephthalate and reaction with ethylene glycol to polyethylene terephthalate) for use in fibers, films or resins. The formation of p-xylene in excess of equilibrium values from toluene alkylation has been reported over a phosphorous or magneisum modified ZSM-5 catalyst[33,34].

(D4) : Ethyltoluene

Ethyltoluene is a precursor for the production of vinyltoluene. Toluene can be alkylated with ethylene over HZSM-5 catalysts[35] to produce ethyltoluene.

(D5) : Linear Alkylbenzenes

The alkylation of benzene with higher molecular weight olefins or alkylchlorides in the 10 to 18 carbon range gives a product called detergent alkylate. This is subsequently sulfonated and converted to detergent. The reaction is carried out using Friedel-Crafts catalyst, e.g. hydrogenfluoride or aluminium chloride in an excess of benzene at 30-60°C.

(D6) : Cresols

Commercially phenol is alkylated over boronfluoride. The amount of orthosubstitution is greater with phenol due to the less steric hindrance offered by hydroxyl group. Phenol is alkylated with linear or branched olefins at 30-60°C using Friedel-Crafts catalysts like hydrogenfluoride or aluminium chloride. The resultant product is used in the preparation of anti-oxidants, lube oil additives, plasticizers and surface-active agents.

E: COMPOSITION OF ZEOLITES

Zeolites are crystalline aluminosilicates represented by the general formula:

$$M_{2/n}O.Al_2O_3.XSiO_2.YH_2O$$

where X > 2 and 'n' is the valence of the cation M. The maximum value of X, for naturally occurring zeolites is 10 and approaches infinity for some of the synthetic materials. The structure

consists of a three dimensional net work of AlO_4^- and SiO_4 tetrahdedra linked to each other by sharing the oxygen ions. The excess negative charge on the aluminium ion is balanced by an alkali metal ion which can be partially or completely exchanged with other mono-, di or trivalent ions. The SiO_4, AlO_4^- network forms honeycombed structure consisting of cavities and channels of molecular dimensions. The more common Si/Al zeolites contain in the as-synthesised form Na as counter ions together with water. By ion-exchange various cations may be introduced. Application of heat removes water and leaves the zeolite in its active form. The nature and number of cations profoundly affects the pore size in the zeolite which in turn changes the sorption and catalytic properties. The unique characteristics of their aluminosilicate framework and the presence of well-defined channel systems in the zeolites have made possible a variety of industrial applications.

F: SYNTHESIS OF ZEOLITES

Natural zeolite materials have been known for more than 200 years and 40 different species have been identified in the past 50 years. But, among these of interest to catalysis, only a few are found in large deposits (clinoptilolite, erionite, mordenite and phillipsite) while others are extremely rare (faujasite, Offretite). The formation of such zeolites with volcanic glass and saline water as reactants must have occurred in the temperature range 25-75^oC and at pH > 13, requiring several hundred years for crystallization[36-38].

In early 1950s synthetic zeolites with low silica to alumina ratios (<10) were synthesized. Their synthesis involved use of highly basic (pH > 13) synthesis gels comprising of reactive silica, an alumina source and alkali or alkaline earth metal hydroxides, and were usually crystallized at around 100°C temperatures. Well known examples of such zeolites are A[39], X[40], Y[41], L[42] and mordenite[43]. Later, the preparations were modified by introducing organic quarternary cations into the gel containing silica, alumina and alkali[44]. Recent progress in zeolite synthesis has been the discovery of the high silica zeolites beta and ZSM (Zeolite Socony Mobil) series using alkylammonium cations and amines[45,46]. Zeolites have been synthesized replacing silicon with germanium and aluminium with gallium[47].

G : CLASSIFICATION OF ZEOLITES

Until now, 40 species of natural zeolites and more than 160 synthetic zeolites have been identified. Classification of zeolites has been made on the basis of their morphological characteristics, crystal structure, chemical composition, effective pore diameter and natural occurrence. The classification of zeolites based on morphology was made initially by Bragg[48]. This was further modified by Meier[49] and Barrer[50] according to the secondary building units present in them.

Zeolites have been classified on the basis of silica-alumina ratios[51] into three types, viz. low, intermediate and high silica/alumina zeolites. Typical examples of the low

silica/alumina ratio zeolites are A, X and sodalite which possess Si/Al ratios between 1 and 1.5. Examples of the intermediate silica/alumina zeolites (Si/Al = 2 to 5) are Y, L, large pore mordenite and omega, while examples of high Si/Al zeolites (Si/Al = 10 to several thousands) are ZSM-5, ZSM-11, EU-1 and EU-2, dealuminated Y, mordenite and erionite. Silica molecular sieves (silicalite-1 and silicalite-2) contain Si/Al from several thousand to infinity. Barrer[50] and Sand[52] have classified zeolites into three groups viz., small (e.g. Linde A ZK-5, RhO and Chabazite), intermediate (ZSM-5, ZSM-11, ZSM-23, ZSM-48, ferrierite, stillbite) and large pore (Linde X, Y, L, gmelinite, mordenite, ZSM-20) zeolites based on differences in their effective pore diameter.

H : INDUSTRIAL IMPORTANCE OF ZEOLITES

A number of commercially important catalysts and processes based on zeolites have been developed and are listed in Table 1.1.

I STRUCTURE OF ZEOLITES

(I.1) : Mordenite

Mordenite is a naturally occurring silica-rich zeolite (Si:Al $\sim$ 5) which also can be synthesised readily[53]. Meier determined the structure of fully hydrated form of sodium mordenite[54]. The mordenite framework is characterised by a micropore system composed essentially of parallel elliptical cylinders of maximum and minimum crystallographic free diameters of 7.0 and 5.7 A^{o}, respectively. These main channels being

TABLE 1.1 : INDUSTRIAL PROCESSES BASED ON SHAPE SELECTIVE ZEOLITES*

Process	Objective	Major Chemical/Process characteristics
Selectoforming	Octane number is increased in gasoline LPG production	Selective n-paraffin cracking
M-forming	High yield, octane number increases in gasoline	Cracking depending on degree of branching;aromatic alkylation and cracking fragments
Dewaxing	Light fuel from heavy fuel oil. Lube oil with low temperature pour point	Cracking of high molecular weight, n- and monomethyl paraffins
Xylene isomerization	High yield of p-xylene product	High through put long cycle
Ethylbenzene	High yield of ethylbenzene, elimination of $AlCl_3$ handling	life, suppression of side reactions
Toluene disproportionation	Benzene and xylenes from toluene	
Methanol to gasoline	Methanol (from coal or natural gas), conversion to high grade gasoline	Synthesis of hydrocarbons only, restricted to gasoline range (C_4 to C_{10}) including aromatics

*Ref: Weisz, P.B., Pure & Applied Chem., 52, 2091 (1980)

interconnected by smaller side channels. The straight channel is 12 ring pore system, while the intersecting one is composed of 8 rings system having highly puckered apertures.

The structure of mordenite is shown in Fig. 1.1.

(I.2) : Faujasite (Y)

The basic building block of zeolite Y (Faujasite) is a truncated octahedron (sodalite cage) consisting of a three dimensional network of SiO_4 and AlO_4^- tetrahedra. The octahedra are connected at four of the hexagonal faces by hexagonal prismatic structures, resulting in a tetrahedral arrangement of the truncated octahedra. There is however a restriction on the arrangement of SiO_4, AlO_4^- tetrahedra governed by Lowensteins[55a] stability rule, which states that two Al atoms cannot share the same oxygen atom when in tetrahedral coordination. The three dimensional framework encompasses the giant supercage elliptical in shape and approximately 13A^o in diameter. The supercages are connected through 12 membered ring openings approximately 8A^o in diameter. The pore opening to sodalite cage (6.6A^o) is through oxygen ring of approximately 2.2A^o. The cations in zeolites occupy different non-framework positions or sites. The various cation sites in faujasite are shown in Fig. 1.2.

(I.3) ZSM-12 Zeolite

ZSM-12 belongs to pentasil family of zeolite and has linear non-interpenetrating channel system whose pore opening is characterised by 12-ring aperture of 5.5 x 5.9 A^o [010]

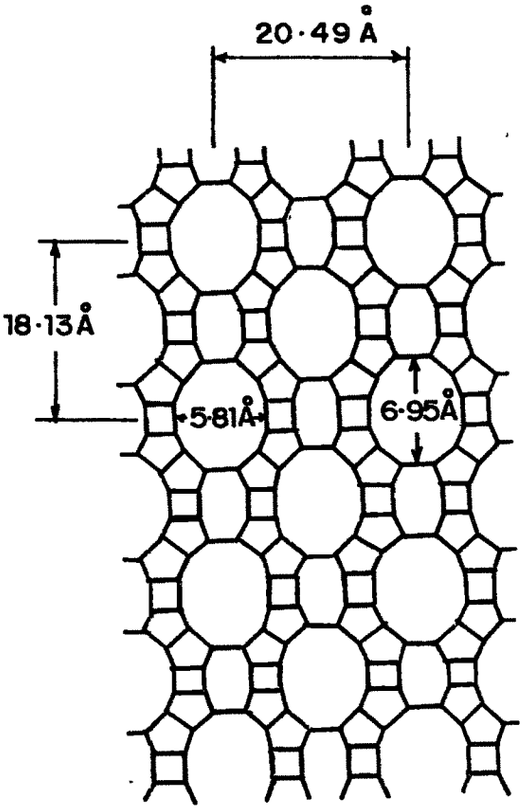

FIG. 1·1 : CROSS-SECTIONAL VIEW OF MORDENITE[54]

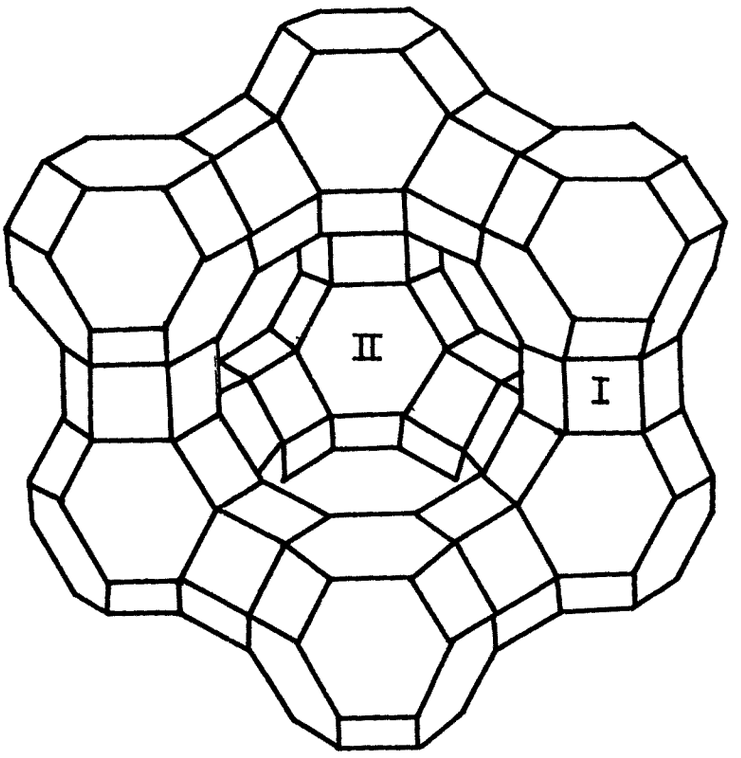

A

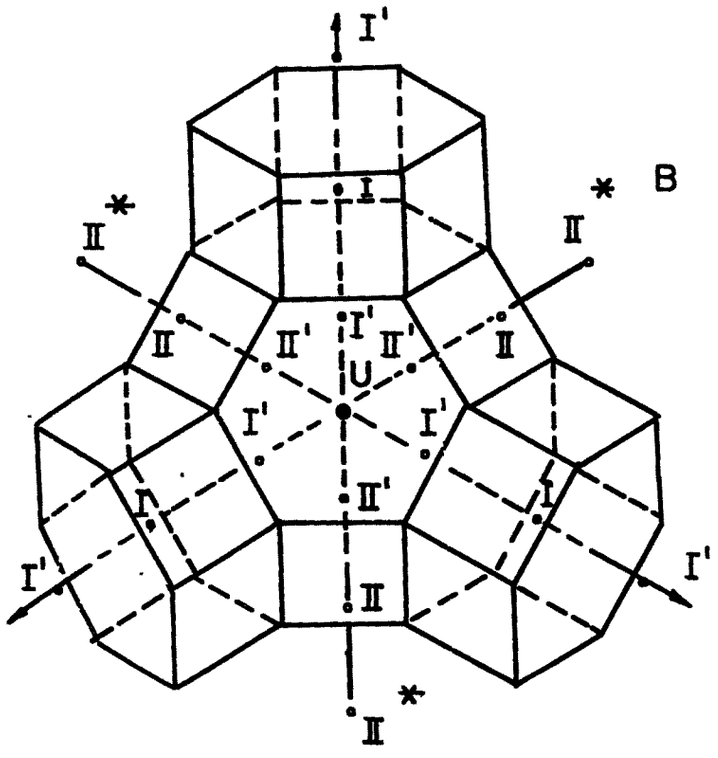

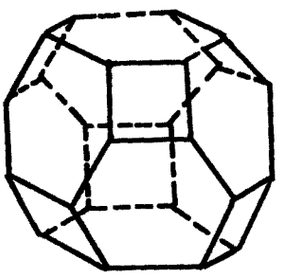

C

FIG. I·2 A–PERSPECTIVE VIEW OF PART OF THE FAUJASITE STRUCTURE
I & II ARE THE CATION SITES (Ref:55c)
B–IDEALIZED PROJECTION OF SODALITE UNIT WITH CATION SITES (Ref:55b)
C–SODALITE UNIT.

direction[56]. The structure is shown in Fig. 1.3.

(I.4) ZSM-5 Zeolite

The framework structure of ZSM-5 has been solved by Kokotailo et al[57]. The framework of ZSM-5 contains a novel configuration of linked tetrahedra [Fig.1.4(a)] consisting of eight five-membered rings. These units join through edges to form chains (Fig. 1.4(b). The chains can be connected to form sheets and the linking of the sheets leads to a three-dimensional framework structure. The sheets paralle to (010) and (100) are shown in Figs. 1.4(c) and 1.4 (d) respectively. The ZSM-5 framework can be generated by linking the sheets of Fig. 1.4(c) across mirror planes forming four and six-membered rings. It belongs to the pentasil family of zeolites and has inter-secting channel system, with ten-membered ring openings. One set of channel is sinusoidal running parallel to (001) and other straight being parallel to (010) as shown in Fig. 1.4 (e).

Table 1.2 presents the structural data of these zeolites.

Unit Cell Composition

The crystallographic compositions of the unit cell in Na-mordenite[54], NaY[41,58], NaZSM-12[56] and NaZSM-5[57] are:

Na-mordenite : $Na_8[Al_8Si_{40}O_{96}]\ 24H_2O$

NaY : $(Na_2Ca)_{32}(Al_{64}Si_{128}O_{384})\ 250H_2O$

NaZSM-12 : $Na_2[Al_2Si_{26}O_{56}] \sim 4H_2O$

NaZSM-5 : $Na_4[Al_4Si_{92}O_{192}]\ 18H_2O$

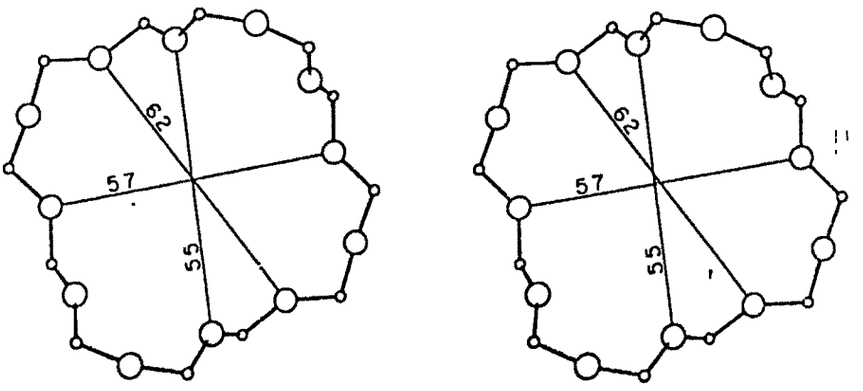

12-ring viewed along [010]

FIG. I.3 FRAMEWORK OF 12 RING PORE SYSTEM IN ZSM - 12 ZEOLITE*

* Ref. W.M. MEIER AND D.H. OLSON "ATLAS OF ZEOLITE STRUCTURE TYPES", P-109, 1987(Pub. Butterworths, London)

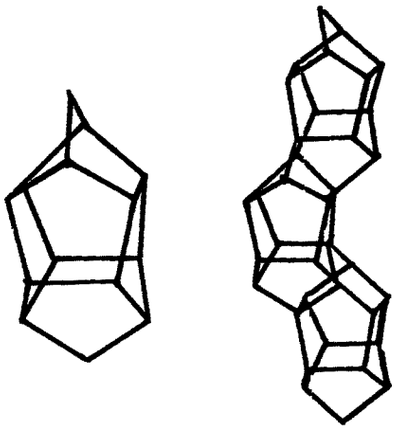

a b

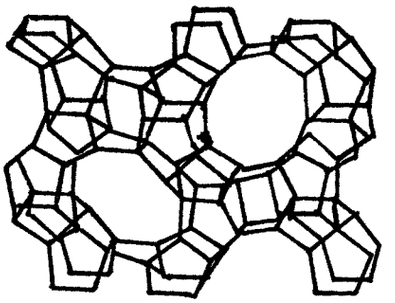

c

a) CHARACTERISTIC CONFIGURATION OF ZSM-5
b) LINKAGE OF ZSM-5

c) SKELETAL DIAGRAM OF 010 FACE

d) SKELETAL DIAGRAM OF 100 FACE

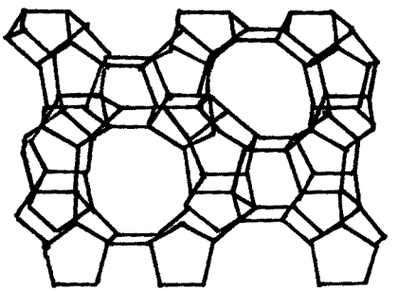

d

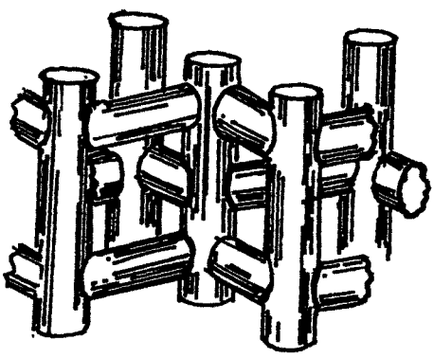

e

e) CHANNEL STRUCTURE OF ZSM-5 ZEOLITE

FIG. 1·4 – STRUCTURE OF ZSM-5 ZEOLITE.

TABLE 1.2 : SUMMARY OF CRYSTAL DATA OF SOME ZEOLITES*

Zeolite	Unit Cell formula	Unit Cell parameter (A^o)	Symmetry	Void vol. (cc/g)	Aperture size (A^o)	Framework density T atoms/1000A^o3
Mordenite	$Na_8[Al_8Si_{40}O_{96}]24H_2O$	a = 18.1 b = 20.5 c = 7.5	Ortho-rhombic	0.14	5.8x7.0	17.2
Faujasite (Y)	$(Na_2,Ca,Mg)_{29}[Al_{58}Si_{134}O_{384}]240H_2O$	a = 24.7	Cubic	0.35	8.0	12.7
ZSM-12	$Na_n[Al_nSi_{28-n}O_{56}] \sim 4H_2O$ with n < 2.5	a = 24.9 b = 5.0 c = 12.2	Mono-clinic	0.30	5.5 x 5.9	19.4
ZSM-5	$Na_n[Al_nSi_{96-n}O_{192}] \sim 16H_2O$ with n < 27	a = 20.1 b = 19.9 c = 13.4	Ortho-rhombic	0.27	5.2 - 5.3 5.3 - 5.8	17.9

*(Ref: Meier , W. M. and Olson, D.H., "Atlas of Zeolite Structure Types, 1987, pub. Butterworths, London)

The number of aluminium atoms per unit cell is obtained from the relation[56]

$$N_{Al} = 96/1 + R$$

where $R = N_{Si}/N_{Al}$ and N_{Si} and N_{Al} are gm. atoms of silicon and aluminium respectively. For ZSM-12 structure $n < 2.5$ whereas it is typically about 3 for ZSM-5. $N_{Al} + N_{Si}$ are the total number of tetrahedra per unit cell. The total number of tetrahedra in the unit cell of mordenite, NaY, NaZSM-12 and NaZSM-5 are 48, 192, 28 and 96 respectively. The factor R varies from 5 to 12.5 for mordenite, for type Y it varies from 1.5 to 3 whereas it varies from 10 to 50 and 5 to ∞ for ZSM-12 and ZSM-5 zeolites respectively.

J : **CHARACTERIZATION OF ZEOLITES** (some structure related properties)

(J.1) : X-Ray Diffraction (XRD)

X-ray diffraction is a powerful tool for the identification of zeolite species and has been extensively used to understand the kinetics[59,60] and mechanism of zeolite crystallization. The changes occurring in the lattice parameters on ion-exchange, calcination and thermal and hydrothermal treatment of the sample can also be evaluated by the X-ray technique[60]. Presence of α - quartz in zeolites[61] can be identified and estimated using the characteristic peaks at $2\theta = 26.7$ and 20.9 in the XRD pattern. Quartz is formed during the synthesis under unfavourable conditions. A review has been presented on the crystal structure of exchanged zeolite[62].

(J.2) : Infrared Spectroscopy (IR)

Infrared spectroscopy has been employed extensively to investigate the framework vibrations[63] in different zeolites and is complimentory to X-ray analysis. In addition to the framework studies, the ir spectroscopy has been extensively employed for the characterization of surface acidity[64]. The absorption bands at 3600 cm^{-1} and 3720 cm^{-1} correspond to strong and weak Bronsted acid sites respectively. It is found that the main Si-O, Al-O bands occur at about 1100 cm^{-1} and is related to the Si/Al ratio of the zeolite framework[65]. Ward has reviewed its applications for study of zeolites surface and surface reactions[66]. In addition to framework studies the IR spectroscopy has been successfully employed for the characterization of surface acidity and structural hydroxyl groups in ion-exchanged zeolites[67,68].

(J.3) : Thermal Analysis

Thermoanalytical data (DTA, TG, DTG) of zeolites have been extensively used for evaluating the rate of decomposition of occluded organic as well as water molecules from the zeolite cavities. The thermal stability has been estimated from the high temperature exotherm and is related to the Si/Al ratio in the zeolite samples[69]. The weight loss which occurs at about 500-700^{o}C has been ascribed to the dehydroxylation of acidic OH groups and the data are used for the estimation of the number of acid sites in the zeolite sample. Thermal stability of the zeolites A, X and Y type[70-72] and mordenite[73] is found to be dependent on the type of cation present in the zeolite. The

influence of cation on the thermal stability of Y type zeolites has been reported[72]. Zeolites, in general, possess high thermal stability as compared to other conventional sorbents and catalysts.

(J.4) : Sorption and Diffusion in Zeolites

A special feature of zeolites is its well defined pore structure with a large internal surface area. The nature of the pore structure can be varied by suitable modification like cation exchange, ultrastabilization and dealumination which strongly influence the sorption and catalytic properties of the zeolite. A large number of adsorbate molecules such as water, benzene, ammonia which are strongly adsorbed have been used to study the nature of zeolite-adsorbate interactions[41,74-78]. Flanigen et al and Chen measured sorption properties of silicalite and siliceous mordenite and attributed their hydrophobic nature to the absence of water adsorption sites[79,80]. Anderson et al reported the sorption properties of silicalite and pentasil zeolite and have classified the sorbate/sorbent system into two (fast and slow) categories[81]. Sorption and diffusion plays a role of paramount importance in molecular shape selective catalysis[82,83]. The screening of the molecules of different size and shape determines the reactant and product selectivity. The molecules with high diffusivity will react preferentially and selectively while molecules which are excluded from zeolite interior will only react on the external non-selective surface of the zeolite. Similarly, products with high diffusivity will

α, β and γ corresponding to ranges of temperature of desorption of ammonia, 330-370 K, 423-473 K and 693-773 K were distinguishable for fresh catalyst. In case of partially deactivated catalyst β state was absent and α state was strongly reduced. Meyers et al[90] studied the acidity of dealuminated mordenites by TPD of ammonia and found good agreement for the Al content determined by TPD with diverse analytical procedures (XRD, XPS, NMR).

(J.6) : Scanning Electron Microscopy (SEM)

SEM is useful for morphological analysis of crystalline phases. Shape and size of crystals of parent zeolite and modified catalyst can be seen. The agglomeration of crystallite into clusters can also be detected in SEM photograph.

(J.7) : Nuclear Magnetic Resonance (NMR)

High resolution magnetic angle spinning (MAS) ^{29}Si NMR together with high powder solid state ^{27}Al and ^{23}Na NMR have proved to be a powerful tool in the investigation of zeolite structure. The ^{29}Si NMR was successfully used to characterise the structure of various natural[91, 92] and synthetic zeolites such as faujasites[93-97], ZK-4[98-101] mordenite[102] and pentasil materials[103-108]. ^{29}Si NMR spectroscopy is able to resolve crystallographically non-equivalent sites in zeolites and to determine short-range silicon-aluminium ordering in their structure. Quantitative determination of Si/Al ratio in the zeolite framework can also be derived from the NMR data[90,94,96]. In addition, ^{29}Si NMR lines belonging to silanol groups in dealuminated faujasites[109] and in ZSM-5 zeolites[110] were

unambiguously identified using the cross-polarization technique.

^{27}Al high resolution MAS NMR was used to discriminate between framework (tetrahedrally coordinated) and extra-framework (octahedrally coordinated) aluminium[111]. The line width analysis provided valuable information on the interaction of Al atoms with neighbouring cations and/or on their hydration[112,113].

Meyers et al[90] dealuminated the commercially available H-mordenite by thermal and acid treatments and confirmed loss of aluminium from the mordenite lattice by ^{29}Si and ^{27}Al MAS NMR. Hays et al studied the effects of cation exchange, acid leaching and steam calcination on the location and extent of framework aluminium removal[114]

(J.8) : <u>X-ray Photoelectron Spectroscopy (XPS)</u>

XPS has been used extensively in surface analysis and can give qualitative information about surface structure. The valance electronic density of the states can be measured and energy level shifts can be used to determine the atoms involved in chemisorption bonds. Chemical shifts in core level binding energies measured in XPS can often be used to distinguish between atoms in adsorbed state, atoms incorporated within the first layer and atoms which have penetrated within several layers to form compounds. Tempere[115,116], Defosse[117], Knecht[118] and Finster[119] investigated the surface composition of A-, X- and Y type zeolites and compared them to their bulk composition. ZSM-5 zeolites have also been studied by XPS[120-123].

preferentially diffuse out while the bulkier molecules with low diffusivity will be converted and equilibrated to smaller molecules which will diffuse out, or transferred to larger species which will block the pores leading to deactivation of the catalyst.

(J.5) : Temperature Programmed Desorption (TPD)

The crystalline aluminosilicate zeolites can be considered as solid acids capable of donating a proton (Brönsted acid) or accepting an electron pair (Lewis acid) from the adsorbing molecule[19,84]. Both functions play an important role in various catalytic processes[85].

TPD is an important technique to characterise and estimate acid sites in the zeolite. The various techniques used for acidity measurements have been reviewed by Tanabe and Jacobs[86,19,]. Vedrine et al[87] and Auroux et al[88] have reported acidity of pentasil zeolite ZSM-5. Anderson et al[82] reported results on TPD of ammonia on NaZSM-5, HZSM-5 and silicalite and suggested that acid sites responsible for the TPD maximum at 780 K are the probable sites for hydrocarbon conversion processes. Acidity measurements on ultrastable Y and HZSM-5 zeolites have been carried out by Jacobs et al[89] who characterised acid sites as weak, medium and strong according to the release of ammonia over a large temperature range. The amount of ammonia released above 753 K was considered to represent the very strong sites on HZSM-5. Topsøe et al[64] studied the acidic properties of the catalysts used in methanol reaction. Three different states,

Sawa et al[124] studied the effect of acid concentration on the dealumination of mordenites and used XPS method to estimate changes in Al concentration in the external layer. Meyers et al[90] dealuminated mordenite by thermal and acid treatment and estimated surface aluminium concentration by XPS. Minachev et al published studies on cation exchanged zeolites[125-127].

(J.9) : Ion-Exchange

It is well known that the ion exchange capacity of a zeolite is equivalent to the tetrahedral aluminium content of the zeolite structure. Olson et al[128] reported caesium ion exchange into a series of ZSM-5 zeolites. Cesium ion exchange into a series of hydrogen form of ZSM-5 samples with SiO_2/Al_2O_3 ratio ranging from 89 to 8666 showed a very good stoichiometric correlation indicating that the relation of framework aluminium to ion exchange capacity holds also for the highly siliceous zeolites even at low level of aluminium. The ratio of Cs/Al was found to be slightly lower than unity. Barrer and Townsend[129] studied the ion exchange of transition metal ions like Mn^{2+}, Co^{2+}, Ni^{2+}, Cu^{2+} and Zn^{2+} in ammonium mordenite in aqueous solution over a pH range of 4-7 at 25°C. They found that in no case at 25°C did the degree of exchange of metal ions exceed 50% and pH as well as anions were found to have no significant effect on equilibria. Minachev et al[130] reported 70% exchange of zinc in mordenite under unspecified conditions. Meier concluded that transition metal ions in aqueous solution are only able to exchange with ammonium ions in the main channels of mordenite.

Gal[131], Wolf[132] and Gallei[133] compared the ion exchange properties of mordenite for transition metal with the other zeolites like A, X and Y and concluded that more siliceous the zeolite the less favoured is exchange of the sodium form by Co^{2+}, Ni^{2+}, Cu^{2+} and Zn^{2+} ions. Maes and Cremers[134] studied the ion exchange of the bivalent transition metal ions like Co, Ni, Cu and Zn on synthetic NaX or NaY zeolite at 0.01 total normality and at 5, 25 and 45°C. They found that (i) the overall selectivity of both X and Y zeolites for bivalent transition metal ions increases in the order Ni < Co < Zn < Cu, (ii) in addition to the ion hydration characteristics and ionic radius the exchange is governed by the coordination ability of the transition metal ion.

(J.10) : Deactivation during catalysis

Zeolite catalysts usuallty undergo deactivation during use in catalytic reactions. Rollman and Walsh[135] had demonstrated that the intracrystalline coking of zeolites is a shape selective process which largely depends on the size and architecture of their channels. The zeolite which provide enough space for the synthesis of polyalkylaromatics would therefore deactivate fast. Dajaifve et al[136] explained the location of coke in three zeolites namely mordenite, offretite and ZSM-5 zeolites which differ in the channels system by acidity measurement. The acidity measurements were performed by ammonia adsorption on fresh and deactivated catalysts after 20 minutes on stream in methanol reaction. The strong acid sites present in the mordenite totally disappeared in coked catalysts indicating that the

psuedounidimensional channel of mordenite had been blocked by coke. In case of offretite although the strong acid sites are decreased, treatment at increasing temperature partially regenerated the acid sites indicating that coke was mainly deposited in cages and larger channels. In contrast with the aging of either mordenite or offretite, the range of acid strength in HZSM-5 remain unchanged. In ZSM-5 zeolites, alkyl aromatics cannot react further and lead to coke deposition, because of smaller dimension of ZSM-5 channels. Karge et al[137] have demonstrated the decisive role of olefin compounds in the deactivation of mordenite catalyst. When the olefin was polymerised under reaction conditions, two-third of the ethylene feed was converted into polymeric form in carbonaceous deposits after 40 minutes time on stream, the remainder to light hydrocarbons. The IR spectra of HM showed the bands of only saturated hydrocarbons and a remarkable weakening of the band of acid hydroxyl groups (3605 cm^{-1}). The formation of saturated species was practically irreversible. The rate of deactivation of X type zeolites in the vapour phase alkylation of benzene with ethylene was very high[138]. The molecular weight of coke occluded within the pores of REX zeolite was twice that of the alkylated product. The composition of this residue was similar to that obtained when ethylene alone was passed over the catalyst. Increasing the system pressure from atmospheric to 500 psig improved the aging characteristic of the catalyst.

The role of surface species formed by adsorption of olefins onto the zeolites, studied by IR[139], provides further insight

into the mechanism of deactivation of zeolites in alkylation. The surface species were characterised by the absence of unsaturated =CH and C=C stretching bands in the IR spectrum and the presence of saturated C-H bending and stretching bands. The introduction of olefin prior to the addition of benzene to the catalyst did not alkylate benzene. However, alkylation took place when olefin was added to the zeolite containing presorbed benzene. It was concluded that the high molecular weight hydrocarbons entrapped in the zeolite pore system were probably a result of deactivation. The higher the olefin to aromatic ratio in the feed, the higher was the rate of catalyst deactivation. In the vapour phase, the aromatic loading was significantly lower than that in the liquid phase and the occurrence of irreversible olefin adsorption was significantly enhanced in the former case compared with the latter[140].

K : OBJECTIVES OF THE PRESENT WORK

The present work was undertaken with the following objectives:

1. To alter the acidity of the synthetic mordenite zeolite by dealumination with acid and to correlate the activity of these dealuminated zeolites in the isopropylation of benzene with their physico-chemical properties.

2. To alter the acidity of synthetic mordenite by incorporation of elements like La, P, Si and study their catalytic activity in the isopropylation of benzene.

3. To compare the catalytic activity of the faujasite (Y) and its modification (by ion exchange) in the isopropylation of benzene.

4. To synthesize and study the uses of zeolites ZSM-5 and ZSM-12 in the isopropylation of benzene and compare their catalytic activity with that of mordenite.

5. Application of ZSM-5 type zeolites in the alkylation of phenol.

REFERENCES

1. J.J. Mcketta, "Encyclopedia of Chemical Processing and Design", Marcel Dekker, Inc., New York, 2387 (1977).
2. K.L. Nelson and H.C. Brown, "The Chemistry of Petroleum Hydrocarbons", Vol.3, Reinhold Publishing corp., New York, Chap. 56, p.465 (1955).
3. S.H. McAllister, McAllister, "The Chemistry of Petroleum Hydrocarbons", Vol.3, Reinhold Publishing Corp., New York, Chap. 37, p.579 (1955).
4. C. Rodziewanowski, Ber. 28, 1137 (1895).
5. M.M. Balsohn, Bull. Soc. Chim.(2) 31, 539 (1879).
6. A. Brochet, Compt. Rend. 117, 115 (1893).
7. S.J. Slanina, F.J. Sowa and J.A. Nieuland, J. Am. Chem. Soc. 57, 1547 (1935).
8. A.V. Topcheiv, "Alkylation with Olefins", Elsevier, Amsterdam (1964).
9. A Contribution by Anglo - Iranium Oil Co. Ltd., Humble Oil and Refining Co., Shell Development Co., Standard Oil Development Co. and Texas Co., Oil Gas J. 38, No.27, 104 (1939).
10. S. Bekermann, J.C. Morrell and G. Egloff, "Catalysis", Reinhold Publishing Corp., New York, p. 963, 1004 (1940).
11. S.H. McAllister, J. Anderson and E.F. Bullard, Chem. Eng. Prog. 43, 189 (1947).
12. Kh. M. Minachev, Ya. I. Isakov, V.N. Mirzabekova and V.I. Bogomolov, Neftekhim 13, 407 (1973).

13. Kh. M. Minachev and Ya. I. Isakov, Dokl. Akad. Nauk. SSSR 170, 99 (1966).

14. A.P. Bolton and C.H. Jewitt, Unpublished data, Union Carbide Corp., Linde Divn.

15. P.E. Pickert, A.P. Bolten and M.A. Lanewala, AIChE Meeting, 59th Columbus, Ohio (1966).

16. H.G. Karge and J. LadeBeck, "Catalysis by Zeolites", (Eds. B. Imelik et al.), Elsevier Scientific Publ. Co., p. 151 (1980).

17. I.M. Koleshikov, G.M. Panchenkov and V.A. Tret´Yakova, Russ. J. Phy. Chem. 41, 586 (1967).

18. I.M. Kolesnikov, G.M. Panchenkov and V.A. Tret´yakova, Russ. J. Phy. Chem. 45, 965 (1971).

19. P.A. Jacobs, "Carboniogenic Activity of Zeolites", Elsevier Sci. Publ. Co., p. 164 (1977).

20. W.O. Haag and D.H. Olson, U.S. Patent 4,136,128 (1979); C.A. 90, 137446 C (1979).

21. W.W. Kaeding, Eur. Pat. Appl. 12, 504 (1980); C.A. 94, 30321 p (1981).

22. G.T. Burress, Eur. Pat. Appl. 12, 514 (1980); CA 94, 46930 x (1981).

23. L.J. Velenyi and S.R. Dolhyj, U.S. Patent 4,283,583 (1981); CA 95, 150142 y (1981).

24. C. Price, Org. React. 3, 58 (1949).

25. T. Kotanigawa, M. Yamamoto, K. Shimokawa and Y. Yoshida, Bull. Chem. Soc. Japan 44, 19 (1961).

26. General Electric Company U.S. Patent 3,44,6856 (1964).

27. P.B. Venuto, L.A. Hamilton, P.S. Landis and J.J. Wise, J. Catal. 5, 81 (1966).

28. S. Namba, T. Yashima, Y. Itaba and N. Hara, "Catalysis by Zeolites" (Eds. B. Imelik et al.), Elsevier Scientific Publ. Co., p. 105 (1980).

29. S. Balsama, P. Beltrame, P.L. Carniti, L. Forni and G. Zuretti, Appl. Catal. 13, 161 (1984).

30. P.D. Chantal, S. Kaliaguine and J.L. Grandmaison, Appl. Catal. 18, 133 (1985).

31. (A) C. Naccache, Proc. IX Ibero-American Symposium on Catalysis, Lisbon, p. 132 (1984).

(B) F.X. Cormerais, G. Perot, F. Chevauer and M. Guisnet, J. Chem. Res. 5, 362 (1980).

(C) J.P. Vandenberg, J.P. Wolthuizen and J.H.C. Vanhoof, Proc. 5th Int. Conf. on Zeolites, Naples, p. 649 (1980).

(D) J.H.C. Vanhoof, "Chemistry and Chemical Engineering of Catalytic Processes" (Eds. Sijjhof and Noor Hoff), Germantown, p. 599 (1980).

32. M. Marczewski, G. Perot and M. Guisnet, "Studies in Surface Sci. and Catalysis" (Eds. M. Guisnet et al.), Elsevier Scientific Publ. Co., p. 273 (1988).

33. W.W. Kaeding, L.B. Young, C.C. Chu, B. Weinstein and S.A. Butter, J. Catal. 67, 159 (1981).

34. W.W. Kaeding and L.B. Young, U.S. Patent 4,034,053 (1977).

35. K.H. Chandavar, Ph.D. Thesis, Pune University (1983).

36. D.W. Breck, "Zeolite Molecular Sieves", Structure, Chemistry and Use, Publ. Wiley Interscience, New York (1974).

37. F.A. Mumpton, Mineralogy and Geology of Natural Zeolites, Short Course Notes, Min-Soc. Am., Washington (1977).

38. L.B. Sand and F.A. Mumpton, (Eds.), Natural Zeolites, Occurence, Properties, Use, Pergamon Press, Oxford (1978).

39. D.W. Breck, W.G. Eversole, R.M. Mitton, T.B. Reed and T.L. Titomas, J. Am. Chem. Soc., 78, 5964 (1956).

40. R.M. Milton, U.S. Patent 2882 244 (1959).

41. D.W. Breck, U.S. Pat. 3130 007 (1964).

42. D.W. Breck, U.S. Pat. 3 216 789 (1965).

43. U.S. Pat. 34 42 795 (1969).

44. R.M. Barrer and P.J. Danny, J. Chem. Soc. 971 (1961).

45. B.M. Lok, T.R. Cannan and C.A. Messina, Zeolites 4, 289 (1984).

46. O.M. Dzhight and A.V. Kiselev, Trans. Far. Soc. 67, 458 (1971).

47. R.M. Barrer, J.W. Baynham, F.W. Bultitude and W.M. Meier, J. Chem. Soc., p. 195 (1959).

48. W.L. Bragg, "The Atomic Structure of Minerals", Cornell University Press, Ithaca, New York (1937).

49. W.M. Meier, Molecular Sieves, Soc. of Chem. Ind., London, p. 10 (1968).

50. R.M. Barrer, "Hydrothermal Chemistry of Zeolites", Academic Press, London (1983).

51. E.M. Flanigen, Proceedings of 5th International Conference on Zeolites, Rees, L.V.C. (Ed.), Heyden and Sons, London (1980).

52. L.B. Sand, Econ Geol., p. 191 (1967).

53. L.B. Sand, "Molecular Sieves", p. 71, Society of the Chemical Industry (London) 1968.

54. W.M. Meier, Z. Krist. 115, 439 (1961).

55a. W. Loewenstein, Am. Minesol. 39, 92 (1942).

55b. J.V. Smith, "Molecular Sieve Zeolites-I", Advan. Chem. Ser., 101, E.M. Flanigen & L.B. Sand, Am. Chem. Soc., Washington D.C., p.171 (1971).

55c. T.I. Barry and L.A. Ray, J. Phys. Chem. Solids, 29, 1395 (1968).

56. R.B. Lapierre, A.C. Rohrman, Jr., J.L. Schlenker, J.D. Wood, M.K. Rubin and W.J. Rohrbaugh, Zeolites 5, 346 (1985).

57. G.T. Kokotailo, S.L. Lawton, D.H. Olson and W.M. Meier, Nature 272, 437-438 (1978).

58. M.L. Costenoble, W.J. Mortier and J.B. Uytterhoeven, J.C.S. Faraday Trans. I, 72, 1877 (1976).

59. A. Gulfaz and L.B. Sand, Adv. Chem. Ser. 121, 140 (1973).

60. E. Dempsey, G.H. Kuhl and D.H. Olson, J. Phys. Chem. 73, 387 (1969).

61. J.D. Hanowalt, H.W. Rin and L.K. Frevel, Ind. Eng. Chem. 10, 457 (1938).

62. J.V. Smith, "Molecular Sieve Zeolites-I", Advan. Chem. Ser. 101, E.M. Flanigen and L.B. Sand, Am. Chem. Soc., Washington D.C., 1971, p. 171.

63. E.W. Flanigen, H. Khatami and H.A. Szymanki, Adv. Chem. Ser. 102, 374 (1973).

64. N. Topsøe, K. Pederson and E.G. Derouane, J. Catal. 70, 41 (1981).

65. D. Lohodmy-Sarac and J.L. White, J. Phys. Chem. 75, 2408 (1971).

66. J.W. Ward, Chapter 2, "Zeolite Chemistry and Catalysis" (Eds. Rabo, J.A.), ACS Monograph, 171 (1976).

67. J.W. Ward, "Molecular Sieve Zeolites-I", Advan. Chem. Ser. 101, Am. Chem. Soc., Washington D.C., p. 380 (1971).

68. P.E. Eberley, Jr., and C.N. Kimberlin, Jr, "Molecular Sieve Zeolites-II", Advan. Chem. Ser. 102, (Ed. E.M. Flanigen et al.), Am. Chem. Soc., Washington D.C., p. 374 (1971).

69. Ref. 36, p. 449 (1974).

70. R.M. Barrer and D.A. Langley, J. Chem. Soc., 3804, 3811, 3817 (1958).

71. R.M. Barrer and G.C. Bratt, J. Phys. Chem. Solids 12, 130, 146 (1959).

72. R.M. Barrer and A.F. Denny, J. Chem. Soc., 4684 (1964).

73. H.K. Beyer, J. Chem. Soc., Faraday Trans I, 73, 1111 (1977).

74. H.W. Habgood, Can. J. Chem. 42, 2340 (1964).

75. A.L. Klyachko, A.T. Gurvich and A.M. Rubinstein, Bull. Acad. Sci. USSR Chem. Sci., 687, 1355 (1967).

76. B. Coughlan and J.J. McEntee, Proced. Royal Irish Acad. 76B, 473 (1976); R.M. Barrer and R.M. Gibbons, Trans. Far. Soc. 61, 948 (1965).

77. R.M. Barrer and B. Coughlan, Molecular Sieves, Publ. Society of Chemical Industry, London, p. 233, 241 (1968).

78. B. Coughlan and S. Kilmartin, J. Chem. Soc., Far. Trans. I, 71, 1809 (1975).

79. E.M. Flanigen, J.M. Bennett, R.W. Grose, J.P. Cohen, R.L. Patton, R.M. Kirchner and J.V. Smith, Nature 271, 512 (1978).

80. N.Y. Chen, J. Phy. Chem. 80, 60 (1976).

81. J.R. Anderson, K. Foger, T. Mole, R.A. Rajadhyaksha and J.V. Sanders, J. Catal. 58, 114 (1979).

82. P.W. Weisz, Pure and Applied Chem. 52, 2091 (1980).

83. E.G. Derouane, B. Imelik et al. (Editors), "Catalysis by Zeolites", p.5 (1980).

84. P.A. Jacobs, "Carboniogenic Activity of Zeolites", Elsevier Sci. Publ. Co., p. 33 (1977).

85. V.J. Frilette, P.B. Weisz and R.L. Golden, J. Catal. 1, 301 (1962); British Pat. 886,716 (1962).

86. K. Tanabe, "Solid Acids and Bases", Academic Press, N.Y., p. 5, Chapter II.

87. J.C. Vedrine, A. Auroux, V. Bolis, P. Dejaifve, C. Naccache, P. Weirzchowski, E.G. Derouane, J.B. Nogi, J.P. Gilson, J.H.C. Van Hooff, J.P. Van der Berg. and J.P. Wolthieuzen, J. Cat. 59, 248 (1974).

88. A. Auroux, V. Bolis, Weirzchowski, P.C. Gravelle and J.C. Vedrine, J. Chem. Soc., Faraday Trans. I, 75, 2544 (1979).

89. P.A. Jacobs, J.B. Uytterhoeven, M. Styeyns, G. Froment and J. Weitkamp, "Proc. 5th Int. Conf. on Zeolites", Naples, Italy, Heyden and Sons, London, 604 (1980).

90. B.L. Meyers, T.H. Fleisch, G.J. Ray, J.T. Miller and J.B. Hall, J. Catal. 110, 82-95 (1988).

91. J. Klinowski, J.M. Thomas, C.A. Fyfe and J.S. Hartman, J. Phys. Chem. 85, 2590 (1981).

92. E. Lippmaa, M. Magi, A. Samoson, M. Tarmak and G.J. Engelhardt, J. Am. Chem. Soc. 103, 4992 (1981).

93. G. Engelhardt, E. Lippmaa and M. Magi, J. Chem. Soc. Chem. Commun. 712 (1981).

94. G. Engelhardt, U. Lohse, E. Lippmaa, M. Tarmark and M. Magi, Z. Anorg. Allg. Chem. 482, 49 (1981).

95. S. Ramdas, J.M. Thomas, J. Klinowski, C.A. Fyfe and J.S. Hartman, Nature 292, 228 (1981).

96. J. Klinowski, S. Ramdas, J.M. Thomas, C.A. Fyfe and J.S. Hartman, J. Chem. Soc. Faraday Trans. II, 78, 1025 (1982).

97. D.E.W. Vaughan, M.T. Melchair and A.J. Jacobson, A.C.S. Symposium Series No.218, "Intra Zeolite Chemistry", (Eds. G.D. Stucky and F.G. Dwyer), Am. Chem. Soc., Washington D.C., p. 231 (1983).

98. M.T. Melchior, A.C.S. Symposium Series No.218 "Intra Zeolite Chemistry" (Eds. G.D. Stucky and F.G. Dwyer), Am. Chem. Soc., Washington D.C., p. 243 (1983).

99. J.M. Thomas, C.A. Fyfe, J. Klinowski and G.C. Gobbi, J. Phys. Chem. 86, 3061 (1982).

100. M.T. Melchior, D.E.W. Vaughan, R.H. Jarman and A.J. Jacobson, Nature 298, 455 (1982).

101. R.H. Jarman, M.T. Melchoir and D.E.W. Vaughan, A.C.S. Symposium Series No.128 "Intrazeolite Chemistry" (Eds. G.D. Stucky and F.G. Dwyer), Am. Chem. Soc., Washington D.C., p. 267 (1983).

102. G. Debras, J. Nagy, Z. Gabelica, P. Bodart and P.A. Jacobs, Chem. Lett. 199 (1983).

103. B. Nagy J., J.P. Gilson and E.G. Derouane, J. Chem. Soc., Chem. Commun. 1129 (1981).

104. C.A. Fyfe, G.C. Gobby, J. Klinowski, J.M. Thomas and S. Ramdas, Nature 296, 530 (1982).

105. P.A. Jacobs, M. Thielen, B. Nagy J., G. Debras, E.G. Derouane and Z. Gabelica in Proc. 6th Int. Zeolite Conference (Eds. D. Olson and A. Bisio), Butterworths, Guildford, p. 783 (1984).

106. B. Nagy J., Z. Gabelica, Z. Debras G., P. Bodart, E.G. Derouane and P.A. Jacobs, J. Mol. Catal. 20, 327 (1983).

107. Z. Gabelica, B. Nagy J., P. Bodart, G. Debras, E.G. Derouane and P.A. Jacobs in "NATO Advanced Study Institute on Zeolites: Science and Technology" (Eds. F.R. Ribeiro et al.), Martinus Nijhoff Den Haag, p. 193 (1984).

108. B. Nagy J., Z. Gabelica, E.G. Derouane and P.A. Jacobs, Chem. Lett. 2003 (1982).

109. G. Engelhardt, U. Lohse, A. Samoson, M. Magi, M. Tarmark and E. Lippmaa, Zeolites 2, 59 (1982).

110. B. Nagy J., Z. Gabelica and E.G. Derouane, Chem. Lett. 1105 (1982).

111. C.A. Fyfe, G.C. Gobbi, J.S. Hartman, J. Klinowski, and J.M. Thomas, J. Phys. Chem. 86, 1247 (1982).

112. B. Nagy J., Z. Gabelica, G. Debras, E.G. Derouane, J.P. Gilson and P.A. Jacobs, Zeolites 4, 133 (1984).

113. E.G. Derouane, B. Nagy J., N. Blom and Z. Gabelica, Zeolites 2, 299 (1982).

114. G.R. Hays, W.A. VanErp, N.C.M. Alma, P.A. Couperus, R. Husi and A.E. Wilson, Zeolites 4, 377 (1984).

115. J.F. Tempere, D. Delafosse and J.P. Contour, Chem. Phys. Lett. 33, 95 (1975).

116. J.F. Tempere, D. Delafosse and J.P. Contour, "Molecular Sieve-II" (Ed. J.R. Katzer), Adv. Chem. Ser. 40, 76 (1977).

117. C. Defosse, B. Delmon and P. Canesson, "Molecular Sieve-II", (Ed. J.R. Katzer), Adv. Chem. Ser. 40, 86 (1977).

118. J. Knecht and G.Z. Stork, Anal. Chemie 283, 105 (1977).

119. J. Finster and P. Lorehz, Chem. Phys. Lett. 50, 223 (1977).

120. E.G. Derouane, J.P. Gilson, Z. Gabelica, M. Desbuquoit and J. Verbist, J. Catal. 71, 447 (1981).

121. J.C. Vedrine, A. Auroux, P. Dejaifve, V. Ducarone, H. Hoser and Zhous, J. Catal. 73, 147 (1982).

122. S. Badrinarayanan, R.I. Hegde, I. Balkrishnan, S.B. Kulkarni and P. Ratnasamy, J. Catal. 71, 439 (1981).

123. J.M. Stenzel, J.R. Diehl, L.J. Douglas, C.A. Spitler, J.E. Crawford and G.A. Melson, Colloids and Surfaces 4, 331 (1982).

124. M. Sawa, M. Niwa and Y. Murakami, Appl. Catal. 53, 169-181 (1989).

125. Kh.M. Minachev, G.V. Antoshin, E.S. Spiro and H.I. Isakov, Izv. Akad. Nauk. SSSR, Ser. Khim., p. 2131 (1973).

126. Kh.M. Minachev, G.V. Antoshin, E.S. Spiro and T.A. Navruzov, Izv. Akad. Nauk SSSR, Ser. Khim., p. 2134 (1973).

127. Kh.M. Minachev, G.V. Antoshin and E.S. Spiro, Izv. Akad. Nauk. SSSR, Ser. Khim., p. 1012 (1974).

128. D.H. Olson, W.O. Haag and R.M. Lago, J. Catal. 61, 390-396 (1980).

129. R.M. Barrer and R.P. Townsend, JCS Faraday Trans. I. 72, 661 (1976).

130. B.W. Burbridge, I.M. Keen and M.K. Eyles, Adv. Chem. Ser., 1971, 102, 401; Kh. Minachev, V. Garanin, T. Isakova, V. Kharlamov and V. Bogomolov, Adv. Chem. Ser., 102, 440 (1971).

131. I.J. Gal, O. Jankovic, S. Malcic, P. Radovanov and M. Todorovic, Trans. Faraday Soc. 67, 999 (1971).

132. F. Wolf, D. Ceacareanu and K. Pikhowski, Z. Phys. Chem. (Leipzig) 252, 50 (1973).

133. E. Gallei, D. Eigenbach and A. Ahmed, J. Catal. 33, 62 (1974).

134. A. Maes and A. Cremers, JCS, Faraday I, 71, 265 (1975).

135. D.E. Walsh and L.D. Rollman, J. Catal. 56, 195 (1979).

136. P. Dejaifve, A. Auroux, P.C. Gravelle, J.C. Vedrine, Z. Gabelica and E.G. Derouane, J. Catal. 70, 123 (1981).

137. H.G. Karge and J. Ladebeck, "Catalysis by Zeolites" (Eds. B. Imelik et al.), Elsevier Scientific Publ. Co., p. 151 (1980).

138. P.B. Venuto, Chem. Tech., p. 215 (1971).

139. T.J. Weeks, A.P. Bolten, Proc. 3rd Intern. Congr. Mol. Sieves, Zurich, p. 426 (1973).

140. A.P. Bolton, "Zeolite Chemistry and Catalysis" (Ed. J.A. Rabo), Am. Chem. Soc., Monograph No. 171, Washington D.C., p. 779 (1976).

****

CHAPTER - 2

SYNTHESIS, MODIFICATION AND CHARACTERIZATION OF ZEOLITES

****

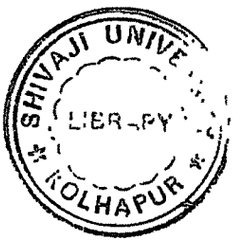

2.1 SYNTHESIS OF MORDENITE

General method of synthesis of zeolites has been described in Chapter-1. In this chapter the actual synthesis and modification is described.

In a typical synthesis of large port mordenite the following procedure was adopted.

Sodium silicate 168.24g (composition: SiO_2 = 27.2, Na_2O = 8.4, H_2O = 64.4% weight (g)) was added to 200 gm of deionised water. An acid aluminium sulphate solution was made taking 12.6 gm of salt [composition: $Al_2(SO_4)_3.18H_2O$) in 226 gm of water. This solution was then slowly added under stirring to the previously prepared sodium silicate solution. The resulting gel having pH = 11.0±2 was then transferred to a stainless steel autoclave (capacity 1000 ml) and kept at 120°C for 96h as these are the optimum synthesis conditions reported.[1] After the reaction was terminated the autoclave content was quenched in cold water. The crystalline product (36 gm) was filtered, washed with hot deionised water till free of sulphate ions, dried in an air oven at 120°C for 24h and calcined in flowing air at 540°C for 10-12h in a static air furnace. The chemical composition of fully crystalline mordenite sample estimated by wet-chemical analysis and atomic absorption spectroscopy (AAS) was SiO_2 = 79.5%, Al_2O_3 = 13.55 and Na_2O = 6.75% (g) (SiO_2/Al_2O_3 molar ratio = 9.98).

2.2 MODIFICATION OF MORDENITE

A. Dealuminated mordenite

The as synthesized Na-mordenite was refluxed with 0.01N HCl (10 mls of HCl/gm of zeolite) for 4h, filtered, washed till free of chloride ions and residue dried at 120°C. The treatment was repeated. The sodium content was reduced to 0.4% Na_2O and the SiO_2/Al_2O_3 ratio increased to 13.0. The sample was designated as HM. This sample (HM) was further treated with hydrochloric acid to obtain dealuminated mordenites of varying SiO_2/Al_2O_3 molar ratios. These Al-deficient materials were filtered, washed with hot deionised water to free from chloride ions, and then dried at 120°C for 12h. The treatment procedure is summarized in Table 2.1. Samples were designated as HDM (H-dealuminated mordenites).

B. Phosphorus impregnated mordenites

These samples were prepared by impregnating H-mordenite (Norton's H-zeolon 100) with appropriate quantity of O-phosphoric acid in aqueous solution. The well homogenised slurry was slowly evaporated at 95°C for 12h and calcined in the muffle furnace at 450°C for 10h to give the corresponding catalyst in oxide form. The samples were designated as PHM.

C. Surface silynation of mordenite

Synthetic zeolon-900 (1/8)" dia extrudates with SiO_2/Al_2O_3 molar ratio 10, obtained from Norton Chemical Co. Worcester Mass, USA, was further treated to make surface silynated catalyst. H-mordenite was suspended in n-hexane and contacted with calculated amount of tetraethyl ortho silicate to give surface silynated

Table 2.1

Preparation of dealuminated mordenites

Sample*	Acid treatment+	Unit cell composition
NaM	-	$H_{1.2}Na_{6.84}[(AlO_2)_{8.03}(SiO_2)_{39.97}]$
HM	-	$H_{5.84}Na_{0.46}[(AlO_2)_{6.3}(SiO_2)_{41.76}]$
HDM-(54)	5N HCl boil 12h	$H_{1.27}Na_{0.44}[(AlO_2)_{1.71}(SiO_2)_{46.29}]$
HDM-(86)	(a) 5N HCl boil 24h (b) 8N HCl boil 12h	$H_{0.97}Na_{0.12}[(AlO_2)_{1.09}(SiO_2)_{46.91}]$
HDM-(106)	(a) 8N HCl boil 24h (b) 8N HCl boil 24h	$H_{0.78}Na_{0.09}[(AlO_2)_{0.87}(SiO_2)_{47.12}]$
HDM-(147)	Product of HDM-106 boiled with 8.5N HCl for 24h	$H_{0.58}Na_{0.06}[(AlO_2)_{0.64}(SiO_2)_{47.4}]$

Product of (a) used for second treatment (b)

* Figures in parenthesis indicate SiO_2/Al_2O_3 molar ratio.

\+ Treatment temperature 98°C.

mordenite. The mixture was first stirred on a magnetic stirrer and was further refluxed for 6h. Finally n-hexane was removed completely by evaporation. The catalyst was dried and calcined before the catalytic studies.

D. Rare-earth exchanged mordenite

D.1 Na-RE Mordenite: The synthetic mordenite (section 2.1) was treated with calculated amount of RE^{3+} ion from a solution containing 3.03% RE_2O_3 by weight. Samples with higher degree of exchanges were obtained by repeated treatments at 95°C. Samples with 22,43,51 and 62% RE^{3+} ion exchanged were prepared and air dried in an air oven for 24h, cooled, powdered, sieved and stored over saturated ammonium chloride solution at 25°C.

D.2 HRE Mordenite: H-mordenite (Norton's H-zeolon 100) was treated with calculated amount of RE^{3+} ion from the solution containing 3.03% RE_2O_3 by weight at 95°C. Samples with higher degree of exchanges were obtained by repeated treatments and dried in an air oven at 120°C for 24h, cooled, powdered, sieved and stored over saturated ammonium chloride solution at 25°C.

2.3 PREPARATION OF RARE EARTH EXCHANGED Y ZEOLITE

Binder free Linde NaY(SK-40) zeolite having Si/Al ratio of 2.68 was obtained from Union Carbide Co., USA and was used for preparation of ion exchanged zeolites.

For cation exchange sample was treated with calculated amount of RE^{3+} ion from the solution containing 3.03% RE_2O_3 by

weight at 95°C. Higher exchanged samples were obtained by repeated treatments. All the samples after ion exchange were filtered, washed free of chloride ion , dried in an air oven at 120°C for 24h, cooled, powdered, sieved and stored over saturated ammonium chloride solution at 25°C.

2.4 SYNTHESIS OF ZSM-12 ZEOLITE

The synthesis of ZSM-12 zeolite was carried out as reported in the patent.[2] Reagents used in the preparation of ZSM-12 zeolite were silicon-dioxide (microsil II, 95.0 wt% SiO_2, 4.85 wt% H_2O, Leuchtstoffwerk, India), Aluminium sulphate hexadecahydrate (Merck), Tetra ethyl ammonium bromide (Merck, Schuchardt), Sodium hydroxide pellets (97% cp), oxalic acid (Loba Chemie, GR) and deionised water.

Typically, zeolite ZSM-12 was synthesized from a gel containing tetraethyl ammonium bromide having a molar composition:

$$22.4\ Na_2O : 32.0\ (TEA)_2O : Al_2O_3 : 260\ SiO_2 : 3600\ H_2O$$

A slurry was made containing 11.9 gms of microsil silica by adding a solution containing aluminium sulphate hexadecahydrate (0.345 g) and tetraethyl ammonium bromide (24.6 g) dissolved in 100 g of deionised water. To this, was then added a solution of NaOH (3.0 g) and oxalic acid (1.5 g) (prepared by dissolving NaOH and $(COOH)_2.2H_2O$ in 125.0 g of deionised water) under stirring. After the mixture was stirred for 1h at room temperature, the gel slurry (pH= 13.0) was transferred to a 300 mls stainless steel

autoclave and allowed to crystallize under static conditions at 170°C for 6 days. After terminating the reaction the solid crystalline product was filtered, washed and dried at 120°C. The as-synthesized product of this system was calcined at 550°C in a flow of air for 10-12h. The sodium form (NaZSM-12) thus obtained was ammonium exchanged using 5N aqueous ammonium nitrate, filtered, washed and dried at 120°C and then calcined at 550°C for 10h to obtain protonic (H^+) form. Before use as a catalyst the sample (HZSM-12) was compacted binder free and crushed to 10-22 mesh size.

2.5 SYNTHESIS OF ZSM-5 ZEOLITE

The synthesis of high silica ZSM-5 type zeolite was carried out as reported in patent.[3] The following raw materials were used for the synthesis:

Sodium silicate: Composition (wt%) SiO_2 = 27.2 g
Na_2O = 8.4 g and water = 64.4 g
Aluminium sulphate: $Al_2(SO_4)_3.16H_2O$ (E.Merck)
Sulphuric acid: (wt%) 98 (BDH Analytical grade)
Triethyl-n-propyl ammonium bromide TEPA Br (Synthesized in the laboratory)

Appropriate amounts of aluminium sulphate and sulphuric acid were dissolved in deionised water to yield solution A. A calculated quantity of TEPA Br was added to a solution of sodium silicate of required strength to yield solution B. The two solutions A and B were then mixed in a stainless steel reactor

vessel (capacity 250 mls) with continuous stirring to form a free flowing gel which had the molar composition:

4.38 $(TEPA)_2O$, 27.6 Na_2O, Al_2O_3, 87.7 SiO_2, 32.62 H_2O

The vessel was then closed as quickly as possible to prevent sorption of CO_2 from air. The reaction vessel was placed in an air oven at the required temperature and left at this temperature ($180\pm5^{o}C$) for sufficient time usually about 24 to 96h depending on SiO_2/Al_2O_3 ratio of the gel mix. The reactor was cooled after completion of crystallization and contents were filtered and washed with water till the filtrate was free of the anion. The resulting sample was dried in a static air oven at $120^{o}C$ for overnight. A part of the sample was used to determine crystallinity by XRD. The remaining sample was slowly heated to $550^{o}C$ and held at this temperature for 8h to decompose intracrystalline organic (TEPA) base. The sample (NaZSM-5) was then cooled and kept over saturated ammonium chloride solution by repeated exchange with 5M ammonium chloride solution under reflex at $95^{o}C$ on water bath, sodium ions in NaZSM-5 were exchanged with NH_4^+ ions. The sample was then dried at 100^{o} and calcined at $550^{o}C$ to convert to NH_4ZSM-5 to the H^+ form (HZSM-5). It was then cooled and kept over saturated ammonium chloride solution.

2.6 CHARACTERIZATION

A. Chemical Analysis

All zeolite samples were analysed by wet chemical/gravimetric methods. SiO_2 was estimated gravimetrically and other elements like Al,Na,Fe etc. were analysed using atomic

absorption spectroscopy (AAS).

Procedure: An accurately weighed amount of the sample (≅ 200-500 mgs) was ignited in a platinum crucible up to 800°C for 2h, cooled in a desiccator over activated silica gel and weighed. This was repeated till the sample showed constant weight. The % loss in weight on ignition due to H_2O and occluded organics was thus determined (Anhydrous weight of the sample thus calculated after obtaining % LOI was used for calculating % SiO_2, Al_2O_3, Na_2O etc. and all results were expressed on anhydrous basis). The sample was then treated with 15 mls of 1:1HF along with 2-3 drops of concentrated H_2SO_4 and evaporated gently. This was repeated twice. The sample was then heated strongly, dried and weighed. % SiO_2 was calculated from the weight loss obtained as a result of loss of silica as SiF_4. The sample so obtained was fused with 2g $K_2S_2O_7$ and dissolved in warm water to get a known volume of solution in a standard flask. The solution was then analysed by AAS for elements like Al, Na, Fe, etc..

Estimation of RE_2O_3: The % RE_2O_3 in the zeolite was estimated gravimetrically by precipitation as oxalates.

About 1-2 gm of accurately weighed sample was treated with 25-30 mls of 1:1 hydrochloric acid and evaporated gently to dryness. The procedure was repeated thrice to bring the rare earth in the solution. The solution was then filtered, washed thoroughly and made up to known volume in a standard flask. Out of this stock solution 50 ml was used for precipitation as rare earth oxalates as follows:

In the 50 ml of solution 2-3 drops of methyl violet indicator were added. To this liquor ammonia was added till the solution showed blue-green colour. The same was then boiled and 60 ml of 12% oxalic acid was added slowly under continuous stirring to get the curdy precipitate of RE-oxalate which was filtered through Whatman No.40 filter paper and washed with 2% oxalic acid solution. The residue was then ignited and weighed as RE_2O_3. % RE_2O_3 was calculated as

$$\% RE_2O_3 = \frac{\text{Weight of residue after ignition}}{\text{Weight of anhydrous sample}} \times 100$$

B. X-ray Diffraction (XRD)

The X-ray diffractograms were recorded using Philips 1700 X-ray diffractometer with Ni filtered CuKα radiation (λ = 1.5405 A^o) in the range of 2θ = 6 to 50^o. The interplaner distances 'd' for Na-mordenite (SiO_2/Al_2O_3 = 10) obtained from values of 2θ along with published 'd' values for mordenite are shown in Table 2.2. Fig. 2.1 shows X-ray diffraction pattern of mordenite. The values of 'd' and the relative intensities of peaks with respect to the most intense peak at 2θ = 25.8 are in agreement with those reported in literature.[1]

Crystalline purity of dealuminated mordenites prepared in section 2.2A after equilibrating over saturated ammonium chloride solution for 24h were determined by comparing the sum of the peak heights of the [3 3 0], [1 5 0], [2 0 2], [3 5 0] and [4 0 2 3 3 2] reflections (2θ = 19 to 31) with that for Hzeolon-100 (SiO_2/Al_2O_3 = 13) scanning at 2^o/min. The X-ray diffraction

Table 2.2

Lattice spacing, (d), and relative intensity (I/I_o) values for Na-Mordenite

2θ	Interplaner spacing 'd' Å(obs)	Interplaner spacing 'd' Å*	Relative intensity I/I_o(obs)	Relative intensity I/I_o*	
6.8	12.99	13.4	20.18	40	ms
8.8	10.04	-	8.26	-	
9.9	8.93	8.85	39.45	50	ms
13.6	6.51	6.49	34.86	55	ms
14.0	6.32	-	19.27	-	
14.8	5.98	-	8.26	-	
15.4	5.75	5.66	13.76	15	mw
19.75	4.49	4.50	31.19	25	ms
22.4	3.97	3.98	66.97	60	vs
23.3	3.81	-	11.00	-	
23.8	3.74	-	11.93	-	
25.8	3.45	3.42	100	100	vs
26.4	3.37	-	64.22	-	
27.8	3.21	3.15	55.05	-	s
31.0	2.88	-	27.52	-	

vs = very strong, s = strong, m = medium, w = weak.

* Adv. Chem. Ser. 101, ACS, Washington, D.C., 127 (1971).

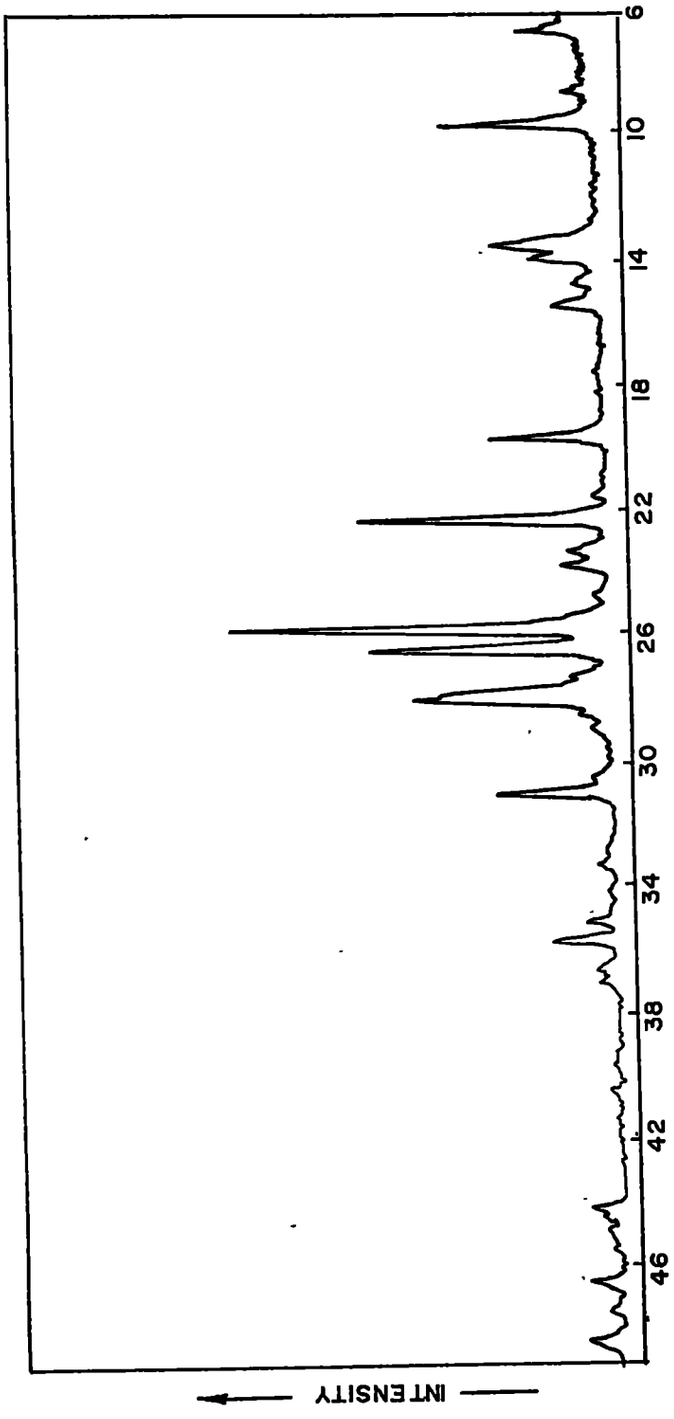

FIG. 2.1 XRD PATTERN OF MORDENITE

patterns of all the dealuminated mordenite with different SiO_2/Al_2O_3 ratio are similar (Fig.2.2). All samples were highly crystalline and were in the range of 90-98%.

No evidence of lattice degradation was apparent and was in agreement with that reported.[4] d spacings and relative intensities for mordenite samples is represented in Table 2.4. Lattice parameters of dealuminated mordenites were determined in the presence of 10% silicon-powder internal standard, (Alfa-Inorganics). Samples were step scanned at 0.5^{o}/min and CuK α, reflections were determined from the peak intensity. Eight reflections ($43\text{-}61^{o}$ 2θ) were normally used in the determinations. [0 10 0], [6 8 0], [0 0 4], [7 1 3], [10 0 0], 5 3 4], [8 4 3] and [8 8 2] reflections identified overwhelmingly with a single hkl set. The cell constants and unit cell volume of dealuminated mordenites are shown in Table 2.3. There is contraction in unit cell dimension which result in decrease in unit cell volume upon aluminium removal from the crystal lattice by acid treatment in agreement with the reported work.[5,6]

The X-ray diffraction pattern of phosphorus impregnated mordenites were found to be similar and products were well crystalline. The XRD pattern of HRE(54)MD is shown in Fig.2.3. d spacings and relative intensities for rare-earth exchanged mordenites are described in Table 2.14.

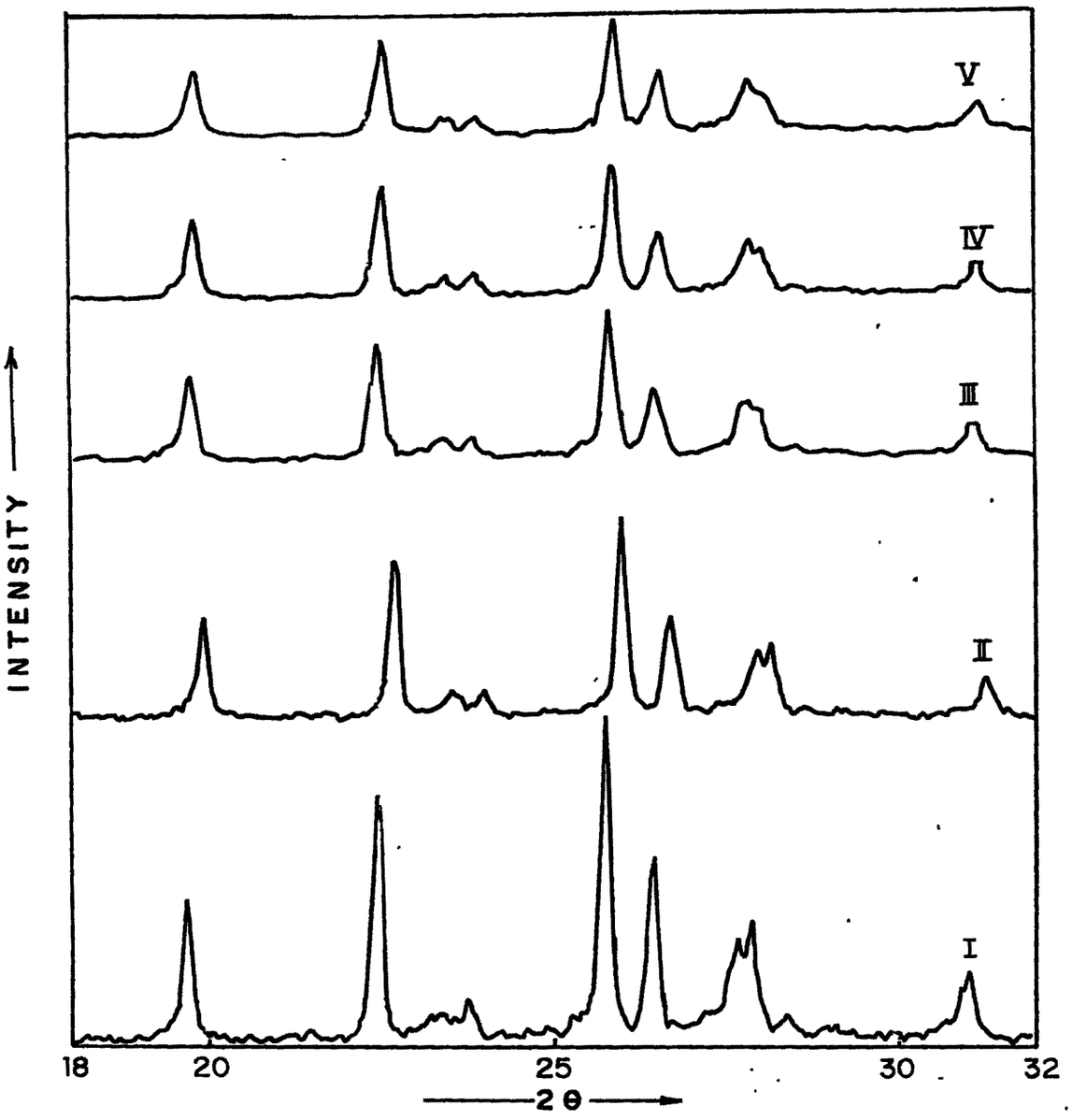

FIG.2.2: XRD PATTERNS OF MORDENITE SAMPLES SiO_2/ Al_2O_3 RATIO : I-13, II-54, III-86, IV-106 AND V-147.

Table 2.3

Cell constant and unit cell volume of dealuminated mordenites

Zeolite	Al/uc	Cell constant, A°			Unit cell volume $(A^{\circ})^3$
		a	b	c	
Na-mordenite	6.84	18.209	20.35	7.516	2786.06
H-mordenite	6.30	18.164	20.342	7.486	2766.02
HDM-(54)	1.71	18.116	20.234	7.479	2741.60
HDM-(86)	1.09	18.097	20.256	7.472	2739.20
HDM-(106)	0.87	18.057	20.299	7.465	2736.40
HDM-(147)	0.64	18.057	20.256	7.461	2729.03

Table 2.4

d spacings and relative intensities of mordenite samples

	Na-mordenite		H-mordenite		HDM-(54)		HDM-(86)		HDM-(106)		HDM-(147)	
hkl	d(Å)	I/I_ox100	d(Å)	I/I_ox100	d(Å)	I/I_ox100	d(Å)	I/I_ox100	d(Å)	I/I_ox100	d(Å)	I/I_ox100
110	12.98	20.18	13.38	34.02	13.58	49.79	13.38	33.85	13.58	57.85	13.18	38.64
020	10.04	9.17	10.04	30.41	10.15	44.75	10.04	33.63	10.27	48.34	10.04	33.62
200	8.92	39.44	8.92	42.32	8.95	96.2	9.01	97.0	9.11	97.5	8.92	99.2
111	6.50	34.86	6.50	51.03	6.50	68.6	6.50	56.95	6.55	67.35	6.50	56.95
130	6.32	19.72	6.32	16.49	6.32	20.97	6.41	11.65	6.32	23.55	6.23	18.99
021	5.98	8.25	5.98	9.02	5.98	10.83	5.98	9.86	6.06	11.57	5.98	10.69
310	5.74	14.22	5.74	23.71	5.74	27.27	5.78	26.45	5.78	29.33	5.74	25.10
240	4.65	31.19	4.48	47.42	4.48	56.64	4.48	53.36	4.50	60.74	4.78	55.45
150	3.96	66.05	3.93	77.31	3.94	85.31	3.94	81.61	3.96	86.77	3.93	81.22
241	3.81	11.0	3.79	16.23	3.79	17.48	3.79	19.05	3.79	19.0	3.76	18.99
002	3.73	12.84	3.72	10.30	3.72	16.08	3.72	17.26	3.73	16.52	3.70	17.90
202	3.45	100	3.45	100	3.45	100	3.45	100	3.45	100	3.44	100
350	3.37	64.22	3.34	51.54	3.36	52.09	3.34	53.36	3.37	52.89	3.34	50.65
530	3.20	55.50	3.20	47.42	3.20	45.45	3.19	49.77	3.20	45.45	3.19	45.85
312	3.18	54.12	3.18	48.45	3.18	44.05	3.18	43.49	3.18	41.73	3.18	43.23
061	3.09	7.33	3.11	7.73	3.06	4.89	3.11	8.52	3.07	4.95	3.11	7.86

Table 2.4 (Continued)

d spacings and relative intensities of mordenite samples

	Na-mordenite		H-mordenite		HDM-(54)		HDM-(86)		HDM-(106)		HDM-(147)	
hkl	d(Å)	I/I_ox100	d(Å)	I/I_ox100	d(Å)	I/I_ox100	d(Å)	I/I_ox100	d(Å)	I/I_ox100	d(Å)	I/I_ox100
261	2.92	6.88	2.90	7.22	2.90	-	2.92	-	2.92	-	2.92	-
620	2.88	27.98	2.86	21.90	2.86	24.47	2.86	25.33	2.88	23.96	2.86	25.32
621	2.68	4.58	2.69	2.57	2.68	2.44	2.68	3.58	2.70	4.13	2.68	3.05
370	2.61	2.75	2.60	2.06	2.60	2.09	2.59	3.13	2.57	1.65	2.60	1.75
442	2.54	6.88	2.52	4.12	2.52	4.89	2.52	5.38	2.53	5.37	2.53	5.37
280	2.50	16.97	2.49	9.02	2.49	9.44	2.49	10.98	2.49	10.04	2.50	9.92
480	2.20	3.21	2.20	3.09	2.25	3.49	2.19	3.81	2.25	3.05	2.20	2.89
732	2.03	8.25	2.02	11.08	2.02	16.08	2.02	14.34	2.02	14.04	2.02	14.19
841	2.0	5.96	1.99	5.67	1.99	5.94	1.99	7.17	2.0	6.61	1.99	7.42
930	1.94	9.63	1.93	7.98	1.93	9.79	1.93	9.41	1.93	9.09	1.93	10.48
752	1.90	4.12	1.89	2.57	1.89	2.79	1.89	3.13	1.90	2.06	1.89	3.49
114	1.86	9.63	1.86	7.73	1.86	9.09	1.86	9.41	1.86	8.26	1.86	9.82

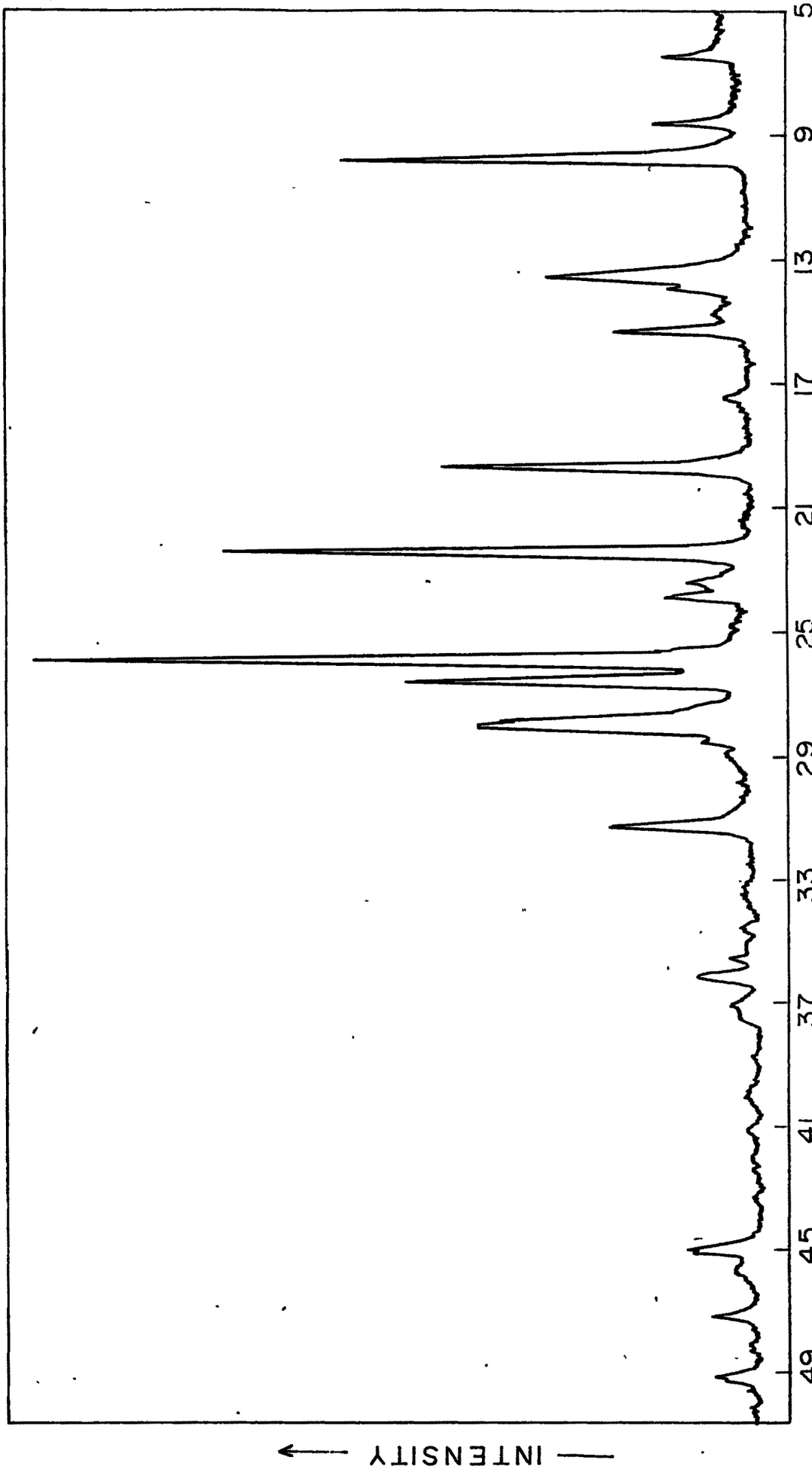

FIG. 2.3 XRD PATTERN OF HRE(54) MORDENITE

C. Infrared Spectroscopy (IR)

The framework I.R. vibration spectra were recorded on Pye-unicam SP3-300 spectrometer using Nujol mull technique with KCN as an internal standard. I.R. spectra of the samples with different SiO_2/Al_2O_3 ratio are given in Fig.2.4(a). Table 2.5 shows characteristic stretching frequencies for H-mordenite (SiO_2/Al_2O_3 = 10).

Fig. 2.4(a) shows the framework I.R. spectra (in the region 200-1300 cm^{-1}) of dealuminated mordenites. The structure sensitive range of the I.R. spectra show the prominent bands 560-580, 640, 710 and 1060 cm^{-1}) characteristic of a zeolite framework. Spectra of HDM with varying SiO_2/Al_2O_3 ratio show shifts of several bands (560-580 to 580-590, 640-655 and 1060-1075 cm^{-1}) to high wave numbers, a decrease in the prominent band intensity at 710 cm^{-1} and the development of a shoulder at 820 cm^{-1}. The intensity of the 820 cm^{-1} band continuously increased with an increase in SiO_2/Al_2O_3 ratio.

The removal of aluminium atom can also be explained on the basis of three factors: (1) zeolite bands attributed to asymmetric and symmetric stretching vibrations of the TO_4 tetrahedral (T = Si or Al) shifting to high wave numbers (i.e. bands at 560-580, 640, and 1060 cm^{-1} present in the crystall lattice[7]) and considered as representative of Al-deficient framework sites, as observed in faujasites.[8,9] (2) On the basis of published results,[9] the band at 730 cm^{-1} is assigned to "isolated" AlO_4^- tetrahedra and its intensity decreases linearly with Al content. According to Tarte,[10] the vibration of these

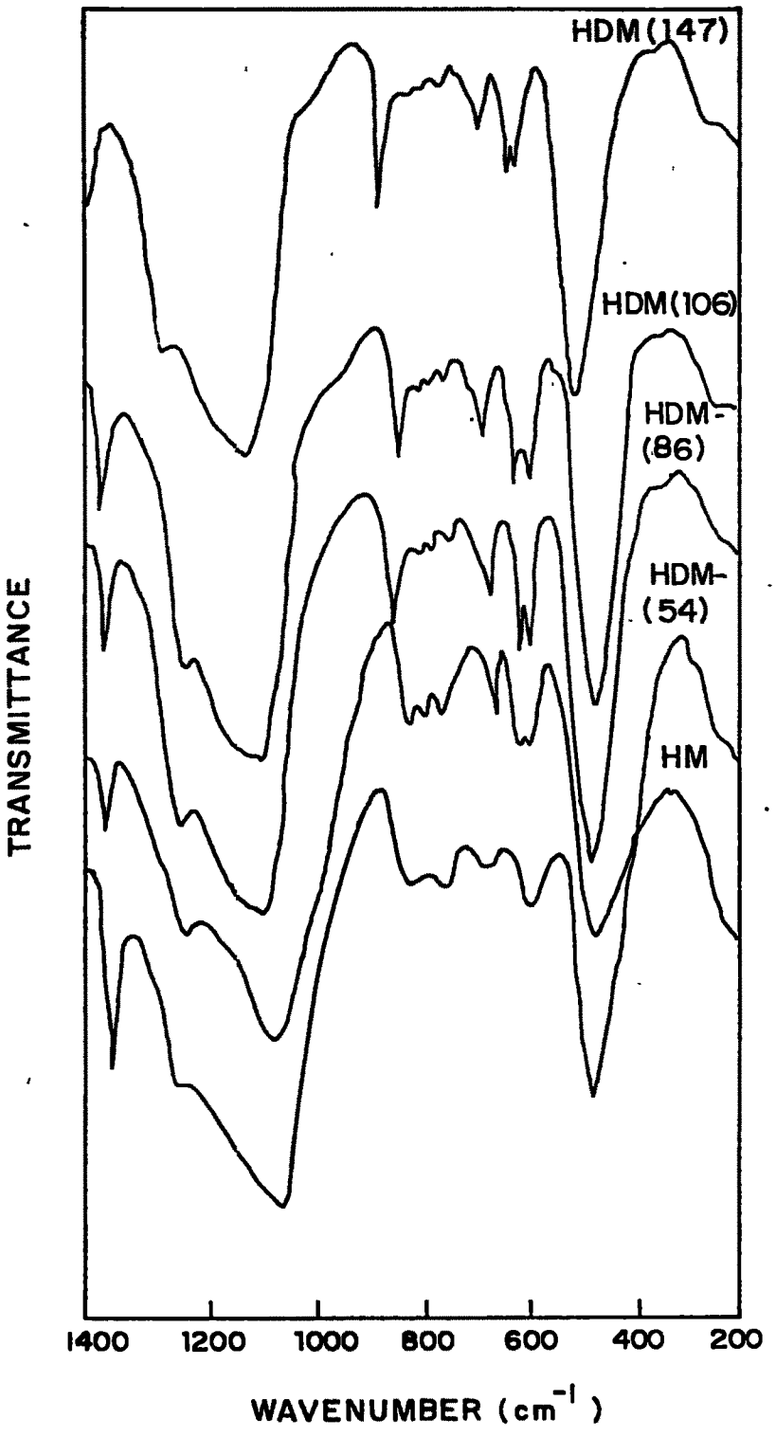

FIG.2.4a-l.r. FRAMEWORK VIBRATION SPECTRA OF HM & DEALUMINATED MORDENITES.

Table 2.5

Framework vibration frequencies for H-mordenite*

(SiO_2/Al_2O_3 = 9.95)

Wave Number (cm^{-1})		Assignment
370	vwsh	Pore opening
448	ms	T-O BEND
555	w	DBL RING
571	w	DBL RING
621	w	-
690	wb	Symmetric stretch
715	wb	Symmetric stretch (Internal)
771	wb	Symmetric stretch
795	wb	Symmetric stretch (External)
1046	s	Asymmetric stretch (Internal)
1180	vwsh	Asymmetric stretch
1216	w	Asymmetric stretch (External)

s = strong, ms = medium strong, m = medium, mw = medium weak, w = weak, vw = very weak, sh = shoulder, b = broad.

* E.M. Flanigen, H. Khatami, H.A. Szymanski, Advances in Chem. Series, 101, 201 (1971).

"isolated" AlO_4^- tetrahedra are in the 800-650 cm^{-1} region. The existing broad 710 cm^{-1} band in mordenite spectra is thus due to framework aluminium and also its intensity varies with the number of AlO_4^- tetrahedra. (3) Formation of Si-O bands[11] with simultaneous removal of Al atoms has been observed in Y zeolite[12,13] or deammoniated NH_4 mordenite.[14] The newly formed T-O bond (820 cm^{-1}) in the symmetrical stretching range in HDM mordenites at sites available due to vacancy by Al between SiO_4 tetrahedral previously linked to AlO_4^- tetrahedra agrees with that reported.[15]

D. Thermal Analysis

The thermoanalytical curves (DTA,TG,DTG) of aluminium deficient mordenites were recorded using NETZSCH STA 409 (FRG) Thermal-analyser under following conditions:

(i)	Sample weight	-	30 mgs
(ii)	Heating rate	-	10^oC/min
(iii)	Sensitivity: (a) DTA	-	0.1 mV
	(b) DTG	-	0.2 mV
	(c) TGA	-	0-25 mgs
(iv)	Atmosphere	-	Flowing air

in the temperature range 25^o to 1000^oC using α -alumina as a reference material. Typical thermograms of HM and HDM-147 samples are shown in Fig.2.4(b) and Fig. 2.4(c) respectively. Fig.2.4(d) shows TGA curves of HDM samples with various SiO_2/Al_2O_3 ratio. It is seen that T_{max} (Temperature corresponding to maximum of

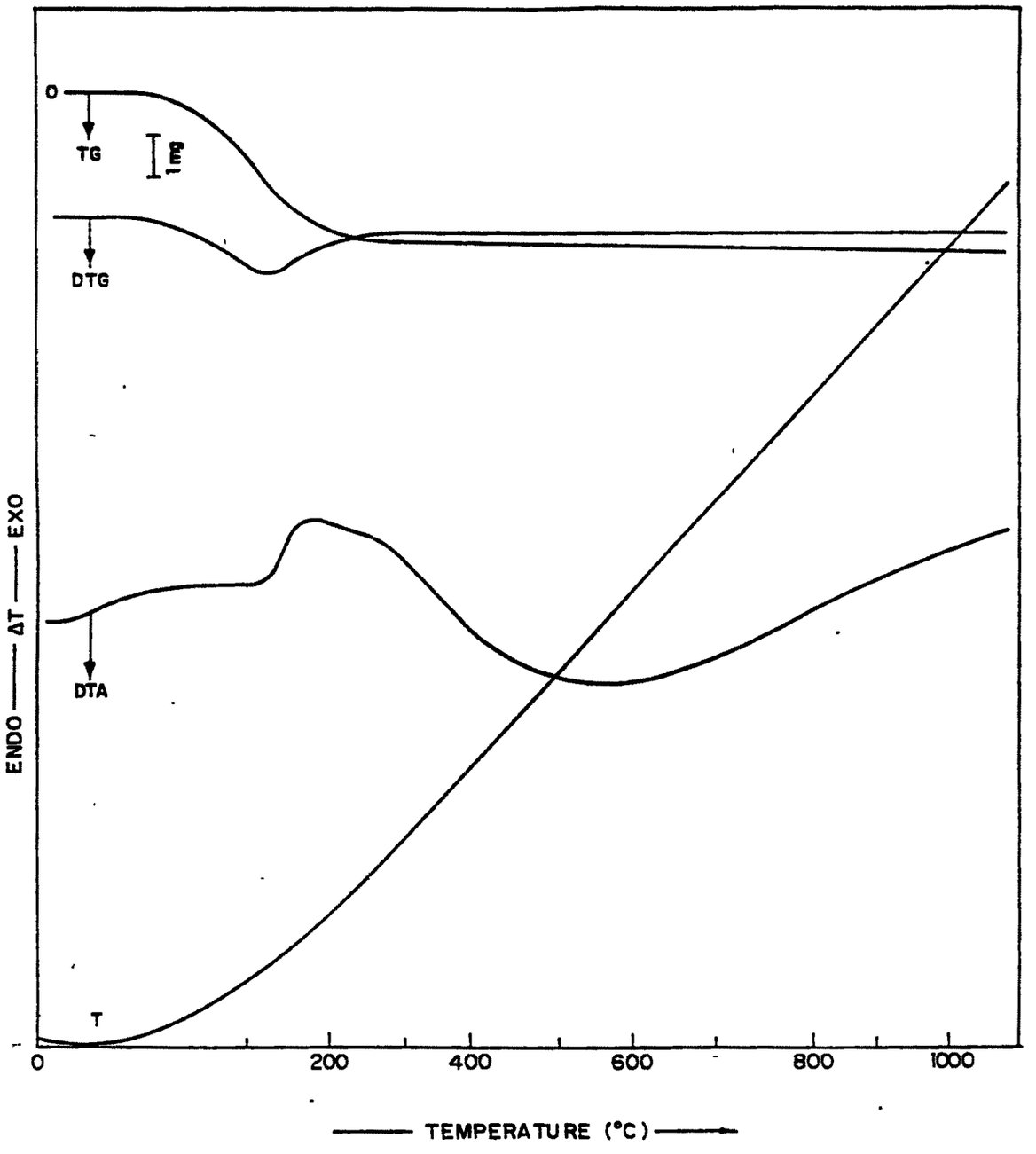

FIG 2·4b: TG, DTG AND DTA THERMOGRAMS OF HMORDENITE ZEOLITE, SiO_2 / Al_2O_3 : 13

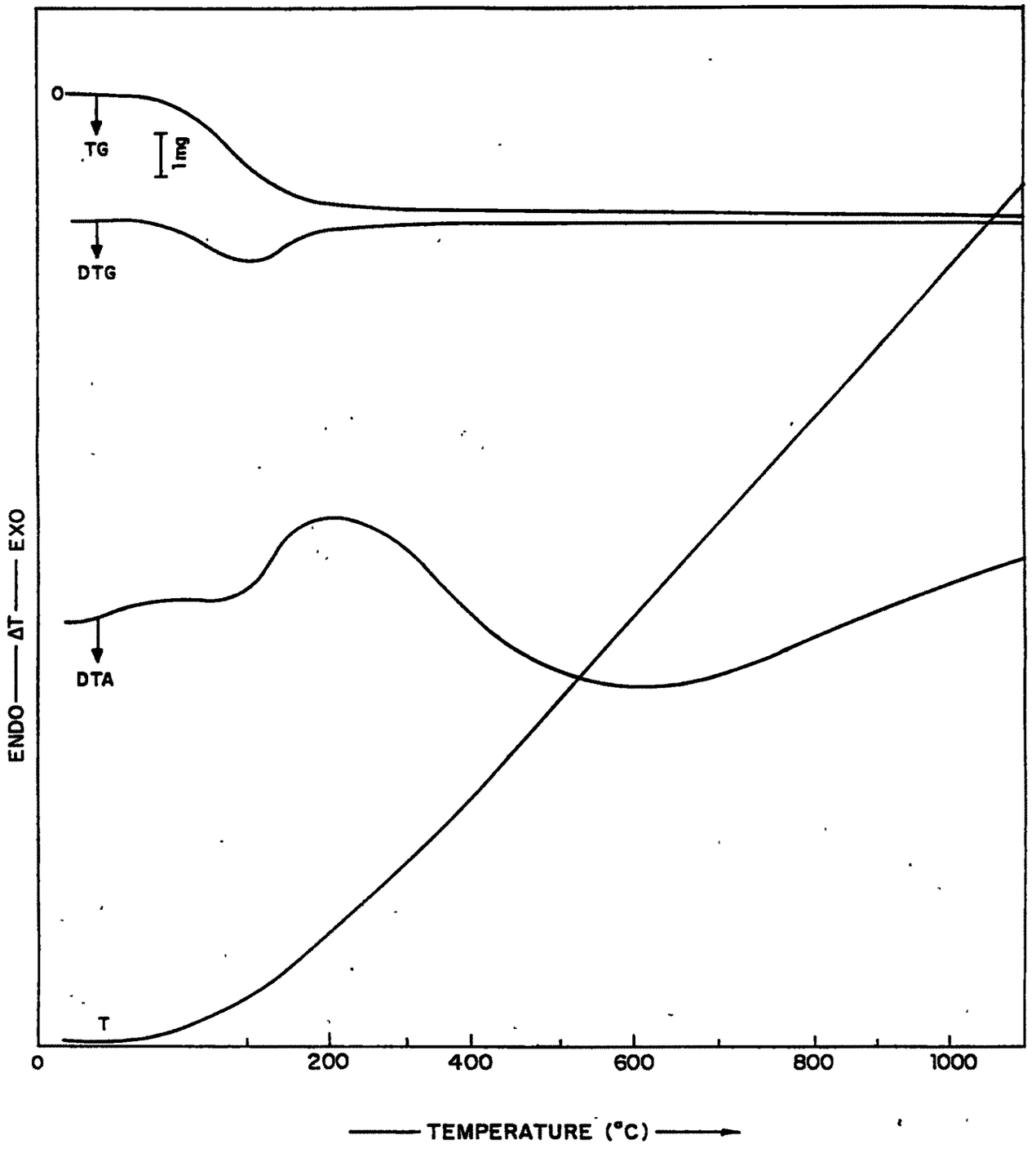

FIG 2·4c : TG , DTG AND DTA THERMOGRAMS OF DEALUMINATED HMORDENITE ZEOLITE , SiO_2/Al_2O_3 : 147

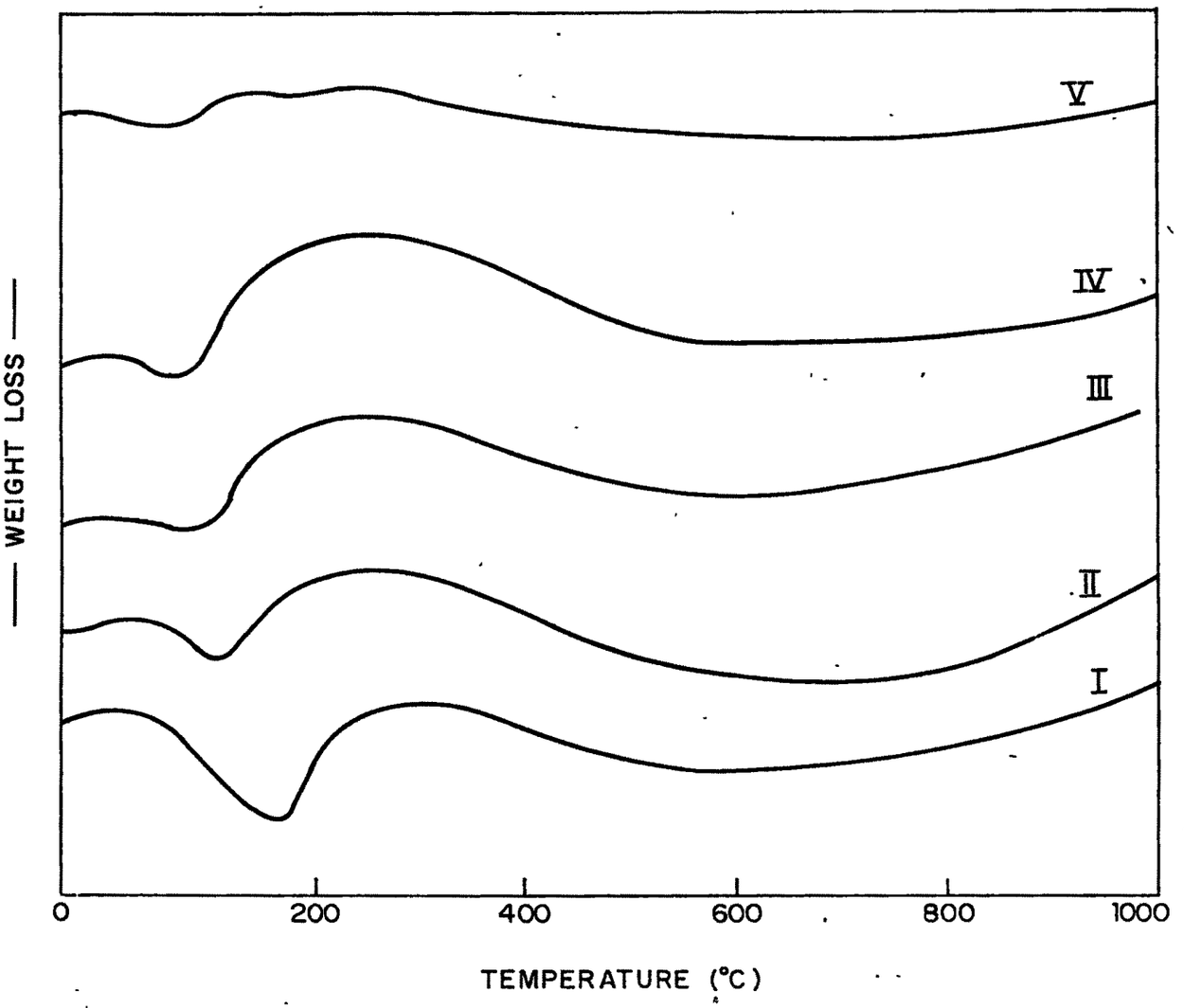

FIG. 2·4d - T. g. a. CURVES OF H-DEALUMINATED MORDENITES WITH VARIOUS SiO_2/Al_2O_3 RATIO.

I - HM , II - HDM (54), III - HDM (86), IV - HDM (106) V - HDM (147).

endotherm) continuously decreases with progressive Al extraction from the zeolite framework. Thus, with the reduction in the number of sodium ion, dehydration of the zeolite becomes faster and occurs at lower temperature, as observed in case of Y-type zeolites.[16] It is also seen that neither of these samples exhibit an exothermic peak up to 1000°C due to structural collapse, indicating high thermal stability.

The TG curves of phosphorus impregnated mordenites (PHM) were recorded on SETARAM PC 92 thermal analyser. For scanning the curves 30-35 mgs sample was used in a platinum crucible, the heating rate being 10° per minute and the temperature range 25° to 1000°C. Assuming that one molecule of water is liberated by the dehydration of two hydroxyl groups, an attempt has been made to calculate the number of surface hydroxyl groups per unit cell from the TGA curves (Fig. 2.4(e)) of the samples in the temperature range 400 to 750°C. The values obtained for the samples impregnated with phosphorus are given in Table 2.6. A reduction in the concentration of hydroxyl groups/u.c. of the impregnated samples indicates that some of the surface hydroxyl groups are eliminated by incorporation of phosphorus, the extent of elimination increasing with increasing amount of impregnating material. These results are further supported by catalytic reactions carried out over the above catalysts.

E. Sorption Measurements

The sorption measurements of water and hydrocarbon vapours was carried out using McBain type quartz spring gravimetric

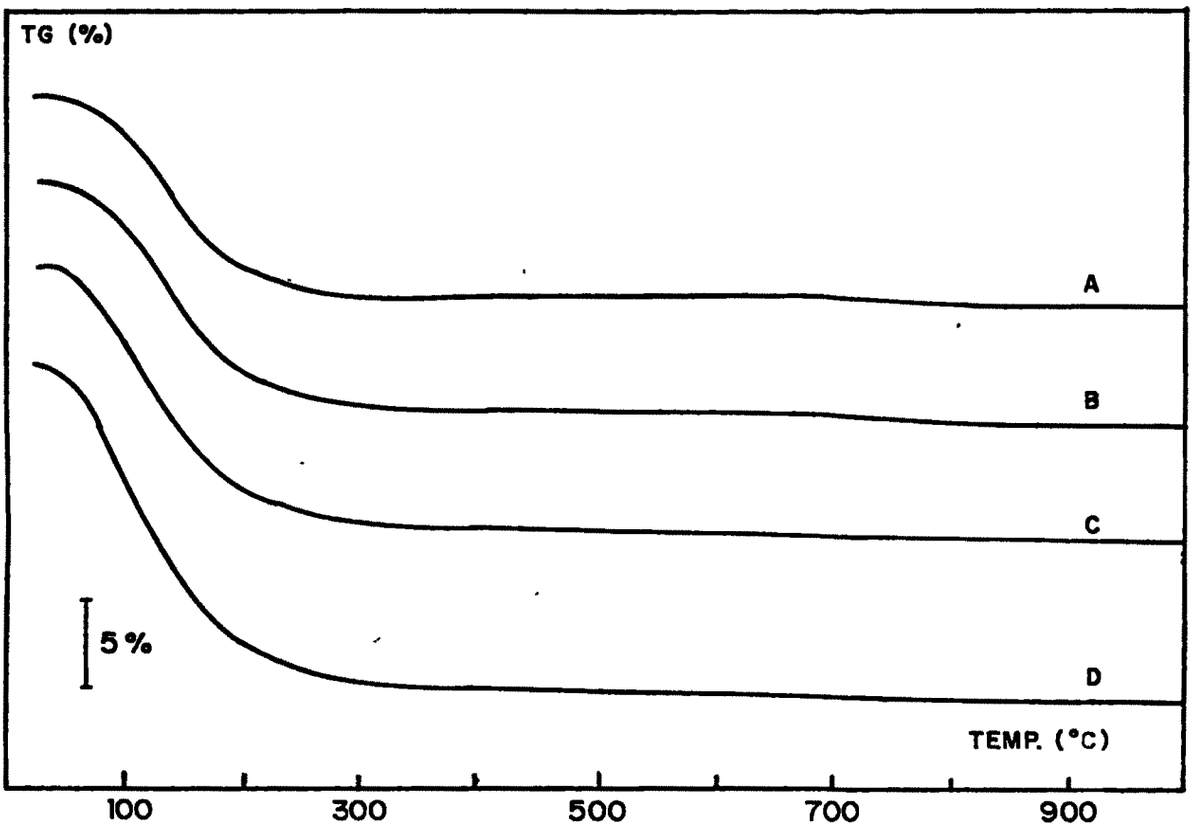

FIG. 2.4e : TG CURVES OF HM AND PHM MORDENITES. A : HM , B : PHM (0·64) C : PHM (3.0), D : PHM (5.0).

Table 2.6

Thermogravimetric data of HM and PHM zeolites

Zeolite*	Percent weight loss			Number of hydroxyl groups per u.c.
	Total	Dehydration up to 400°C	Dehydration 750-400°C	
HM	12.86	11.83	1.03	3.31
P(0.32)HM	11.64	10.66	0.98	3.15
P(0.64)HM	12.10	11.18	0.90	2.92
P(1.0)HM	12.49	11.66	0.83	2.70
P(3.0)HM	13.33	12.66	0.67	2.22
P(5.0)HM	15.16	14.57	0.59	1.98

* Figures in parenthesis indicate percentage phosphorus impregnated.

balance. A schematic diagram of the set-up is illustrated in Fig.2.5. A sensitive calibrated silica spring was used for the measurement of the weight changes.

The zeolite sample (250 mg) was pressed into a pellet and weighed in the aluminium bucket which was attached to the spring. The assembly was evacuated by means of a two stage rotary pump and mercury diffusion pump to a vacuum of about 10^{-6} torr. The sample was activated at 400°C in vacuum to desorb water from zeolite pores. After the zeolite sample had reached a constant weight, the temperature was lowered to the desired value, by immersing the sample tube in a thermostat. To study the equilibrium and rate of adsorption, the sorbate was admitted to the sample and the weight gain was recorded as a function of time at constant temperature and pressure. After recording the equilibrium adsorption, the catalyst was evacuated and heated to 400°C at 10^{-6} torr and used for the next sorption measurement. All sorption measurements were carried out at 25°C and relative pressure P/P_o = 0.5. Critical and kinetic diameters of some sorbate molecules are presented in Table 2.7.

Sorption of water, n-hexane, benzene, cyclohexane and isopropylbenzene (cumene) in the H-form of siliceous mordenite (HM and HDM) are shown in Table 2.8. The adsorption properties of mordenites depend upon the SiO_2/Al_2O_3 ratio, and all samples studied were of large port type. With an increase in SiO_2/Al_2O_3 ratio, the water adsorption decreases, while there is marginal increase[4,17] in the sorption of benzene, cyclohexane, and also cumene, which is comparable to the reported[18] values. A

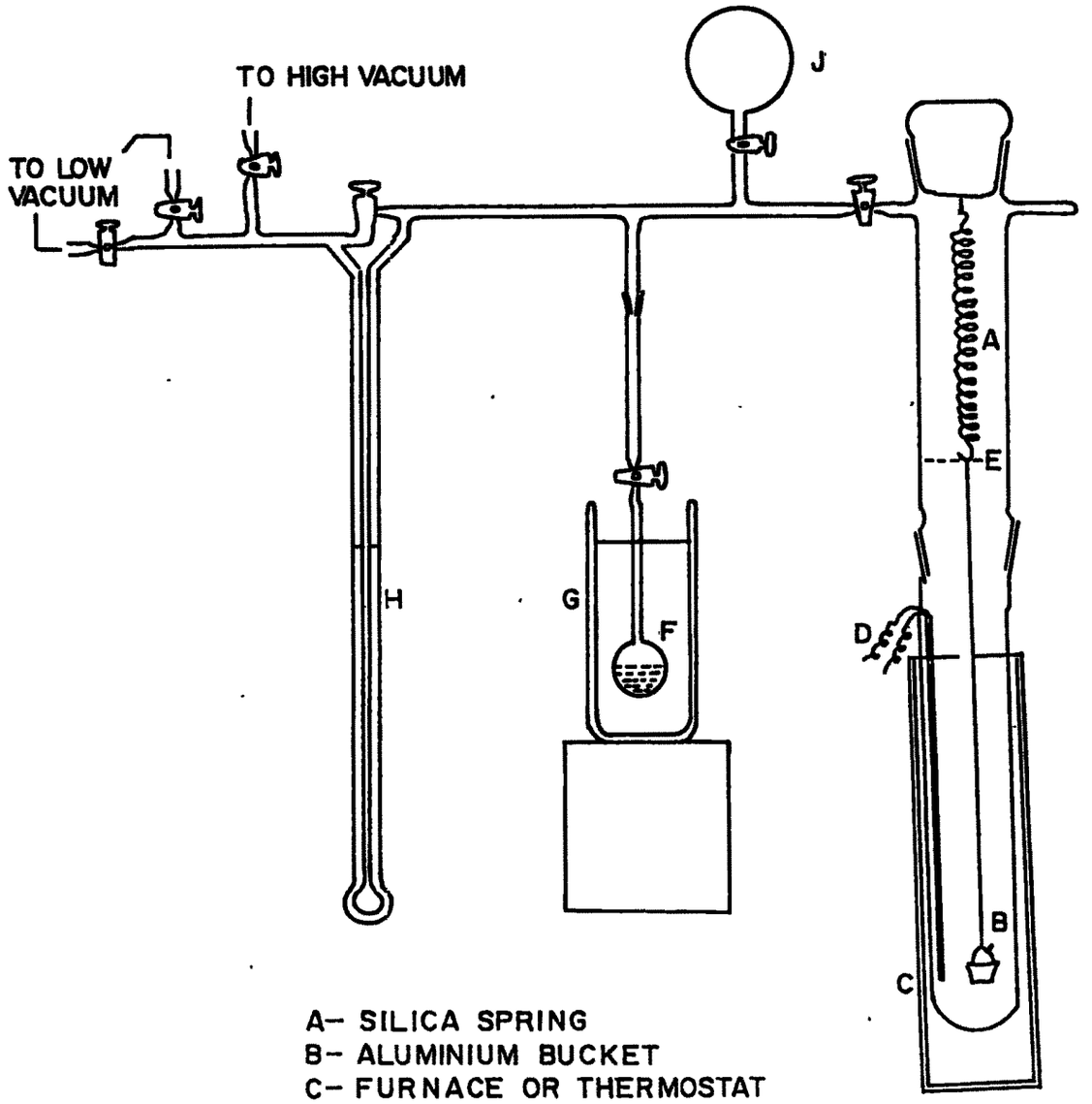

A– SILICA SPRING
B– ALUMINIUM BUCKET
C– FURNACE OR THERMOSTAT
D– THERMOCOUPLE
E– REFERENCE POINT
F– LIQUID BULB
G– THERMOSTAT
H– MANOMETER
J– GAS RESERVOIR

FIG. 2.5 GRAVIMETRIC ADSORPTION UNIT

Table 2.7

Critical and kinetic diameters of some sorbate molecules

Sorbate	Critical[a] diameter nm	Kinetic[b] diameter nm
n-Hexane	0.49	0.43
2-Methyl pentane	0.59	0.53
3-Methyl pentane	-	0.55
2,3-Dimethyl butane	-	0.61
Cyclohexane	0.61	0.60
Benzene	0.67	0.58
n-Heptane	0.45	0.43
Toluene	0.67	0.58
p-Xylene	0.67	0.58
o-Xylene	0.74	0.68
m-Xylene	0.71	0.70
1,3,5-Trimethyl benzene	0.78	0.75
Ammonia, methanol	0.35-0.37[c]	0.38[d]
Water	0.32	0.27[d]
Cyclopropane		0.42

a - Ref. 23 b - Ref. 24

c - Ref. 25 d - Ref. 26

Table 2.8

Sorption of water and hydrocarbon on HM and HDM-mordenites

Sample	SiO_2/Al_2O_3 ratio	Adsorption capacity (Molecules/uc)				
		Water	n-hexane	Benzene	c-hexane	cumene
HM	13.0	35.04	3.18	4.08	2.87	1.40
HDM(54)	54.0	28.55	3.45	4.12	3.14	1.84
HDM(86)	86.0	27.62	3.68	4.15	3.27	1.88
HDM(106)	106.0	25.54	3.62	4.21	3.32	2.23
HDM(147)	147.0	23.50	3.86	4.34	3.38	2.47

continuous increase in n-hexane sorption capacity shows that n-hexane has access to more surface than that accessible to either benzene or c-hexane. This can also be explained on the basis of the molecular size and, hence, could also enter those cavities that occur periodically along the walls of the main adsorption tubes (channels). The amount adsorbed vs time plots for different hydrocarbons are shown in Fig.2.6.

Table 2.9 describes the equilibrium sorption capacities of phosphorus impregnated mordenites. It is seen that a progressive increase in the incorporation of phosphorus decreased the sorption capacity (m.moles/g) since these species are known to penetrate into the channels of the zeolite and blocking the pores partially.[19] This blocking effect is more pronounced with PHM (3.0) and PHM(5.0) samples in which adsorption is very small.

F. Surface Area

The surface area plays an important role in the catalytic activity. The nitrogen sorption was used for the estimation of the surface area and the micropore volume. The sorption was measured on `Accusorb Unit' (Micromeritics Model 2100E) volumetrically at liquid nitrogen temperature (-195°C). The surface occupied by nitrogen molecule was taken to be 16.2 A^2.[20] The surface area was calculated using the BET[21] equation

$$\frac{P}{V(P_o-P)} = \frac{1}{VmC} + \frac{C-1}{VmC} \cdot \frac{P}{P_o}$$

where P = adsorbate pressure

P_o= saturation pressure

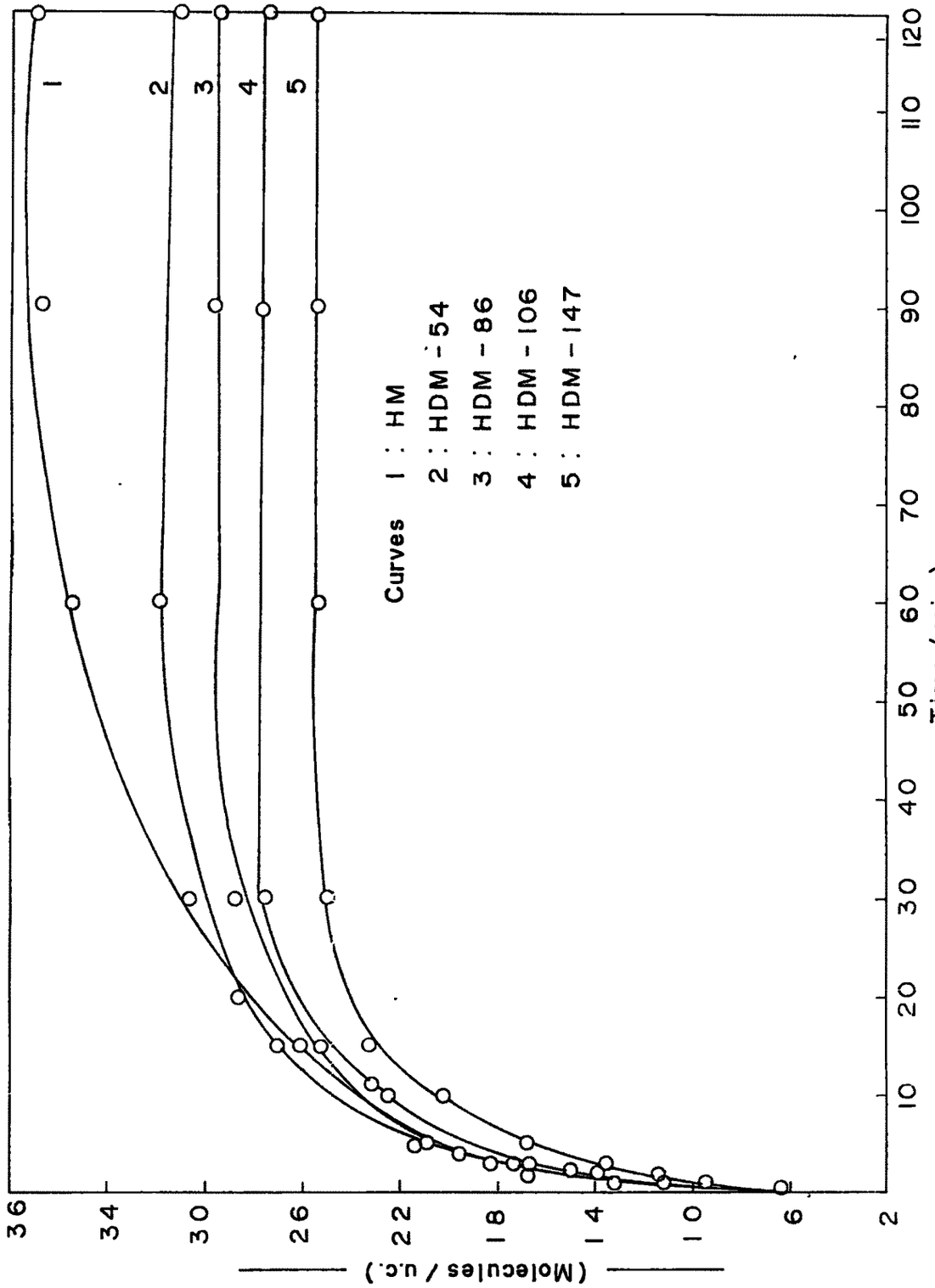

FIG. 2·6a: KINETICS OF WATER SORPTION

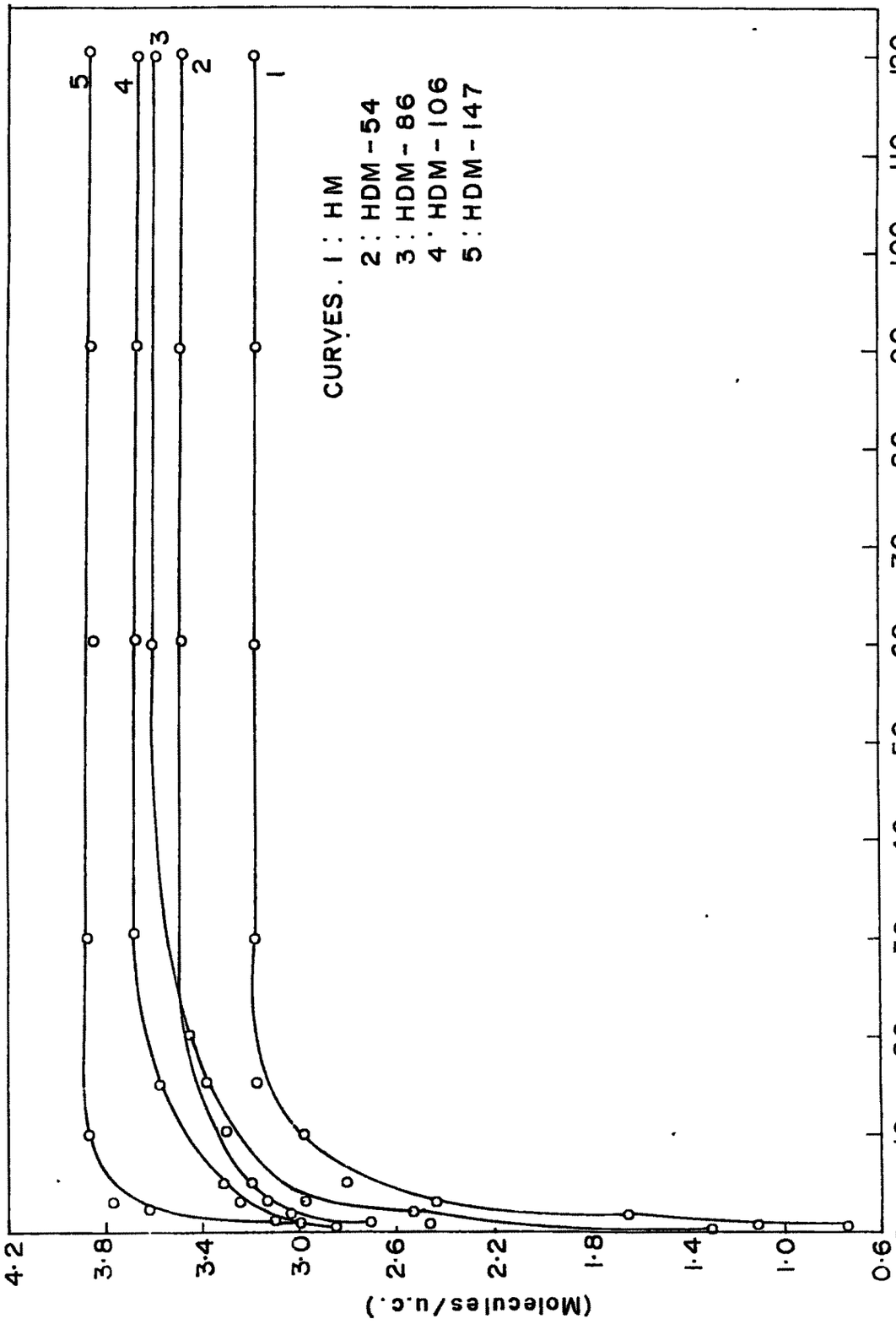

FIG.2·6b: KINETICS OF N-HEXANE SORPTION.

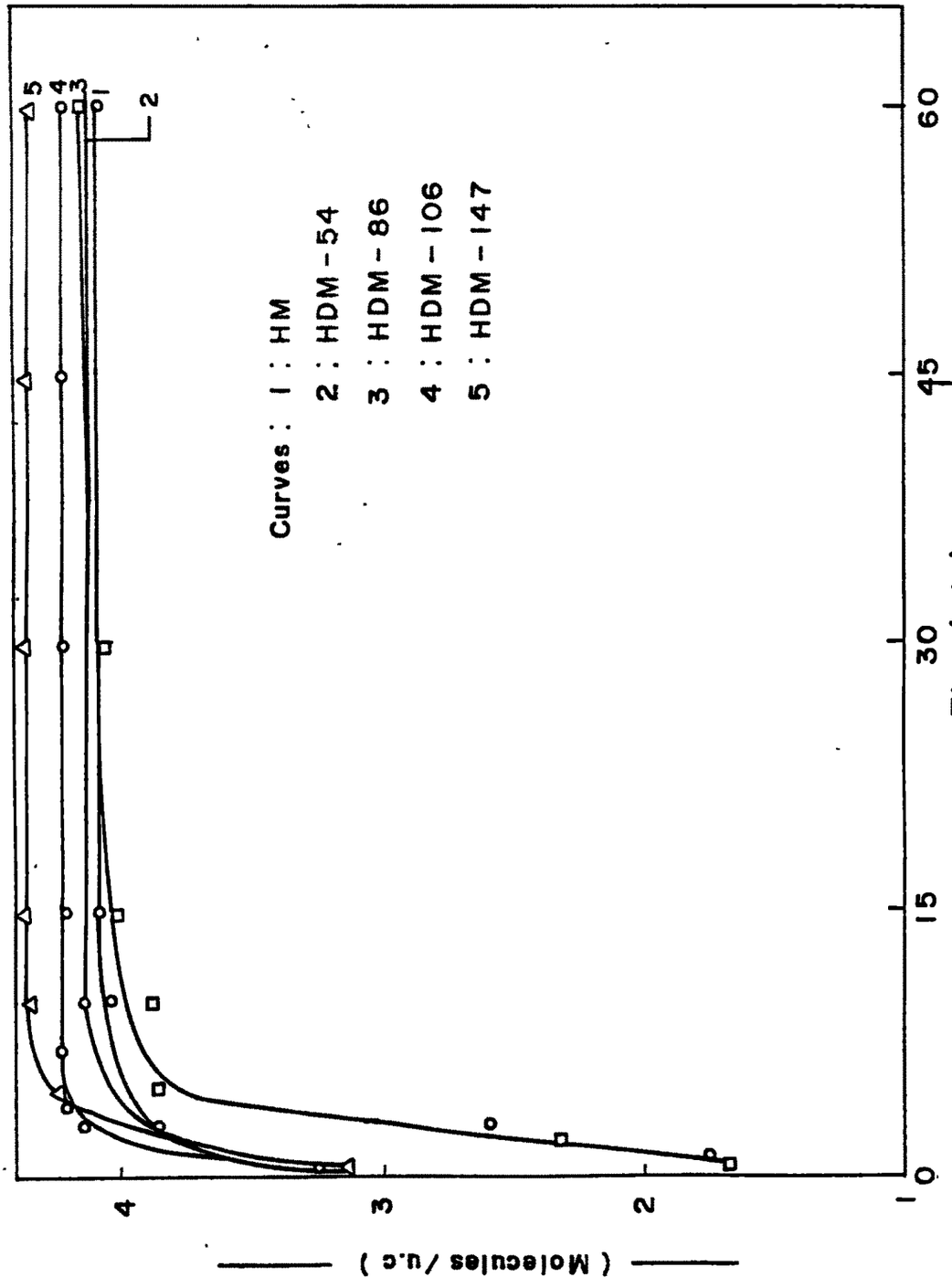

FIG.2·6c:KINETICS OF BENZENE SORPTION

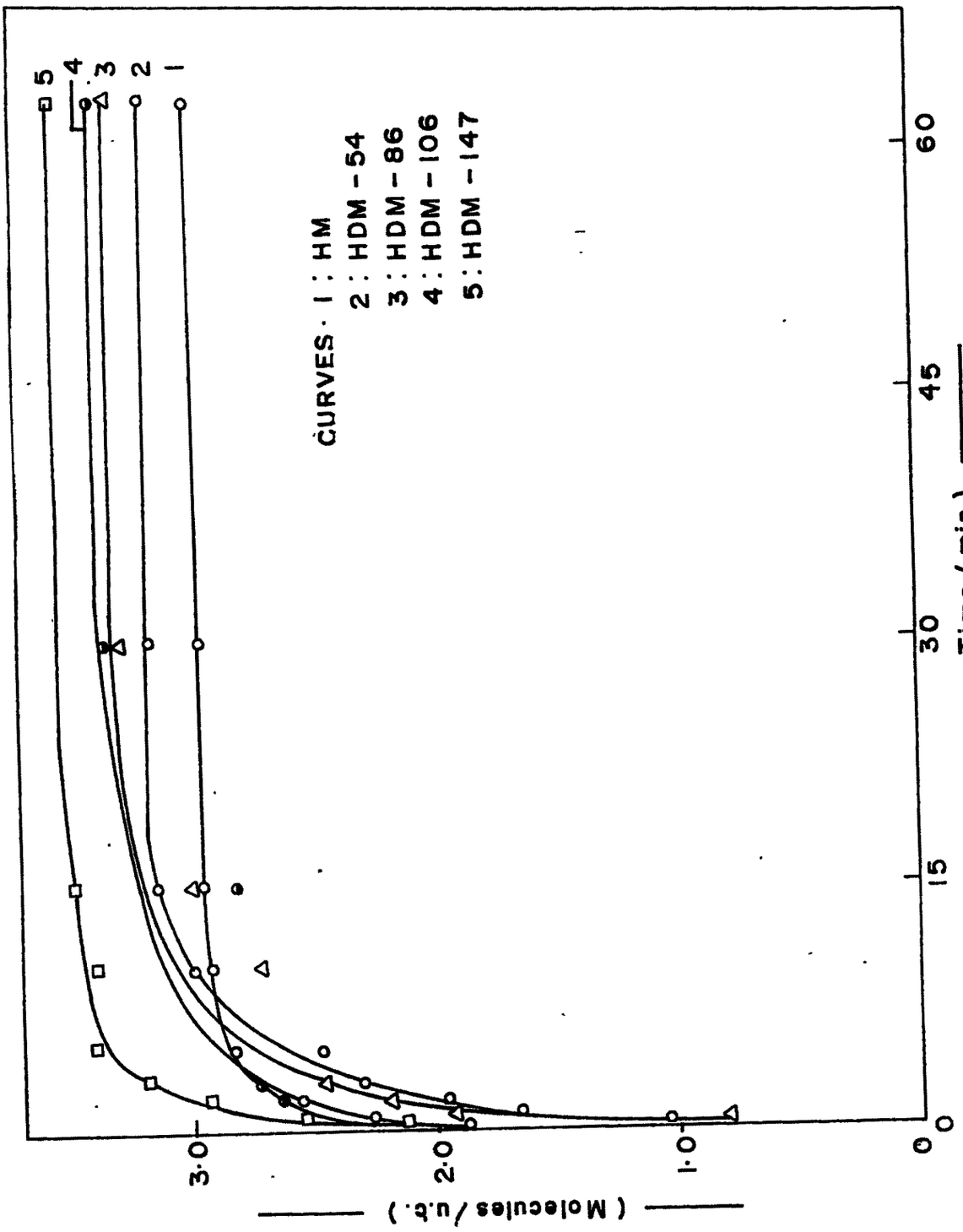

FIG.2·6d:KINETICS OF CYCLOHEXANE SORPTION.

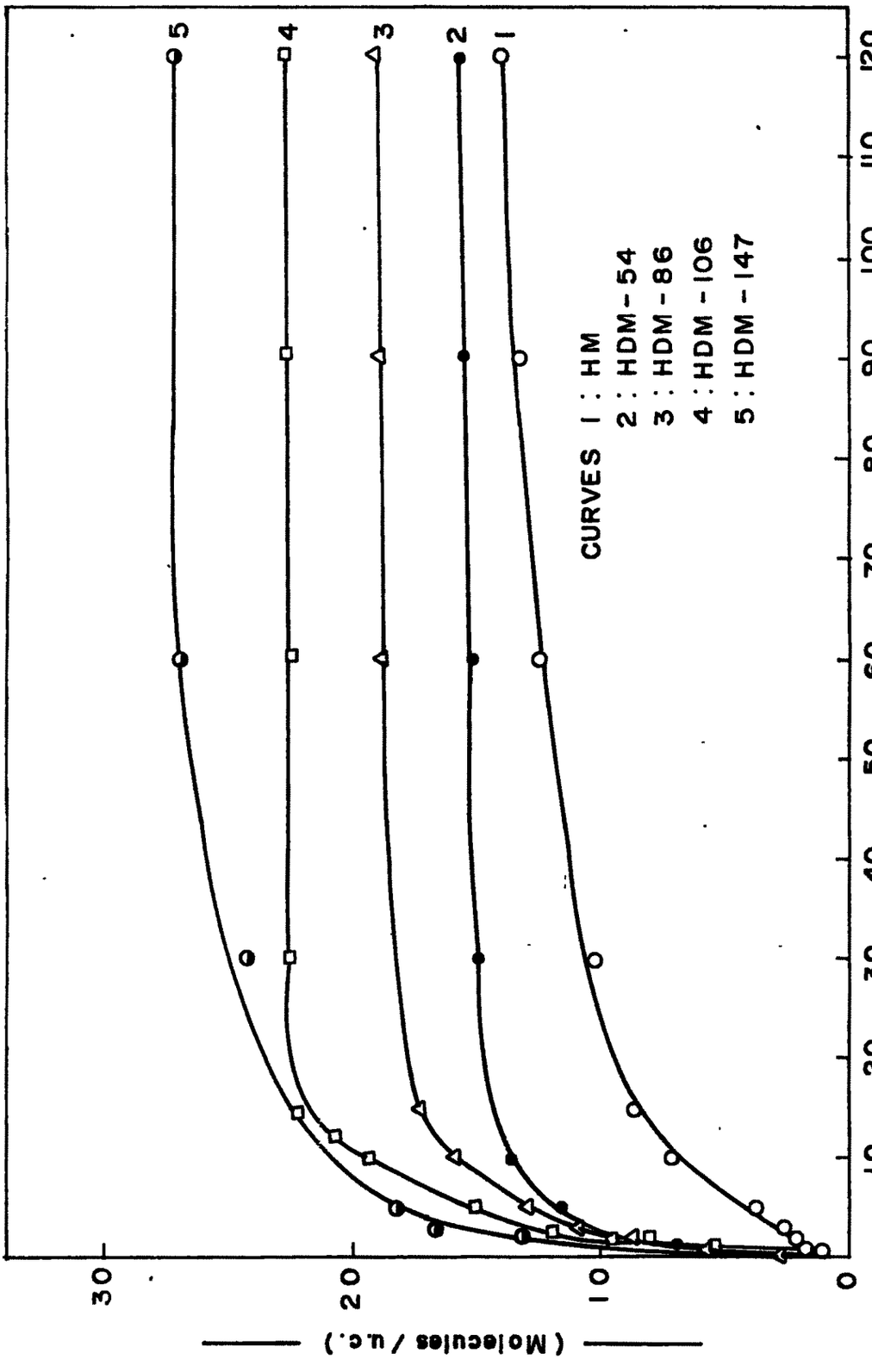

FIG. 2·6e : KINETICS OF CUMENE SORPTION.

Table 2.9

Equilibrium sorption capacities and void volume of HM and PHM zeolites

Zeolite[a]	Sorption (m.moles/g)[b]					Void volume cc/g
	Water	n-hexane	Benzene	cumene	n-propyl-benzene	
HM	9.33	0.85	1.24	0.38	0.49	0.1082
P(0.32)HM	8.79	0.75	1.05	0.44	0.52	0.0962
P(0.64)HM	9.82	0.79	0.93	0.39	0.46	0.1012
P(1.0)HM	10.11	0.61	0.73	0.31	0.36	0.0903
P(3.0)HM	8.5	0.11	0.14	0.06	0.07	0.0135
P(5.0)HM	11.89	0.03	0.09	0.02	0.023	-

a = Figures in parenthesis indicate % phosphorus impregnated.

b = Sorption values at 25°C and P/P_o = 0.5.

Vm= monolayer capacity

C = constant, characteristic of adsorbate-adsorbent interaction.

A typical BET plot for samples (HM & HDM-147) is shown in Fig.2.7. Surface area of the sample is evaluated from the slope of the straight line.

The adsorption isotherms constructed for the samples of different SiO_2/Al_2O_3 ratios are shown in Fig.2.8. The micropore volume which can be derived from type I adsorption isotherm was calculated using Dubinin equation[22]:

$$\log_{10} V_a = \log_{10} V_o - D (\log P/P_o)^2$$

where V_a is the volume adsorbed per unit mass of the adsorbent, V_o is the volume of adsorbed phase or the pore volume, P/P_o is the relative pressure, D is a constant, varying with temperature and the adsorbate-adsorbent interaction. A plot of $\log_{10} V_a$ against $(\log P/P_o)^2$ should, therefore, be a straight line (Figs. 2.9(a) and 2.9(b)). The intercept which is equal to $\log_{10} V_o$ can be obtained and would lead to the micropore volume V_o

$$V_a = V_o (Q_g/Q1)$$

where Q_g and Q1 being the density of the adsorbate in the gas and liquid phase respectively.

The surface area and pore volume of the aluminium-deficient mordenites are listed in Table 2.10. It can be seen that with increase in SiO_2/Al_2O_3 ratio, surface area and micropore volume are increased. The parent mordenite (HM) has relatively low

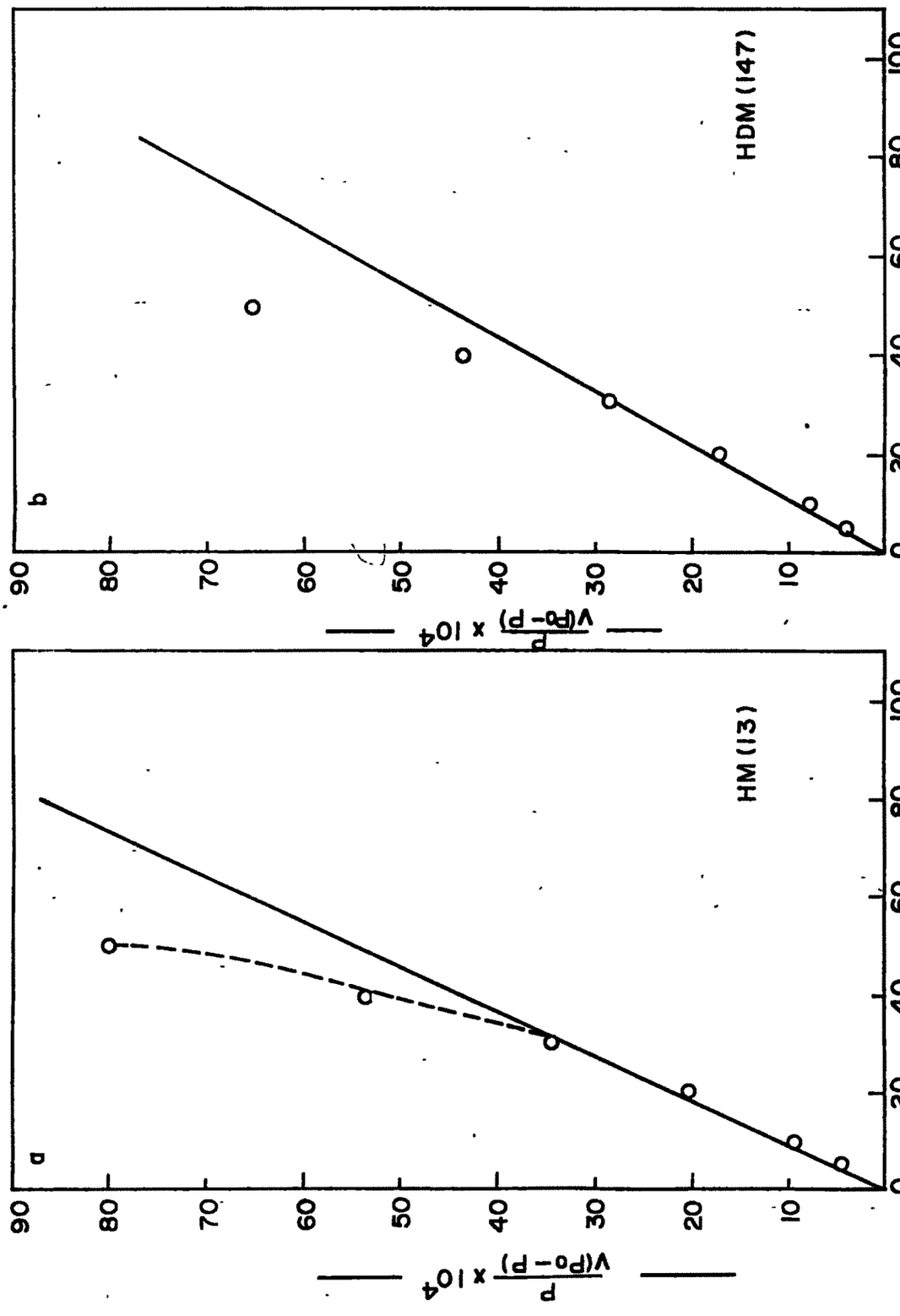

FIG. 2.7 B.E.T PLOTS FOR NITROGEN SORPTION AT −195 °C

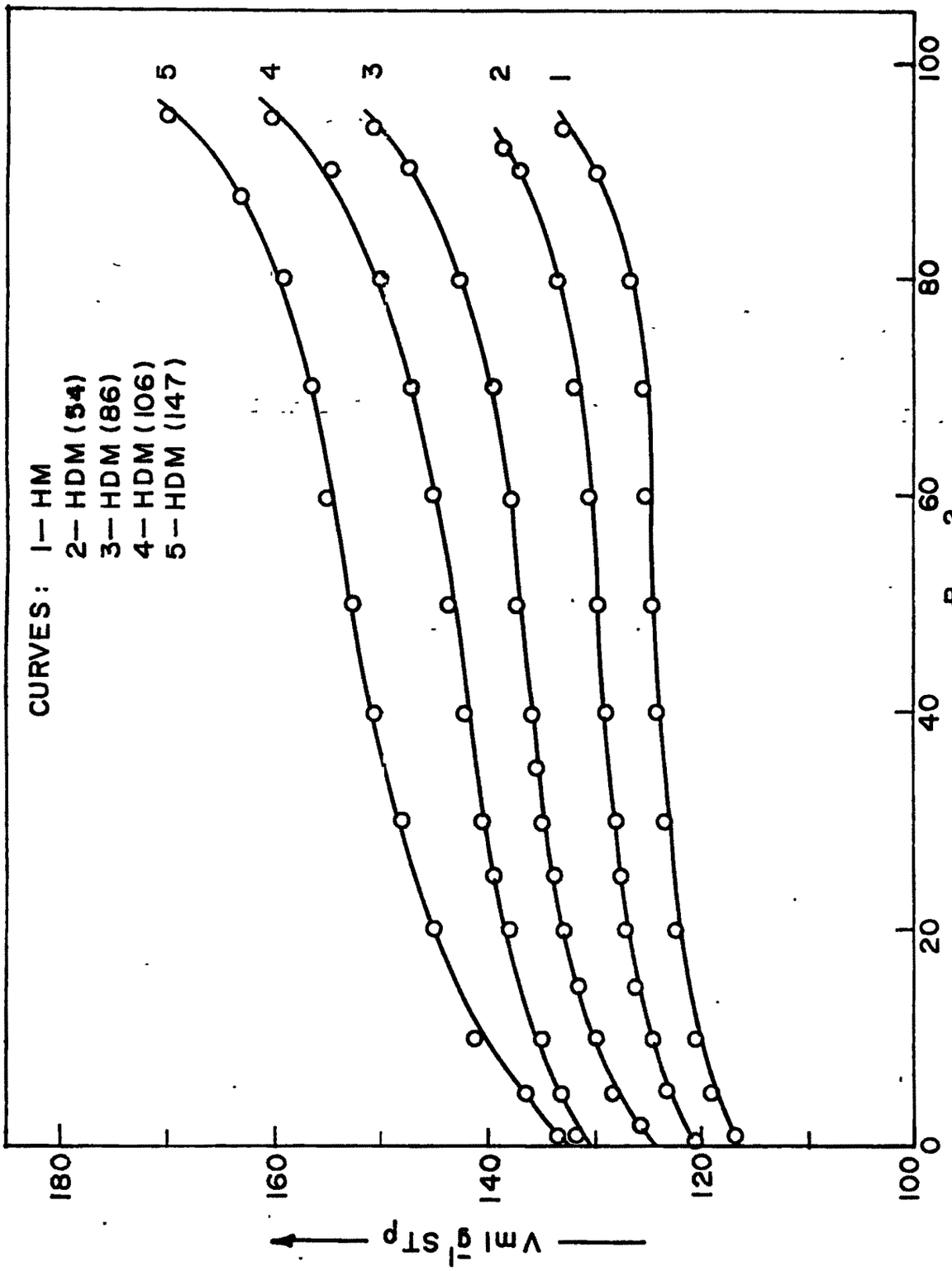

FIG. 2.8 N_2 ADSORPTION ISOTHERM AT —195°C

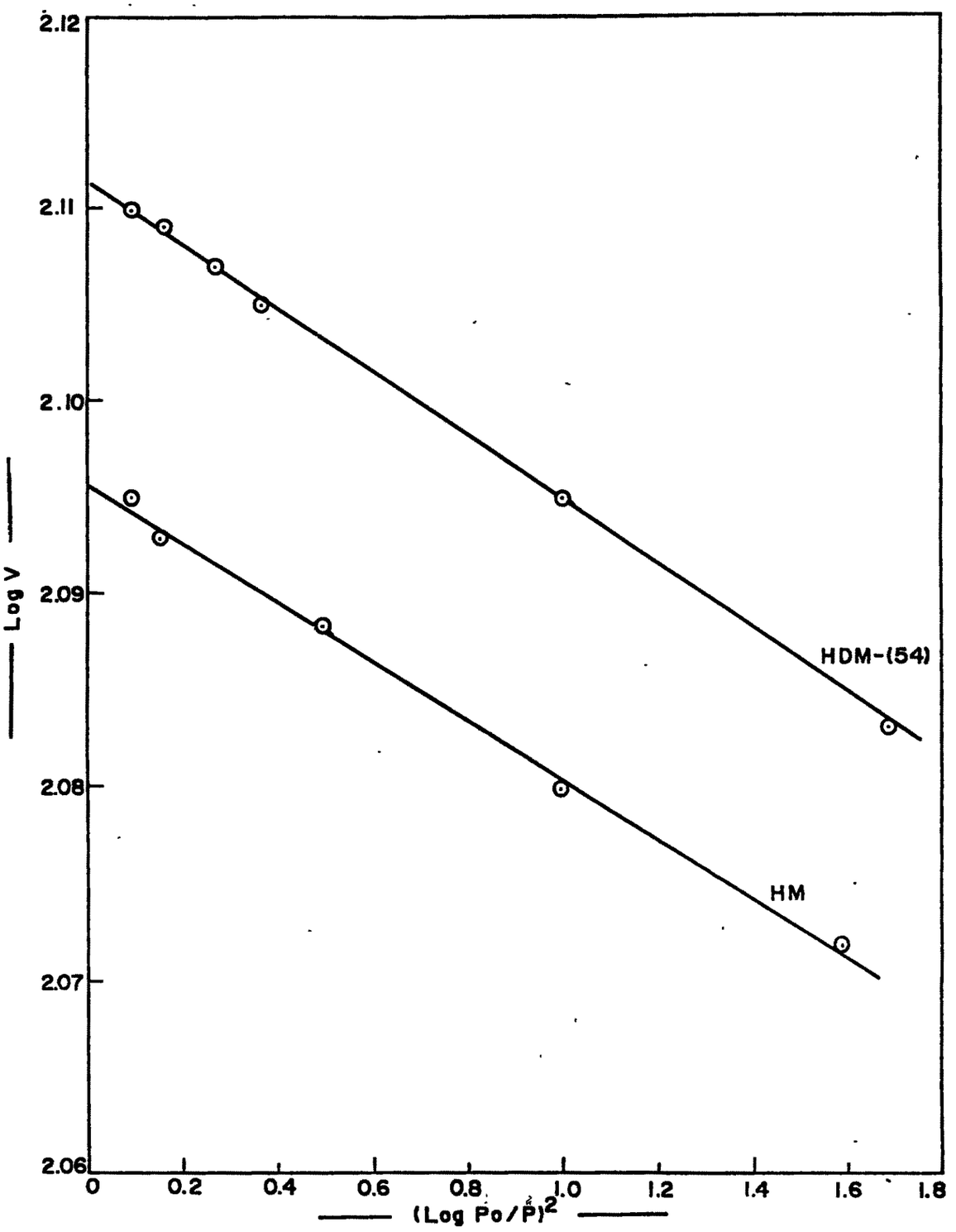

FIG. 2.9a DUBININ PLOTS FOR ADSORPTION OF NITROGEN AT -195°C

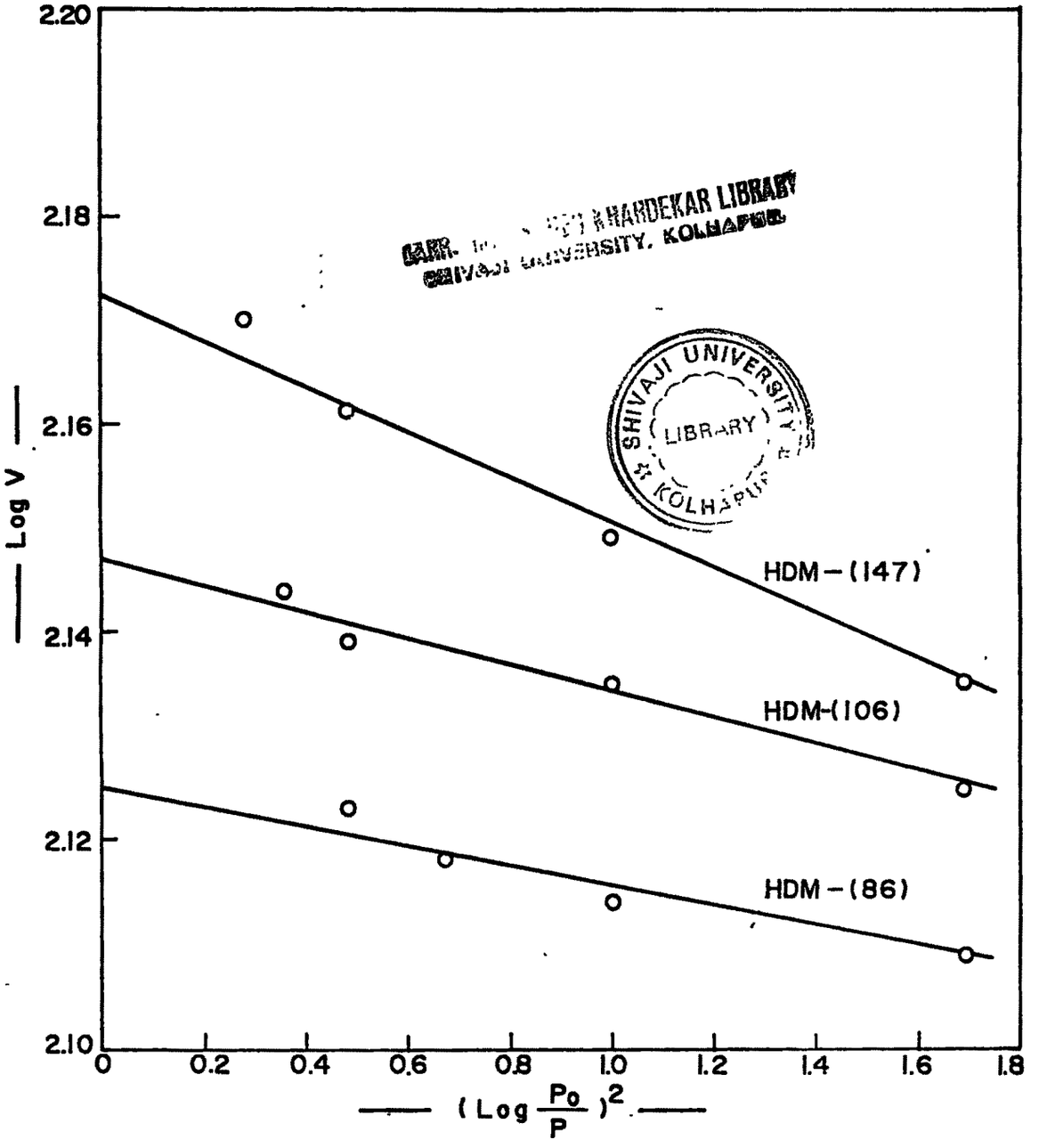

FIG. 2.9 b DUBININ PLOTS FOR ADSORPTION OF NITROGEN AT –195°C

Table 2.10

Surface area and pore volume of mordenite samples

Sample	SiO_2/Al_2O_3 ratio	log V	N_2 saturation capacity mls/g	Dubinin pore volume		BET surface area M^2/g
				cc/g	m.moles/g	
HM	13	2.096	124.59	0.189	5.56	472
HDM-(54)	54	2.115	129.27	0.1964	5.78	490.1
HDM-(86)	86	2.125	133.35	0.2026	5.96	545.2
HDM-(106)	106	2.147	140.3	0.213	6.27	559.4
HDM-(147)	147	2.172	148.76	0.226	6.65	569.2

surface area and low internal zeolite microporosity. This may be due to presence of considerable amorphous material blocking or filling the micropores. The effect of this amorphous material is reflected in the hydrocarbon selectivity in alkylation (Table 3.6). The low ratio of IPB/nPB suggest that there is amorphous material in the pore channel which sterically restricts the formation of the more bulky IPB. Once the non-crystalline material is removed by acid extraction, IPB/nPB ratio is increased. Further acid treatments increased in micropore volume and surface area in agreement with the findings of Meyers et al.[27] A decrease in pore volume is also observed (Table 2.9) when phosphorus is incorporated in the mordenite. It has been suggested that compounds of modifier species occupy portion in the channels thus effectively reducing their volume.[28]

G. Characterization of acid sites

The acidity in the zeolite is believed to be the result of isomorphous substitution of trivalent aluminium for tetravalent silicon in the framework. Such substitution creates a negative charge on the aluminium atom which is neutralised by the presence of a cation or a proton. In the latter case, a Brönsted acid site is created. Lewis sites which can be the charge compensating cations or trigonal aluminium atoms at oxygen deficient sites or at cation positions are also present in zeolites.[29,30]

The active centres for most of the zeolite based organic reactions are Brönsted acid sites and their number and strength

depend upon several factors like type of zeolite and its Si/Al ratio, nature of aluminium distribution in the zeolite and their location.[29-31]

Many techniques have been used for the characterization of the acid sites namely infrared spectroscopy,[32,33] microcalorimetry,[34] electron spin resonance and temperature programmed desorption.[27,35-38]

TPD of NH_3 has been used in the present study to characterise and evaluate acid sites in dealuminated mordenites. The experimental set-up is shown in Fig.2.10. 0.4 gm of the zeolite sample (HM or HDM, 10-20 mesh) was taken in a microreactor. It was initially heated to 400°C at a rate of 10°C min^{-1} in a flow of pure and dry nitrogen and then coupled to sorptiometer for evacuation. It was activated at 400°C for 2 hours and cooled to 150°C. A calibrated volume of NH_3 (RCF, 99.5%) was admitted to the sample which was further allowed to cool to 25°C. The equilibrium adsorption of NH_3 was determined at 25°C and 200 mm pressure. The loosely bound ammonia was evacuated at the same temperature. Equilibrium adsorption was once again determined at the same temperature and pressure. The difference between the amounts adsorbed during the first and second determinations was taken as the chemisorbed ammonia.

The microreactor was then coupled to the on-line GC after allowing sufficient time to stabilise the GC. The sample was heated at a linear rate of 10°C min^{-1} with carrier gas flow rate of 60 ml min^{-1} and the TPD spectrum was obtained with percentage

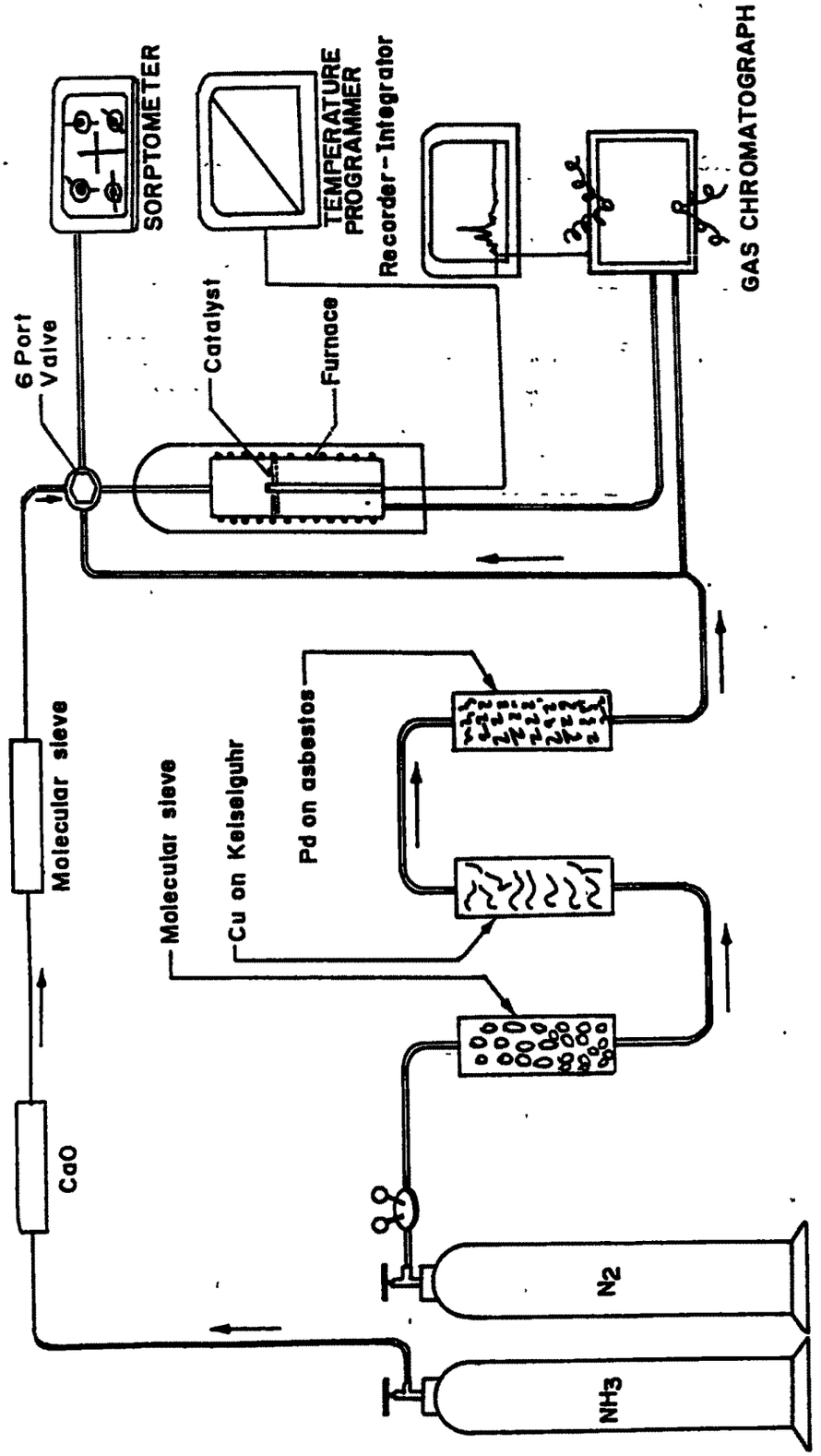

FIG. 2.10 SCHEMATIC DIAGRAM OF TPD UNIT

area of the peaks. The total volume chemisorbed at 25°C obtained by volumetric measurements and the area% of the desorption peaks are then used to calculate the acid strength distribution in the sample.

Results and Discussion

The temperature programmed desorption spectra of ammonia and the acidic properties of HM and HDM zeolites are shown in Fig.2.11 and Table 2.11 respectively. The profiles indicate only peaks having two maxima unlike in HZSM-5 zeolites.[35] The first peak corresponds to weak+medium and second one is for stronger acid sites. First peak ranging from 107 to 135°C and second one around 530°C. There is a variation in the peak maximum for the stronger peak corresponding to degree of dealumination. Lowest being for HDM-147 at 433°C and highest for that of HM at 546°C. The differences are due to the number of acid centres associated with the parent zeolite. Accordingly the calculated values of the acid sites/u.c. of zeolite are given in Table 2.11 corresponding to both weak and strong acidic centres. Thus dealumination reduces both weak and stronger acidic sites. The catalytic studies indicate that (Presented in Chapter 3, Table 3.6) almost all catalysts show complete conversion of isopropanol (% propylene conversion varied from about 100 to 91) but the higher aluminium containing sample deactivated faster. Catalytic activity is highest around 210°C which is corresponding to weak+medium sites rather than stronger sites. At higher temperature non-selective products formation is observed due to

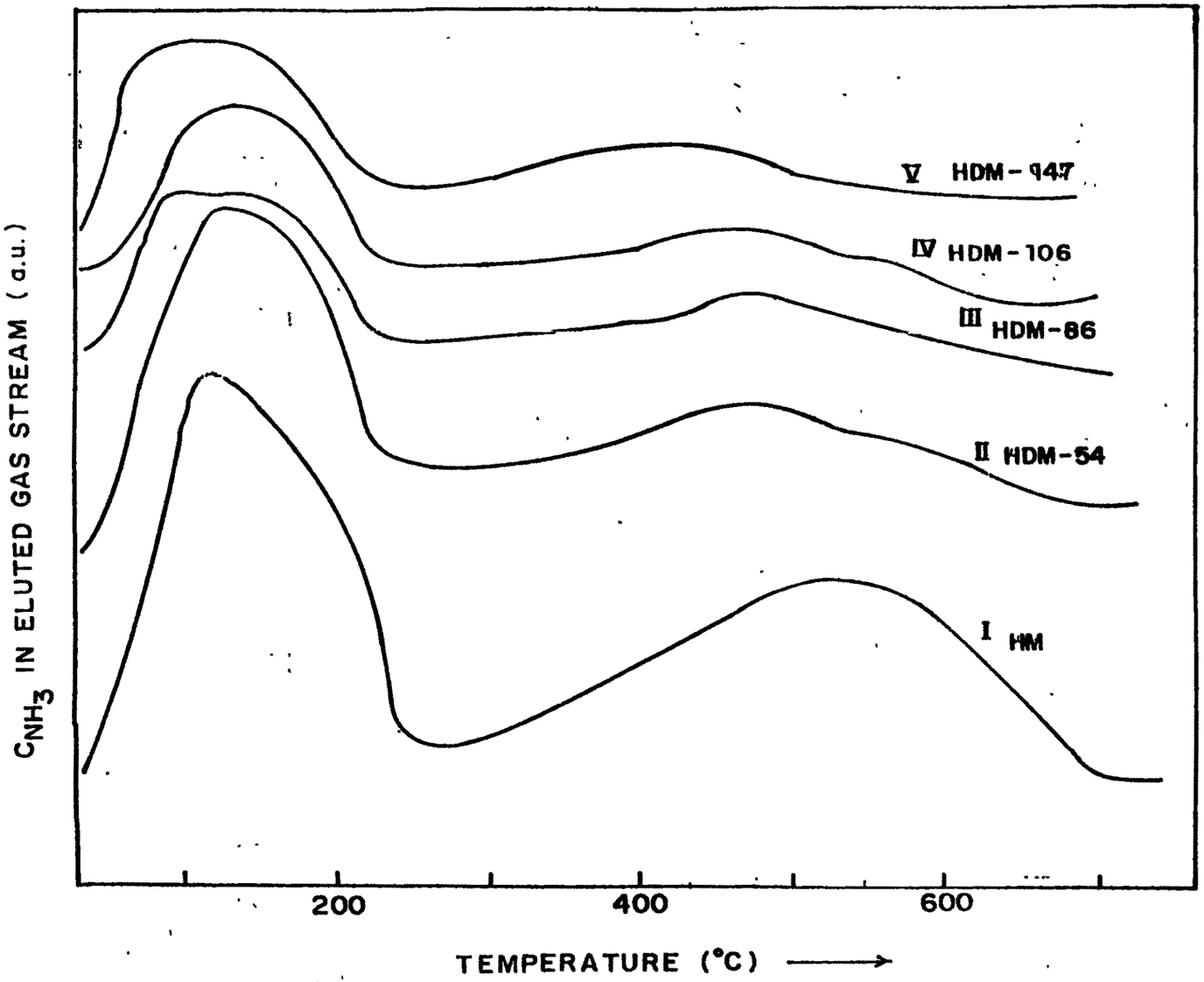

FIG. 2·11 - TPD CHROMATOGRAMS OF HYDROGEN MORDENITE AND DEALUMINATED MORDENITES.

Table 2.11

The concentration of surface acid sites

Sample	SiO_2/Al_2O_3	Al/u.c.	T_{max} (Strong sites) ^oC	Acid sites/u.c.		
				Weak+Medium	Strong	Total
HM	13.0	6.44	546	9.6	5.5	15.1
HDM-(54)	54.0	1.71	488	4.0	1.4	5.4
HDM-(86)	86.0	1.09	480	3.2	1.0	4.2
HDM-(106)	106.0	0.89	470	2.8	0.65	3.45
HDM-(147)	147.0	0.64	433	3.0	0.35	3.35

stronger acid sites leading to cracking. Thus the lowest aluminium containing mordenite shows stable activity which is mainly attributed to lower number of stronger acid sites.

H. XPS of dealuminated mordenites

In the present study, attempt has been made to find 'Al' concentration in the external layer of acid leached mordenites by using highly surface sensitive XPS technique.

The XPS measurements were performed with a XPS spectrometer (Vacuum Generator ESCA 3MK II) MgKα X-ray source ($h\nu$ = 1253.6 eV) was used. The slit width was 4 mm and analyzer energy was 50 eV. The surface Si/Al atomic ratio for zeolites was calculated by employing the relation,[39,40]

$$Si/Al = \frac{I_{si}}{I_{Al}} \times \frac{\sigma(i)Al}{\sigma(I)Si} \times \frac{(E_k si)^{1/2}}{E_k Al)^{1/2}}$$

where

I_{si} and I_{Al} = Intensity

$\sigma(i)Si$ and $\sigma(i)Al$ = Photoionization cross section

$E_k Si$ and $E_k Al$ = Kinetic energy of Si and Al respectively.

The XPS parameters of the dealuminated mordenites are summarised in Table 2.12. A binding energy of 103.3 eV for the Si_{2p} level was used as internal standard for all samples. The binding energy (BE) and FWHM (Full width at half maximum) values of O_{1s}, Al_{2p} and Si_{2p} determined from the spectra (Fig.2.12) are given in Table 2.12. It is seen from Table 2.13 that the aluminium concentration of HM was less than the bulk aluminium

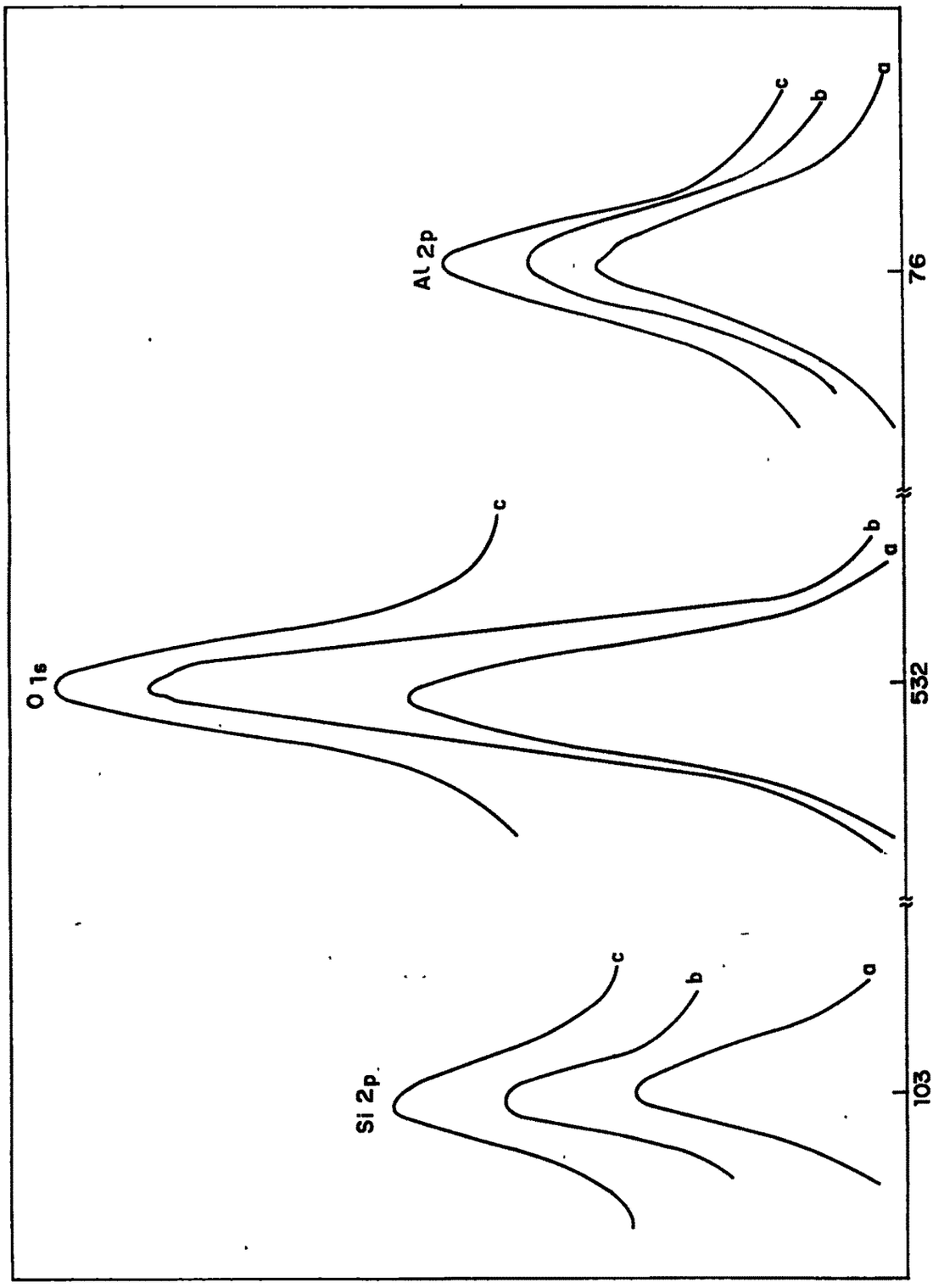

FIG.2.12 : XPS SPECTRA OF H MORDENITES. CURVES a) HM b) HDM-I c) HDM-IV

Table 2.12

XPS parameters of dealuminated mordenites*

Sample	Si_{2p}		O_{1s}		Al_{2p}	
	B.E.	FWHM	B.E.	FWHM	B.E.	FWHM
HM	103.5	3.0	532.8	3.6	75.4	3.48
HDM-(54)	103.6	2.76	531.0	3.3	75.6	3.36
HDM-(86)	103.6	3.0	535.0	3.36	76.6	3.84
HDM-(106)	103.8	3.0	533.3	3.48	75.6	3.60
HDM-(147)	103.5	2.88	533.0	3.0	75.5	3.6

* B.E. and FWHM in eV

Table 2.13

XPS data on treated mordenites

Sample	$(Si/Al)_{bulk}$	$(Si/Al)^a$	$(Si/Al)^b$
HM	6.7	19.89	20.0
HDM-(54)	27.0	33.72	34.43
HDM-(86)	43.0	99.05	101.6
HDM-(106)	53.0	104.94	107.1
HDM-(147)	73.5	162.54	162.0

a : Calculated following the method described in Ref.39.

b : Calculated following the method described in Ref.40.

concentration. On dealumination, the aluminium concentration in the external layer decreased considerably. The finding is in agreement with the work reported.[41] Both BE and FWHM for Al_{2p} in the samples are constant within experimental error, which implied that the same species of Al must be present in all the samples. (The peak intensities for Al_{2p} increases with increasing dealumination. This may be due to some aluminium species sticking out from channel upon acid leaching.)

I. Nuclear Magnetic Resonance

The loss of aluminium from the mordenite lattice on acid treatments was confirmed by ^{29}Si and ^{27}Al NMR. The solid state ^{29}Si and ^{27}Al MAS NMR spectra were recorded at ambient temperature using a Bruker MSL-300 FT-NMR spectrometer. 3000 FID's were accumulated before FT to get spectra with good S/N ratio. A 5S delay time was used for 90^{o} pulse. TMS was used as the external reference for the ^{29}Si signal, while an aqueous solution of $AlCl_3$ provided the reference peak for ^{27}Al. MAS was kept at 3.5 KHz for all samples.

Results and Discussion

^{29}Si MAS NMR: ^{29}Si MAS NMR of samples with SiO_2/Al_2O_3 ratio 13,86 and 147 are shown in Fig.2.13A. The spectrum of sample HM(13) shows two distinct peaks at -105 and -112 ppm which are assigned to Si(1Al) and Si(0Al) unit respectively. In addition to that peak at -105 ppm arises not only from Si(1Al) but also arise from Si(OH) group.[42] After dealuminating with HCl (Sample HDM-86) the part of aluminium has been removed from framework mordenite

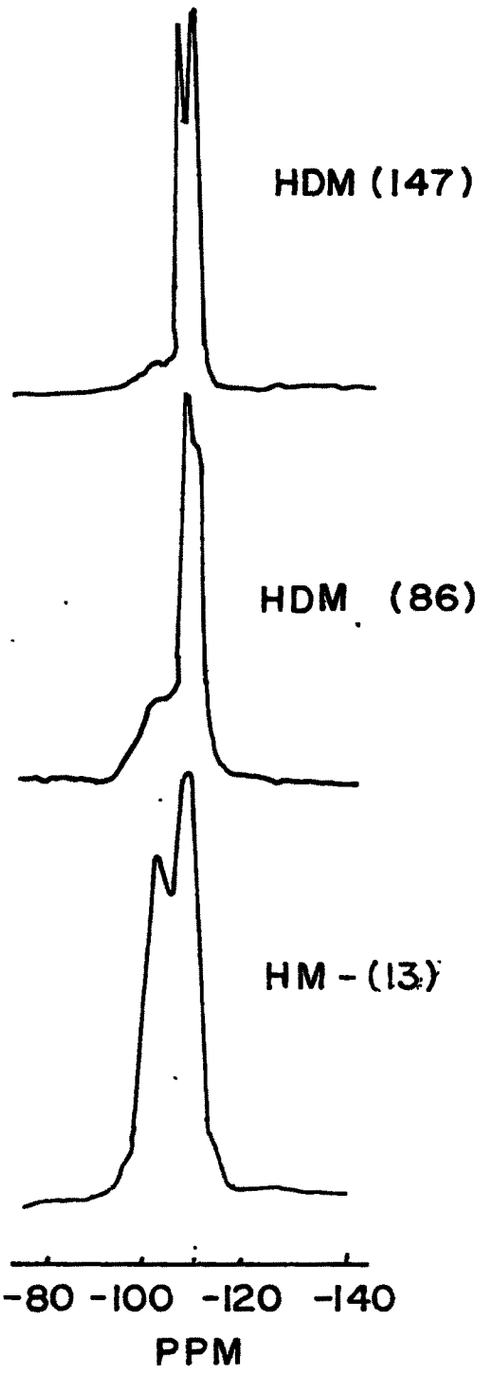

FIG. 2-13a- ^{29}Si NMR SPECTRUM OF HM AND DEALUMINATED MORDENITES

structure which has been clearly seen from the spectrum where Si(1Al) peak at -105 ppm decreased which is direct evidence of removal of aluminium from framework without disturbing framework structure as is further confirmed by XRD (Fig.2.2). Further dealumination leads to complete disappearance of peak at -105 ppm and fine crystallographic sites arises from the highly dealuminated sample with SiO_2/Al_2O_3 ratio 147 (Peak at -112 ppm split into two). Other workers have observed similar results for mordenite and its dealuminated products.[27,42-44]

^{27}Al MAS NMR: The spectrum of ^{27}Al MAS NMR of HM(13) and HDM(147) samples are shown in Fig.2.13B. It is seen from spectrum A that there are two different environments of aluminium present in the sample. The peak at 55 ppm has been assigned to aluminium in the tetrahedral coordination present in the framework whereas peak near 0 ppm has been assigned to aluminium in octahedral (non-framework) environment.[27,45] After dealumination aluminium from the framework can be removed as an octahedral soluble species. This is further confirmed by the decrease in peak intensity at 0 ppm of sample with SiO_2/Al_2O_3 ratio 147 shown in spectrum B.

J. Scanning Electron Microscopy (SEM)

The morphology of the zeolite crystals was studied by SEM (Sterioscan Model 150, Cambridge, UK). The sample was dusted on aluminium pegs and coated with an Au-Pd evaporated film. The SEM photographs of mordenites with varying SiO_2/Al_2O_3 ratio are shown in Fig.2.14A. Upon modification the observations are as below:

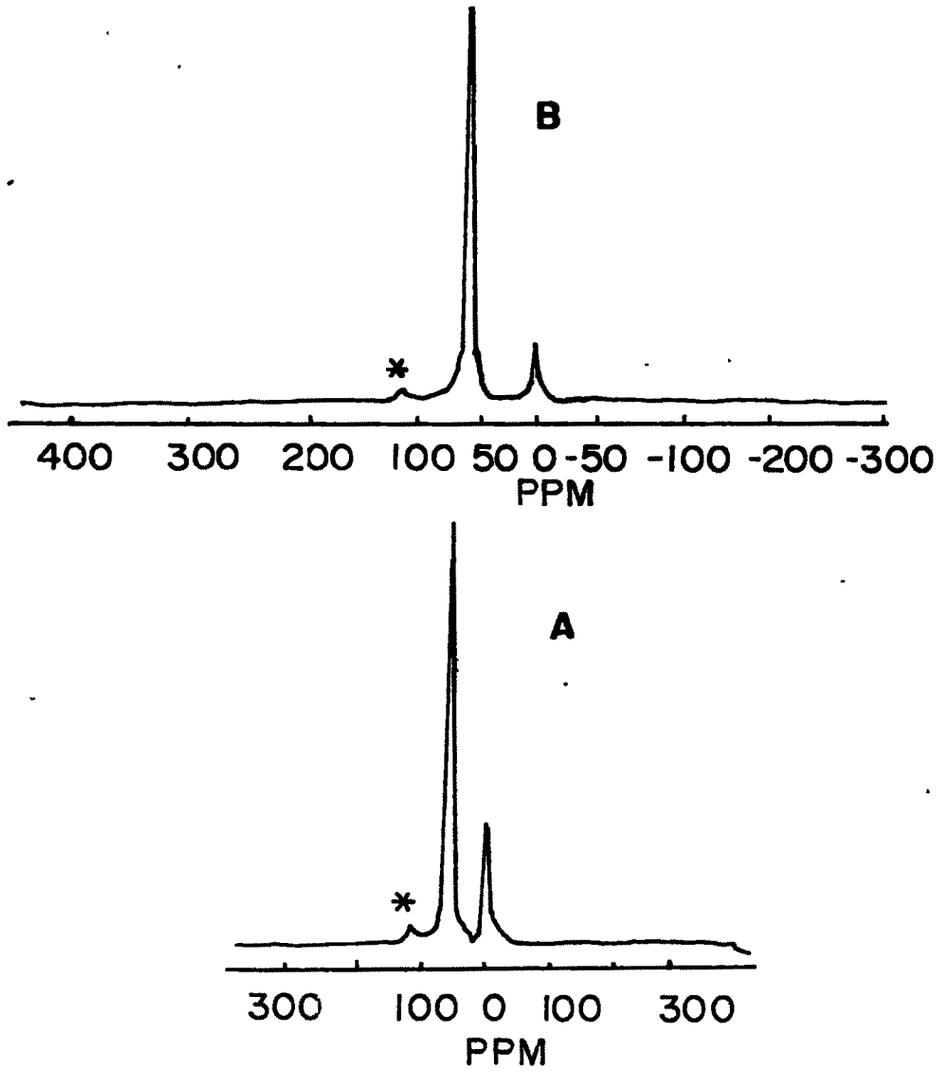

FIG. 2·13b - ^{27}Al NMR SPECTRUM OF A) HM AND B) HDM - 147. * SSB. (SPINNING SIDE BAND.)

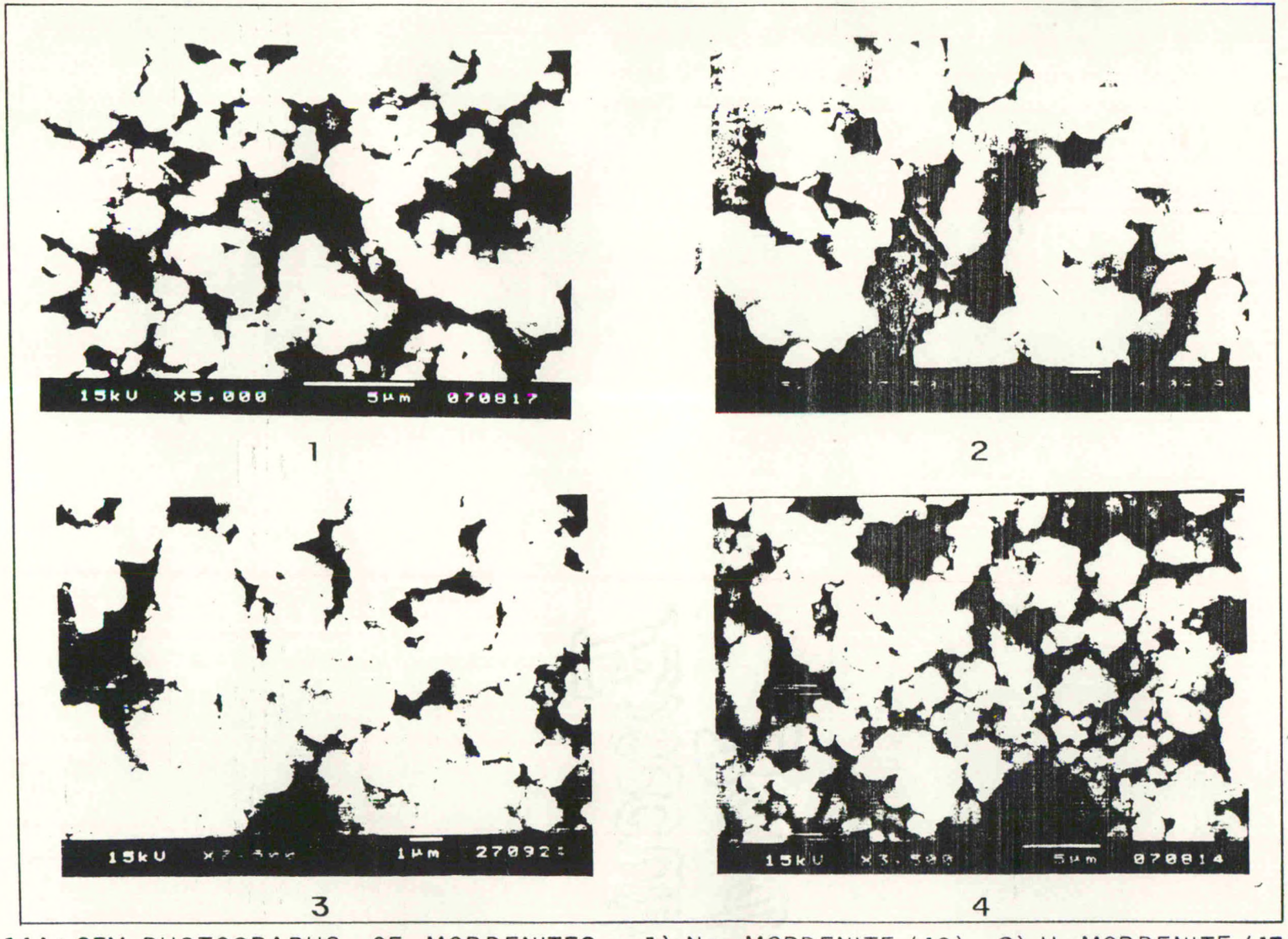

FIG. 2.14A : SEM PHOTOGRAPHS OF MORDENITES . 1) Na – MORDENITE (10) , 2) H – MORDENITE (13) 3) HDM (54) , 4) HDM (147). (FIGURES IN PARENTHESIS INDICATE SiO_2/Al_2O_3 RATIO)

Sample	SiO_2/Al_2O_3 ratio	Size (μm)	Shape
Na-mordenite	9.96	1.4	Cylindrical
HM	13	1.5-1.8	Oblong
HDM-54	54	2.1-2.5	Irregular
HDM-147	147	2.6-3.2	Oval shape

It is seen that with increase of SiO_2/Al_2O_3 ratio crystallite size increased which is also reported for pentasil zeolites.[46b,c]. The SEM photographs of ZSM-5 zeolites are shown in Fig.2.14B. The observations are given below:

SiO_2/Al_2O_3 ratio	size (μm)	Shape
36	$\cong$ 1.1	Nearly spherical
86	$\cong$ 2.5	Nearly spherical
200	$\cong$ 10-12	Cuboidal

The crystals show morphology similar to those reported.[46a] The crystallite of the samples increases with the ratio.[46b,c]

2.7 CHARACTERIZATION OF RE-MORDENITES

(a) XRD:

The XRD patterns of rare-earth exchanged mordenites were obtained in a similar manner as described in section 2.6B. The data of the exchanged zeolite samples showed that the crystallinity is retained in general in all the samples. However, on progressive increase of RE^{3+} ions a slight decrease in crystallinity was observed (Intensity was changed from 95.6 for

1

2

3

FIG. 2.14B : SEM PHOTOGRAPS OF ZSM-5 ZEOLITES OF DIFFERENT SiO_2/Al_2O_3 RATIOS.
(1) 36 , (2) 86 , (3) 200.

HRE(27)MD to 93.56% for HRE(68)MD when compared with parent zeolite) which could be due to the higher scattering factor of heavy rare earth ions.

The XRD pattern of HRE(54)MD is illustrated in Fig.2.3. The peak height I and the position of the X-ray diffraction peak as a function of 2θ where θ is the Bragg angle, were estimated from the spectrometer chart. From these, the relative intensities (I/I_o x 100) where I_o is the intensity of the strongest line or peak and d is the interplaner distance in A^o, were calculated. The values of (d) and relative intensities obtained from the X-ray diffractograms are given in Table 2.14 for the various exchanged mordenite samples.

The lattice constants and unit cell volume are described in Table 2.16. The reduction in unit cell volume is attributed to the dealumination during the exchange of cation.[6] The unit cell formulae of exchanged mordenites are shown in Table 2.15.

(b) Nitrogen sorption:

Typical set of isotherm for nitrogen sorption is presented in Fig.2.15. The figures show that the uptake decreases with increasing rare earth exchange cations in zeolites act as sorption centres, hence their distribution among ion exchange sites changes their sorption behaviour. Replacement of proton by multivalent cations would lead to lattice distortion and unit cell contraction and hence decrease in nitrogen uptake.[46d]

Table 2.14

d spacings and relative intensities of rare-earth exchanged mordenites

Zeolite	H-mordenite		HRE(27)MD		HRE(45)MD		HRE(54)MD		HRE(68)MD	
hkl	d(Å)	I/I_ox100	d(Å)	I/I_ox100	d(Å)	I/I_ox100	d(Å)	I/I_ox100	d(Å)	I/I_ox100
110	13.79	8.31	13.58	20.38	13.58	12.52	13.58	12.25	13.79	16.66
020	10.27	8.31	10.15	20.87	10.96	16.91	10.27	13.97	10.27	15.99
200	9.20	41.57	9.01	57.24	9.04	40.50	9.01	56.77	9.11	55.40
111	6.60	24.94	6.50	36.89	6.55	32.56	6.55	28.82	6.60	31.08
310	5.86	17.94	5.74	21.84	5.82	20.66	5.78	19.78	5.82	21.17
040	5.12	3.50	5.06	5.58	5.10	5.42	5.06	4.30	5.09	5.40
311	4.57	41.13	4.48	47.08	4.52	44.25	4.50	43.44	4.52	43.24
150	4.00	76.58	3.96	75.24	4.00	77.45	3.94	73.97	3.98	75.67
331	3.86	12.91	3.79	10.67	3.83	9.60	3.79	9.67	3.81	9.9
002	3.79	14.00	3.73	12.80	3.76	10.85	3.79	12.90	3.75	12.61
022	3.50	10.0	3.45	100	3.47	100	3.43	100	3.47	100
060	3.41	56.45	3.36	46.6	3.36	46.6	3.34	48.8	3.38	50.9
132	3.26	42.28	3.20	38.30	3.22	35.9	3.32	35.64	3.22	38.28

Table 2.14 (Continued)

d spacings and relative intensities of rare-earth exchanged mordenites

Zeolite	H-mordenite		HRE(27)MD		HRE(45)MD		HRE(54)MD		HRE(68)MD	
hkl	d(Å)	I/I_ox100	d(Å)	I/I_ox100	d(Å)	I/I_ox100	d(Å)	I/I_ox100	d(Å)	I/I_ox100
511	3.22	42.01	3.18	36.8	3.20	36.95	3.29	38.7	3.21	40.54
261	2.90	22.32	2.86	20.8	2.89	20.04	2.85	20.86	2.89	21.62
080	2.55	4.81	2.53	3.88	2.55	4.17	2.67	3.44	2.54	4.05
352	2.53	11.15	2.49	8.49	2.51	8.35	2.61	11.18	2.56	9.90
732	2.04	11.59	2.02	10.92	2.03	9.39	2.10	10.32	2.03	10.13
443	2.03	5.03	1.99	4.12	2.01	3.34	2.07	4.08	2.01	4.05
680	1.96	7.65	1.93	6.79	1.95	6.88	2.0	7.09	1.94	10.13
482	1.92	2.62	1.89	2.18	1.92	1.87	1.96	2.15	1.90	2.25
004	1.88	7.0	1.85	6.06	1.88	6.68	1.92	7.31	1.87	7.20

Table 2.15

Unit cell formulae of rare-earth exchanged mordenites

Zeolite*	Unit cell formula	Mole% RE_2O_3	No. of uc/ gm x 10^{-20}
H-mordenite	$H_{6.60}Na_{0.18}(AlO_2)_{6.78}(SiO_2)_{41.22}$	-	2.09
HRE(27)MD	$H_{4.77}Na_{0.17}RE_{0.61}(AlO_2)_{6.77}(SiO_2)_{41.23}$	0.024	2.03
HRE(45)MD	$H_{3.56}Na_{0.17}RE_{1.01}(AlO_2)_{6.76}(SiO_2)_{41.24}$	0.039	1.99
HRE(54)MD	$H_{2.93}Na_{0.16}RE_{1.22}(AlO_2)_{6.75}(SiO_2)_{41.25}$	0.046	1.98
HRE(68)MD	$H_{1.98}Na_{0.016}RE_{1.53}(AlO_2)_{6.73}(SiO_2)_{41.27}$	0.056	1.95

* Figures in parenthesis indicate percentage exchange of rare earth cation.

Table 2.16

Lattice constants and unit cell volume of rare-earth exchanged mordenites

Zeolite	Lattice constant (Å)			Unit cell volume($Å^3$)
	a	b	c	
H-mord	18.014	20.528	7.505	2775.21
HRE(27)MD	18.058	20.426	7.512	2770.94
HRE(45)MD	18.164	20.342	7.486	2766.31
HRE(54)MD	18.127	20.333	7.504	2765.61
HRE(68)MD	18.107	20.344	7.582	2755.17

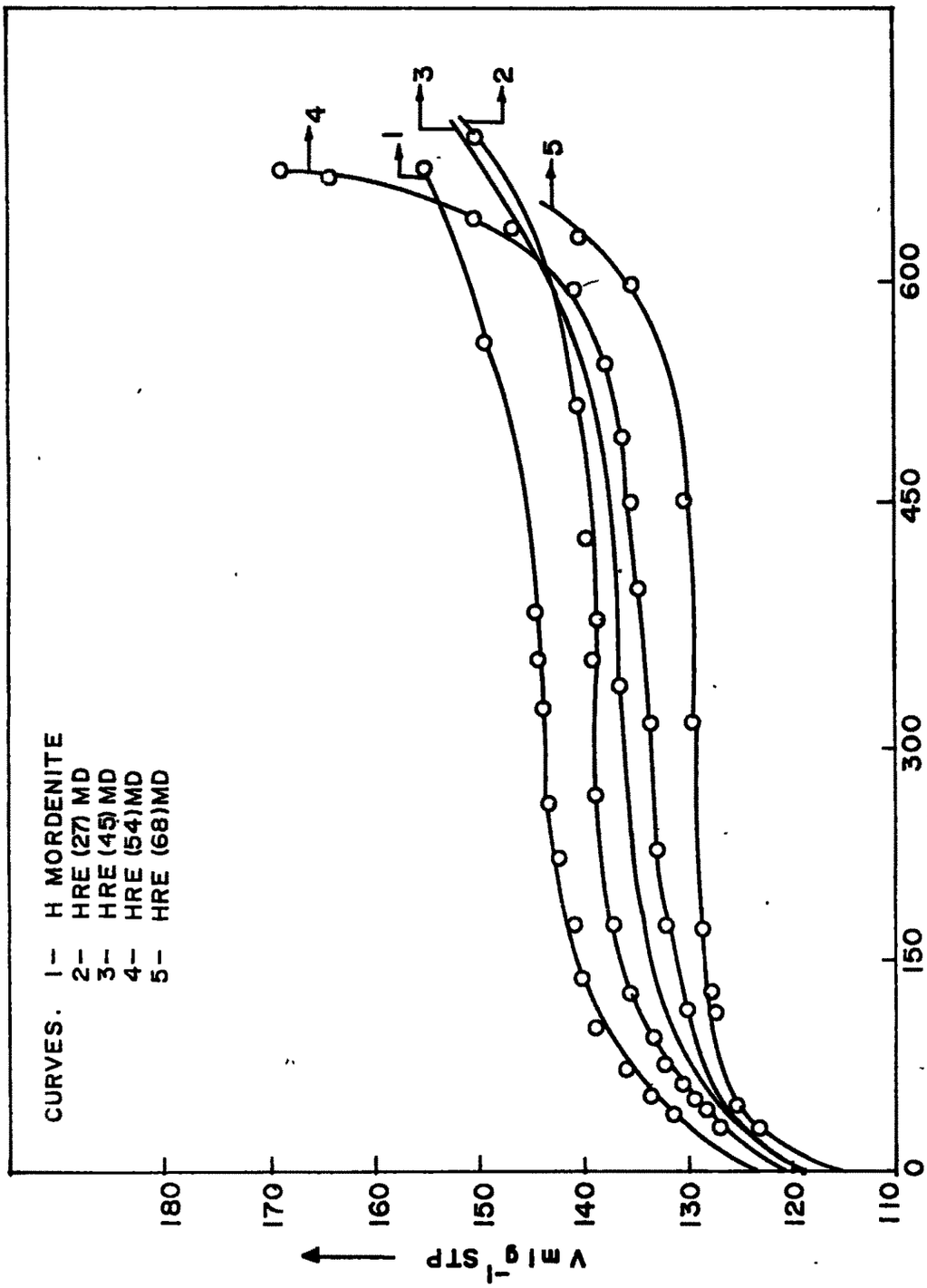

FIG. 2.15 ISOTHERMS OF NITROGEN SORPTION AT — 195°C

(c) Surface Area:

The sorption isotherm depend on the amount of gas sorbed at equilibrium pressure. Langmuir and BET equations were applied to calculate surface area. A typical plot for HRE(54)MD is shown in Fig.2.16. It is seen that Langmuir plot is linear over a wide range of relative pressure. Similar results are reported for nitrogen sorption in Pd-mordenite.[47] Saturation capacity of nitrogen and surface area of rare-earth exchanged mordenites are shown in Table 2.17.

(d) Free energy change in sorption:

Sorption is an exothermic process and is accompanied by decrease in the surface free energy. When one mole of sorbate is transferred reversibly and isothermally from a standard pressure P_o to equilibrium pressure P, the decrease in Gibb's free energy is given by the relationship

$$\Delta G = \Delta\mu = RT\ln P/P_o$$

where ΔG is the convenient thermodynamic measure of the chemical affinity of a particular sorbate at fixed temperature T. The affinities of nitrogen sorption at $-195^{o}C$ for all exchanged zeolites calculated as a function of coverage are shown in Table 2.18. There is fall in affinity with increased uptake upto a pressure = 500 torr and then show decrease at higher pressure. This situation corresponds to multilayer formation and capillary condensation. The affinity for nitrogen sorption decreases with the increase in RE^{3+} content. The affinity coefficient for nitrogen sorption is shown in Table 2.19.

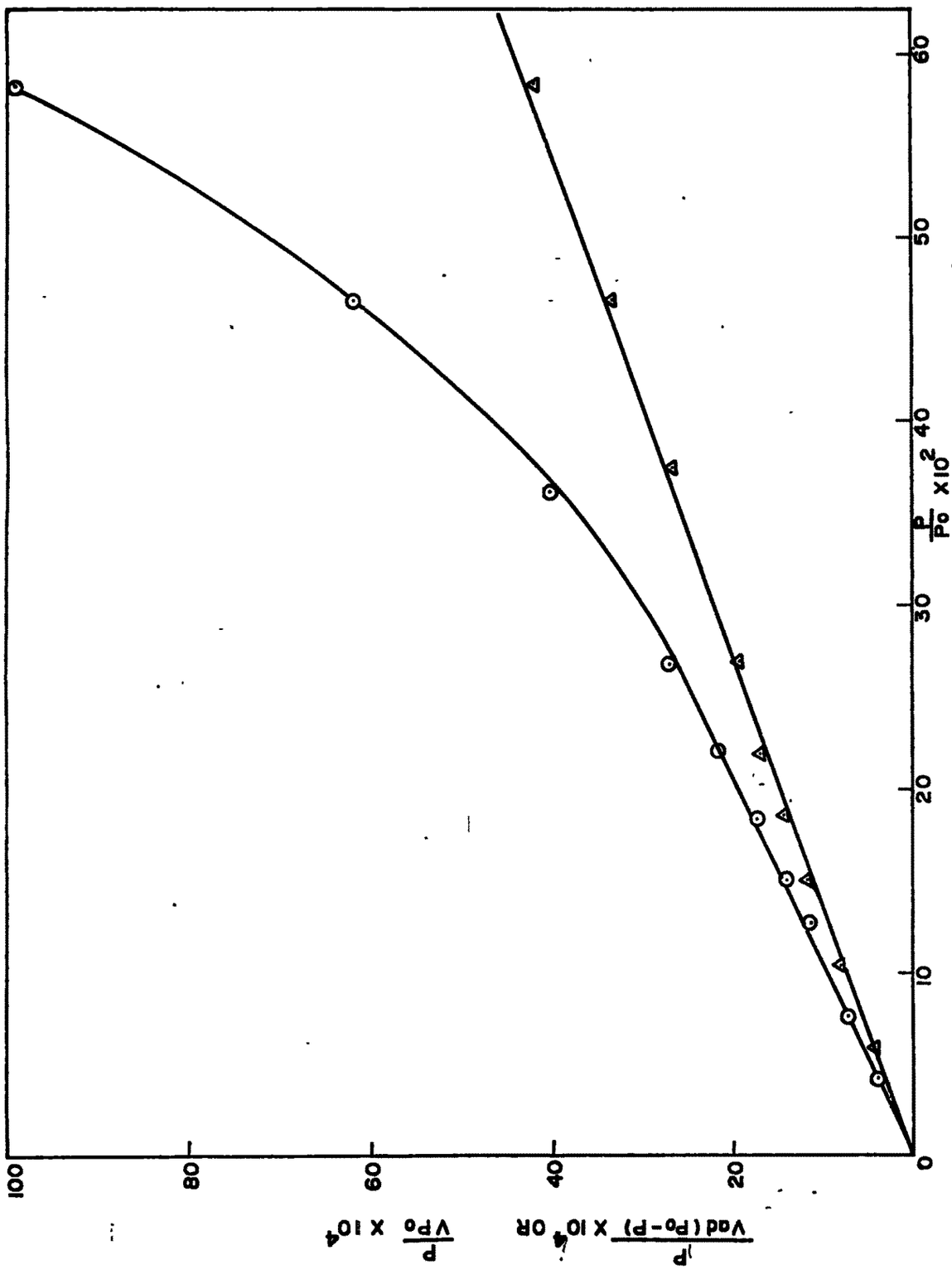

FIG.2.16 BET ⊙ AND LANGMUIR ▲ PLOTS FOR NITROGEN SORPTION AT −195°C ON HRE(54) MD

Table 2.17

Saturation capacity (nitrogen) and surface area of rare-earth exchanged mordenites*

Zeolites	Saturation capacity molecules/u.c.		Surface area (m^2/g)	
	Langmuir	BET	Langmuir	BET
H-mordenite	18.38 (142.85)	15.72 (122.22)	621.84	532.02
HRE(27)MD	18.29 (137.25)	14.80 (111.11)	597.44	483.18
HRE(45)MD	18.68 (136.38)	14.42 (105.26)	593.67	458.19
HRE(54)MD	18.71 (135.00)	14.30 (103.22)	587.65	449.34
HRE(68)MD	18.14 (129.16)	13.95 (99.35)	562.23	432.50

* Figures in parenthesis indicate mls/g. of nitrogen.

Table 2.18

Chemical affinity of rare-earth exchanged mordenites for nitrogen sorption at $-195^{o}C$

H-mordenite		HRE(27)MD		HRE(45)MD	
Molecules/uc	$-\Delta\mu$ KJ/mole	Molecules/uc	$-\Delta\mu$ KJ/mole	Molecules/uc	$-\Delta\mu$ KJ/mole
16.93	1.90	16.36	2.07	16.60	2.34
17.22	1.74	16.50	1.88	17.07	2.21
17.53	1.53	16.65	1.76	17.40	2.01
17.88	1.29	16.80	1.63	17.56	1.78
18.04	1.10	17.04	1.48	17.72	1.59
18.14	0.92	17.20	1.32	17.29	1.43
18.33	0.78	17.44	1.15	17.95	1.29
18.46	0.67	17.68	0.94	18.03	1.19
18.56	0.53	17.84	0.66	18.16	1.06
18.64	0.46	17.93	0.46	18.24	1.01
18.67	0.41	18.01	0.33	18.27	0.95
18.86	0.27	18.09	0.21	18.42	0.83
19.27	0.16	18.82	0.03	18.64	0.66
19.97	0.03	20.13	0.01	18.85	0.49
21.98	0.01			19.10	0.35
				19.39	0.25
				19.78	0.12
				20.20	0.07
				20.98	0.03

Table 2.18 (Continued)

Chemical affinity of rare-earth exchanged mordenites for nitrogen sorption at $-195^{o}C$

HRE(54)MD		HRE(68)MD	
Molecules/uc	$-\Delta\mu$ KJ/mole	Molecules/uc	$-\Delta\mu$ KJ/mole
17.36	2.34	17.04	2.29
17.71	1.96	17.55	2.16
18.12	1.44	17.57	1.93
18.26	1.18	17.81	1.70
18.40	0.99	17.87	1.51
18.54	0.89	17.97	1.42
18.68	0.72	18.03	1.20
18.83	0.51	18.09	1.09
18.96	0.35	18.14	0.09
19.04	0.25	18.24	0.91
19.17	0.20	18.25	0.85
19.38	0.13	18.28	0.72
19.88	0.08	18.29	0.67
21.14	0.03	18.35	0.51
		18.33	0.36
		18.46	0.25
		18.67	0.12
		19.02	0.07
		19.91	0.04

Table 2.19

Sorption of water and hydrocarbon vapour on rare-earth exchanged mordenite

Zeolite	Equilibrium sorption (Molecules/uc)					Void volume cc g^{-1}	$\frac{B}{\beta^2} \times 10^6$
	H_2O	n-hexane	Benzene	Cumene	Cyclohexane		
H-mord	26.43	2.38	3.57	1.08	2.15	0.221	9.68
HRE(27)MD	25.1	1.74	2.24	0.87	1.37	0.214	9.46
HRE(45)MD	24.8	1.70	2.20	0.81	0.65	0.203	5.30
HRE(54)MD	24.2	1.60	2.20	0.57	0.50	0.199	5.41
HRE(68)MD	23.09	1.53	2.0	0.16	0.36	0.197	3.79

(e) Void Volume:

The Dubin equation[22]

$$\log_{10} V_a = \log_{10} V_o - D(\log P/P_o)^2$$

$$\text{where } D = \frac{0.434BT^2}{\beta^2} = \text{constant here.}$$

B = constant independent of temperature and characteristic of sorbent pore structure.

β is the affinity coefficient.

T is the temperature

was applied to nitrogen adsorption isotherm and from the intercept of the plot of $\log_{10} V_a$ against $(\log P/P_o)^2$, void volume of the exchanged zeolites was computed. The Dubinin plots are presented in Fig.2.17. It is seen that the plots are linear for nitrogen sorption with slight deviation at higher pressure due to multilayer formation and capillary condensation. The void volume decreases from 0.22 to 0.197 cc g^{-1}. The result indicates that channels are modified by cation exchange with RE^{3+} and this influences the uptake of gases to a considerable extent.

(f) Sorption of water and hydrocarbon

Table 2.19 presents void volume, and sorption of water and hydrocarbon vapours of rare-earth exchanged mordenites at 25°C and $P/P_o = 0.5$. All sorption measurements were carried out as described in previous section. The decrease in water sorption capacity is attributable to dealumination[6] during cation exchange. A reduction in uptake of Benzene, cumene, cyclohexane and n-hexane vapours is a consequence of unit cell contraction

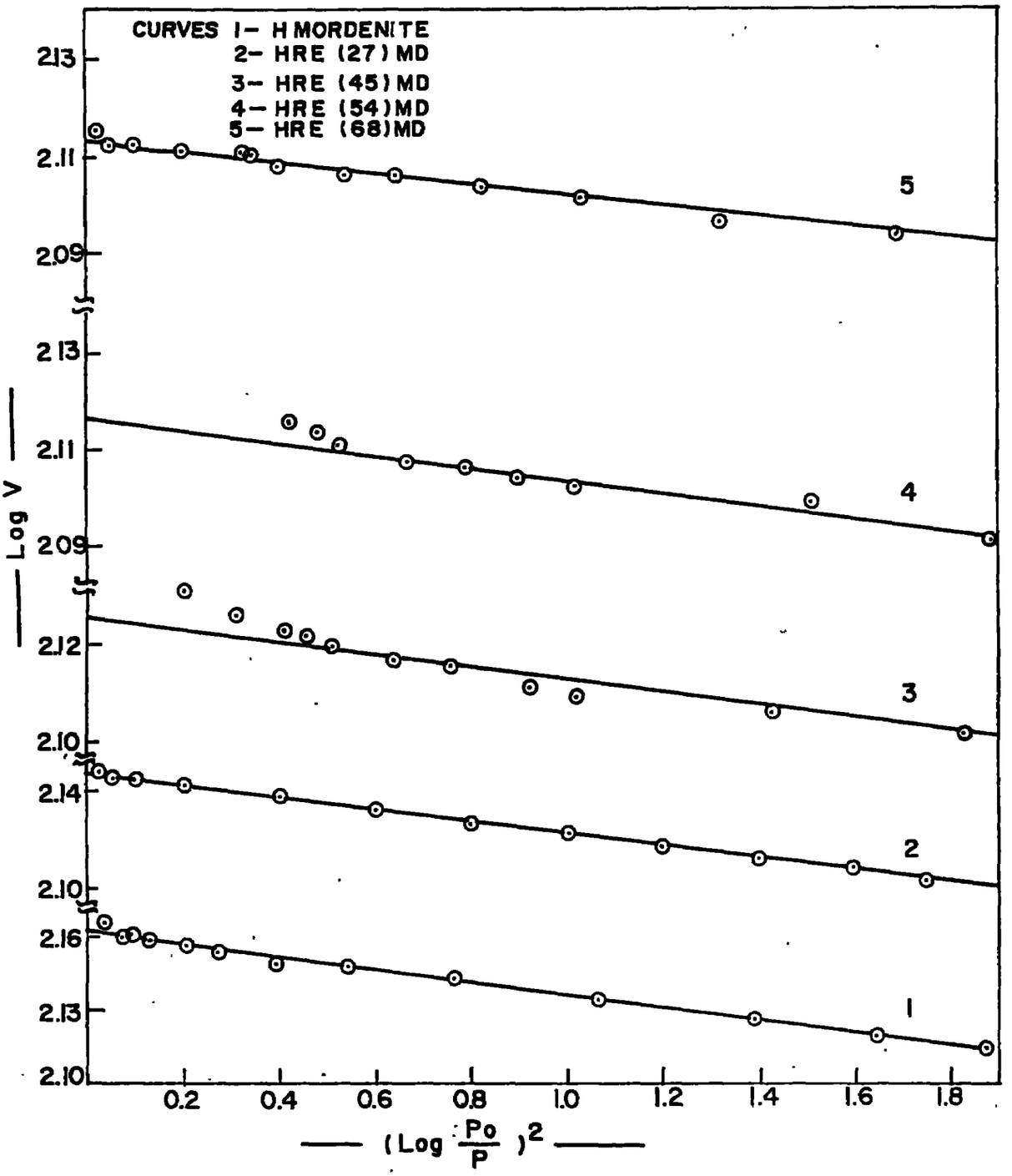

FIG. 2.17 DUBININ PLOTS FOR THE ADSORPTION OF NITROGEN AT −195 °C

due to the presence of larger hydroxy rare-earth cations.[46d]

2.8 ZSM-12 ZEOLITE

The XRD pattern of NaZSM-12 zeolite is shown in Fig.2.18. The interplanar spacings 'd' in A^{o} obtained from values of 2θ against the observed relative intensities for synthesized NaZSM-12 zeolite with the reported is presented in Table 2.20.

The values of 'd' and the relative intensities of peaks with respect to the most intense peak at 2θ = 20.8 are in agreement with those reported confirming the indentify of the sample as NaZSM-12.[2]

2.9 ZSM-5 ZEOLITE

The interplanar specings 'd' in A^{o} obtained from values of 2θ are shown in Table 2.21 and Fig. 2.19. The intense peaks occuring at 2θ = 7.9±0.1 and 23±0.22 are characteristic of ZSM-5 type zeolite. The values of 'd' and the relative intensities of peaks with respect to the most intense peak at 2θ = 23^{o} are in agreement with those reported in the literature.[3]

2.10 CHARACTERIZATION OF RARE-EARTH EXCHANGED Y ZEOLITE

The XRD and IR spectra for exchanged zeolites were scanned as described in section 2.6B and C respectively.

Results and discussion

(a) The X-ray diffraction patterns of hydrated samples of Y type

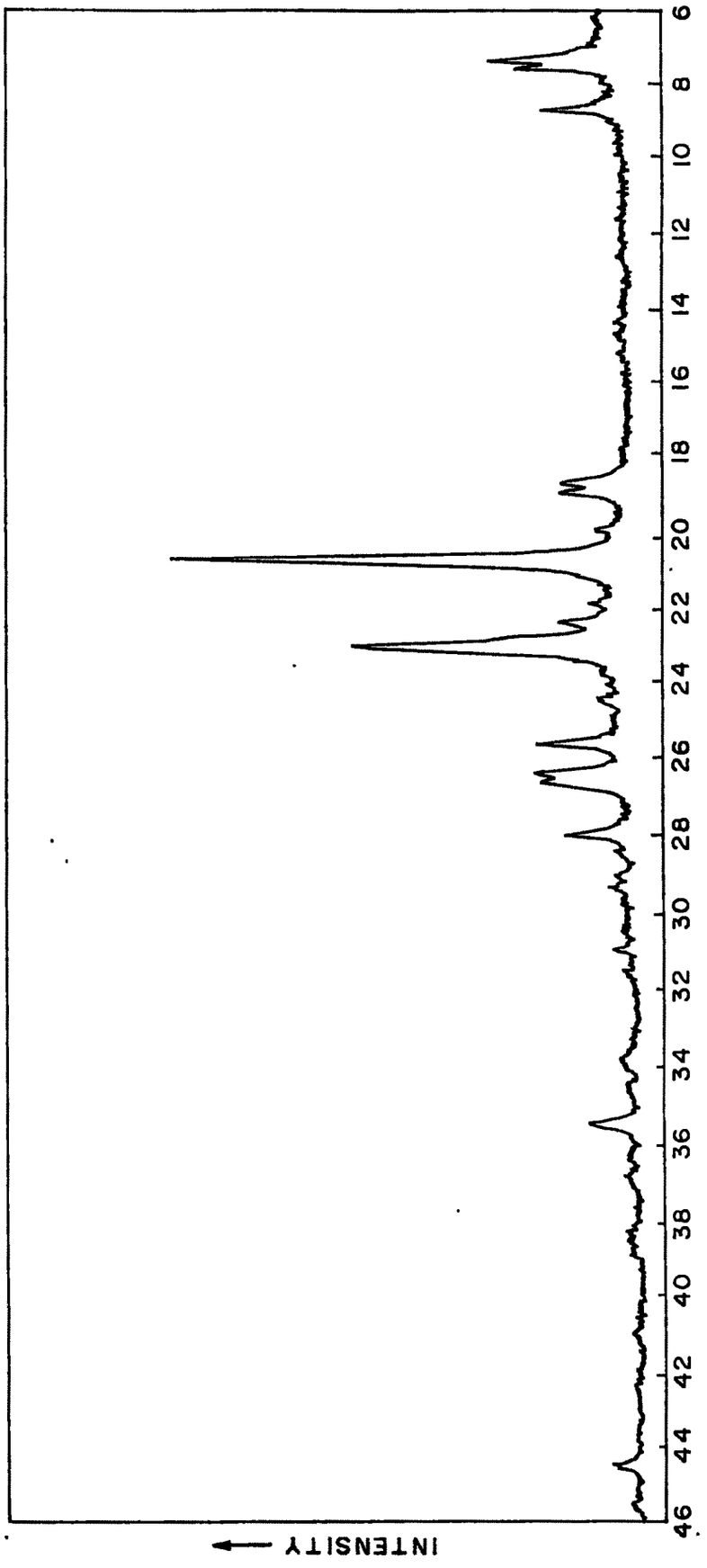

FIG. 2·18- X-RAY DIFFRACTION PROFILE OF ZSM-12 ZEOLITE

Table 2.20

d-spacings and relative intensities for ZSM-12 zeolite

Observed				Reported*	
d(Å)	I/I_o	d(Å)	I/I_o	d(Å)	I/I_o
11.93	30	4.45	03	11.90	27.0
11.62	20	4.26	100	11.60	10.0
-	-	4.07	02	11.15	10.0
10.04	16	-	-	10.02	35.0
9.72	05	3.98	05	9.72	5.0
-	-	3.86	58	6.02	5.0
-	-	-	-	5.57	5.0
-	-	3.75	05	4.96	5.0
-	-	-	-	4.75	14.0
-	-	3.63	05	4.20	11.0
6.04	05	3.46	20	4.45	6.0
-	-	3.37	20	4.28	100.0
5.57	05	3.33	18	4.10	8.0
-	-	-	-	3.98	14.0
-	-	3.18	12	3.85	67.0
4.96	05	3.07	01	3.75	5.0
4.74	10	3.04	03	3.71	9.0
4.65	10	-	-	3.65	7.0

* Ref. 2

Table 2.21

Lattice spacing, (d), and relative intensity (I/I_o) values for NaZSM-5

2θ	Interplanar spacing 'd' A^o (obs)	Interplanar spacing 'd' A^o *	Relative intensity I/I_o(obs)	Relative intensity I/I_o *
7.9	11.15	11.10±0.2	62.3	s
8.80	10.04	10.0 ±0.2	45.4	s
11.90	6.70	-	7.0	-
13.90	6.36	6.3 ±0.1	13.8	w
14.80	5.99	6.04±0.1	15.4	w
15.55	5.71		10.8	-
15.90	5.57	5.56±0.1	13.8	w
19.20	4.62	4.60±0.08	7,7	w
20.80	4.27	4.25±0.08	13.8	w
22.12	4.02	-	6.2	-
23.00	3.86	3.85±0.07	100.0	vs
23.9	3.72	3.71±0.05	52.3	s
24.41	3.64	-	30.8	-
29.30	3.04	3.04±0.03	12.3	w
29.90	2.99	2.99±0.02	16.9	w
30.39	2.94	2.94±0.02	7.7	w

* Ref. 3

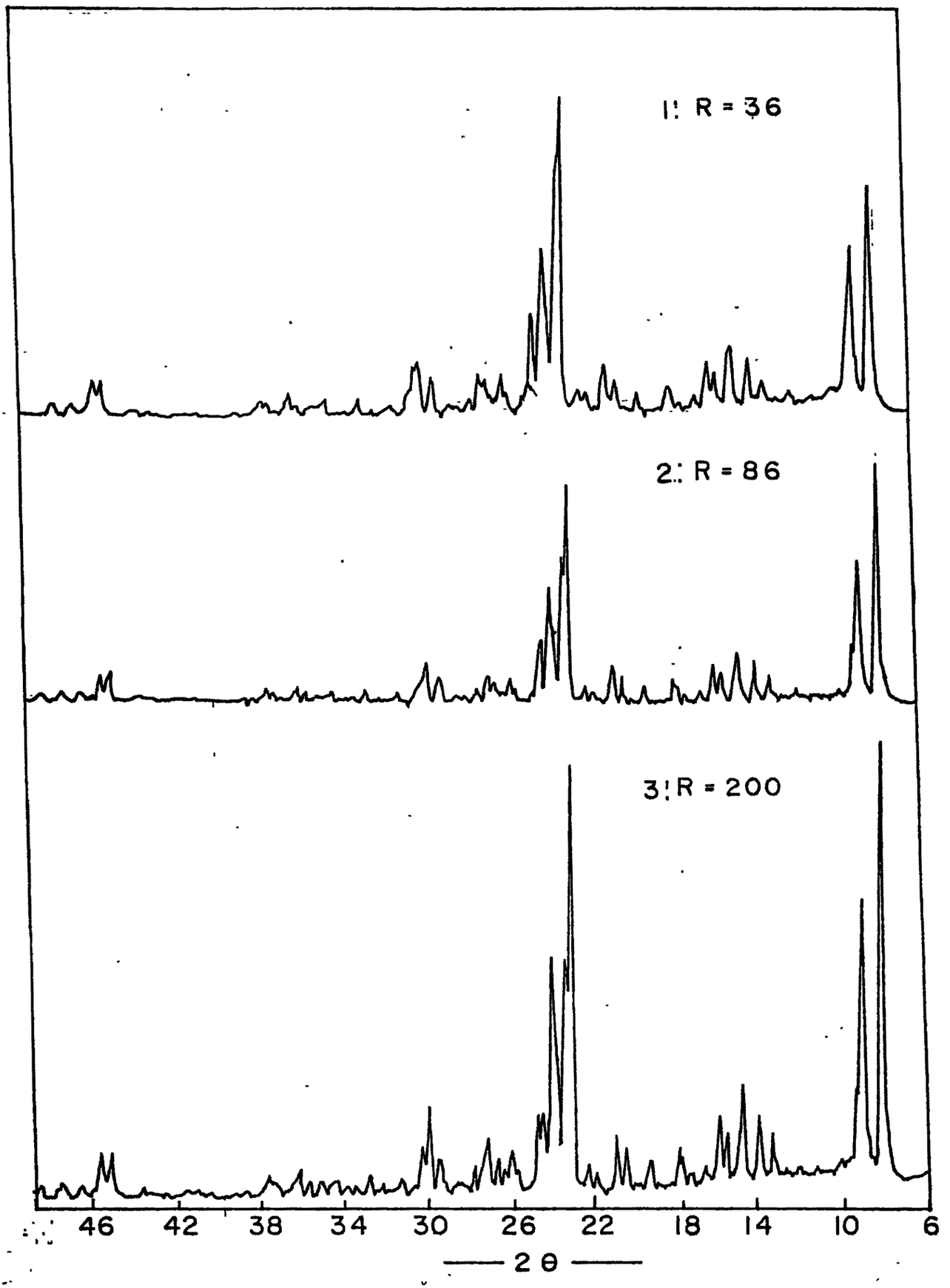

FIG.2.19: XRD PATTERNS OF HZSM-5 ZEOLITES SiO_2/Al_2O_3 FOR 1) 36, 2) 86 AND 3) 200

zeolites exchanged with RE^{3+} at various levels of exchanges are shown in Fig.2.20. The XRD pattern of NaY confirms the reported data.[6] The XRD data for exchanged zeolite samples show that the crystallinity is retained in all the samples. However, on progressive increase of RE^{3+} ions in the NaY, the intensities of the peaks decrease, which could be due to the higher scattering factor of heavy lanthanum ions. For the RE^{3+} exchanged samples the intensity of all diffraction lines is in the order:

$$NaY > RE(32)Y > RE(60)Y > RE(83) > RE(92)$$

The Table 2.22 summarizes ΣS values (sum of peak heights for planes 331,533,642 and 751)[48] and the relative line intensities for all reflections in accordance with the assignments of Breck.[6] The relative intensities are calculated by assuming the strongest line in NaY as 100%.

The average values of lattice constants 'a_o' calculated from the principal reflections are also listed in Table 2.22. All the a_o values are smaller than the values for the parent NaY crystal. The contraction in unit cell parameter was attributed to the dealumination[6] or by specific cation movement.[49]

(b) Infrared spectra

The spectra were analysed according to the band assignments of Flanigen et al[11] and are grouped into two classes, those due to (a) internal vibrations of TO_4 tetrahedron (T= Si or Al) which is primary structural unit and (b) vibrations related to linkages between tetrahedra.. These are sensitive to secondary building

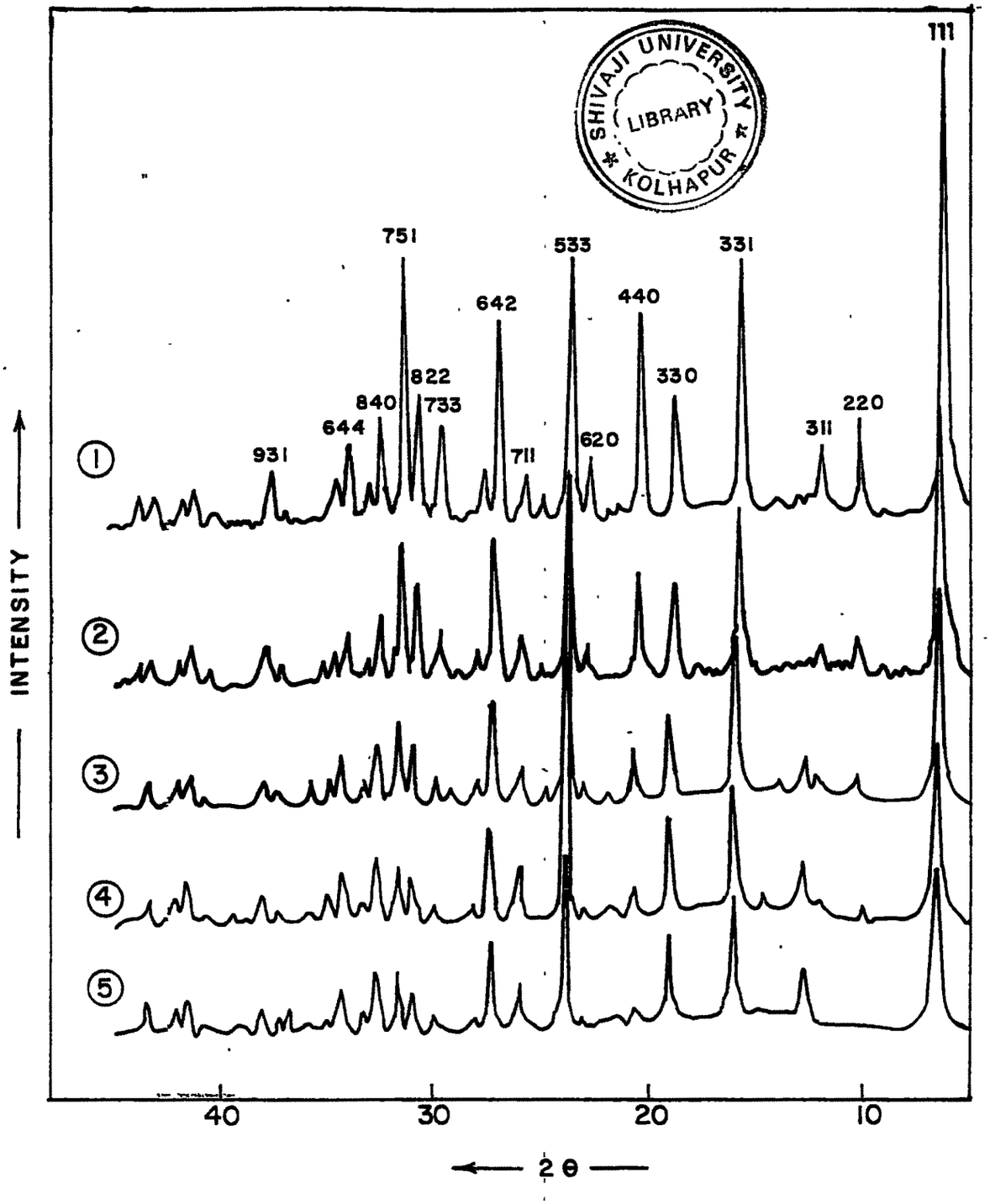

FIG.2.20-X-RAY DIFFRACTROGRAMS OF (1)NaY, (2)RE(32)Y (3) RE (60) Y, (4)RE (83) Y, (5) RE (92) Y.

Table 2.22

X-ray powder diffraction data for rare-earth exchanged zeolites

Zeolite	NaY	RE(32)Y	RE(60)Y	RE(83)Y	RE(92)Y
a_o (Å)	24.71	24.66	24.60	24.56	24.52
≥S	49.7	33.1	26.5	24.2	23.2
hkl					
111	100	68	44	41	32
220	21	7	5	-	-
311	16	4	-	-	-
331	59	34	32	24	26
333	28	20	18	20	18
440	45	20	11	5	9
620	13	7	4	-	-
533	65	44	38	37	36
551	10	8	8	8	10
642	45	29	21	18	18
553	12	6	4	-	3
733	20	10	4	4	3
822	27	16	13	12	8
751	61	29	18	13	13
840	19	-	13	13	14
664	18	11	10	8	9
931	7	5	5	5	3

units as well as the pore opening bands.

The different IR assignment[11] bands are summarized below:

			cm^{-1}
1.	Internal	Asym. stretch (<--OT--> <--O)	1250-950
	tetrahedra	Sym. stretch (<-- OTO -->)	720-650
		T-O band	500-420
2.	External	Double ring	650-500
	linkages	Pore opening	450-500
		Sym. stretch	750-820
		Asym. stretch	1150-1050

Fig.2.21 shows IR spectra for NaY and exchanged samples in the region 250-1250 cm^{-1} and Table 2.23 gives assignments of the bands. The IR spectra of NaY confirms the spectra reported by Flanigen et al[11] and shows bands at 1005,780,710,575,460,380, and 350 cm^{-1}, the strongest (asym. stretch) band being at 1005 cm^{-1}. The band at 575 cm^{-1} is characteristic double ring (D6R) band and that at 380 cm^{-1} is assigned to the pore opening, both the above bands are structure sensitive bands, with exchange of Na^{+} with RE^{3+} ions, the shoulder bands at 1130 cm^{-1} and 380 cm^{-1} shift to higher frequencies, while those at 780,575 and 460 cm^{-1} shift to lower values. These observations are consistent with the result reported.[11,50-52]

For RE exchanged zeolites, the shift to higher frequency is possible due to dealumination[51] and subsequent contraction of the unit cell which is confirmed by XRD data discussed earlier. Cation exchange with polyvalent ions apparently causes

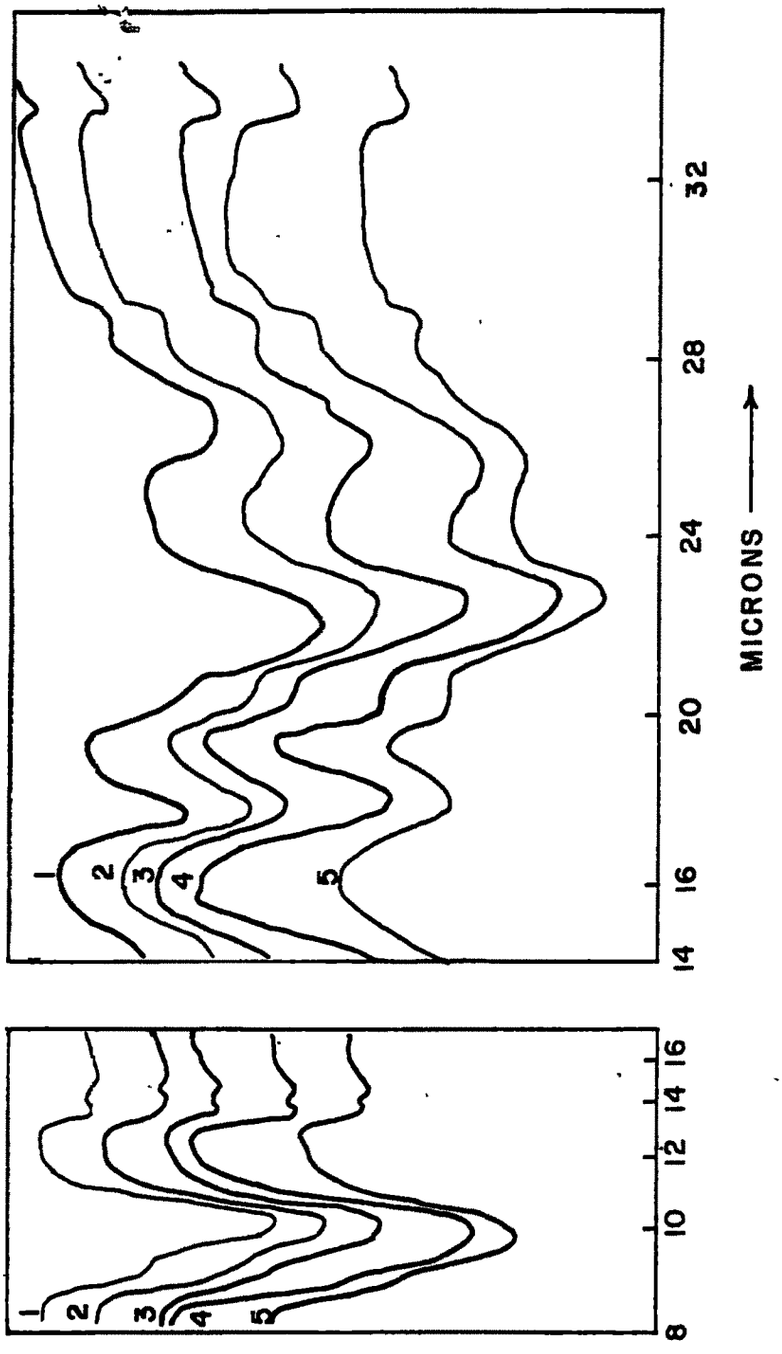

FIG.2;21.IR SPECTRA OF CATION EXCHANGED ZEOLITES (1) NaY, (2) RE(32)Y, RE(60)Y, (4) RE(83)Y, (5) RE(92)Y

Table 2.23

Infrared spectral data for rare-earth exchanged Y zeolites

Zeolite	Asymmetric stretch		Symmetric stretch		Double rings	T-O Bend		Pore opening		
NaY	1130 msh	1005 s	780 w	710 m	575 m	494 mwsh	460 ms	380 m	350 w	301 vw
RE(32)Y	1140 mwsh	1010 s	770 w	715 w	571.4 m	492 mwsh	452.5 ms	386 m	350 w	300 vw
RE(60)Y	1140 wsh	1020 s	765 m	715 m	568.2 m	491 mwsh	448.5 ms	389 m	350 w	299 vw
RE(83)Y	1140 vwsh	1025 s	770 w	720 m	561.8 m	494 msh	442.5 ms	392 m	350 w	298 vw
RE(92)Y	1135 wsh	1030 s	768 w	725 m	560.2 mb	497 msh	439.5 ms	394 m	350 w	297 vw

s = strong
ms = medium strong
m = medium
w = weak
mw = medium weak
vw = very weak
sh = shoulder
b = broad

dealumination or framework distortion as a consequence of the polyvalent ions occupying screened sites in the zeolite lattice. From the IR spectra, we conclude that introduction of polyvalent ions in the Y zeolite produces characteristic shifts in the frequencies of various bands. The shifts are attributable to lattice distortion caused by the heavy atoms occupying the screened positions in the zeolite lattice. The IR bands become broad, intense and shoulders more sharp and pronounced showing a stabilization of the lattice. These results are in accordance with the lattice energy calculation by Romanovskii.[53]

(c) Thermal properties

The thermoanalytical curves (DTA,TG) were recorded on an automatic Derivatograph, MOM-Budapest (Type 00-102)B described by Paulick et al.[54] α-alumina was used as reference material. For scanning the curves 200 mgs sample was used, heating rate being 10^{o} per minute and temperature range 25^{o} to 1000^{o}C.

The DTA,TG curves for NaY and RE^{3+} exchanged zeolites are presented in Fig.2.22.

Results and discussion

The TG curves show that the dehydration of zeolites starts around 40-60^{o}C and is complete at about 400^{o}C. The rate of drhydration of the zeolite is found to depend on the concentration of substituted cation. The TG curves indicate two different stages of water loss, the first between 40^{o}C to 400^{o}C and the second up to a temperature of structure collapse of the

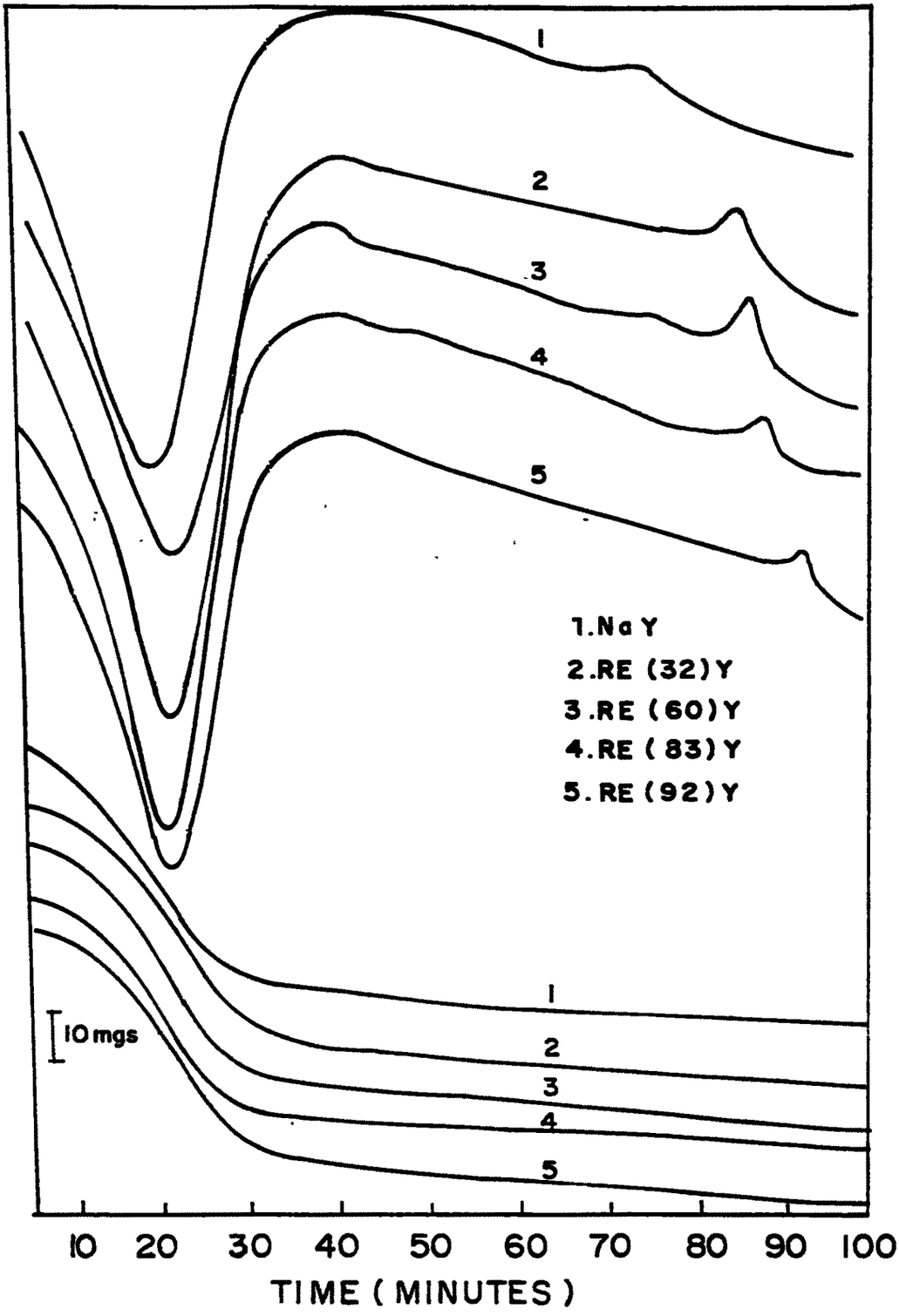

FIG. 2·22 DTA AND TG CURVES OF RARE EARH EXCHANGED Y ZEOLITES

zeolite. The former loss gradually amounts to about 90% of the total weight loss and is attributed mainly to zeolitic water molecules which are physically absorbed. The second stage weight loss consists of dehydroxylation process.

TG analysis: The TG curves in Fig.2.22 show that the rate of water loss from NaY is faster than that from exchanged samples suggesting a strong bond between RE^{3+} than between Na^{+} and water. The temperature range for complete dehydration however decreases from 465°C for NaY to 420°C for RE(92)Y. Furthermore, the weight loss beyond 500°C suggests that the concentration of OH groups increase with RE^{3+} content in the zeolite.

The total weight loss estimated from the TG curves shows a continuous increase of water content with RE^{3+} concentration and the weight loss due to dehydroxylation increasing from 2.25% for NaY to 3.5% for RE(92)Y.

DTA analysis: The DTA curves of RE exchanged zeolite are presented in Fig.2.22. All the samples show a strong endotherm indicating desorption of zeolitic water. The endotherm maxima shift from 180°C for NaY to 205°C for RE(92)Y due to stronger bonding of water molecules with RE^{3+} ions. The dehydroxylation endotherm in REY becomes more pronounced with RE^{3+} content and increases from 460°C to 500°C, indicating enhanced thermal stability and catalytic activity (discussed in Chapter 3) on account of larger number of OH groups. The high temperature exotherm for NaY Occurs at 810°C while that for RE(92)Y at 970°C, indicating a marked increase[50,51] in the thermal stability of the

RE zeolites. The thermo-analytical data of exchanged zeolites is presented in Table 2.24.

(d) Nitrogen sorption:

Typical sets of isotherms for the sorption of nitrogen are presented in Fig.2.23. It is seen that the uptake decreases with increasing degree of rare-earth exchange in the Y type zeolite. The sorption data reported[55] for the CO_2 in trivalent cationic forms of Y type zeolites also indicated decrease in the uptake.

The nitrogen molecules are not sorbed in the sodalite cages of zeolites X and Y and therefore the cations located in sites I and I' are inaccessible to this molecule. This is due to larger kinetic diameter of nitrogen molecule ($3.64A^{o}$)[24] as compared to the diameter of the largest opening ($2.6\ A^{o}$) to the sodalite cage through the six membered oxygen ring. Thus, the uptake of nitrogen is due to sorption in the α cage in X and Y type zeolites. Therefore, the reduction in the nitrogen capacity upon RE^{3+} exchange appears to be a consequence of the modification in the α cage. Since cation acts as sorption centres, the change in their distribution must cause such changes in the sorption properties. However, the cation distribution data reported[56] for La^{3+} ions showed their absence in zeolite Y; therefore the influence of cations on the N_2 sorption is ruled out.

It has been shown[57] that low temperature dehydration (below $400^{o}C$) results in partial hydrolysis of the La^{3+} ions to form a divalent hydroxy complex ($LaOH^{2+}$) ions located in site I' to the extent of 16 per unit cell or 2 each in sodalite (β) cage.

Table 2.24

Thermoanalytical data of rare-earth exchanged Y zeolites

Zeolite	% loss in weight for complete			Temperature (^{o}C) of			
	Dehydration	Dehydroxylation	Structural collapse	Minimum of endotherm	Complete dehydration	Dehydroxy-lation	Maximum of exotherm
NaY	27.0	28.5	29.3	185	465	665	810
RE(32)Y	26.5	28.5	29.7	205	430	460,750	910
RE(60)Y	26.0	29.0	29.8	200	425	470,770	930
RE(83)Y	-	-	-	193	445	480,880	945
RE(92)Y	26.0	29.0	30.5	200	420	500,860	970

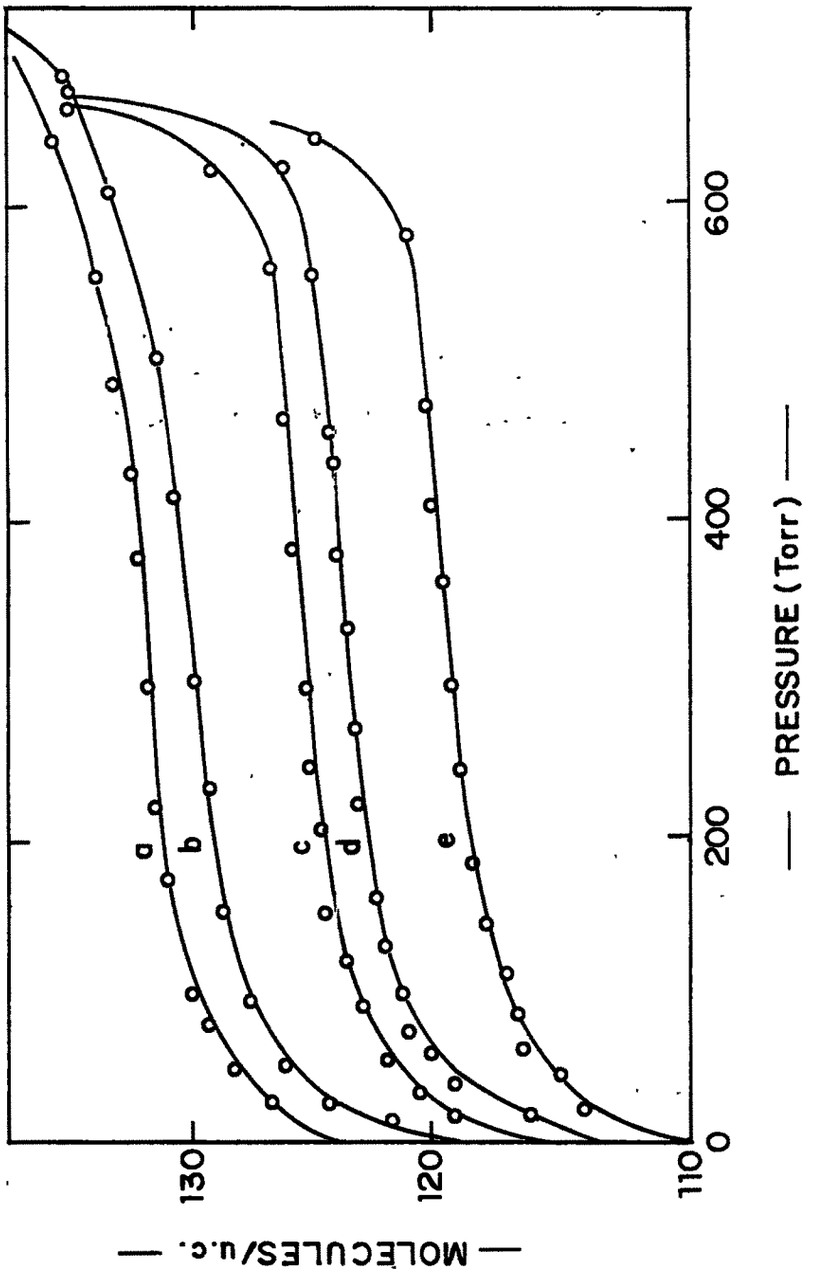

FIG. 2.23: ISOTHERMS FOR THE SORPTION OF NITROGEN OVER RARE-EARTH EXCHANGED Y ZEOLITES AT - 195°C.
a) NaY b) RE(32)Y c) RE(60)Y d) RE(83)Y AND e) RE(92)Y.

Simultaneously, the proton attaches to a framework oxygen to form a hydroxyl group. Increased number of RE^{3+} in the zeolite cages or hexagonal prisms would thus cause some distortions in the pores and intracrystalline voids due to strong interaction with lattice oxygens. Similarly increased cation density may cause a strong cationic repulsion which may cause lattice distortion. Such lattice distortion is reported[58] for calcium exchanged X type zeolites. Such intracrystalline deformation would change the geometry of the super cages and this should be reflected in the sorption capacity. The X-ray diffraction data discussed earlier in this chapter, in fact confirm the lattice deformation or change in the crystallinity of the RE^{3+} exchanged zeolite. Fig.2.20 and 2.21 indicate a decrease in the intensities of the X-ray peaks particularly 533 peak which is reported[59] to be least affected by cation exchange. Similarly the data reported in Table 2.22 show a contraction in the unit cell with progressively increasing RE^{3+} content in the Y type zeolites. The X-ray crystallinity, as determined by summing out the peak heights of four selected XRD reflections,[60] (Planes 331,533,642 and 751) is found to decrease with RE^{3+} exchange (Table 2.22).

(e) Surface area

Langmuir and BET plots have been constructed for the adsorption of nitrogen in the zeolites. Typical Langmuir and BET plots for RE(92)Y are shown in Fig.2.24. The adsorption data on all the zeolites gave similar plots. The Langmuir equation was shown to be applicable to the sorption of nitrogen/methane mixture in the zeolite 4A.[20] Therefore, the surface areas have

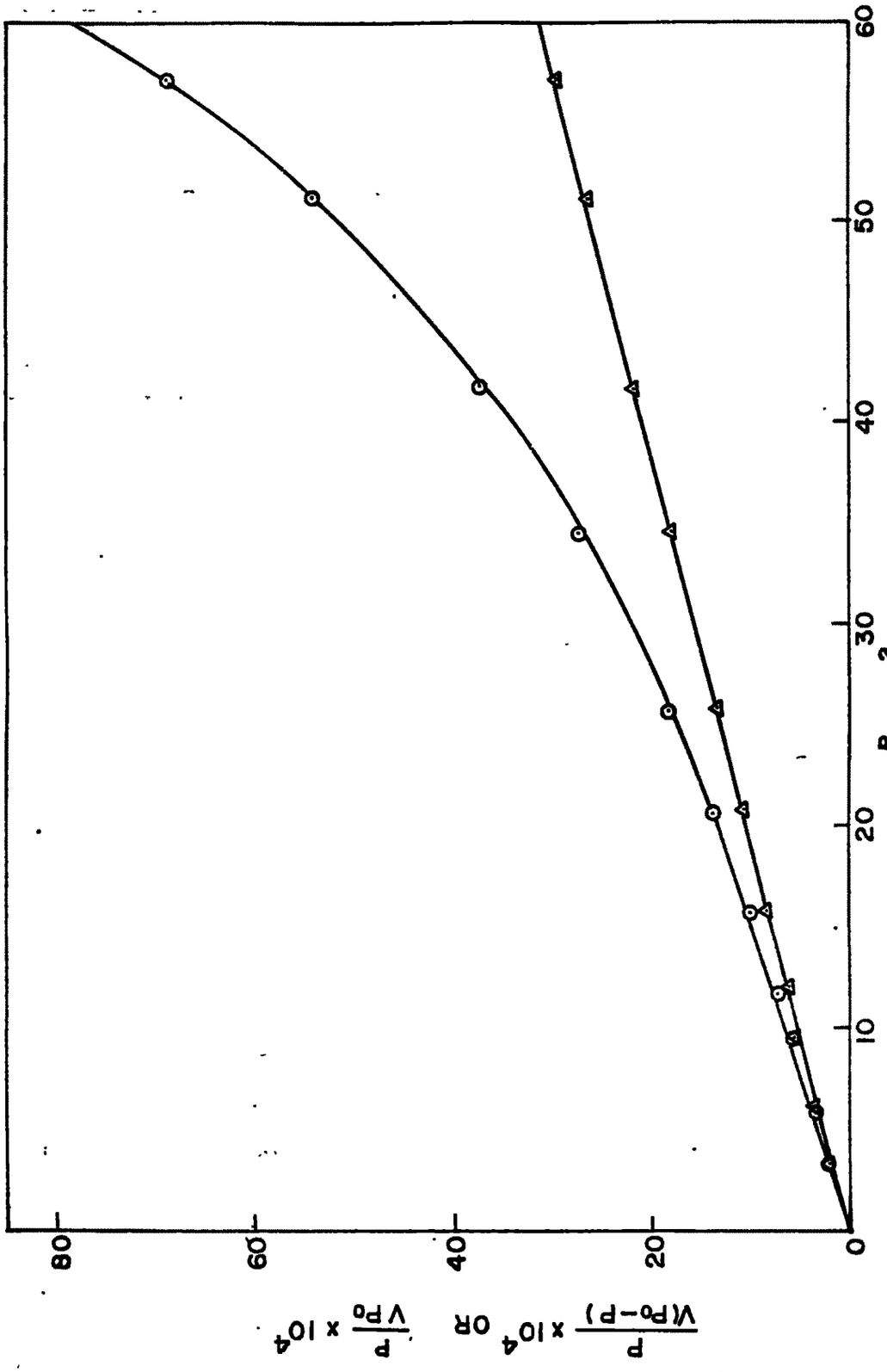

FIG. 2.24 B.E.T. (○) AND LANGMUIR Δ PLOTS FOR NITROGEN SORPTION AT −195°C ON RE(92)Y

been determined from the Langmuir equation and compared with the BET surface area in Table 2.25(a).

(f) Free energy change on sorption

Gibb's free energy (ΔG) has been discussed in previous section [2.7(d)] and in the same way was calculated for all the exchanged Y zeolites as a function of amount of gas adsorbed at $-195^{o}C$. Table 2.25(b) shows a sharp fall in the affinity with increased uptake (Up to a pressure 500 torr) and slow decrease at higher pressure due to multilayer formation and capillary condensation. The affinity sequence for introgen at $-195^{o}C$ for the rare-earth exchanged zeolite is represented as

$$NaY > RE(32)Y > . . . . > RE(92)Y$$

A decrease in affinity with coverage for water has been reported.[61]

(g) Saturation capacity and affinity coefficients

The Dubinin equation[22] has been explained in sections [2.6(f) & 2.7(e)]. The equation was applied for nitrogen sorption at $-195^{o}C$ over rare-earth exchanged Y zeolites. Fig.2.25 shows the plot of log V against $(\log P_o/P)^2$. The saturation values as (molecules/unit cell) evaluated from the intercepts and the constant B are summarized in Table 2.26.

The nitrogen molecules are sorbed only in the α cages, the void volumes obtained from these plots represent the changes in the volume of the super cages brought about by the cation exchange. The data from Table 2.26 indicate that the void volume

Table 2.25(a)

Saturation capacity (nitrogen), surface area and equilibrium sorption of rare-earth exchanged Y zeolites

Zeolites	Saturation capacity (molecules/u.c.)[a]		Surface area (m^2/g)		Sorption(molecules/unit cell)*	
	Langmuir	BET	Langmuir	BET	Water	Benzene
NaY	131.2 (231.5)	120.6 (210.0)	1014	919	228	44.5
RE(32)Y	131.0 (221.2)	120.3 (202.0)	969	885	252	43.1
RE(60)Y	125.2 (209.6)	114.4 (193.0)	918	846	234	42.6
RE(83)Y	121.5 (200.0)	109.2 (182.0)	876	787	225	37.2
RE(92)Y	122.4 (198.4)	110.5 (179.0)	869	785	215	36.4

* Sorption values at 25°C and $P/P_o = 0.5$

a Figures in parenthesis indicate mls/g of zeolite.

Table 2.25(b)

Chemical affinity of rare-earth exchanged Y zeolites for nitrogen sorption at -195°C

NaY		RE(32)Y		RE(60)Y		RE(83)Y		RE(92)Y	
Molecules /u.c.	$-\Delta\mu$ KJ mole^{-1}	Molecules /u.c.	$-\Delta\mu$ KJ mole^{-1}	Molecules /u.c.	$-\Delta\mu$ KJ mole^{-1}	Molecules /u.c.	$-\Delta\mu$ KJ mole^{-1}	Molecules /u.c.	$-\Delta\mu$ KJ mole^{-1}
127.0	2.30	123.6	2.32	118.8	2.32	116.40	2.30	114	2.3
128.0	1.86	125.6	1.86	120.8	1.83	118.20	1.83	115.4	1.86
129.0	1.60	126.4	1.58	121.8	1.58	119.40	1.58	116.20	1.58
129.4	1.40	127.1	1.42	123.0	1.40	120.6	1.38	117	1.40
130.0	1.16	128.0	1.14	123.4	1.20	121.6	1.18	117.50	1.18
131.0	1.00	128.6	0.97	124.4	1.00	122.40	1.00	117.80	1.00
131.6	0.82	129.84	0.82	125.20	0.66	123.00	0.76	118.40	0.80
131.8	0.66	129.8	0.66	125.80	0.56	123.40	0.66	119.20	0.58
132.8	0.38	130	0.44	126.0	0.38	123.70	0.56	119.60	0.38
133.4	0.20	130.8	0.36	126.60	0.24	124.00	0.38	120.2	0.20
133.8	0.14	131.4	0.20	127.80	0.14	124.60	0.20	122	0.10
		133.2	0.14			125.80	0.12		

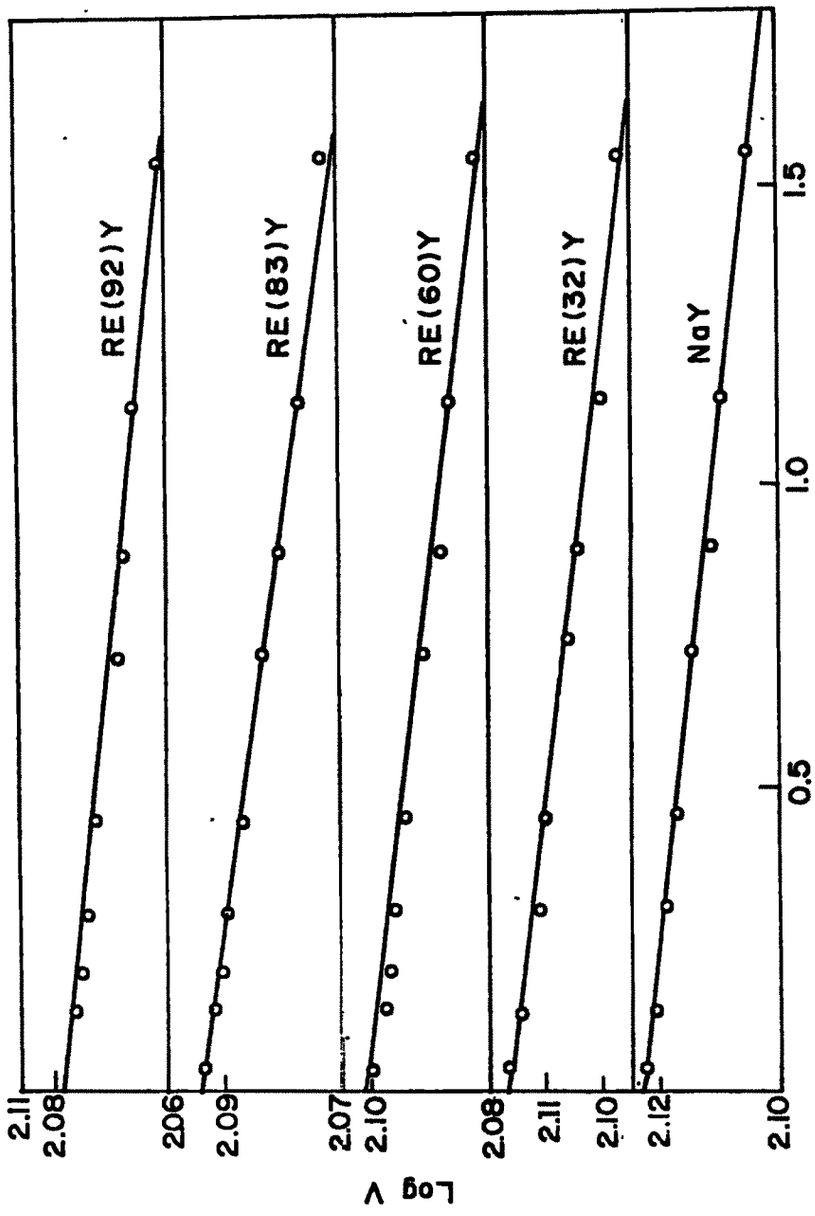

FIG. 2.25 DUBININ PLOTS FOR NITROGEN SORPTION AT-195°C

Table 2.26

Saturation capacity (nitrogen) and affinity coefficients from Dubinin plots at -195°C

Zeolites	a_s molecules/u.c.	void volume mls/gm	$B/\beta^2 \times 10^6$
NaY	132.7	0.35	4.42
RE(32)Y	130.8	0.33	4.93
RE(60)Y	126.0	0.31	4.67
RE(80)Y	124.3	0.31	5.65
RE(92)Y	119.7	0.29	4.23

decreases from 0.355 cc/g in NaY to 0.29 cc/g in RE(92)Y. The data for NaY is consistent with the reported[62] value (0.36 cc/g).

The results indicate that the cavities in the Y type zeolites are modified by cation exchange with RE^{3+} ions and influence the uptake of gases to a considerable extent.

(h) Sorption of water and benzene

The polarity and relatively smaller size are two important characteristics, due to which water molecules are employed as probes for evaluating structural changes in zeolites brought about by cation exchange. On account of the smaller size 2.65A°[24] water molecule can penetrate[61] the smaller voids, the hexagonal prisms and sodalite cages in the zeolite and interact with the cations present therein. Benzene on the other hand, has a larger critical diameter (5-85A°)[24] and is sorbed in the larger cavities super cages (α cages) only. Therefore, from the rate of sorption and equilibrium capacities, the volume of the sorbent surface and also the sorbent-sorbate interaction can be determined.[63]

The sorption kinetics of benzene and water vapours on NaY and RE^{3+} exchanged zeolites are represented in Fig.2.26. The sorption rate and equilibrium sorption capacity for water is highest in NaY and decreases with increasing RE^{3+} exchange. The equilibrium sorption initially increases up to 60% RE^{3+} exchange and falls down with further exchange. The uptake of water follows the sequence

$$NaY < RE(32)Y < RE(60)Y > RE(83)Y > RE(92)Y$$

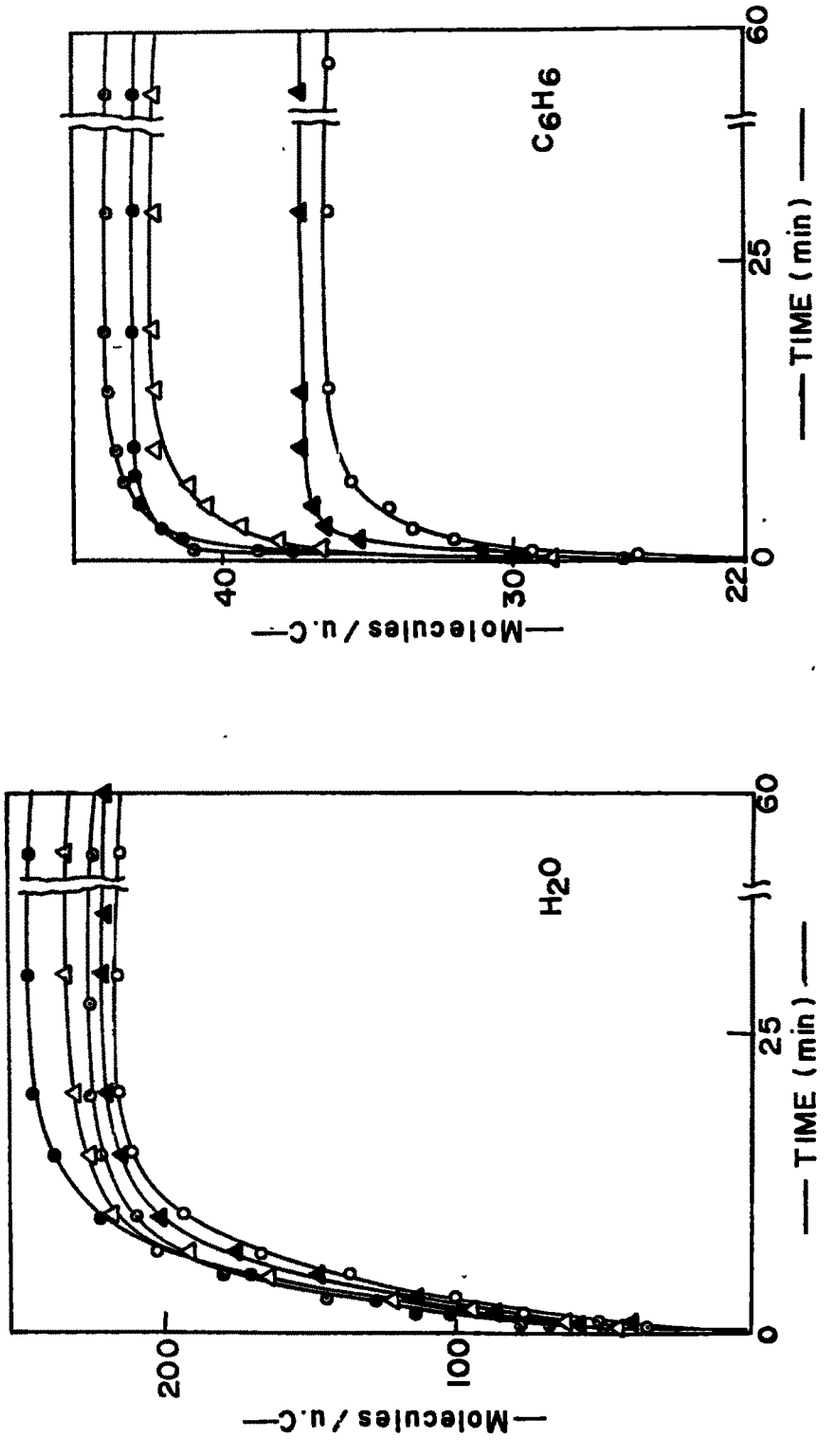

FIG. 2.26 SORPTION KINETICS OF WATER AND BENZENE ⊙—NaY, ●—RE(32)Y
△—RE(60)Y, ▲—RE(83)Y, ○—RE(92)Y

The initial increase in uptake upto 60% RE^{3+} exchange is due to interaction of water molecule with cations occupying comparatively screened positions (S_I',S_{II} and S_{III}'). The reduction in water uptake on further RE^{3+} exchange could possibly be attributed to lattice distortion which is based on the XRD studies discussed earlier. This confirms the earlier work[64] on water vapour sorption on sodium and lanthanum zeolites. Likewise, the uptake of benzene is found to decrease with RE^{3+} content in the Y zeolite. Table 2.26 shows the change in the sorption capacity for water, benzene and nitrogen as a function of RE^{3+} exchange. There is decrease in uptake of N_2, water and benzene on ion exchange with RE^{3+}.

(i) Acidity of rare-earth exchanged Y zeolites

The total acidity of rare-earth exchanged Y zeolites was measured by n-Butylamine titration adopting the following procedure.

The sample of about 1.0 gm was activated in dry air at 400°C in a muffle furnace (heating rate 2°C/min) for 4h. It was closed air tight and placed in a dessicator to cool to ambient temperature. The sample was transferred to a dry conical flask containing 50 ml of benzene (Dried with 3A molecular sieve) as quickly as possible. Three drops of butter yellow (1% solution) were added. The contents were stirred for 10 minutes and total acidity was determined by titration with 0.13m nBA solution. The first titration served to obtain approximate estimate of the total acidity. Subsequently titration was carried out by the

Table 2.27

The composition and acidity of rare-earth exchanged Y zeolites

Zeolite	Unit cell composition	Number of unit cell per gm x 10^{-19}	Mole% RE_2O_3	Acidity m eq/gm
NaY	$Na_{61}(AlO_2)_{58}(SiO_2)_{134}$	4.68	0	0.015
RE(32)Y	$Na_{40}RE_7(AlO_2)_{58}(SiO_2)_{134}$	4.52	0.0260	0.37
RE(60)Y	$Na_{21}RE_{10.5}(AlO_2)_{58}(SiO_2)_{134}$	4.50	0.0425	0.89
RE(83)Y	$Na_{10}RE_{14.7}(AlO_2)_{58}(SiO_2)_{134}$	4.42	0.0582	1.25
RE(92)Y	$Na_5RE_{16.2}(AlO_2)_{58}(SiO_2)_{134}$	4.36	0.066	1.21

addition of 0.25-0.5 millilitre of nBA while watching for a color change and stirring vigorously in a meanwhile using magnetic stirrer. By repeating the titration few times (3-4) a reproducible titre value for the acidity in the sample was obtained.

The acidity was expressed as meq./g of the dry sample. The composition and acidity data is expressed in Table 2.27.

2.11 CONCLUSIONS

(1) The variation of SiO_2/Al_2O_3 ratio of mordenite by dealumination does not influence XRD and IR patterns of mordenite except the intensities of XRD peaks. There is decrease in unit cell volume upon dealumination. The XRD patterns of modified zeolites were found to be similar to parent zeolite and products were crystalline. A decrease in intensities of rare-earth exchanged zeolites was noticed.

The intensity of 820 cm^{-1} bond in IR spectrum of dealuminated mordenites continuously increased with increase in SiO_2/Al_2O_3 ratio.

IR spectra of rare-earth Y zeolites showed the characteristic band become broad, intense and shoulder more sharp and pronounced indicating the stabilization of lattice on cation exchange.

(2) The DTA/TG analyses can be used to estimate the thermal stability as well as number of acid sites of the catalyst

samples.

(3) The sorption of water and hydrocarbons showed that with increase in the SiO_2/Al_2O_3 ratios, the zeolites tend to become more hydrophobic. There is marginal increase in the sorption of benzene, cyclohexane and cumene.

It can be concluded from the nitrogen sorption data that with progressive dealumination non-crystalline material from the channels of the mordenite is removed which in turn increased micropore volume estimated by Dubinin plots. The compounds of modifier species block the channel and effectively reduce the void volume of the catalyst. Result indicates that the cavities of the Y type zeolite are modified by rare-earth exchange and influence the uptake of gases to considerable extent.

(4) TPD of NH_3 leads to the estimation of number and strength of acid sites distribution in the catalyst sample and shows a good correlation with the activity. It may be concluded from the result that dealumination reduces both weak and stronger acid sites. The stable activity of dealuminated mordenite is attributable to the lower number of stronger acid sites.

(5) XPS data showed that on dealumination aluminium concentration in the external layer decreased considerably.

(6) The dealumination has been confirmed by the use of ^{29}Si and ^{27}Al MAS NMR.

-------- 0 --------

REFERENCES

1. P.K. Bajpai, Zeolites 6, 2 (1986).
2. E.J. Rosinski and M.K. Rubin, U.S. Patent 3832 449 Mobil Oil Corp., U.S.A. (1974).
3. R.J. Argauer and G.R. Landolt, U.S. Patent 3702886 (1972).
4. R.M. Barrer and E.V.T. Murphy, J. Chem. Soc.(A) Inorg. Phys. Theor. 2506 (1970).
5. G. Engelhardt, U. Lohse, E. Lippmaa, M. Tarmark and M. Magi, Z. Inorg. Allg. Chem. 482, 49 (1981).
6. D.W. Breck and E.M. Flanigen, "Molecular Sieves", Soc. Chem. Ind. London, p.47 (1968).
7. S. Ueda, T. Fukushima and M. Koizumi, J. Clay. Sci. Jpn. 22, 18 (1982).
8. P. Pichat, R. Beaumont and D. Bartomeuf, Compt. Rendus. Sci. Acad. Sci. C; Chim. 272, 612 (1971).
9. R. Pichat, R. Beaumont and D. Barthomeuf, J. Chem. Soc., Faraday Trans.I 70, 1402 (1974).
10. P. Tarte, Spectrochim. Acta A 23, 2127 (1967).
11. E.M. Flanigen, H.A. Szymanski and H. Khatami, Adv. Chem. Ser.-101, p.201 (1971); E.M. Flanigen in "Zeolite Chemistry and Catalysis", ACS Monograph Vol.171, Am. Chem. Soc., Washington D.C., p.80 (1976).
12. G.T. Kerr, J. Phys. Chem. 71, 4155 (1967).
13. G.H. Kuhl, in Proc. of the IIIth International Conference on Molecular Sieves, p.227 (1973).
14. R.M. Barrer and J. Klinowski, J. Chem. Soc., Faraday Trans.I 71, 690 (1975).

15. B.H. Ha and D. Barthomeuf, J. Chem. Soc., Faraday Trans. I 75, 2366 (1979).

16. A.J. Chandwadkar and S.B. Kulkarni, J. Thermal Anal. 19, 313 (1980).

17. K. Itabashi, T. Fukashima and K. Ge. Igawa, Zeolites 6, 30 (1986).

18. P.E. Eberly, Jr. and C.N. Kimberlin, Jr., Ind. Eng. Chem. Prod. Res. Dev. 9(3), 335 (1970).

19. W.W. Kaeding, L.B. Young, C.C. Chu, B. Weinstein and S.A. Butter, J. Catal. 67, 159 (1981).

20. H.W. Habgood, Canadian J. Chem. 36, 1384 (1958).

21. S. Brunauer, P.H. Emmett and E. Teller, A. Am. Chem. Soc. 60, 309 (1938).

22. M.M. Dubinin, J. Colloid Interface Sci. 23, 487 (1967).

23. R. Le, Van Mao, O. Pilati, A. Marzi, G. Leofanti, A. Vella and V. Ragaini, React. Kinet. Cat. Lett. 15, 293 (1980).

24. D.W. Breck, "Zeolite Molecular Sieves", Structure, Chemistry and Use, Publ. Wiley Interscience, New York, p.636 (1974).

25. R.M. Barrer and D.A. Ibbitson, Trans. Faraday Soc. 40, 206 (1944).

26. E.M. Flanigen, J.M. Bennett, R.W. Grose, J.P. Cohen, R.L. Patton, R.M. Kirchner and J.V. Smith, Nature 1271, 512 (1978).

27. B.L. Meyers, T.H. Fleisch, G.J. Ray, J.T. Miller and J.B. Hall, J. Catal. 110, 82-95 (1988).

28. N.Y. Chen, W.W. Kaeding and F.G. Dwyer, J. Am. Chem. Soc. 101, 6783-84 (1979).

29. P.A. Jacobs, "Carboniogenic Activity of Zeolites", Elsevier Sci., Publ. Co., p. 164 (1977).

30. P.A. Jacobs, "Carboniogenic Activity of Zeolites", Elsevier Sci. Publ. Co., p.33 (1977).

31. P.A. Jacobs, J.A. Martens, J. Weitkamp and H.K. Beyer, Faraday Discussions 72, 353 (1981).

32. J.W. Ward, Chapter 2 "Zeolite Chemistry and Catalysis" (Ed. Rabo, J.A.) ACS Monograph, 171 (1976).

33. P.A. Jacobs and R.V. Ballmoos, J. Phys. Chem. 86, 3050 (1982).

34. E.G. Derouane, B. Imelik et. al. (Editors), "Catalysis by Zeolites", p.5 (1980).

35. N. Topsøe, K. Pederson and E.G. Derouane, J. Catal. 70, 41 (1981).

36. J.R. Anderson, K. Foger, T. Mole, R.A. Rajadhyaksha and J.V. Sanders, J. Catal. 58, 114 (1979).

37. G.P. Babu, S.G. Hegde, S.B. Kulkarni and P. Ratnasamy, J. Catal. 81, 471-477 (1983).

38. K.H. Chandawar, S.B. Kulkarni and P. Ratnasamy, Appl. Catal. 4, 287-295 (1982).

39. C.D. Wagner, Anal. Chem. 44, 1052 (1972).

40. P. Alnot and J. Oliver, J. Electron Spectroscopy and Related Phenomena 49, 159-173 (1989).

41. M. Sawa, M. Niwa and Y. Murakami, Appl. Catal. 53, 169-181 (1989).

42. P. Bodart, J.B. Nagy, G. Debras, Z. Gabelica and P.A. Jacobs, J. Phys. Chem. 90, 5183 (1986).

43. G. Debras, J. Nagy, Z. Gabelica, P. Bodart and P.A. Jacobs, Chem. Lett. 199 (1983).

44. G.R. Hays, W.A. Van Erp. N.C.M. Alma, P.A. Couperus, R. Husi and A.E. Wilson, Zeolites 4, 377 (1984).

45. C.A. Fyfe, G.C. Gobbi, J.S. Hartman, J. Klinowski and J.M. Thomas, J. Phys. Chem. 86, 1247 (1982).

46a. A. Erdem and L.B. Sand, J. Catal. 60, 241 (1979).

46b. M. Ghamami and L.B. Sand, Zeolites 3, 155 (1983).

46c. H. Nakamoto and H. Takahashi, Chem. Letters, 1739 (1981).

46d. V.P. Shiralkar and S.B. Kulkarni, Z. Phys. Chemie, Leipzig 265, 2, s.313-320 (1984).

47. J. Hopper, Ph.D. Thesis, Louisiana State University and Agricultural and Medical Engineering College, p.335, University Microfilms, Inc. Ann. Arbor. Michigan (1969).

48. J.W. Ward, J. Catal. 26, 451 (1972).

49. D.H. Olson and H.S. Sherry, J. Phy. Chem. 72, 4095 (1968).

50. D. Ballivet, P. Pichat and D. Barthomeuf, "Molecular Sieves-II", Advan. Chem. Ser. 121, Am. Chem. Soc., Washington D.C., p.469 (1973).

51. J. Scherzer, J.L. Bass and F.D. Hunter, J. Phy. Chem. 79, 1194, 1200 (1975).

52. A.A. Kubasov, K.V. Topchieva and R.N. Ratov, Russ. J. Phy. Chem. 47, 1023 (1973).

53. B.V. Romanovskii, Russ. J. Phy. Chem. 45, 270 (1970).

54. F. Paulick, J. Paulick and L. Erdey, Talanta 13, 1405 (1966).

55. B. Coughlan and S. Kilmartin, J. Chem. Soc., Far. Trans.I 71, 1809 (1975).

56. J.V. Smith, J.M. Bennett and E.M. Flanigan, Nature 215, 241 (1967).

57. Ref. 24, pp.460-482.

58. F.D. Hunter and J. Scherzer, J. Catal. 20, 246 (1971).

59. A.H. Badran, J. Dwyer, N.P. Evmerides and J.A. Manford, Inorg. Chim. Acta 21, 61 (1977).

60. D.W. Breck, U.S. Pat. 3130 007 (1964).

61. R.M. Barrer and B.E.F. Fe der, J. Phys. Chem. Solids 21, 1 (1961).

62. D.W. Breck, J. Chem. Education 41, 678 (1964).

63. R.M. Barrer and G.C. Bratt, J. Phys. Chem. Solids 12, 130, 146 (1959).

64. G.V. Tsitsishvili and T.G. Andronikashvili, "Molecular Sive Zeolites-II", Advan. Chem. Ser. 102, Am. Chem. Soc., Washington D.C., p.217 (1971).

****

CHAPTER - 3

STUDIES ON PROPYLATION OF BENZENE

****

3.1 INTRODUCTION

Isopropylbenzene (cumeme) the precursor for phenol, is produced using solid phosphoric acid catalyst by alkylation of benzene with propylene. But there are limitations in the use of this catalyst for cumene process like

1) The catalyst cannot be regenerated.
2) The moisture content has to be regulated precisely to avoid leaching and deactivation of the catalyst.
3) Transalkylation of diisopropylbenzene (formed to an extent of 5% wt) with benzene cannot be carried out and
4) environmental problems associated with the disposal of phosphoric acid sludge.

In view of these limitations there are world wide efforts to find an alternate catalyst system preferably zeolite based for this process. In the following sections studies on propylation of benzene using mordenite based catalysts is described.

3.2 PROPYLATION OF BENZENE OVER MORDENITE

(a) Materials: Benzene and isopropanol were high purity reagents and were used without further purification. Propylene containing 2.7% propane was used.

(b) Procedure: The catalytic alkylation reactions were carried out at atmospheric pressure using a fixed bed, down flow integral reactor. The zeolite H-mordenite (HM) (2g, 10-20 mesh particles) was loaded in a silica reactor, and was first activated in dry

air at 450-500°C for 8 h^{1} and cooled to reaction temperature in the flow of dry nitrogen. Benzene was fed from the top using a syringe feed pump (Model 352, Sage Instrument Co., USA) while propylene was metered through mass-flow controller (Matheson, USA), vaporised in a preheater assembly packed with inert material and then passed through catalyst bed. A schematic diagram of the experimental set up is shown in Fig.3.1. The reaction temperature was maintained constant through the catalyst bed. All temperatures were recorded with a centrally placed calibrated chromel-alumel thermocouple. The vapour from the reactor was cooled by passing through chilled water condensers and analysed at regular intervals using a Shimadzu gas chromatograph (Model GC R1A) fitted with an Apiezone L column and an FID detector. Gaseous products were analysed using a poropak Q column. The analysis conditions are given below.

Instrument : Shimadzu G.C.

Detector (FID) temperature : 175°C (for condensible liquids)

: 100°C (for gaseous products)

Carrier gas (N_2) flow rate : 25 mls/min

Column	Conditions	Product analysed
Apeizon-L (250) (1/8)" ID x 2 m	125°C Isothermal	C_5^+ hydrocarbons
Poropak Q (1/8)" ID x 6'	100°C, 10 minutes programmed at 10°C min^{-1} to 150°C held for 25 minutes	Gaseous products and aqueous layers

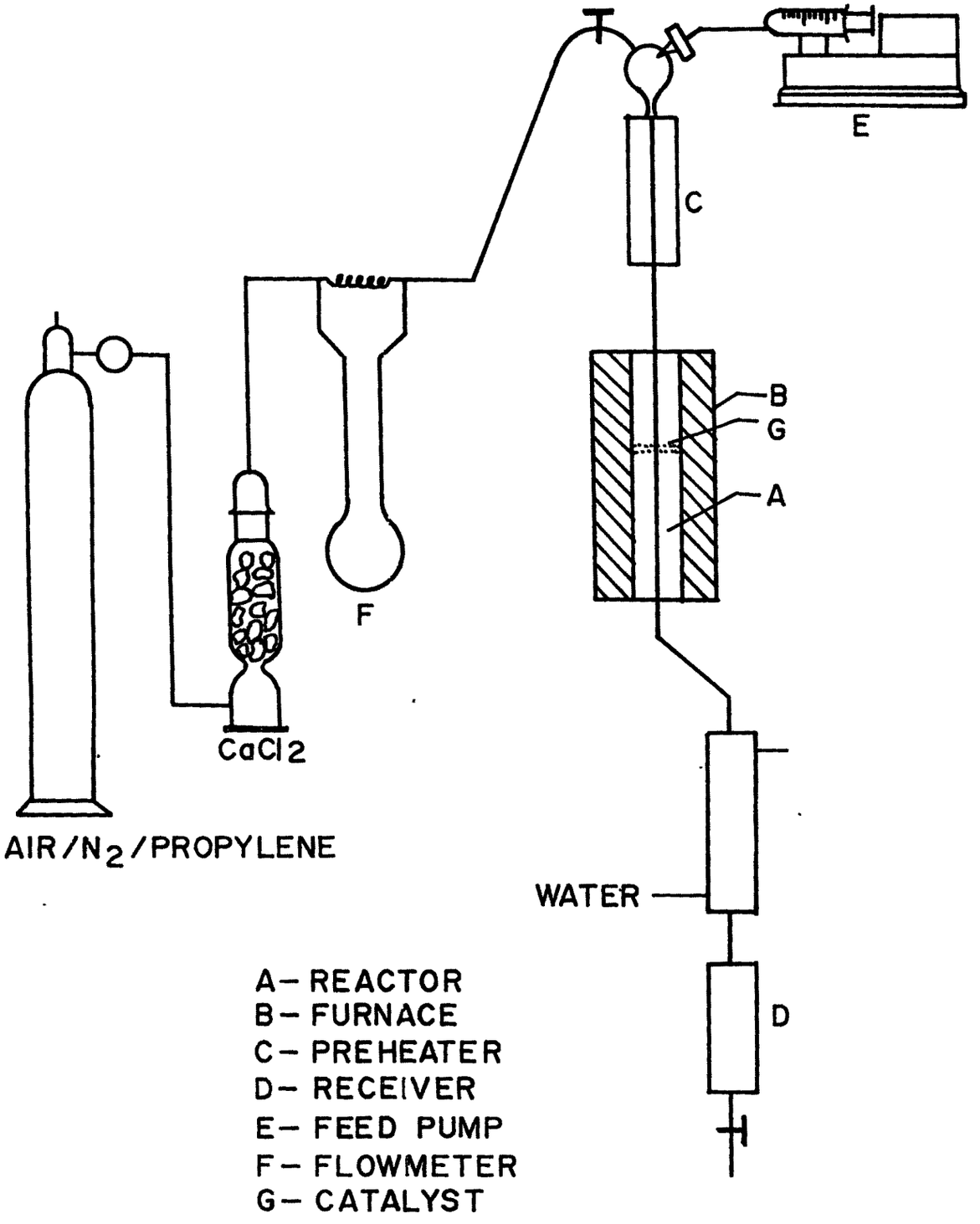

FIG. 3.1 SILICA REACTOR USED FOR CATALYTIC REACTIONS

A typical chromatogram is shown in Fig.3.2. The reproducibility of data was about ± 0.3%.

High pressure reactions were carried out in a "catatest" unit (Geomechanique, Model B, France) shown in Fig.3.3. The stainless steel reactor was used both as a preheater and a reactor. The reactor had an internal diameter (I.D.) of 1.8 cms, with centered thermowell of 0.6 cm diameter. The reactor was provided with four thermocouples for measuring temperatures at four different points in the reactor. The catalyst in the form of extrudates (1/16)" dia (made using alumina binder in equal weight proportion of H-mordenite) was loaded in the middle of the reactor. The top as well as bottom portions were filled with inert alumina balls of 2-3 mm diameter. The catalyst was activated following the procedure described above for the atmospheric pressure reaction. The reaction mixture (Benzene + isopropanol/propylene) was fed by a metering pump into the vaporiser and passed through the catalyst bed. The reaction products from the reactor were cooled in chilled water condenser and collected in a high pressure separator where gaseous and liquid products were separated. The products were collected periodically and analysed by gas chromatography as described above. All calculations were made on the basis of propylene conversion. The percentage conversion and selectivity to isopropylbenzene are defined as follows:

i) Conversion of propylene to isopropylbenzene (cumene) % = $\frac{\text{Moles of isopropylbenzene produced}}{\text{Moles of propylene fed}}$ x100

ii) Σ Alkylates (α) % = Summation of propylene conversion to IPB, nPB and DIPB.

iii) Selectivity to cumene = $\frac{\text{Propylene conversion to IPB}}{\Sigma \text{ Alkylates } (\alpha)}$

iv) Selectivity of IPB between IPB and nPB = $\frac{\text{IPB}}{\text{IPB + nPB}} \times 100$

v) $\frac{\text{DIPB}}{\text{IPB}} \times 100$ = Ratio of moles of DIPB to moles of IPB obtained multiplied by 100

vi) Weight hourly space velocity ($g.\ g^{-1}\ h^{-1}$) = $\frac{\text{Weight in grams of the reactant mixture passed per hour}}{\text{Weight in grams of the catalyst}}$

vii) Contact time (W/F) hr = $\frac{1}{\text{Weight hourly space velocity}}$

viii) TON Turn over number = Number of molecules of benzene converted/u.c./sec.

ix) Yield % = $\frac{\text{IPB obtained}}{100 - \text{Benzene}} \times \text{Total propylene conversion}$

3.3 RESULTS AND DISCUSSION

In the propylation of benzene the major products were isopropylbenzene and diisopropylbenzenes. Small amounts of toluene, xylenes, ethyltoluene, ethylbenzene, n-propylbenzene and butylbenzene were also formed. Polypropylated benzenes (tri and above) were formed only in very small quantities depending on the mole ratio of feed. The relative concentration of the secondary products was dependent on the experimental conditions. For convenient representation, the products other than isopropylbenzene, n-propylbenzene and diisopropylbenzene have

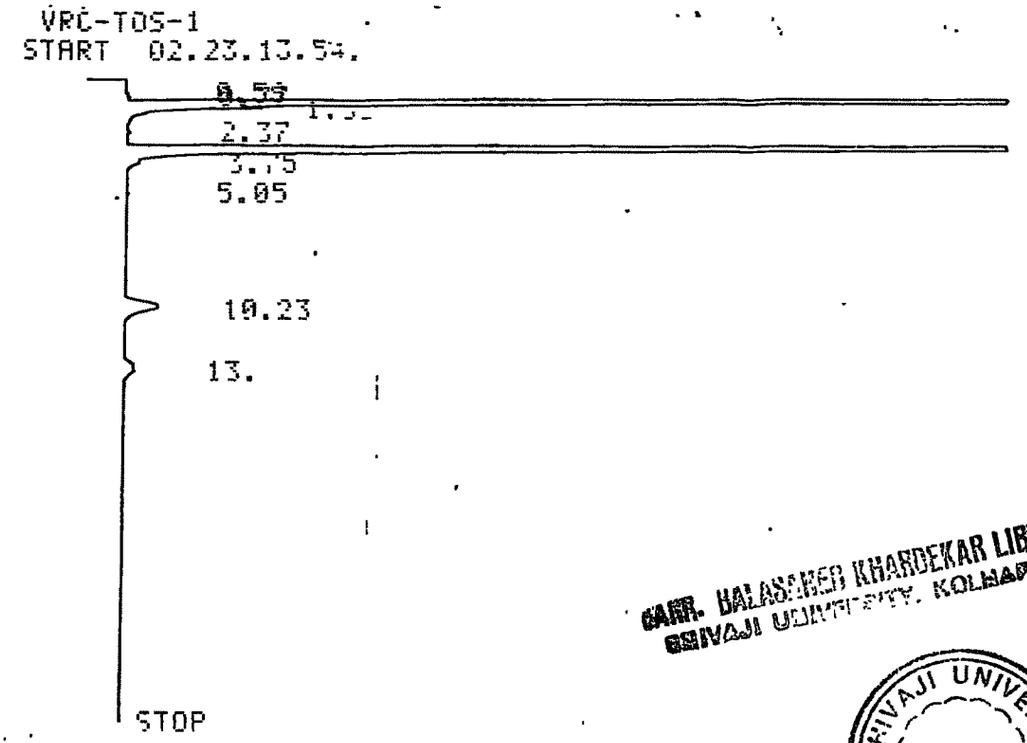

GC-R1A
SMPL # 00
FILE # 5
PEPT # 524
METHOD 41

#	NAME	TIME	CONC	MK	AREA
0		0.77	0.0069	V	490
0		1.02	83.7612	E	5914743
0		1.33	0.0846	T	5979
0		2.37	0.0163		1155
0		3.16	15.2635		1077823
0		3.75	0.0119	T	840
0		5.05	0.0091		648
0		10.23	0.5883		41542
0		13.	0.2578		18210
	TOTAL		99.9499		7061432

FIG. 3.2 A TYPICAL CHROMATOGRAM OBTAINED BY ANALYSIS OF THE REACTION PRODUCTS IN ISOPROPYLATION OF BENZENE.
THE MAIN PRODUCTS ARE BENZENE (RETENTION TIME, tr = 1.02), ISOPROPYL BENZENE (tr = 3.18), n-PROPYL-BENZENE (tr = 3.75), 1,3, DIISOPROPYL BENZENE (tr = 10.23), 1,4 DIISOPROPYL BENZENE (tr = 13.0)

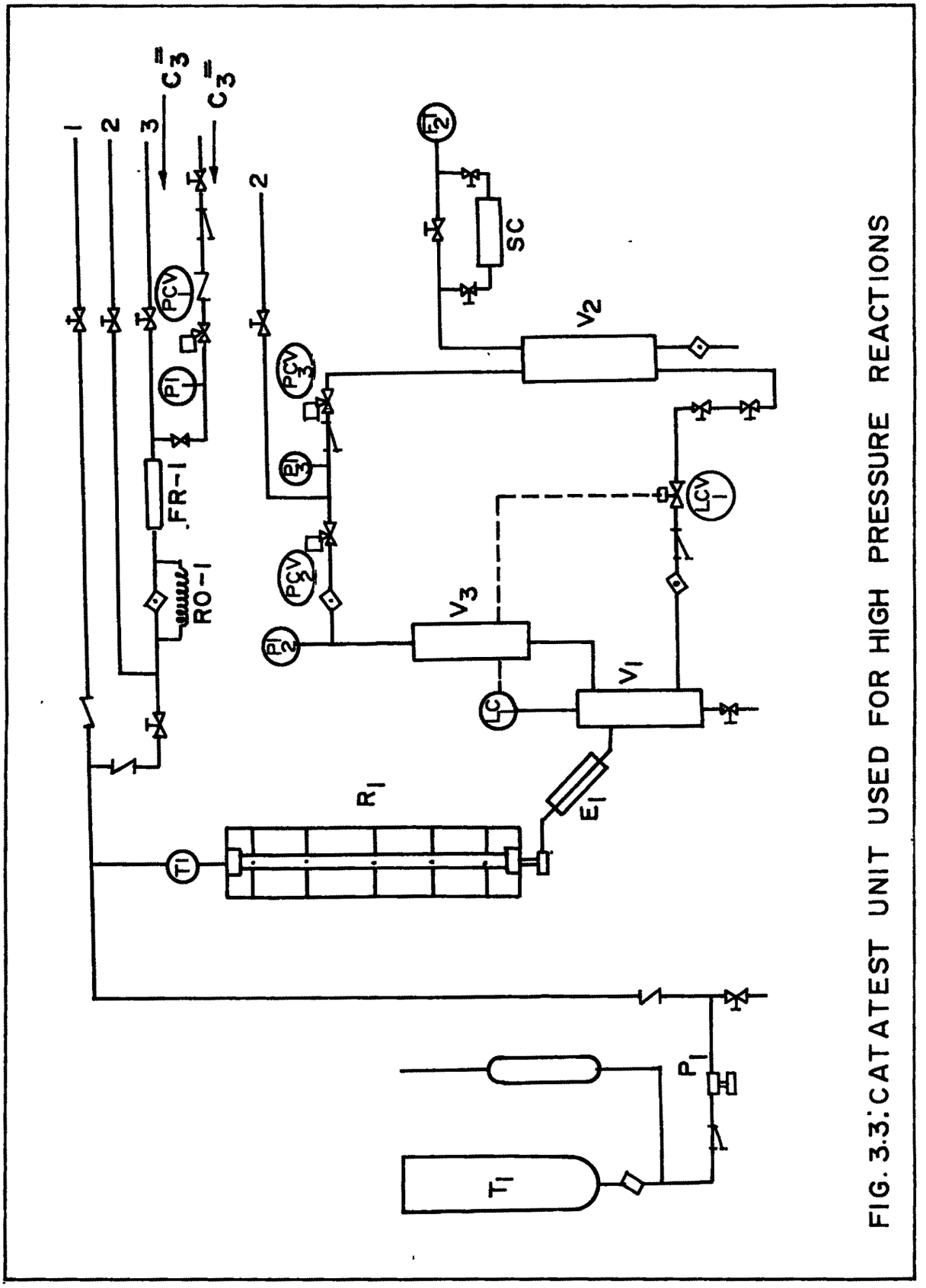

FIG. 3.3: CATATEST UNIT USED FOR HIGH PRESSURE REACTIONS

DESCRIPTION OF THE PARTS OF CATATEST UNIT

T_1	-	Feed Reservoir
P_1	-	Feed Pump
R_1	-	Reactor
E_1	-	Condenser
V_1	-	High Pressure Separator
V_2	-	Product Separator
V_3	-	Uncondensed Gas
LC	-	Level Controller
LCV	-	Level Controlling Valve
TC	-	Thermocouple
PCV	-	Pressure Control Valve
PI	-	Pressure Indicator
SC	-	Gas Sampling Column
FT	-	Wet Flow Meter
RO	-	Capillary
RI	-	Gas Flow Meter
	-	One-way Valve
TI	-	Temperature Indicator
RC	-	Recycle

been grouped into C_8, C_9-C_{11} and HBF (Higher boiling fractions) aromatics, C_8 representing xylenes, ethylbenzene, C_9 aromatics constituting of ethyltoluenes, C_{10}-C_{11} aromatics constituting of those boiling above diethylbenzenes.

A. Influence of Calcination Temperature

The experimental data of the runs carried out at various calcination temperatures but at constant space velocity, reactant mole ratio and reaction temperature is presented in Table 3.1. All the runs were carried at ambient pressure. It is seen that (i) conversion of propylene to alkylbenzenes is maximum at 480°C and it drops at higher calcination temperature. (ii) Yield of n-propylbenzene is maximum at 400°C. Further, a decrease in the concentration of aliphatics and other impurities like toluene and C_8 aromatics is observed. The reduction in activity may be attributed to the effect of calcination temperature on acidity. The thermoanalytical studies indicated decrease in the number of acidic OH groups per unit cell with increase in temperature of calcination (Table 3.2). In zeolites like faujasites and mordenites dehydroxylation causes conversion of Brönsted acid sites to Lewis acid sites. Karge[2] reported the existence of Brönsted and Lewis acid sites even below 450°C but above this temperature Brönsted sites are converted to Lewis sites. Since alkylation reaction need Brönsted acidity the reduction in activity can be correlated with the reduction in Brönsted acid sites upon dehydroxylation.

Above 900°C about 60% loss of acidic OH groups was noticed. XRD analysis of the samples calcined at different temperatures

Table 3.1

Influence of Calcination Temperature on Alkylation Activity
Catalyst: HM. Reaction temp.(°C) = 210
(Benzene: Isopropanol) mole=8, WHSV(h^{-1}) = 2.2

Calcination temp.(°C)	400	480	560	640	720	800
Product weight %						
Aliphatics	0.13	0.11	0.11	1.28	1.42	2.3
Benzene	83.59	82.01	83.67	85.76	86.06	88.17
Toluene	0.08	0.09	0.06	0.04	0.03	-
C_8 Aromatics	0.06	0.05	0.03	0.01	-	-
Cumene	14.92	16.42	14.56	11.85	8.43	6.51
n-propylbenzene	0.55	0.49	0.28	-	-	-
C_9-C_{11} Aromatics	0.03	0.03	0.01	0.02	-	-
DIPB (m)	0.42	0.50	0.44	0.65	2.62	1.44
(o)	-	-	-	-	-	-
(p)	0.22	0.24	0.21	0.29	1.33	1.44
ΣDIPB	0.64	0.75	0.65	0.94	3.95	2.88
HBF	0.06	0.05	0.01	0.09	0.11	0.13
ΣAlkylates (α)%	91.12	99.9	87.7	73.48	79.25	59.8
Selectivity to IPB%	90.8	91.2	92.14	89.5	59.03	60.4

Table 3.2

Thermogravimetric data of H-mordenite zeolite*

Calcination temperature °C	Percent weight loss[a]		Loss of OH group per u.c.
	Total	Dehydroxylation (T-400)°C	
560	14.8	0.4	1.29
680	15.0	0.6	1.93
850	15.35	0.95	3.06
930	15.42	1.02	3.29
1000	15.60	1.2	3.87

* Calculated from TG curve of Fig.2.4b

a Weight loss due to dehydration (At 400°C) = 14.4%

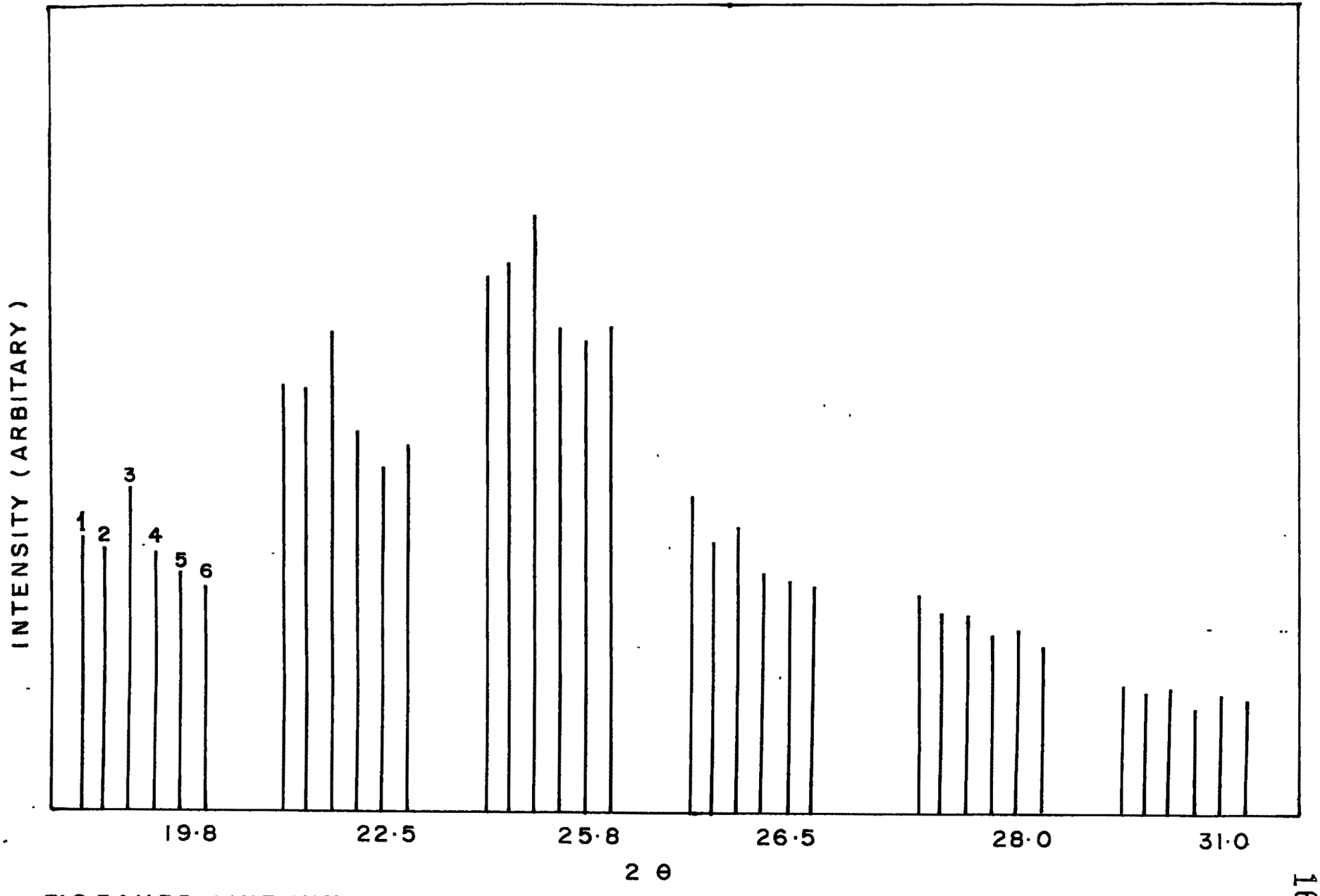

FIG.3.4-XRD LINE INTENSITY OF H-MORDENITE (Si/Al=27) CALCINED AT DIFFERENT TEMPERATURE (°C). 1) T-400, 2) T-480, 3) T-550, 4) T-640, 5) T-720, 6) T-800

(Fig.3.4) indicated complete crystallinity of the zeolite up to 700°C and above that a drop in crystallinity up to 20% was noticed. From these observations it is indicated that with increase in the calcination temperature there is a continuous decrease in the number of acidic hydroxyl groups leading to the decrease in Brönsted acidity needed for alkylation. The optimum calcination temperature was observed in the range of 460-500°C.

B. Influence of Reaction Temperature

The data on the influence of reaction temperature on product distribution is shown in Table 3.3. It is seen that the optimum temperature to produce highest yield of isopropylbenzene at lower content of n-propylbenzene (which is undesirable) lies in the range of 210-215°C. At lower than 210°C, the liquid hydrocarbon product consisted of significant amounts of diisopropylbenzene and polyalkylated products. With the increase in temperature the concentration of isopropylbenzene decreases due to dealkylation and disproportionation of alkylated products resulting in the lower yield and selectivity to isopropylbenzene. Above 230°C the concentration of xylenes and to a lesser degree that of toluene increases. Also increased npB concentration was noticed at higher temperature.

At temperatures below 185°C, the catalyst was found to undergo rapid deactivation within 4-5 h due to blocking of the active sites by strongly chemisorbed organic molecules having low mobility. In the runs carried out above 215°C, no significant change in product distribution was observed for more than 10 h.

Table 3.3

Alkylation of Benzene with Isopropanol over H-Mordenite

Influence of temperature
(Benzene: Isopropanol) mole = 7.32, WHSV (h^{-1}) = 2.2

Temperature (^{o}C)	150	185	215	230	250	275	300
Product weight %							
Aliphatics	0.4	0.48	0.31	0.32	0.11	0.32	0.80
Benzene	90.86	86.5	82.8	83.0	84.4	87.0	91.1
Toluene	-	-	-	0.03	0.06	0.18	0.45
C_8 Aromatics	-	-	0.02	0.08	0.22	0.54	0.87
Cumene (IPB)	5.66	7.4	15.1	15.6	13.75	9.84	4.40
n-propylbenzene	0.01	0.02	0.02	0.14	0.65	1.4	2.06
C_9-C_{11} Aromatics	-	-	0.01	0.04	0.11	0.32	-
DIPB	2.96	5.6	1.72	0.80	0.63	0.32	0.34
HBF	-	-	0.06	0.01	0.04	0.13	-
≥Alkylates(α) %	51.36	80.28	90.23	86.43	78.34	59.82	35.56
iproH---> Propylbenzenes	28.95	37.89	77.21	80.38	73.54	57.40	32.99
Composition (%)							
Isopropylbenzene	99.82	99.73	99.87	99.11	95.48	87.54	68.11
n-propylbenzene	0.18	0.27	0.13	0.89	4.52	12.46	31.89

In all these experiments conversion of isopropanol is complete. After an average of 10 h reaction, the catalyst was regenerated at 500^{o}C using air (for 12 h) and the reproducibility of the catalytic activity was checked.

C. Influence of Space Velocity (WHSV)

Influence of weight hourly space velocity at constant reaction temperature and reactant mole ratio on product distribution is illustrated in Fig.3.5. The figure indicates that increase in space velocity or decrease in contact time (W/F) influences the product pattern. At very low space velocities the selectivities to isopropylbenzene (cumene) is very high around 95-98% with very low diisopropylbenzene formation. At higher space velocities the diisopropylbenzene formation is very high and conversion is reduced. This is due to higher concentration of the reactants near the active sites. Even at higher residence times or low space velocities side products like toluene, n-propylbenzene and xylenes are less.

D. Influence of Benzene to Isopropanol Mole Ratio on Product Distribution

Fig.3.6 illustrates the amount of isopropanol converted to propylbenzenes and selectivity to IPB with varying Benzene to isopropanol mole ratios at constant temperature and velocity.

It is seen that with increase in the mole ratio selective conversion to cumene occurs. At lower mole ratios the formation of diisopropylbenzene is higher which is due to successive

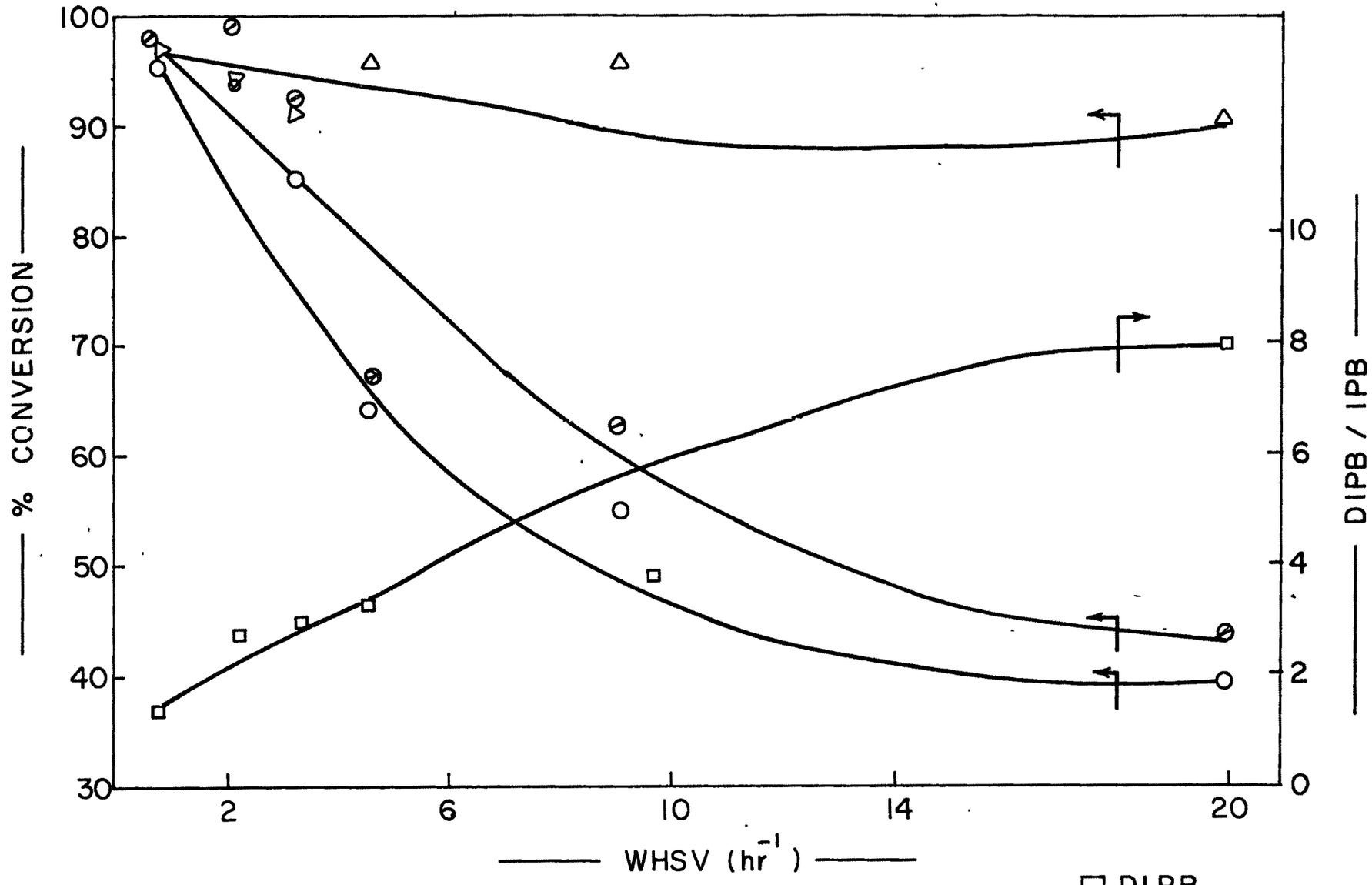

FIG.3·5 INFLUENCE OF WHSV ON PROPYLENE CONVERSION
CAT : HMORDENITE, MR : 8 (Bz : ISOPROPANOL). TEMP. 210 (°C)

FIG 3·6: EFFECT OF REACTANT MOLE RATIO ON PROP. CONVERSION

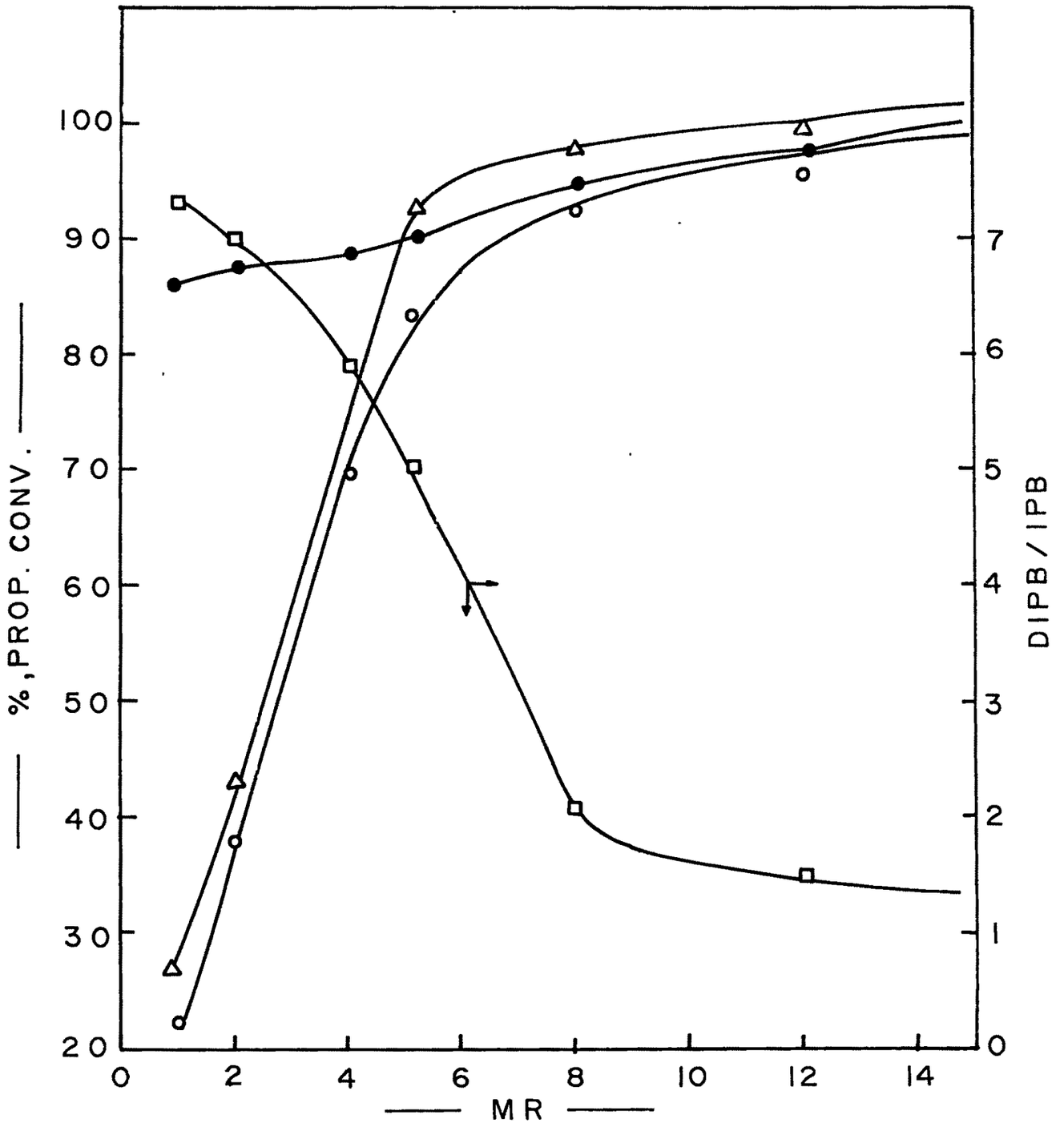

TEMP : 210 °C , WHSV = 2·2 hv^{-1}, PRESS = Atm.

alkylation of monoalkylated IPB. As the concentration of reactants (In particular, of propylene) is higher near the active sites, overall selectivity and conversion are low at low mole ratios. At higher mole ratios the low propylene concentration at active sites selectively produces IPB with very low diisopropylbenzene formation. Other impurities like npB and xylenes are also not noticeable at higher ratios. Even though water is formed as one of the products when isopropanol is used as an alkylating agent, the deactivation is less to that of alkylating with propylene.

Alkylation of benzene with propylene with varying mole ratio of the reactant mixture is shown in Fig.3.7. Although the product pattern is similar as in the case of isporopanol, the temperature needed for the same conversion level is lower. However, the fast deactivation of the catalyst was observed due to oligomerisation of propylene.

E. Influence of Pressure on the Alkylation Activity

Pressure has marked influence on the reaction when propylene is used as an alkylating agent. This is due to the law of mass action. At higher pressures rate of reaction increases but in this particular reaction higher pressure are advantageous as benzene remains in liquid state above 25 kg/cm^2 at 210^oC. This helps washing of the pores by the liquid leading to longer life of the catalyst. The pressure below 25 kg/cm^2 has marked influence on the product pattern leading to the formation of side products. When isopropanol is used as an alkylating agent, even

FIG 3·7: EFFECT OF BENZENE / PROPYLENE MOLAR RATIO ON CONVERSION

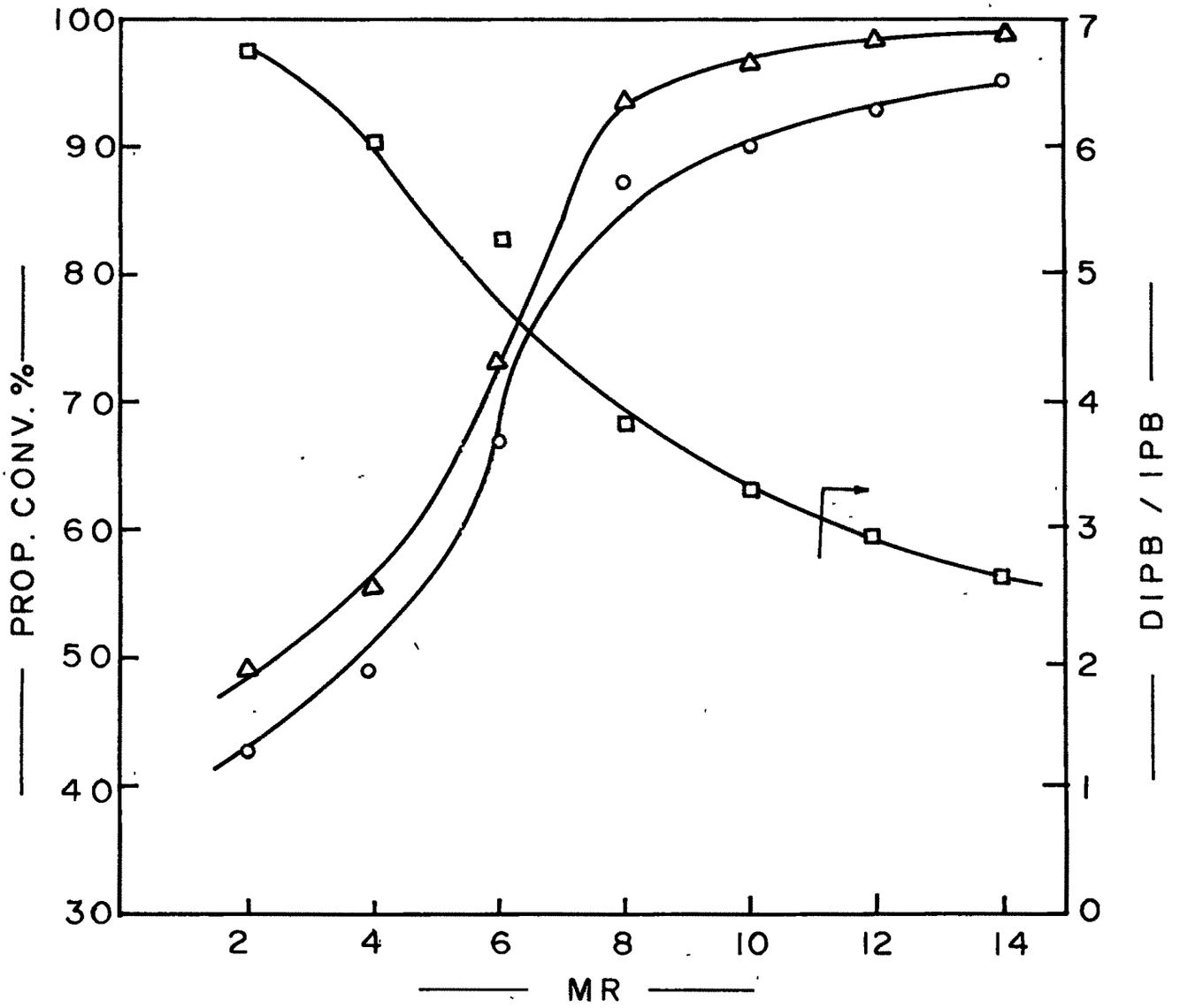

o PROP. CONV. TO CUMENE Δ Σ ALKYLATES (∝)

□ $\frac{DIPB}{IPB}$ x 100

TEMP.: 173 °C, WHSV = 2·2 hr^{-1}, PRESS = Atm.

though pressure has no influence still the product pattern is same as that of propylene. With increase in pressure with both the feeds, the concentration of diisopropylbenzene is increased. Total alkylates also increased with increase in pressure. The conversion of isopropanol/propylene is higher at atmospheric pressure. These are due to the rate of reaction being higher in the gas phase than in the liquid phase. The latter being controlled by diffusion effects. Fig.3.8 represents influence of pressure on alkylation activity.

F. Influence of Time on Stream

An experiment of longer duration was carried out to determine the degree to which ordinary coke deposition would affect the product distribution and conversion of alcohol during propylation of benzene with isopropanol. Experiments were carried out at 210°C, benzene to isopropanol mole ratio 8 and maintaining WHSV at 2.2 (h^{-1}) for more than 100 h. These particular experiments were carried out with mordenites having SiO_2/Al_2O_3 molar ratio 13 and 147. Fig.3.9 and Table 3.4 show the product distribution as a function of time in (h). From the figure it is seen that the catalytic activity drops in case of lower SiO_2/Al_2O_3 ratio over a period of 10-15 h whereas catalyst with higher SiO_2/Al_2O_3 ratio did not show considerable drop in activity over a period of 100 h. The stable activity is due to the lower number of active sites. A catalyst like mordenite with SiO_2/Al_2O_3 ratio 13 has considerable acid centres. Molecules like cumene and benzene are strongly adsorbed on these acid centres. The mobility of these ions decreases due to strong chemisorption.

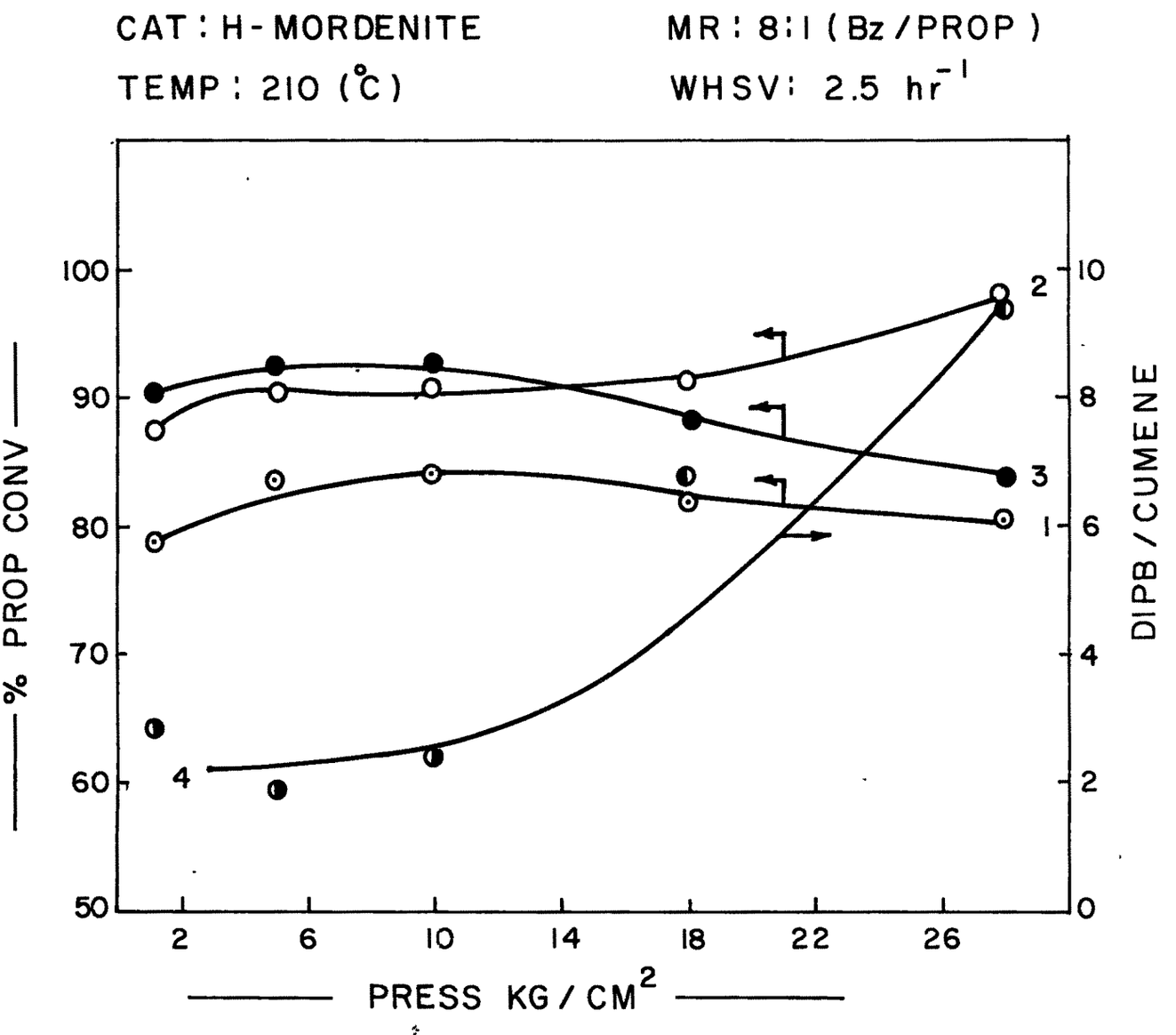

1: PROP CONV TO CUMENE 2: Σ ALKYLATES (α)

3: PROPCONV TO CUMENE / Σ ALKYLATES (α)

4: DIPB / CUMENE

FIG .3·8 INFLUENCE OF PRESSURE ON ALKYLATION ACTIVITY.

FIG 3-9 : EFFECT OF TOS ON ALKYLATION ACTIVITY

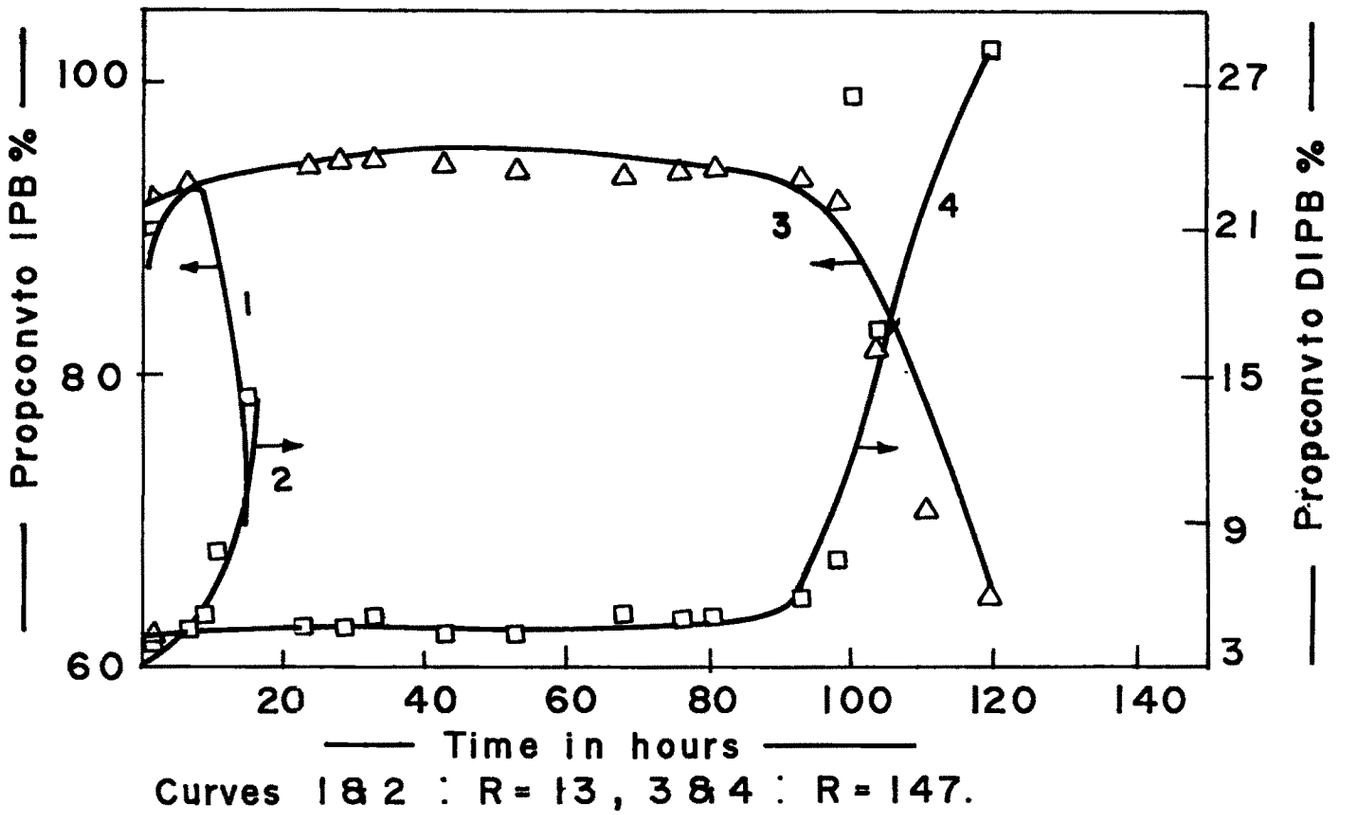

Curves 1 & 2 : R = 13 , 3 & 4 : R = 147.

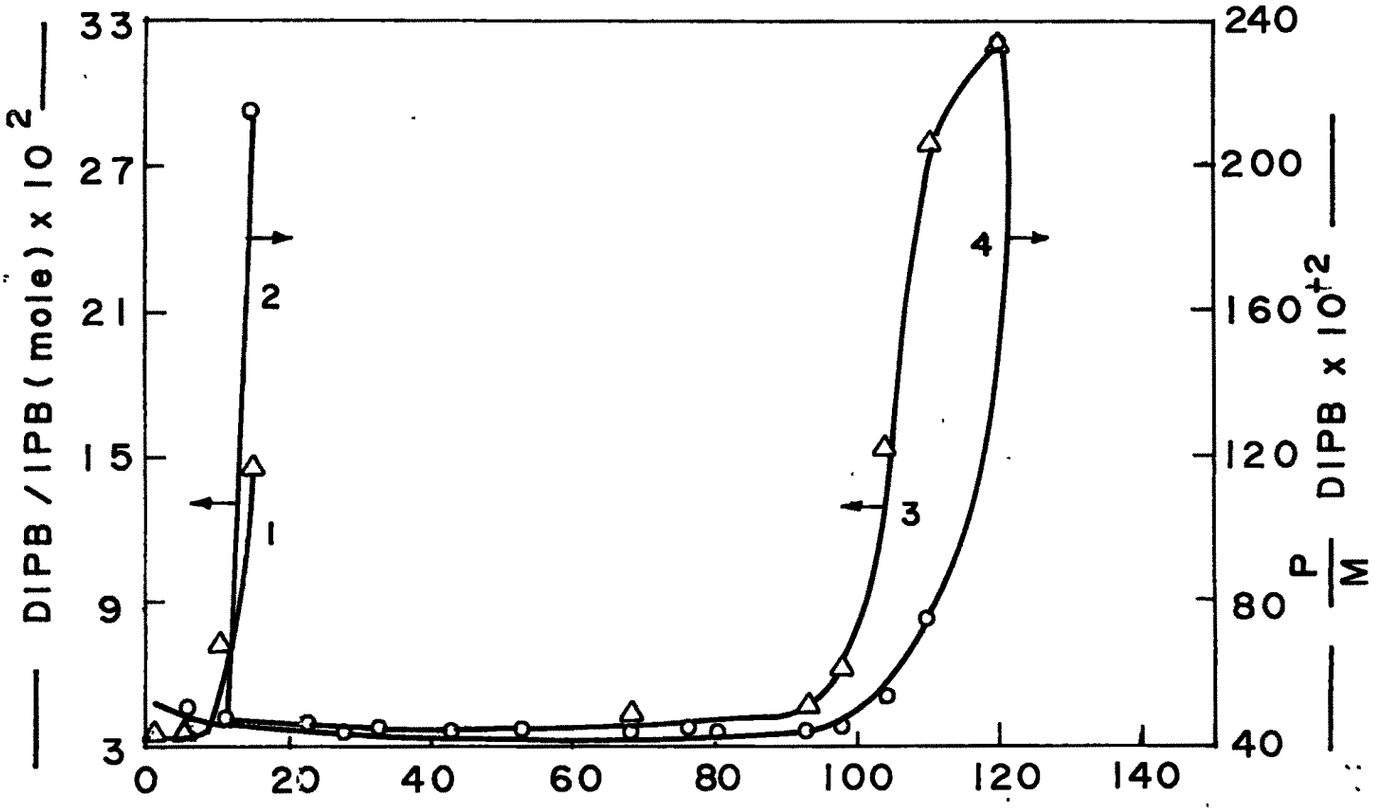

Curves 1 & 2 : R = 13 , 3 & 4 : R = 147

Table 3.4

Influence of Time on Stream on Product Distribution over Mordenite Catalysts

Temperature ^{o}C = 210, (Benzene: Isopropanol) mole = 8, WHSV (h^{-1}) = 2.2

CATALYST	SiO_2/Al_2O_3 = 13					SiO_2/Al_2O_3 = 147						
TOS (hr)	1	3	8	10	15	1	10	28	53	80	104	120
Product weight %												
Aliphatics	0.03	0.06	0.06	0.07	0.88	0.90	0.89	0.92	0.87	0.83	0.70	0.41
Benzene	82.79	82.02	82.56	84.44	94.15	81.9	81.84	81.76	82.55	83.53	84.08	92.78
Toluene	0.03	0.02	0.02	-	-	0.08	0.08	0.10	0.09	0.06	0.06	0.07
C_8 Aromatics	0.10	0.08	0.07	0.02	0.02	0.05	0.06	0.02	0.02	0.01	0.01	-
Cumene	15.37	16.3	15.9	13.52	4.12	15.92	15.88	15.75	15.34	14.84	12.51	4.68
npB	0.95	0.70	0.62	0.25	-	0.38	0.50	0.46	0.29	0.05	0.08	-
C_9-C_{11} Arom	0.03	0.04	0.02	0.06	-	0.01	0.01	-	-	-	0.01	-
DIPB (m)	0.41	0.46	0.44	1.09	0.26	0.51	0.47	0.60	0.57	0.47	1.68	0.61
(o)	-	-	-	-	-	-	-	-	-	-	-	-
(p)	0.22	0.23	0.22	0.53	0.56	0.24	0.23	0.27	0.25	0.22	0.89	1.43
≥DIPB	0.63	0.69	0.66	1.62	0.82	0.75	0.70	0.87	0.82	0.69	2.57	2.04
HBF	0.07	0.08	0.07	0.01	-	0.01	0.03	0.02	0.01	-	0.02	0.02
Prop. Conv. to IPB%	85.3	89.91	88.24	75.03	22.87	88.36	88.13	87.41	85.14	82.36	69.43	25.81
≥Alkylates (α) %	95.75	99.46	97.1	85.41	29.61	96.63	96.65	97.11	93.49	88.31	90.99	42.57
Sel to IPB %	89.08	90.39	90.87	87.84	77.23	91.44	91.18	90.01	91.06	93.26	76.30	60.63

In course of these some of the cumene molecules further react with propanol molecules forming polyalkylated compounds having lower mobility than benzene and cumene due to their bulkier nature. These molecules thus block the channels and deactivate the catalyst by not allowing reactants molecules to enter. This phenomenon is less in case of dealuminated mordenite with higher SiO_2/Al_2O_3 ratio as diffusivity of the benzene and cumene is much faster. Thus the stable activity observed can be explained on the basis of lower number of acidic centres for high SiO_2/Al_2O_3 ratio.

Another phenomenon noticed which is common to both the catalysts is the fall in impurities like toluene, ethylbenzene and higher boiling products. It is also noticeable that with increase in time-on-stream the selectivity of dialkylated products increased along with the increase of p/m diisopropylbenzene. All these phenomenon is due to the gradual coking on the external surface as well as in the interial channels, thus leading to coke induced selectivity.[3,4]

G. Influence of SiO_2/Al_2O_3 Mole Ratio

H-mordenite catalysts having varying SiO_2/Al_2O_3 molar ratio 13, 53, 86, 106 and 147 were used in studies on propylation of benzene with isopropanol. Table 3.5 compares the number of propylene moles converted to alkylated products. It was shown in earlier chapter (Table 2.11) that concentration of surface acid sites decreased with decreasing concentration of aluminium atoms/uc. Table 3.6 and 3.7 show the influence of temperature on

product distribution over catalysts having SiO_2/Al_2O_3 ratio of 13 and 147. The main observations are:

1) A small but significant decrease in the conversion of alcohol to isopropylbenzene is observed with increasing silica/alumina ratio. The observation being more pronounced when sample with R=13 and R=147 are compared.
2) The ipB/npB ratio and diisopropylbenzenes increased with increasing silica/alumina ratio, especially when compared at low reaction temperatures.
3) The extent of cracking of propylbenzenes and secondary reactions to form toluene, ethylbenzene, butylbenzene, etc. are reduced with increasing silica/alumina ratio.

At 210°C the catalyst with SiO_2/Al_2O_3 ratio 13 is significantly more active than other catalysts. The conversion of propylene decreased marginally with increasing dealumination (with increase in SiO_2/Al_2O_3 ratio). The difference observed (Total propylene conversion varied from about 100 to 91%) may be due to the differences in the density of tetrahedral aluminium sites. Alumina tetrahedra become more isolated with decreasing aluminium content. From Table 2.11 it is clear that with progressive dealumination there is reduction in acid sites as well as acid strength of pre-existing sites. However, total acidity decreased with increasing silica/alumina ratio. From Fig.2.11 it is seen that the strongly bound ammonia corresponding to desorption of ammonia molecules at higher temperatures (433°C and above) is progressively decreased with dealumination. Topsøe[5] et al have assigned this high temperature TPD peak to

chemisorption of ammonia by strong acid sites and have assumed that the intensity of this peak should decrease when Si/Al ratio is increased. Thus the above investigations lead to the conclusion that with increasing silica/alumina ratio, the concentration of strong acid sites responsible for the catalytic activity decreases. This is supported by the data in Table 3.5 and 2.11 which dictate the influence of increasing SiO_2/Al_2O_3 ratio on the propylene conversion and the distribution of surface acid sites of weak, medium and strong acid strength respectively.

H. Influence of Pyridine Injection on Alkylation Activity

Bases like pyridine and amines are known to reduce the activity due to the poisoning of active acid sites by reacting with the acidic sites which are active in the zeolite catalysed alkylation reaction.[6] Experiments were carried out to determine optimum level of pyridine. Fig.3.10 shows the conversion of propylene to IPB, total alkylated products and DIPB/IPB plotted against the amount of pyridine. The detailed product distribution is included in Table 3.8. Fig.3.10 shows that with increasing pyridine content in the feed (0 to 80 ppm) the catalytic activity gradually dropped from almost 100% propylene conversion to 75%. The drop is more pronounced from 40 to 80 ppm. Proportionately conversion to IPB is also decreased whereas selectivity to cumene is constant. The fall in activity can be correlated with the reaction of acidic sites with pyridine. The lower conversion of propylene with less acidic zeolite is as expected. The constant selectivity of cumene is due to the differences in site

Table 3.5

Alkylation of Benzene with Isopropanol over Mordenite Catalysts
Influence of SiO_2/Al_2O_3 ratio

Temperature ^oC = 210 (Benzene: Isopropanol) mole = 8

WHSV (h^{-1}) = 2.2

CATALYST	HM-(13)	HDM-(54)	HDM-(86)	HDM-(106)	HDM-(147)
Product weight %					
Aliphatics	0.13	0.20	0.24	0.38	0.52
Benzene	81.92	82.29	82.62	82.80	83.22
Toluene	0.09	0.08	0.08	0.08	0.06
C_8 Arom	0.10	0.09	0.07	0.05	0.04
Cumene	16.50	16.23	15.92	15.88	15.23
npB	0.40	0.32	0.30	0.17	0.08
C_9-C_{11} Arom	0.03	0.04	0.01	0.01	0.03
DIPB (m)	0.50	0.46	0.51	0.38	0.57
(o)	-	-	-	-	-
(p)	0.26	0.24	0.24	0.22	0.25
≥ DIPB	0.76	0.70	0.75	0.60	0.82
HBF	0.06	0.05	0.01	0.02	-
Prop. Conv. to IPB %	91.24	90.07	88.36	88.13	84.52
≥ Alkylates (α) %	99.71	97.6	96.19	94.00	91.70
Sel to IPb %	91.57	92.28	91.86	93.76	92.17

Table 3.6

Alkylation of Benzene with Isopropanol
Catalyst: H-Mordenite (SiO_2/Al_2O_3 ratio = 13)
(Benzene: Isopropanol) mole = 8, WHSV (h^{-1}) = 2.2.

Temperature ^oC	140	210	250	300
Product weight %				
Aliphatics	0.4	0.13	0.30	0.74
Benzene	90.92	81.92	85.29	91.19
Toluene	-	0.09	0.05	0.41
C_8 Aromatics	-	0.10	0.20	0.80
Cumene	5.5	16.50	12.66	4.05
npB	0.29	0.40	0.59	1.89
C_9-C_{11} Arom	-	0.03	0.25	0.80
DIPB (m)	1.89	0.50	0.42	0.08
(o)	-	-	-	-
(p)	0.91	0.26	0.20	0.03
≅ DIPB	2.80	0.76	0.62	0.11
HBF	0.08	0.06	0.03	-
Prop. Conv. to IPB %	30.53	91.24	70.26	22.47
≅ Alkylates (α) %	69.63	99.71	78.62	33.85
$\frac{IPB}{IPB+npB} \times 100$	94.17	97.62	95.54	68.18
$\frac{DIPB}{IPB}$ (mole) x 100	37.72	3.42	3.62	2.01

Table 3.7

Alkylaticn of Benzene with Isopropanol
Catalyst: HDM-147 (SiO_2/Al_2O_3 ratio = 147)
(Benzene: Isopropanol) mole = 8, WHSV (h^{-1}) = 2.2.

Temperature ^oC	140	210	250	300
Product weight %				
Aliphatics	0.44	0.52	0.35	0.58
Benzene	91.32	83.22	86.33	92.05
Toluene	0.08	0.06	0.04	0.32
C_8 Aromatics	-	0.04	0.12	0.63
Cumene	5.20	15.23	10.83	3.20
npB	-	0.08	0.84	1.38
C_9-C_{11} Arom	-	0.03	0.16	0.72
DIPB (m)	0.88	0.57	0.39	0.32
(o)	-	-	-	-
(p)	2.06	0.25	0.53	0.44
Σ DIPB	2.94	0.82	0.92	0.76
HBF	0.02	-	0.41	0.36
Prop. Conv. to IPB %	28.86	84.52	60.10	17.76
Σ Alkylates (α) %	53.02	91.70	72.32	31.65
$\frac{IPB}{IPB+npB} \times 100$	100	99.47	92.8	69.86
$\frac{DIPB}{IPB}$ (mole) x 100	41.92	3.98	6.29	17.59

Table 3.8

Influence of Pyridine injection of Alkylation Activity
Catalyst: HM (SiO_2/Al_2O_3 ratio = 13)
Temperature ^oC = 210
(Benzene: Isopropanol) mole = 8, WHSV (h^{-1}) = 2.2

Pyridine in feed (ppm)	0	40	80
Product weight %			
Aliphatics	0.06	1.02	2.8
Benzene	82.14	81.77	83.77
Toluene	0.03	0.01	0.01
C_8 Aromatics	0.08	0.04	0.01
Cumene	16.33	16.02	12.66
npB	0.49	0.39	0.21
C_9-C_{11} Arom	0.04	0.03	0.01
DIPB (m)	0.51	0.46	0.32
(o)	-	-	-
(p)	0.24	0.21	0.17
≧ DIPB	0.75	0.67	0.50
HBF	0.07	0.05	0.03
Prop. Conv. to IPB %	90.63	88.91	70.26
≧ Alkylates (α) %	99.51	96.57	75.53
Sel to IPb %	91.07	92.06	93.02

EFFECT OF POISONING ON ACTIVITY AND SELECTIVITY
IN ISOPROPYLATION OF BENZENE OVER HMORDENITE
TEMP: 210°C , WHSV : 2.2 hr^{-1} MR 8 (Bz : ISOPROPANOL)

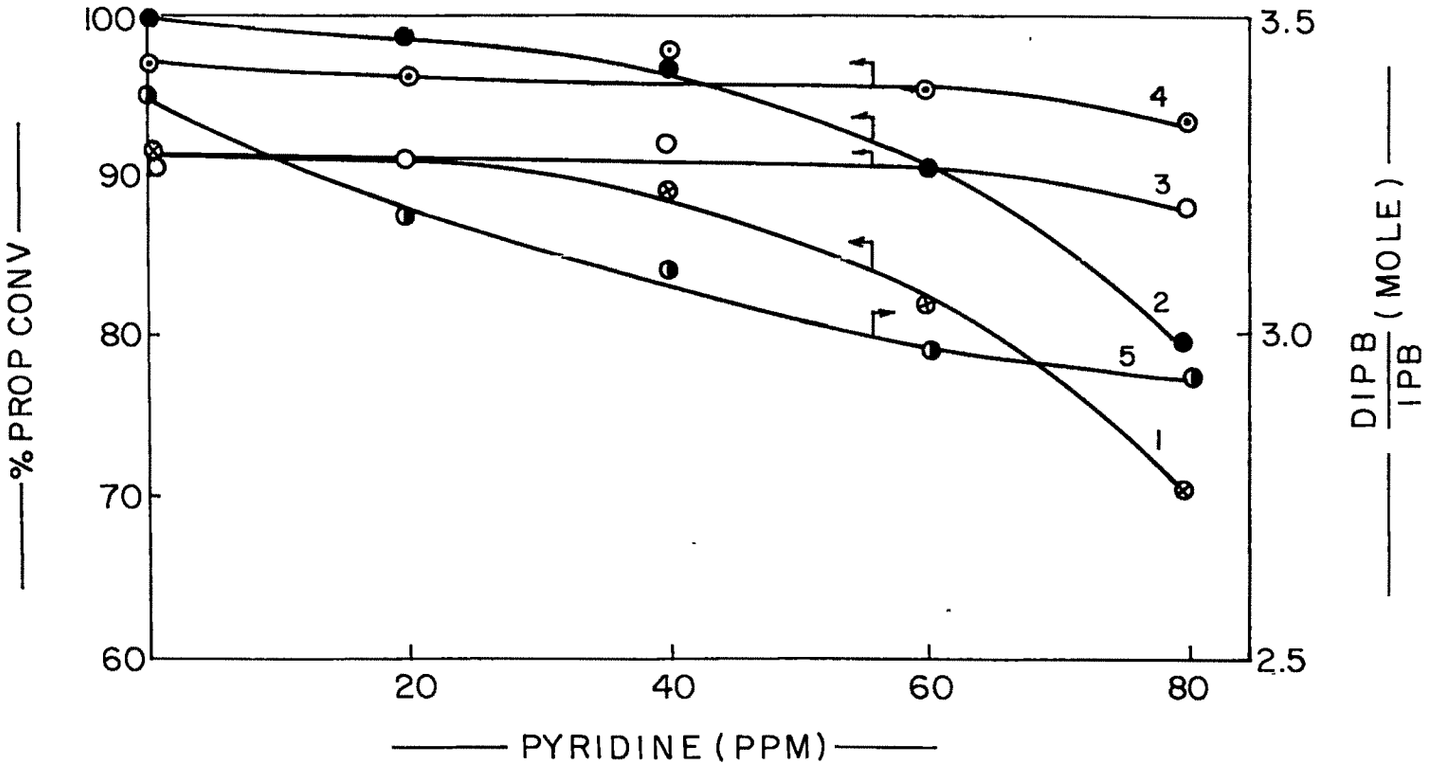

FIG. 3·10: 1 PROP CONV TO IPB 2 Σ ALKYLATE (α)

3 $\frac{\text{PROP CONV. TO IPB}}{\Sigma \text{ ALKYLATE}(\alpha)}$ 4 $\frac{\text{IPB}}{\text{IPB} + \text{NPB}}$

5 $\frac{\text{DIPB}}{\text{IPB}}$ (MOLE)

occupation by pyridine. Up to 60 ppm level the sites needed for alkylation are not much affected eventhough total conversion is reduced. Further increase in pyridine concentration reduced the active sites with a drastic fall in activity. The selectivity being a property of the zeolitic structure, is not much affected due to reduction in acidic sites.

I. Influence of Phosphorous Impregnation on Alkylation Activity

The preparation of phosphorous modified mordenites has been described in section 2.2B. Fig.3.11 shows the conversion of propylene as a function of % phosphorous impregnation. Between 0.5 to 1% of phosphorous there is major change in catalytic activity. When phosphorous content was increased from 3 to 5%, no reaction was noticed. It is suggested by Kaeding and Butter[7] that elemental phosphorous binds the zeolite framework through oxygen as indicated

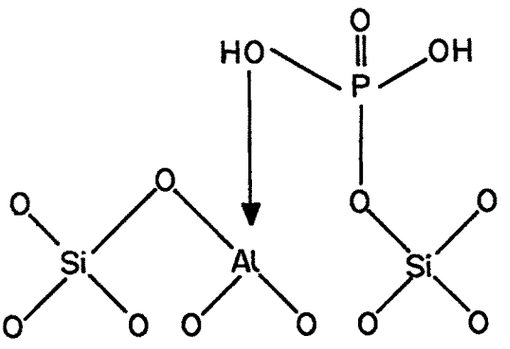

and reduces acidic sites.[8] In the process some of the pore mouth are blocked by the phosphorous complex. Also inside the channel these complexes change the channel tortuosity resulting in the

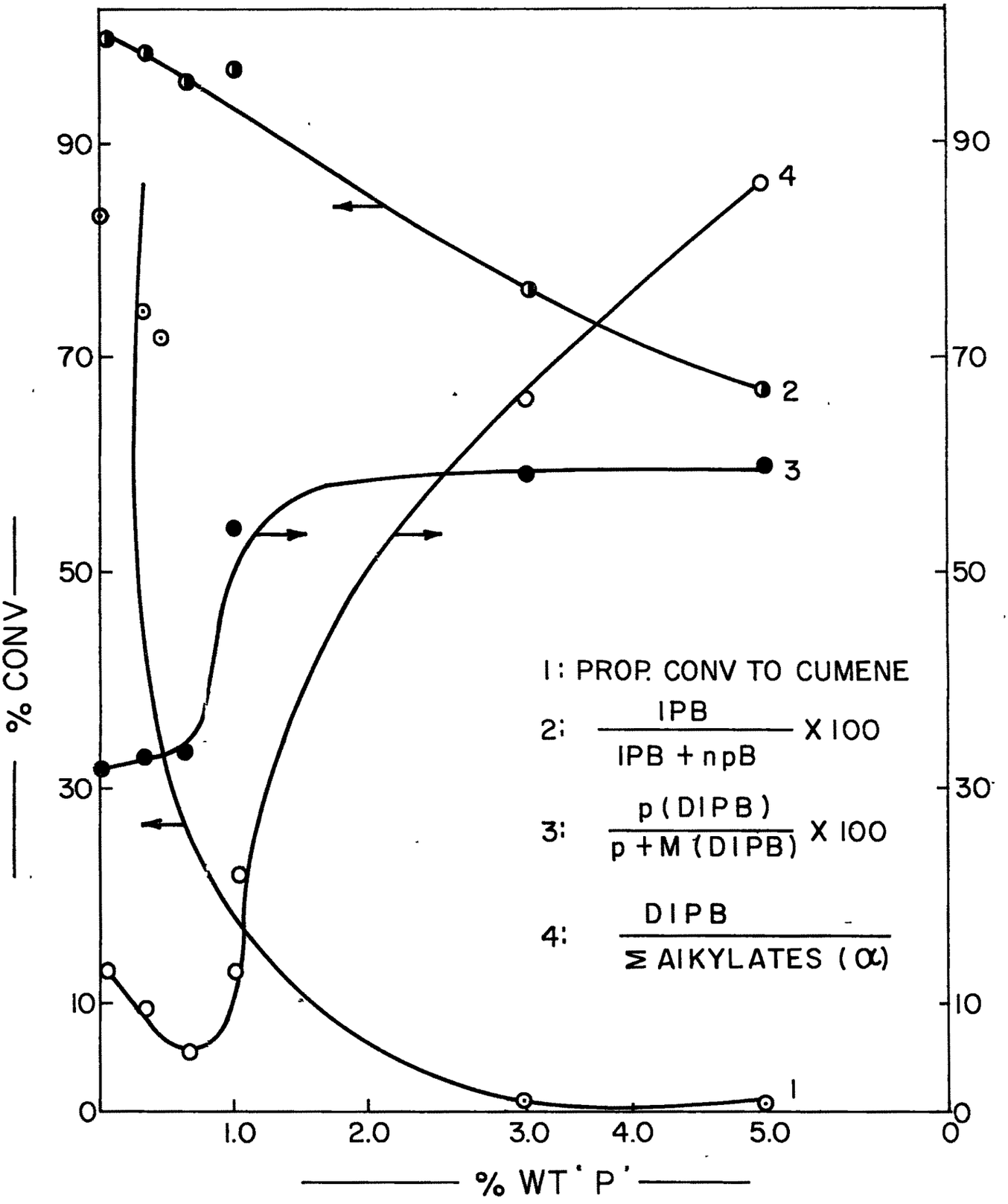

TEMP: 210 (°C), MR: (Bz / Isopropanol): 8, WHSV (hr^{-1}): 2.2

FIG. 3.11 : EFFECT OF 'P' LOADING ON ACTIVITY AND SELETIVITY OVER. H - MORDENITE.

Table 3.9

Influence of phosphorus impregnation on alkylation activity
Temperature ^{o}C = 210
(Benzene: Isopropanol) mole = 8, WHSV(h^{-1}) = 2.2

CATALYST*	HM	PHM (0.32)	PHM (0.64)	PHM (1.0)
Product weight %				
Aliphatics	0.03	0.07	0.11	0.44
Benzene	82.77	83.38	83.97	96.48
Toluene	0.04	0.03	0.03	0.02
C_8 Aromatics	0.11	0.09	0.08	0.01
Cumene	15.37	14.85	14.42	2.45
npB	0.95	0.81	0.63	0.08
C_9-C_{11} Arom	0.03	0.04	0.03	-
DIPB (m)	0.41	0.39	0.38	0.22
(o)	-	-	-	-
(p)	0.22	0.22	0.19	0.26
≧DIPB	0.63	0.61	0.57	0.48
HBF	0.07	0.12	0.16	0.04
Prop. Conv. to IPB%	85.30	82.42	80.03	13.59
Total Prop. Conv.(α)%	95.74	91.92	88.20	17.97

* Figures in parenthesis indicate % phosphorus impregnated

formation of para selective products in the dialkylbenzenes. With increase in phosphorous content the drop in catalytic activity, increasing DIPB formation and increase in p-diisopropylbenzene is observed. On further increase in phosphorous content a drop in activity leading to the decrease in formation of all the products is noticed. The product distribution over phosphorous impregnated mordenite is shown in Table 3.9. It is observed that there is reduction in toluene, ethylbenzene and xylenes which are formed due to cracking on the external surface.[9] A reduction in concentration of surface hydroxyl groups/uc of the impregnated samples is listed in Table 2.6. It is seen that some of the surface hydroxyl groups reduced by incorporation of phosphorous, the extent of reduction is in proportion to the amounts incorporated. These results support the observed results in catalytic activity. There is diminition in pore volume with incorporation of phosphorous as observed by the adsorption studies of cyclohexane and benzene (Table 2.9).

J. Influence of Water Vapour

Propylene was bubbled through water and fed into the reactor along with benzene over the catalyst bed containing H-mordenite. The products were collected at different intervals and analysed. The gaseous products were also collected and analysed separately. Results are presented in Table 3.10 and Fig.3.12. It is seen from the table that there is a decrease in the formation of isopropylbenzene and increase in the diisopropylbenzene when moist propylene is passed through the catalyst bed. The

Table 3.10

Alkylation of Benzene with Propylene

Influence of Steam Injection

Catalyst: HM (SiO_2/Al_2O_3 ratio = 13), Temperature ^oC = 175

(Benzene: Propylene) mole = 7.4, WHSV (h^{-1}) = 2

Product weight %	-	*
Aliphatics	0.09	0.04
Benzene	80.8	82.65
Toluene	0.08	0.01
C_8 Aromatics	0.13	-
Cumene	16.88	14.20
npB	0.56	0.02
C_9-C_{11} Arom	0.10	-
DIPB (m)	0.79	2.20
(o)	-	-
(p)	0.33	0.83
≥ DIPB	1.12	3.03
HBF	0.20	-
Prop. Conv. to IPB %	87.10	73.27
≥ Alkylates (α) %	98.54	96.53
Sel to IPb %	88.39	75.90

* Propylene passed through H_2O trap

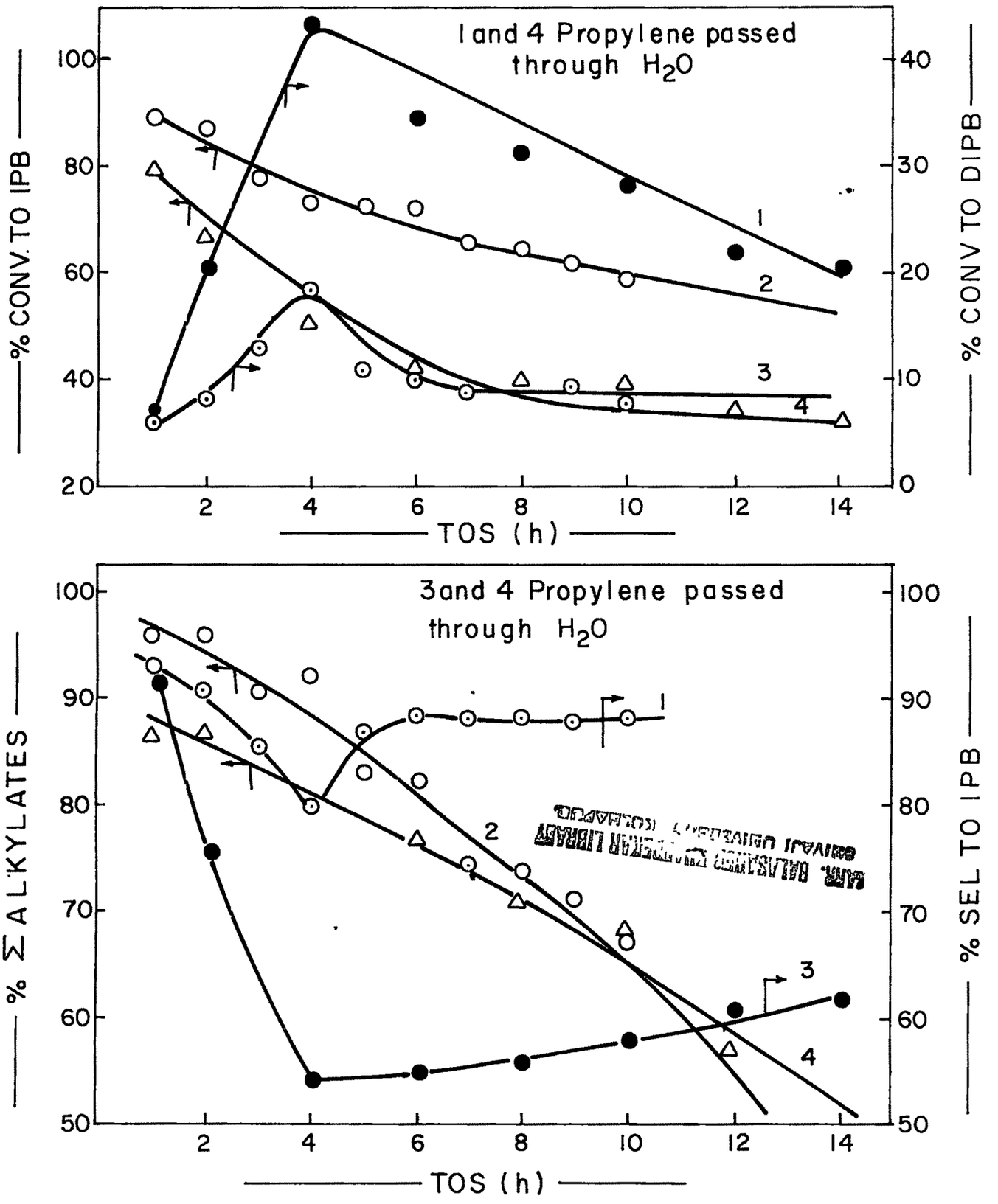

G.3.12 INFLUENCE OF WATER VAPOUR ON PROPYLENE CONVERSION AND SELECTIVITY TO IPB.

impurities (toluene, C_8 aromatics and npB) are reduced indicating the neutralization of some acidic sites with water molecules. The increase in DIPB concentration is due to lower acidity. Both high temperature and acidity are needed for reversible transalkylation reaction. Temperature being constant in reaction with and without water vapour, the high concentration of DIPB may be related to the lower number of acid sites due to which transalkylation and dealkylation of DIPB is reduced. The presence of water (steam) may also facilitate easier removal of DIPB from the pores. This explains the increased yield of DIPB in the presence of water.

When reaction was carried out for longer period up to 15 h on stream (Fig.3.12) conversion to IPB and DIPB decreased, (Even propylene without H_2O also showed decreasing trend).

K. Alkylation of Benzene with Isopropanol over Coked Catalyst

A coked mordenite catalyst was used for alkylation of benzene to cumene. The data is shown in Table 3.11. As can be seen from the table, the conversion of propylene is decreased whereas selectivity to IPB is increased. Among the diisopropylbenzene p-isomer predominates over the m-isomer and also there is no formation of n-propylbenzene over coked catalyst. The deposition of coke within the catalyst pores or on the external surface eliminates strong acid sites responsible for cracking and other secondary reactions. The deposition of coke within the catalyst gradually reduces the pore geometry thus increasing the selectivity to para isomer among the dialkylbenzenes. Absence of higher boiling fractions also support

Table 3.11

Alkylation of Benzene with Isopropanol

Comparison of Fresh and Coked Catalyst

Catalyst: HM (SiO_2/Al_2O_3 ratio = 13), Temperature ^{o}C = 210

(Benzene: Propylene) mole = 8, WHSV (h^{-1}) = 2.2

CATALYST	FRESH	COKED
Product weight %		
Aliphatics	0.10	5.75
Benzene	82.01	92.47
Toluene	.01	0.12
C_8 Aromatics	.05	-
Cumene	16.49	1.49
npB	0.49	-
C_9-C_{11} Arom	0.03	-
DIPB (m)	0.51	0.02
(o)	-	-
(p)	0.24	0.05
≤DIPB	0.75	0.07
HBF	0.05	-
Prop. Conv. to IPB %	91.52	8.27
Sel to IPB %	91.20	93.45
$\frac{\text{DIPB (p)}}{\text{DIPB (m)}} \times 10^2$	47.06	250

the above conclusion. Deposition of coke on the catalyst leading to increased selectivity to IPB suggests coke induced shape selectivity.[10] The most accessible surface acidic sites could be covered to reduce the formation of undesirable products.

L. Determination of External Diffusion Effects

Fig. 3.13 describes influence of variation of catalyst weight at a constant space velocity to study the external diffusion effects. In spite of change in the weight of catalyst to 3 times the conversions and selectivities did not vary much indicating negligible external diffusion effects for flow rates employed in this investigation.

M. Determination of Energy of Activation

The temperature dependance of experimentally determined rate constants in practically all cases is well represented by Arrhenius equation,

$$K = Koe^{-E_a/RT}$$

where,

K = reaction rate constant,

Ko = Arrhenius frequency factor,

E_a = Activation energy for the reaction,

R = Gas constant,

T = Absolute temperature.

If the Arrhenius equation is applicable, a plot of logarithm of rate constant versus reciprocal of absolute temperature should

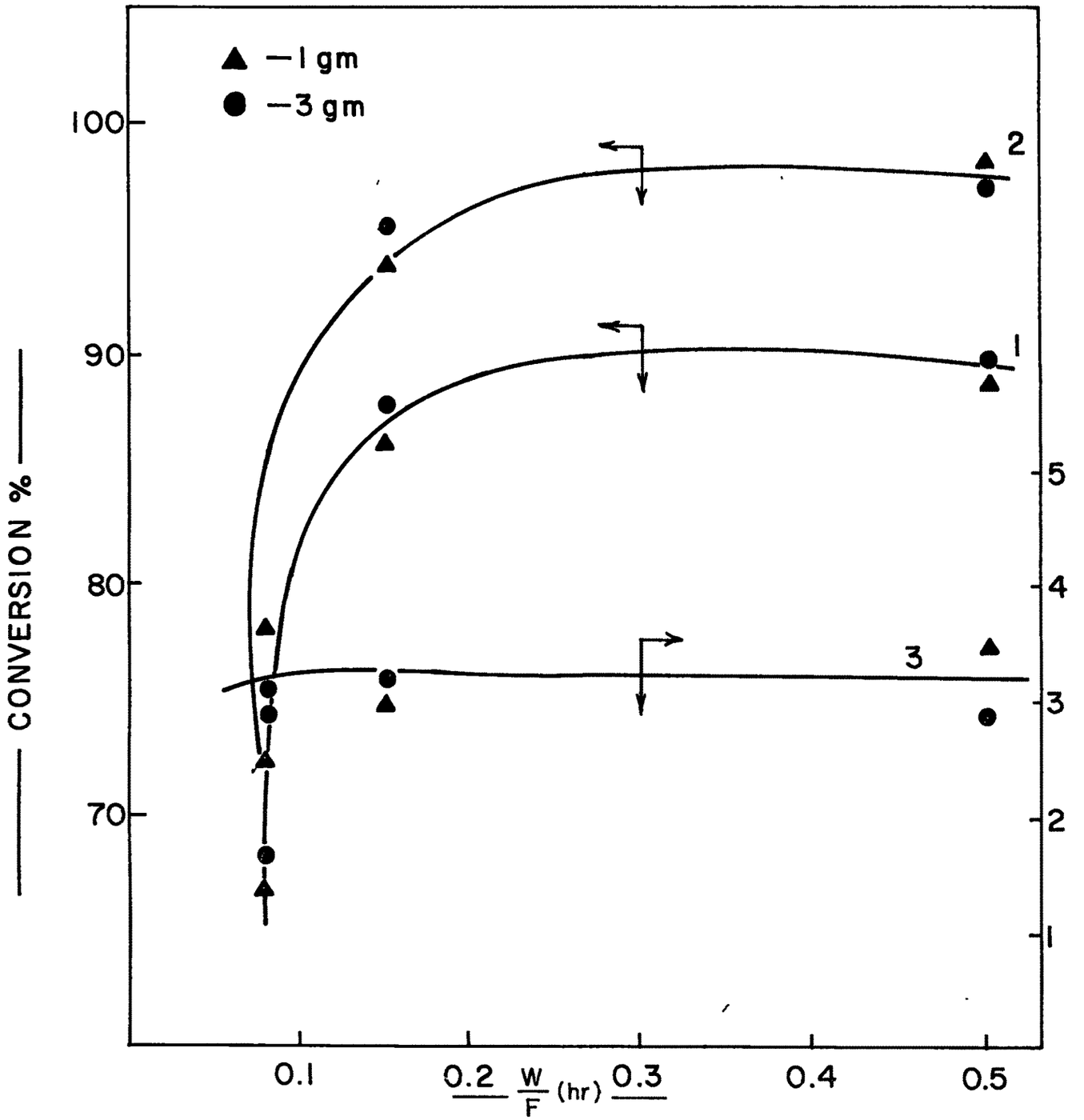

FIG.3-13-THE INFLUENCE OF VARIATION IN CATALYST WEIGHT AT CONSTANT WHSV^{-1} hr

1- ALCOHOLE CONVERSION TO CUMENE

2- TOTAL ALKYLATES (α)

3- DIPB / CUMENE x 100

yield a linear relation. The reaction rate constant at different temperatures were calculated from first order kinetic equation.

$$K = \frac{F}{W} \ln \frac{1}{1-x} \quad \text{where}$$

F = Flow rate of reactant mixture,

W = Weight of the catalyst,

X = Fraction of alcohol converted.

The reaction conditions employed were: Benzene/Isopropanol (mole) =8, WHSV = 2 h^{-1} and at atmospheric pressure.

A pseudo-unimolecular reaction is proposed for isopropylation of benzene using excess of benzene on the assumption that only alcohol is adsorbed on the active acid site to form an electrophilic species and then interacts with benzene in the gaseous phase to form isopropylbenzene. There are evidences which show that olefins react with aromatic hydrocarbons like benzene, in a Rideal type mechanism.[11,12]

An Arrhenius plot for alkylation of benzene with isopropanol over H-mordenite catalyst is shown in Fig.3.14. The activation energy E_a, for the reaction, as determined from the slope of the plot is 9.9 Kcals/g mole. Similar type of study was made by Karge et al and reported a value of 10.5 Kcals/g mole for alkylation of benzene with ethylene.[1]

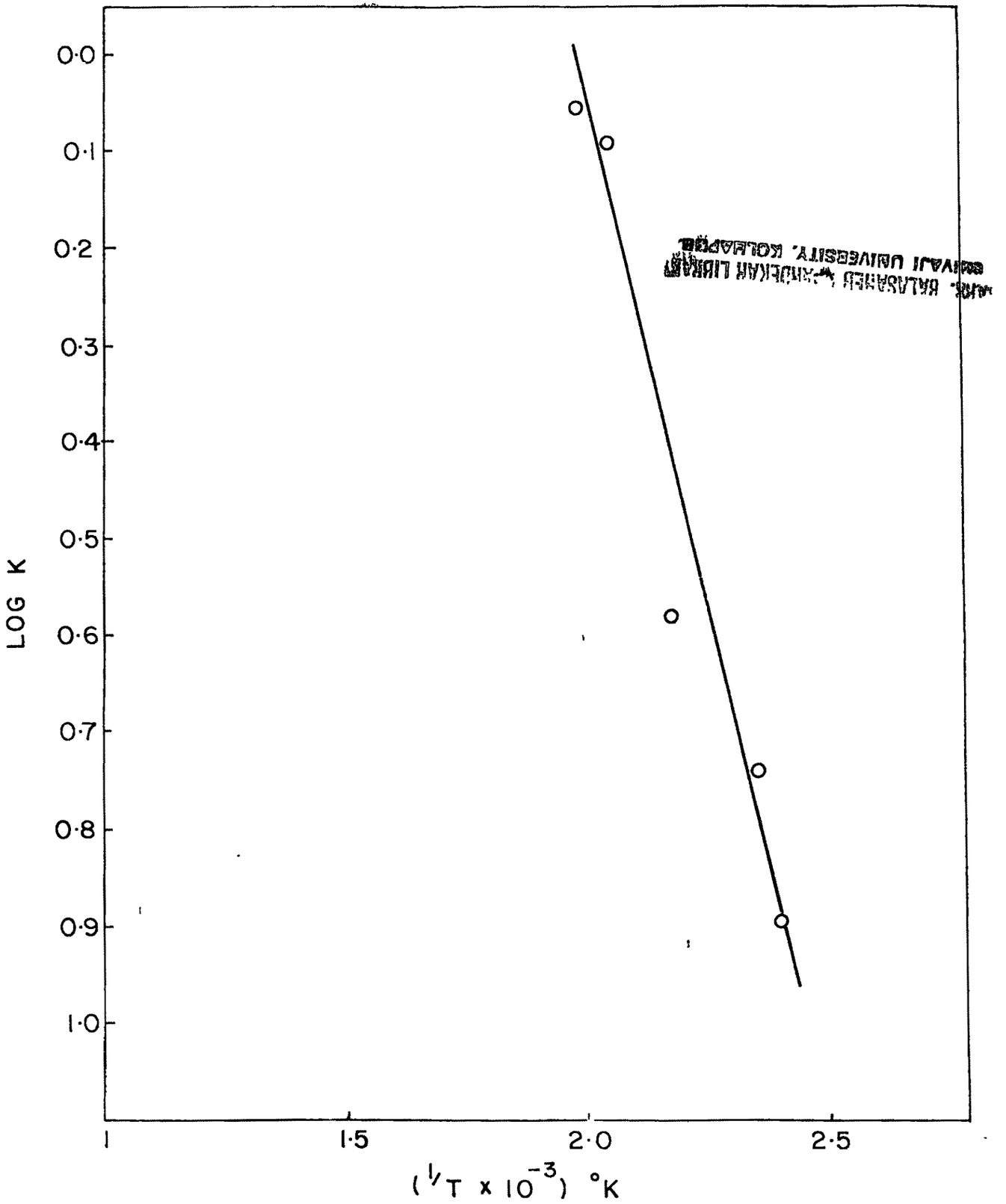

FIG. 3·14-THE ARRHENIUS PLOT FOR ISOPROPYLATION OF BENZENE·

N. Propylation of Benzene using Isopropanol, N-Propanol and Propylene: A Comparison

Studies were carried out using isopropanol, n-propanol and propylene as alkylating agents under identical experimental conditions. The data is included in Tables 3.3, 3.12 and 3.13 respectively.

When propylene was used as an alkylating agent conversions are higher even at 190°C and at higher temperature unreacted propylene was observed in the product stream. When isopropanol was used, higher temperatures were needed for the same conversions. However, the activity of n-propanol was maximum around 275°C. The product pattern in all these cases is similar. Irrespective of the alkylating agent, isopropylbenzene is the major component.

Alkylation of benzene by simple alcohol like n-propanol has been described by Minachev and co-workers over CaY at 532-598 K.[13] The product from n-propanol was largely rearranged isopropylbenzene, as expected for a carbonium ion process in which a primary cation is rearranged to a secondary cation. However, Venuto and Landis reported that significant quantities of n-alkyl aromatics[12] can be obtained from primary alcohols directly by an SN^2 process without requiring prior formation of a carbonium ion and attendant rearrangement possibilities.

Table 3.12

Alkylation of Benzene with n-propanol over H-Mordenite Catalyst

Influence of temperature
(Benzene: n-propanol) mole = 7.32, WHSV (h^{-1}) = 2.0

Temperature (^{o}C)	150	185	215	235	250	275	300	350
Product weight %								
Aliphatics	0.08	0.21	0.54	0.46	2.61	0.58	0.71	0.67
Benzene	94.9	95.08	97.58	90.19	83.62	84.11	85.49	88.42
Toluene	-	-	-	-	0.03	0.04	0.02	0.02
C_8 Aromatics	-	-	-	-	0.03	0.05	0.04	0.04
Cumene (IPB)	0.22	0.44	1.28	6.40	10.23	12.79	12.08	9.84
n-propylbenzene	0.05	0.1	-	0.37	0.31	0.35	0.32	0.34
C_9-C_{11} Aromatics	-	-	-	0.01	0.09	0.15	0.17	0.13
DIPB	0.28	0.12	-	1.70	2.34	1.60	0.92	0.34
HBF	0.04	0.02	-	0.17	0.18	0.12	0.05	0.01
≧ Alkylates (α) %	3.48	3.70	6.54	47.72	71.53	79.21	70.28	54.55
n-proH---> Propylbenzenes	1.37	2.81	6.54	34.6	53.82	67.1	63.4	52.0
Composition (%)								
Isopropylbenzene	81.75	80	100	94.5	97.06	97.34	97.42	96.67
n-propylbenzene	18.25	20	-	5.5	2.94	2.66	2.58	3.33

Table 3.13

Alkylation of Benzene with Propylene over H-Mordenite Catalyst

Influence of temperature
(Benzene: Isopropanol) mole = 7.32, WHSV (h^{-1}) = 2

Temperature (^{o}C)	150	170	190	210	230	250	300
Product weight %							
Aliphatics	0.92	0.45	0.05	0.28	0.69	0.35	0.9
Benzene	85.7	80.73	80.71	82.3	82.13	84.04	87.22
Toluene	-	-	0.04	0.05	0.15	0.13	0.9
C_8 Aromatics	-	0.01	0.06	0.11	0.30	0.34	1.23
Cumene (IPB)	11.87	17.27	17.82	15.42	14.35	13.02	5.63
n-propylbenzene	0.01	0.09	0.24	0.83	1.26	1.48	3.23
C_9-C_{11} Aromatics	-	-	-	0.05	-	0.13	0.35
DIPB	0.95	0.80	0.73	0.58	0.50	0.50	0.13
HBF	0.45	0.59	0.39	0.38	0.43	0.50	0.41
Σ Alkylates α %	73.73	94.75	97.79	94.96	83.53	77.87	50.25
Propylene---> Propylbenzenes	60.7	88.7	92.3	83.04	81.0	66.53	45.3
Composition (%)							
Isopropylbenzene	99.92	99.50	98.7	94.9	90.6	89.79	63.5
n-propylbenzene	0.08	0.5	1.3	5.1	9.4	10.21	36.5

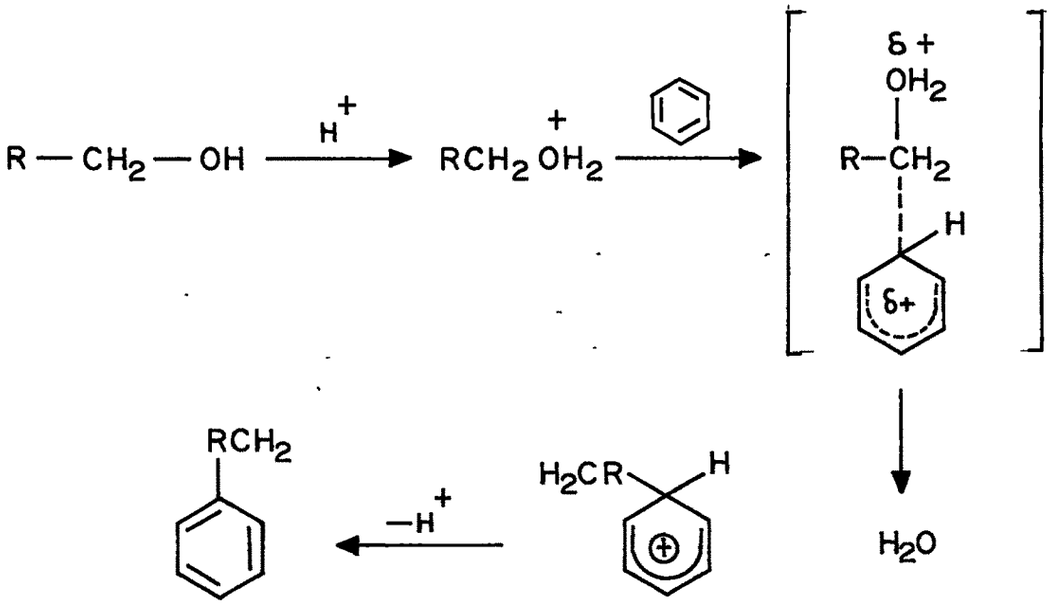

Table 3.14 lists the isomeric composition of isopropylbenzene and n-propylbenzene at various temperatures under thermodynamic equilibrium as calculated by Taylor et al.[14] Accordingly the amount of npB increases with increasing temperature and at temperature above 400 K the composition of npB exceeds that of IPB. Chandawar et al[15] reported increasing amount of npB at higher temperature over HZSM-5 zeolite. The different alkylating agents over mordenite did not indicate much difference in the product pattern. Isopropylbenzene is always in excess than thermodynamic equilibrium at all temperatures. This may be due to presence of stronger acid sites and larger pores in the structure of mordenite. Thus the observed product pattern is different than that reported for the medium pore zeolites.

O. Influence of Silynation on Catalytic Activity

Acidity and pore size are the parameters which independently influence catalytic properties of zeolites. Acidity of H-

Table 3.14

Equilibrium Composition of Propylbenzenes*

Temperature, °K	n-propylbenzene	Isopropylbenzene
298	46.7	53.3
300	46.9	53.1
400	57.7	42.3
500	62.5	37.5
600	66.7	33.3
700	68.9	31.1

* Ref.: W.J. Taylor, D.D. Wagman, M.G. Williams, K.S. Pitzer and R.D. Rossinni, J. Res. Nat. Bur. 37, 95 (1946).

mordenite is controlled by cation exchange and by dealumination. The influence of acidity distribution on isopropylation has been examined. Cation exchange poisons the strong acid sites preferentially, while dealumination reduces acid sites over a whole region.[16] Silynation using SiH_4 has recently been suggested for pore size modification.[17] However, these methods modify the acidity as well as pore structure, so an undesired change in catalytic activity may be introduced. According to studies of Niwa et al[18] the deposition of silica can be explained on the basis of the following reaction.

$$Z\text{-}OH + Si(OC_2H_5)_4 - Z\text{-}OSi(OC_2H_5)_3 + C_2H_5OH$$

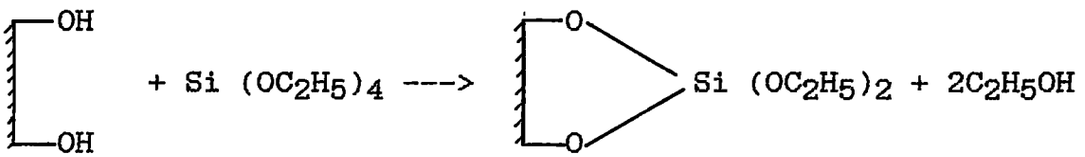

The external hydroxyl groups first will be reacted with orthosilicate which on calcination forms silica-H-mordenite. Due to this the surface acidity (Due to the neutralization of acidic sites by orthosilicate on the external surface) will be reduced thereby reducing the surface reactions. In Fig.3.15 the propylene conversion versus cumulative feed passed is shown. It is seen that although the activity of the fresh catalyst (H-mordenite) shows a continuous drop in propylene conversion, it has higher activity as compared to silynated catalyst. The silanated catalyst shows fast deactivation. The DIPB/IPB also decreases in a span of 60 mls of feed passed whereas unmodified catalyst is stable up to 120 mls.

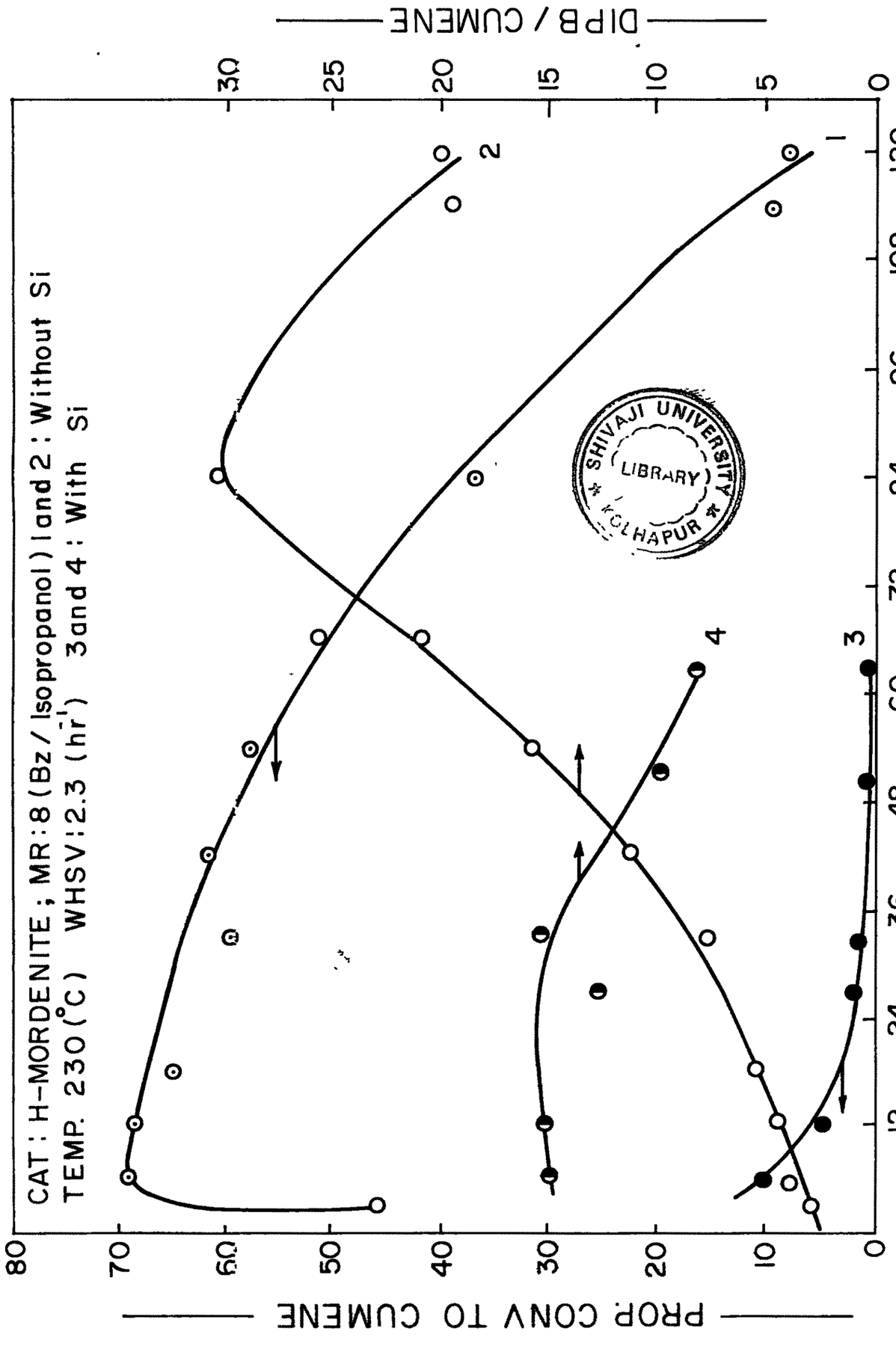

FIG - 3·15 INFLUENCE OF SILYNATION ON ACTIVITY AND STABILITY.

P. Isopropylation of Benzene over Na-RE-Mordenite

The rare-earth exchanged sodium mordenites were studied in isopropylation of benzene at reported optimum activation and reaction temperature[11,19] as a function of Na content in the exchanged zeolites. It is seen from Table 3.15 that with decreasing Na content in the sodium mordenite the conversion of propylene is increased. The reduction in propylene conversion is as expected due to reduction in Brönsted acid centres which are needed for alkylation.[20,21] As the mordenite channels are comparatively larger than medium pore zeolites, the shape selectivity arising out of structural factors is not significant hence the observed near constancy in p/m DIPB.

3.4 ISOPROPYLATION OF BENZENE OVER MORDENITE, ZSM-5 AND ZSM-12 ZEOLITES: A COMPARISON

The product distribution of alkylation of benzene with isopropanol over mordenite, ZSM-5 and ZSM-12 in their acidic form but having comparable SiO_2/Al_2O_3 molar ratio is presented in Table 3.16.

From the table it is evident that mordenite with SiO_2/Al_2O_3 ratio of 86 is more active and selective for the formation of isopropylbenzene than the ZSM-5 type with the same SiO_2/Al_2O_3 ratio. The mordenite structure consist of unidimensional dual pore system with 6.7 x 7.0 A^o (12 MR) and 2.9 x 5.7 A^o (8 MR) connected via side pockets of 2.9 A^o whereas ZSM-5 is having two dimensional channel system (straight channel 5.2 x 5.8 A^o and

Table 3.15

Isopropylation of Benzene over Rare-earth Exchanged Sodium Mordenite

Conditions: Activation temp.= 250°C, Reaction temp.= 250°C

(Bz: Isopropanol) mole = 8, WHSV(h^{-1}) = 2.2

CATALYST	NaRE(22)MD	NaRE(43)MD	NaRE(51)MD	NaRE(62)MD
Na ppm x 10^{-3}	39.0	28.5	24.5	19.0
Product weight %				
Aliphatics	0.35	0.33	0.33	0.21
Benzene	93.98	93.58	93.12	92.76
Toluene	0.03	0.01	-	-
C_8 Aromatics	-	-	-	-
Cumene	4.48	4.85	5.18	5.46
npB	-	-	-	-
C_9-C_{11} Arom	-	-	-	-
DIPB (m)	0.51	0.56	0.65	0.78
DIPB (o)	-	-	-	-
DIPB (p)	0.47	0.49	0.53	0.58
DIPB	0.98	1.05	1.18	1.36
≅ HBF	0.18	0.17	0.18	0.19
Prop. Conv. to IPB %	24.86	26.91	28.75	30.3
≅ Alkylates (α) %	32.92	35.54	38.45	41.48
DIPB($\frac{p}{m}$) x 10^2	92.15	87.5	81.53	74.35

Table 3.16

Alkylation of Benzene with Isopropanol Over Zeolite Catalysts
Temperature ^{o}C = 210
(Benzene: Isopropanol) mole = 8, WHSV(h^{-1}) = 2.2

Product Weight %	CATALYST			
	HDM-(86)	HDM-(147)	HZSM12-(167)	HZSM5-(86)
Aliphatics	0.61	0.32	0.19	0.24
Benzene	82.25	83.47	82.49	85.26
Toluene	0.08	0.06	-	0.23
C_8 Aromatics	0.07	0.04	-	-
Cumene	15.92	15.23	16.25	10.05
npB	0.30	0.08	0.01	0.42
C_9-C_{11} Arom	0.01	0.03	0.01	2.79
DIPB	0.70	0.82	0.86	0.72
HBF	0.05	-	0.09	0.21
Prop. Conv. to IPB %	86.36	84.32	90.2	55.77
Σ Alkylates (α) %	96.19	91.70	97.32	64.02
Sel to IPB %	91.86	92.17	92.68	87.11

sinusoidal channel 5.4 x 5.6 A^{o}) with distance between two intersection of 10 A^{o}. The steric constraint imposed by the channel within the pores favours the secondary reactions leading to products like n-propylbenzene and butylbenzenes. Also this restricts to some extent formation of DIPB and higher aromatics.

The large channel opening of mordenite favours higher selectivity to cumene whose formation along with that of n-propylbenzene may be represented as shown in scheme B of mechanism (Section 3.6). Secondary carbonium ion favours stability considerations and results in the transient species III whose formation is more facile in large pore mordenite.[22] The low selectivity observed in ZSM-5 is on account of its smaller pore openings (5.1 x 5.4 A^{o}).

The product distribution on dealuminated mordenite and HZSM-12 of comparable SiO_2/Al_2O_3 ratio is shown in column 2 and 3 of Table 3.16. It is seen that both catalysts indicate selective formation of cumene with a similar product pattern except that mordenite favours impurities like aliphatics, toluene, n-propylbenzene and C_9 aromatics. Both catalysts have unidirectional linear channels. ZSM-12 having noninterpenetrating channels with pore openings of 5.7 x 6.1 A^{o} and mordenite with 8-membered interconnecting channels. Dealuminated mordenite is having strong acidic sites (0.35 acid sites/u.c.) than ZSM-12 (0.17 acid sites/u.c.) still the product pattern does not vary much than that of ZSM-12, which again shows that large pore zeolites are more selective for propylation reactions. The yield of isopropylbenzene is more in ZSM-12 than in mordenite.

3.5 PROPYLATION OF BENZENE OVER RARE-EARTH EXCHANGED Y ZEOLITE

The preparation of rare-earth exchanged Y zeolite is described in Section 2.3. The experiments were carried out by employing the procedure described in Section 3.1b.

Results and Discussion

The unit cell composition of different rare-earth exchanged faujasite (Y) samples calculated by chemical analysis is presented in Table 2.27. As revealed by X-ray diffraction patterns all the samples were highly crystalline. Sorption capacities for water, benzene and nitrogen saturation capacity of different samples are reported in Table 2.26. With increase in degree of exchange of rare-earth ions, a decrease in the sorption capacity was observed. These samples were tested for isopropylation of benzene.

The alkylation of benzene with propylene to cumene is multistep reaction. The main reaction scheme can be presented as

		ΔH, Kcal/mole
(1)	Benzene + Propylene ----> Cumene	-14.72
(2)	Cumene + Propylene ----> Diisopropylbenzene	-13.94
(3)	Diisopropylbenzene + Benzene $\rightleftharpoons$ 2 Cumene	- 0.78
(4)	Cumene ----> Propylene + Benzene	+15.80

As revealed by thermodynamic data, alkylation reactions (1 and 2) are exothermic and result in liberation of heat. Reactions 3 and 4 are appreciable only at high temperatures.

Selective formation of cumene can be achieved by optimising the reaction parameters, such as activation temperature, benzene to propylene mole ratio, weight hourly space velocity (WHSV), reaction temperature, rare-earth content in zeolite samples and reaction pressure.

A. Effect of Activation Temperature

The effect of activation temperature on cumene formation is shown in Fig.3.16. The maximum conversion of propylene to cumene is observed at about 250-300°C. Ward[23] from his studies concluded that zeolitic activity in a alkylation reaction is caused essentially by Brönsted acid sites. These acid sites on zeolites are produced by polarisation-dissociation of water molecules existing around a multivalent cation.[24]

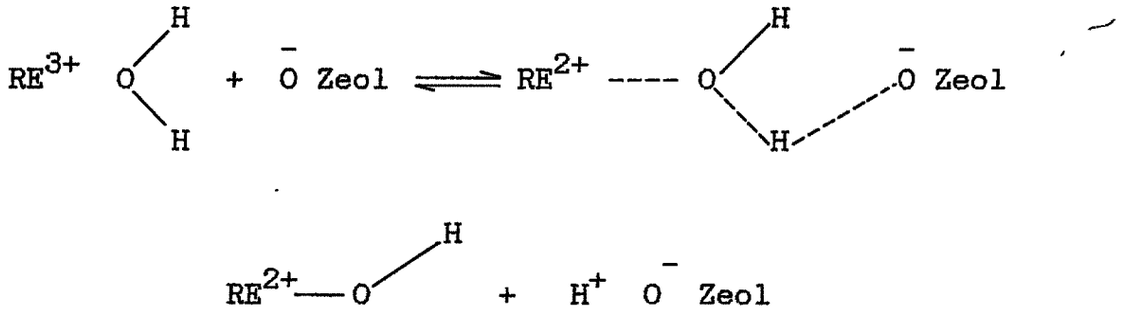

The protons liberated during the dehydration process from framework OH groups responsible for the Brönsted acidity. Eventually, a small multivalent ion like RE^{3+} can produce several of such acidic OH groups. IR measurements have identified[23,25,26] three types of OH groups in REY and HY zeolites. These have adsorption band at about 3740, 3640 and 3520 cm^{-1}. Of these, OH groups giving rise to the 3650 cm^{-1} band are

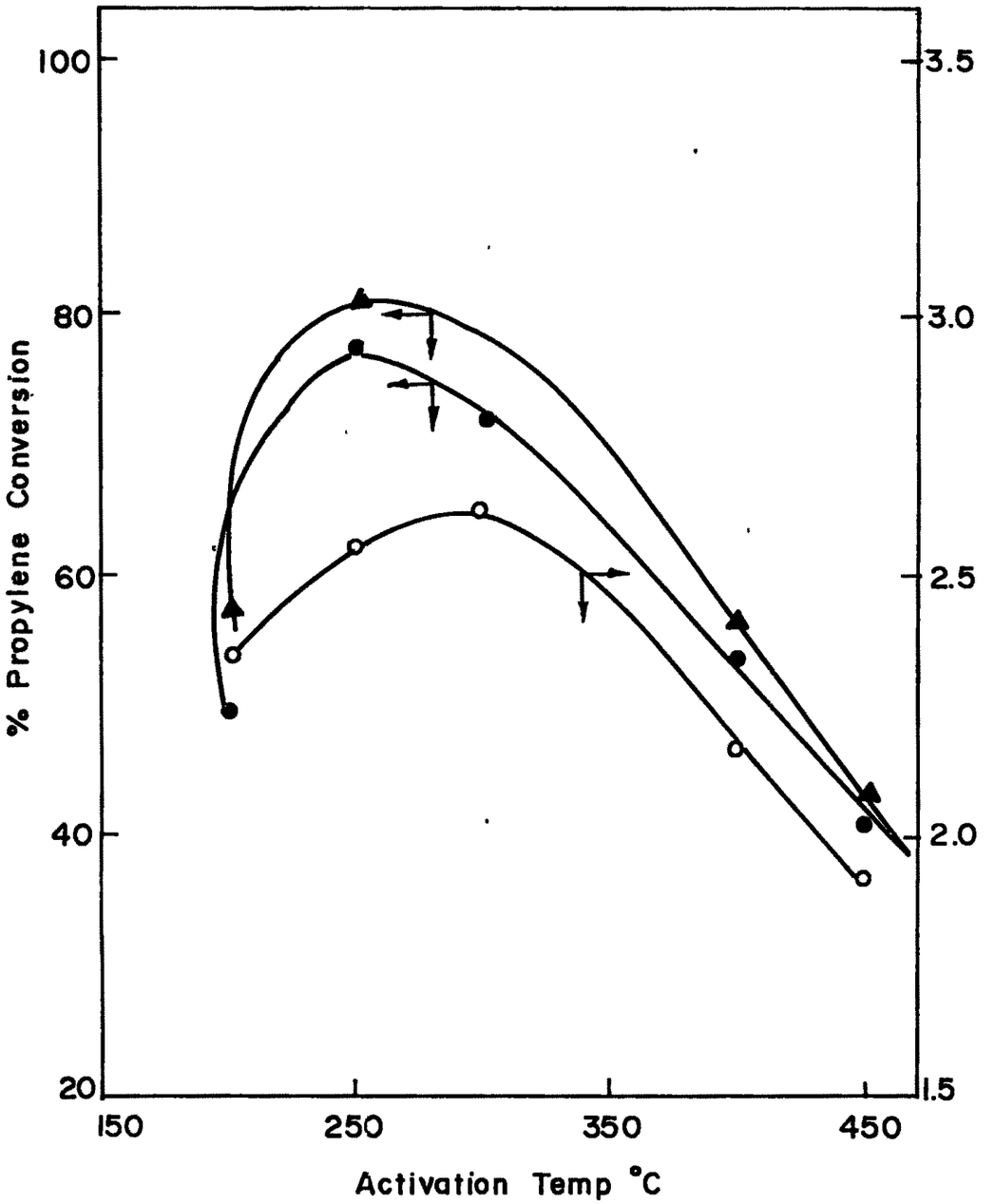

FIG. 3.16 INFLUENCE OF ACTIVATION TEMPERATURE IN THE ISOPROPYLATION OF BENZENE CATALYST : RE(92)Y , REACTION TEMPERATURE 175°C, BENZENE-TO-PROPYLENE MOLE RATIO 8, SPACE VELOCITY: 2.2 h^{-1}, PRESSURE ATMOSPHERIC; (▲) TOTAL PROPYLENE CONVERSION (wt %) , (●) PROPYLENE CONVERSION TO CUMENE (wt %) (O)(DIPB/CUMENE) x 100

located in the cages and are responsible for bronsted acidity of the zeolite. The activation of zeolites in the range 200-400°C shows a large effect on the intensity of this band and is maximum in the range 250-300°C. The thermogravimetry curve in Fig.2.2 for RE(92)y shows that only 1% of water in the hydrated zeolite is lost when zeolite sample was activated at 250°C for a longer period of time indicating no loss of framework hydroxyls, as has happened during the catalyst activation prior to the reaction. The maximum activity observed around 250-300°C may therefore be explained. Lower conversion at activation temperature of 200°C may be due to partial blocking of cages by adsorbed water. Beyond 300°C, the destruction of Brönsted acid sites can be visualised by reversal of the reaction and expulsion of water molecules.

According to Venuto et al[11,27] the mechanism for alkylation reaction involves formation of intermediate (I) which gives secondary carbonium ion (II). This carbonium ion interacts with benzene to give cumene.

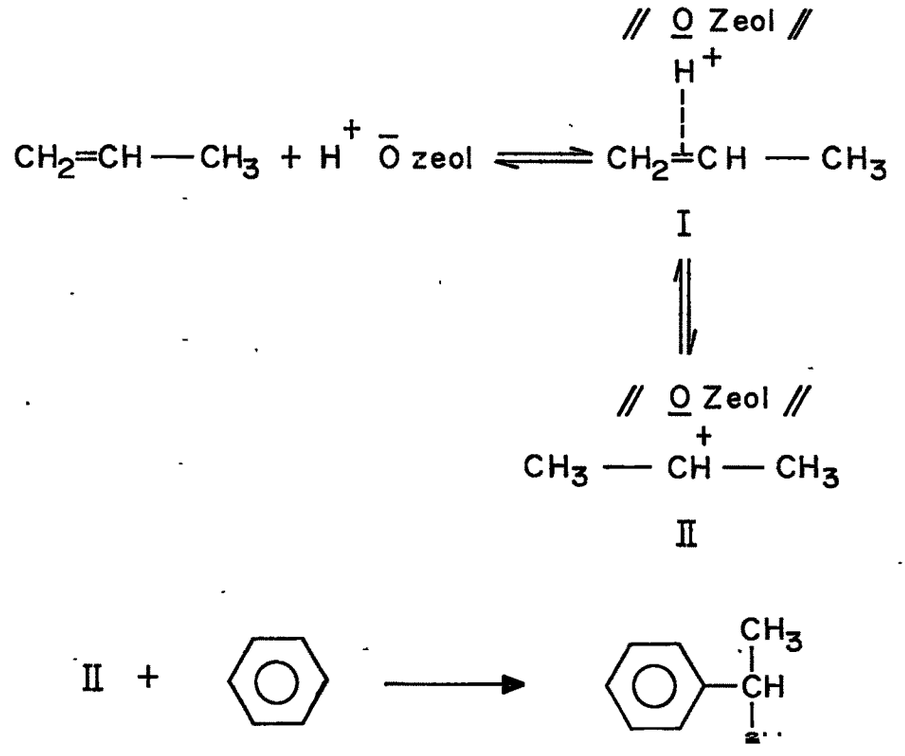

B. Effect of Reaction Temperature

The variation of reaction temperature influences the formation of cumene (Fig.3.17). The optimum conversion of propylene to cumene takes place in the range 175-200°C. Higher temperatures result in cracking rreactions to give unwanted by-products like ethylbenzene and C_7-C_9 aromatics, etc. decreasing the selectivity of propylene to cumene. Cumene also isomerises to n-propylbenzene over acid zeolites at higher temperatures.[28] At lower temperatures, selectivity of propylene to cumene is less because of successive alkylation of cumene to DIPB.

C. Influence of Weight Hourly Space-Velocity (WHSV)

Fig. 3.18 shows the influence of space-velocity on product distribution. Selectivity to cumene is high at lower space velocities having an optimum of 2.5 h^{-1}. Higher space velocities result in decrease in the conversion of propylene leading to low cumene contents and high DIPB amounts.

D. Effect of Benzene to Propylene Mole Ratio

From Fig.3.19 it is evident that higher selectivity of propylene to cumene was observed at higher mole ratios. Due to the presence of higher amounts of propylene at lower mole ratios, successive alkylation of cumene to DIPB takes place. Change in mole ratio also influences the product distribution on account of heat liberated due to exothermicity. In Fig.3.20 the temperature rise observed during the reaction is plotted as a function of mole ratio and space velocity. The temperature rise is more at lower mole ratios and higher space velocities.

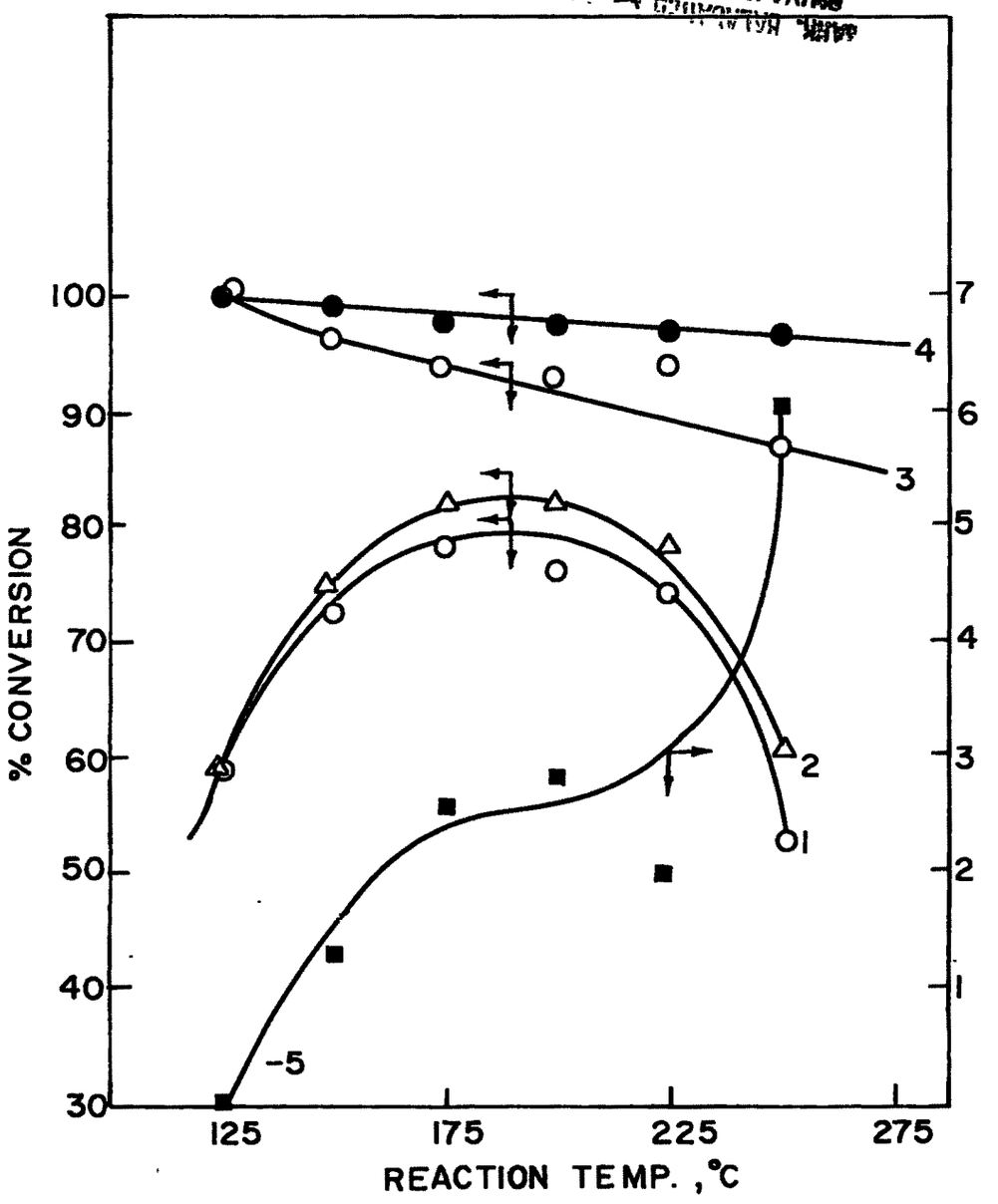

FIG. 3.17 INFLUENCE OF REACTION TEMPERATURE [CATALYST: RE(92)Y, ACTIVATION TEMPERATURE: 250 °C, BENZENE-TO-PROPYLENE MOLE RATIO: 8, WHSV: 2.2 h^{-1}, PRESSURE: ATMOSPHERIC; (1) CONVERSION OF PROPYLENE TO CUMENE (wt %), (2) TOTAL CONVERSION OF PROPYLENE (wt %), (3) % SELECTIVITY OF PROPYLENE TO CUMENE, (4) % SELECTIVITY OF CUMENE BETWEEN CUMENE AND n-PROPYLBENZENE. (5) (DIPB/CUMENE) x100]

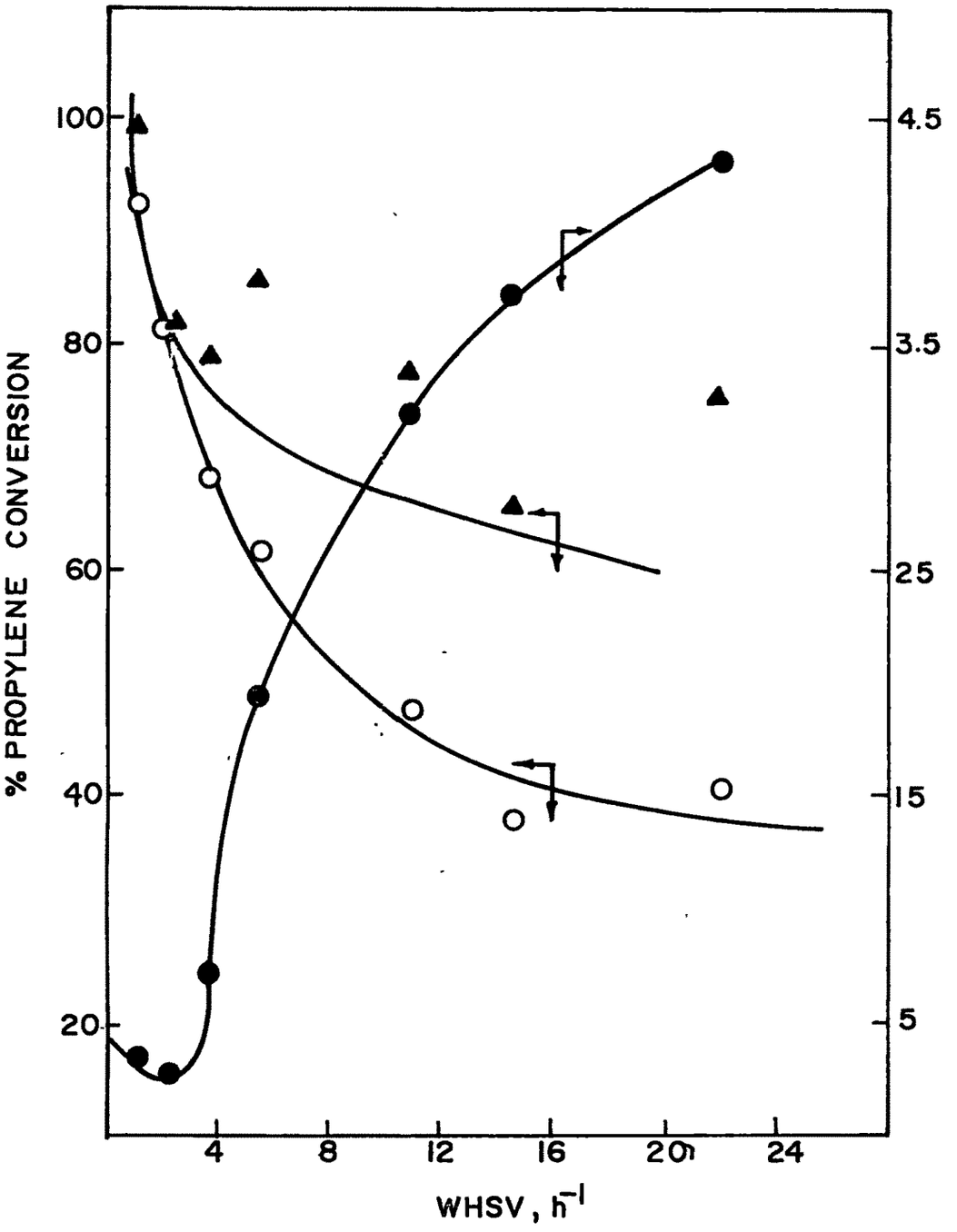

FIG. 3.18 INFLUENCE OF WHSV [CATALYST: RE(92)Y, REACTION TEMPERATURE: 175 °C, BENZENE-TO-PROPYLENE MOLE RATIO: 8, PRESSURE: ATMOSPHERIC; (▲) TOTAL PROPYLENE CONVERSION (Wt %), (○) CONVERSION OF PROPYLENE TO CUMENE (Wt %), (●) (DIPB/CUMENE)x 100]

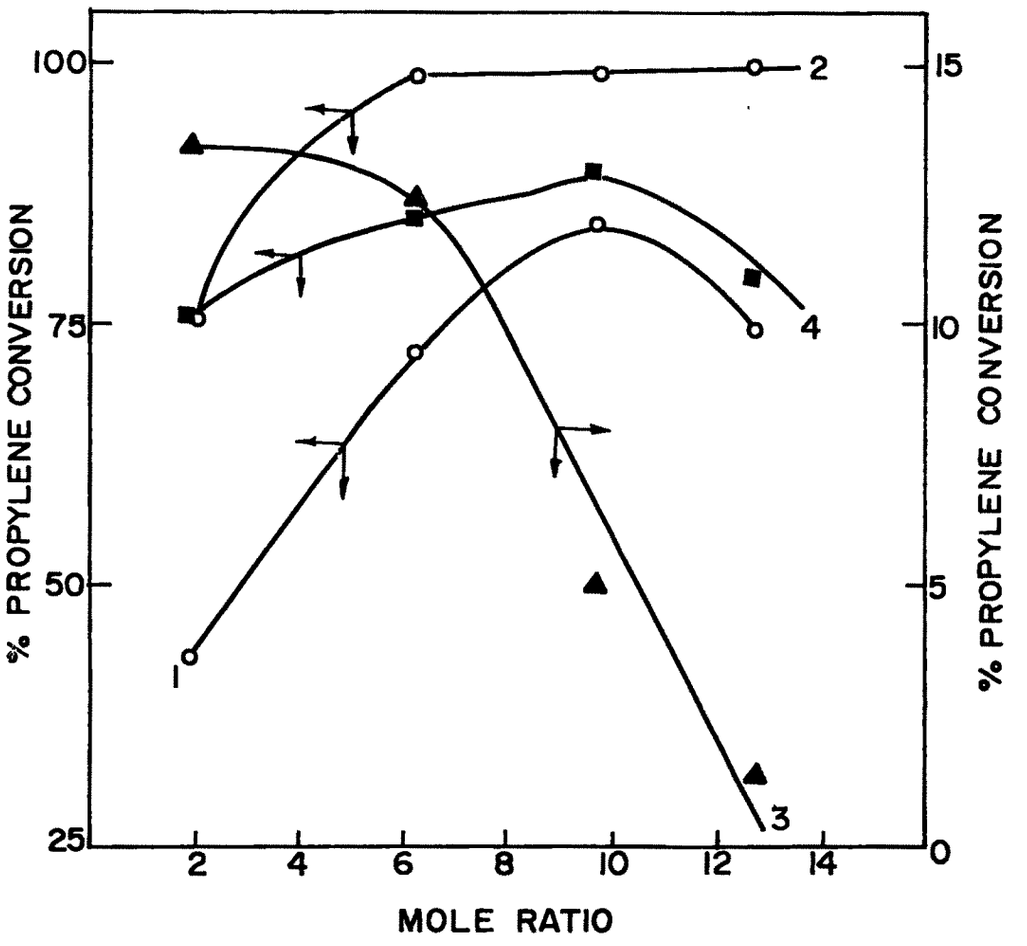

FIG. 3.19 INFLUENCE OF MOLE RATIO [CATALYST: RE(92)Y, REACTION TEMPERATURE: 175°C, BENZENE-TO-PROPYLENE MOLE RATIO: 8, PRESSURE: ATMOSPHERIC; WHSV: 2.2 h^{-1}; (1) PROPYLENE CONVERSION TO CUMENE (wt.%), (2)% SELECTIVITY OF CUMENE BETWEEN CUMENE AND n-PROPYLBENZENE (3) PROPYLENE CONVERSION TO DIPB (wt %), (4) TOTAL PROPYLENE CONVERSION (wt %)]

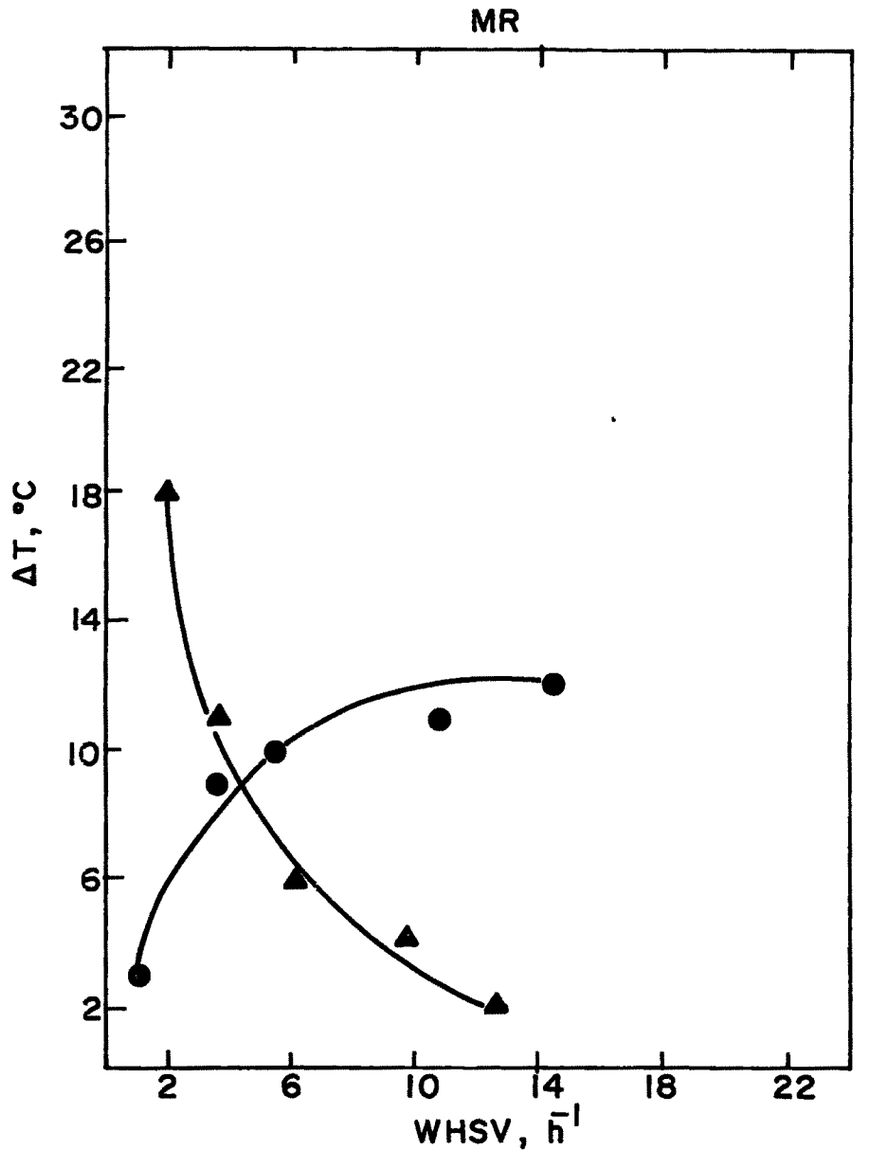

FIG. 3.20 INFLUENCE OF WHSV AND MOLE RATIO ON TEMPERATURE RISE [CATALYST: RE(92)Y, INITIAL TEMPERATURE: 175 °C, PRESSURE: ATMOSPHERIC, (●) WHSV, (h^{-1}), (▲) MOLE RATIO]

E. Effect of Amount of Rare-Earth Content

The thermoanalytical data of rare-earth exchanged faujasites are presented in Table 2.24. With increase in rare-earth content, thermal stabillity and dehydroxylation temperature are increased. In this study, an attempt has been made to correlate acidity and activity of the catalyst, to rare-earth content. Acidity calculated by n-butylamine titrations was observed to increase with rare-earth content. In Table 3.17a and 3.17b conversion of propylene and acidity data of rare-earth exchanged faujasites is presented. Maximum conversion of propylene was observed at 80% exchange with rare-earth ions and also the acidity was found to be maximum. This can be related to accessibility of the active sites to the reactant molecules.[29]

F. Effect of Pressure

Though REY is an active catalyst for the isopropylation reaction, it deactivates within 8-10 h at atmospheric pressure. However, as shown in Fig.3.21 no deactivation was observed at 25 Kg/cm^2 pressure for more than 150 h. At 25 Kg/cm^2 and reaction temperature of 230^oC benzene as well as propylene are in liquid state and the alkylation reaction is a liquid phase reaction. This avoids reactions like oligomerisation which results in the formation of coke. Also it washes out the coke precursors formed, if any. This results in stable and extended activity of the faujasite catalyst. However, an increase in the formation of DIPB was observed at higher pressures.

Table 3.17a

Composition, acidity and conversion to IPB over rare-earth exchanged Y zeolites

Catalyst	Mole % RE_2O_3	Acidity meq/g	% Propylene conversion to IPB
NaY	0	0.015	0
RE(32)Y	0.0260	0.37	28.6
RE(60)Y	0.0425	0.89	83.9
RE(83)Y	0.0582	1.25	90.23
RE(92)Y	0.0660	1.21	77.24

Table 3.17b

Isopropylation of benzene over rare earth exchanged Y zeolites

Influence of rare-earth content

Activation temp.(^{o}C)=250, Reaction temp.(^{o}C)=175
(Benzene:Isopropanol) mole=8, WHSV (h^{-1}) = 2.2

CATALYST	RE(32)Y	RE(60)Y	RE(83)Y	RE(92)Y
Product weight %				
Aliphatics	0.14	0.30	0.58	0.58
Benzene	92.92	82.98	81.92	84.50
Toluene	-	0.07	0.11	0.21
C_8 Aromatics	-	0.25	0.22	0.32
Cumene (IPB)	5.15	15.12	16.26	13.92
npB	-	0.12	0.15	0.11
C_9-C_{11} Arom	-	0.17	-	-
DIPB	1.79	0.99	0.76	0.48
HBF	-	-	-	-
Prop. Conv. to IPB %	28.6	83.9	90.23	77.24
≥Alkylates (α) %	43.31	92.69	97.3	81.8

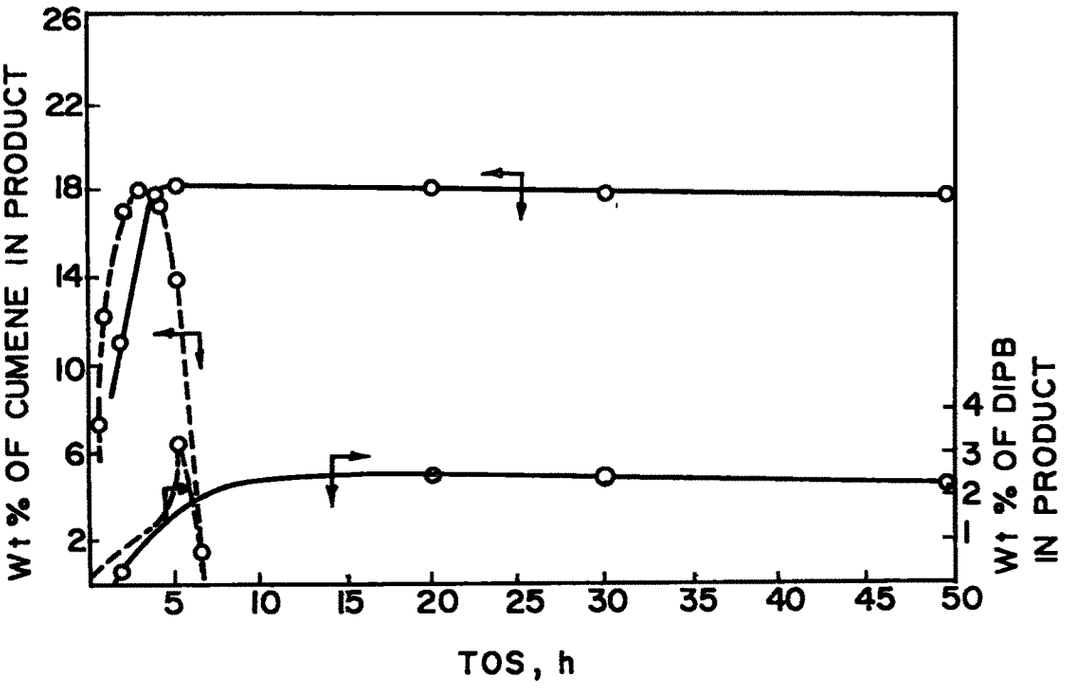

FIG.3.21 INFLUENCE OF PRESSURE ON PROPYLENE SELECTIVITY TO CUMENE AND DIPB [CATALYST: RE (83) Y, REACTION TEMPERATURE : 210°C, WHSV : 2.2 h^{-1}; ——— 25 Kg/Cm^2 PRESSURE, ------- ATMOSPHRIC PRESSURE]

3.6 MECHANISM

A carbonium ion mechanism analogous to that postulated[30] for the ethylation of benzene may be applicable for the propylation of benzene with isopropanol. The isopropanol molecule is activated at a Brönsted acid site of the zeolite resulting in an adsorbed electrophilic species. This is followed by transfer of a isopropyl group to the aromatic ring and transfer of a proton back to a catalyst site.

Scheme A

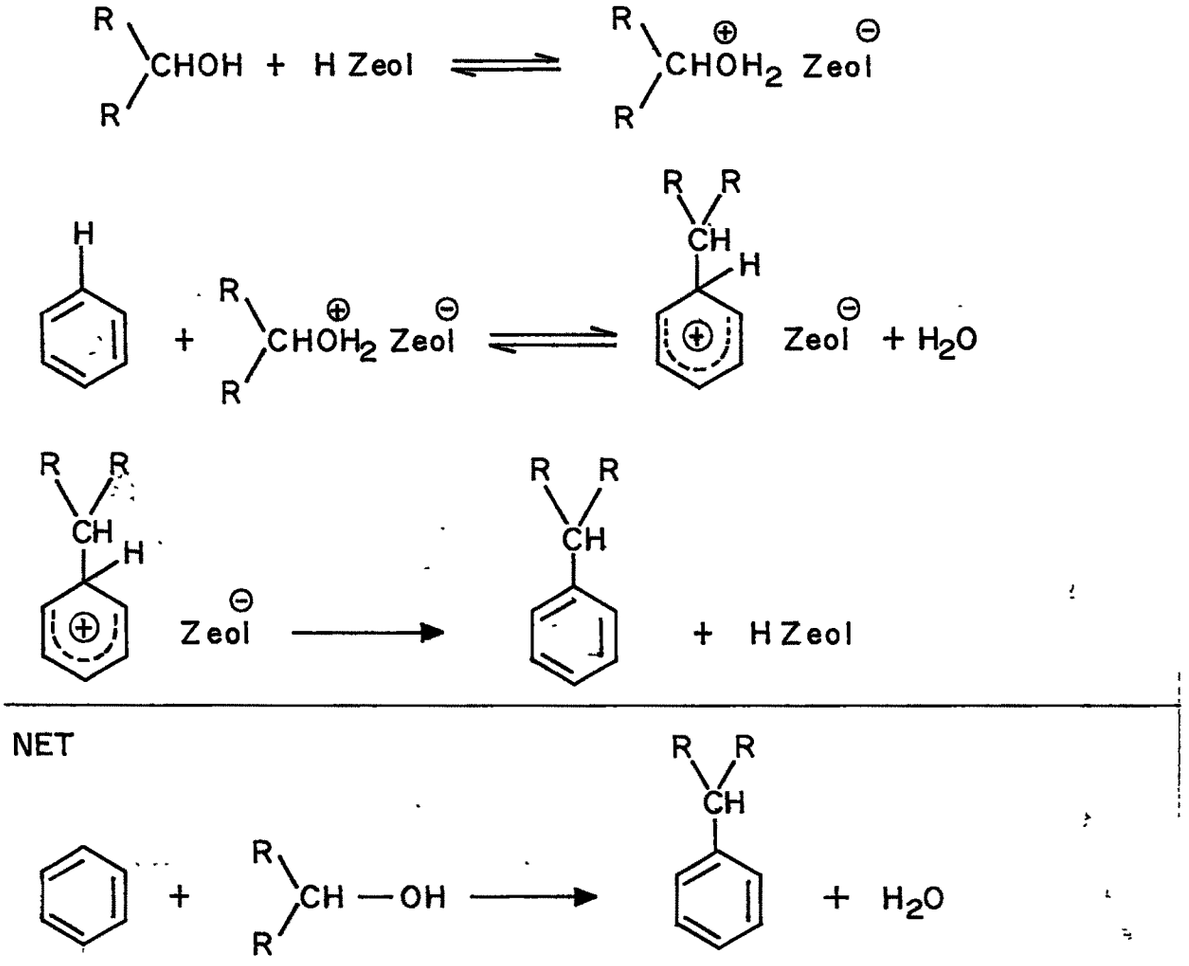

where R = CH_3

The formation of n-propylbenzene occurs as per scheme shown below when propylene is used as alkylating agent.

Scheme B

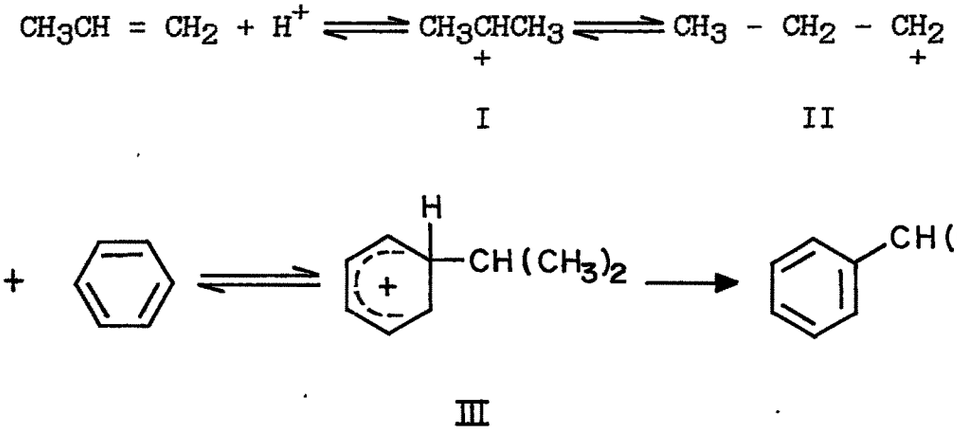

When isopropanol is used as an alkylating agent, eventhough isopropylbenzene is primary product n-propylbenzene formation is observed at high temperatures. It is due to the dealkylation of isopropylbenzene and rearrangement of carbocation of propylene as shown in Scheme B which is more favourable at high temperature.[31]

3.7 CONCLUSIONS

1) The alkylation of benzene with isopropanol to form isopropylbenzene is a Brönsted acid catalysed reaction.

2) The optimum reaction temperature for alkylation of benzene with isopropanol lies around 210°C.

3) The formation of impurities is influenced by reactant mole ratio rather than space velocity. The optimum WHSV and reactant mole ratio are found to be 2.2 h^{-1} and 8:1 (Benzene:Isopropanol) respectively.

4) Pressure has marked influence on the product pattern. At 210^{o} and above 25 Kg/cm^{2} of pressure, benzene being in liquid state, the catalyst life is improved. More DIPB is formed at higher pressure when iropropanol is used as alkylating agent.

5) The different alkylating agent (propylene, isopropanol, n-propanol) did not show any change in product pattern except the change of temperature.

6) On dealumination mordenite showed stable and extended activity.

7) Though isomerisation of isopropylbenzene to n-propylbenzene is temperature dependent reaction, the ipB/npB ratio can be increased with increasing SiO_2/Al_2O_3 ratio and by high temperature calcination of the mordenite catalyst.

8) Incorporation of phosphorous reduces surface hydroxyl groups. Also a reduction in activity and elimination of cracked products was observed.

9) Activity of the rare earth exchanged zeolites can be correlated to Brönsted acidity, which depends up on rare earth content and activation temperature.

REFERENCES

1. J.J. McKetta, "Encyclopedia of Chemical Processing and Design", Marcel Dekker, Inc., New York, 2387 (1977).
2. H.G. Karge, "Molecular Sieves-II", ACS Symposium Series, J.R. Katzer (Editor), 40, 584 (1977).
3. N.Y. Chen, W.W. Kaeding and F.G. Dwyer, J. Am. Chem. Soc. 101, 6783-84 (1979).
4. E.G. Derouane and Z. Gabelica, J. Catal. 65, 486-489 (1980).
5. N. Topsøe, K. Pederson and E.G. Derouane, J. Catal. 70, 41 (1981).
6. V.R. Choudhary and V.S. Nayak, Zeolites 5, 15 (1985).
7. W.W. Kaeding, L.B. Young, C.C. Chu, B. Weinstein and S.A. Butter, J. Catal. 67, 159 (1981).
8. J.C. Vedrine, A. Auroux, P. Dejaifve, V. Ducarone, H. Hoser and S. Zhous, J. Catal. 73, 147 (1982).
9. W.W. Kaeding and S.A. Butter, J. Catal. 61, 155 (1980).
10. J. Klinowski, J.M. Thomas, M.W. Anderson, C.A. Fyfe and G.C. Gobbi, Zeolites 3, 5 (1983).
11. P.B. Venuto, L.A. Hamilton, P.S. Landis and J.J. Wise, J. Catal. 5, 81 (1966).
12. P.B. Venuto and P.S. Landis, Adv. Catalysis 18, 259 (1968).
13. Kh. M. Minachev, V.I. Garanin and Ya.I. Isakov, Russ. Chem. Rev. 35, 903 (1966).
14. W.J. Taylor, D.D. Wagman, M.G. Williams, K.S. Pitzer and R.D. Rossini, J. Res. Nat. Bur. 37, 95 (1946).

15. K.H. Chandavar, S.G. Hegde, S.B. Kulkarni and P. Ratnasamy, J. Chem. Tech. Biotechnol. 34A, 165-173 (1984).

16. C.V. Hidalgo, H. Itoh, T. Hattori, M. Niwa and Y. Murakami, J. Catal. 85, 362 (1984).

17. G. Peeters, A. Thys., P. Devievre and E.F. Vasant, Preprint from the 6th Int. Zeolite Conf., Reno. S-49 (1983).

18. M. Niwa, S. Kato, T. Hattori and Y. Murakami, J. Chem. Soc. Faraday Trans. 80, 3135 (1984).

19. I. Balkrishnan, S.G. Hegde, B.S. Rao, V.P. Shiralkar, C.V. Kavedia, V.R. Chumbhale and S.B. Kulkarni, Proc. 4th Natl. Symp. on Catalysis, Bombay (India), p.421 (1978).

20. H.A. Bensi, J. Catal. 8, 368 (1967).

21. H.W. Kouwenhoven, ACS 121, "Molecular Sieve", (Eds. W.M. Meier and J.W. Uytterhoven), p.529 (1973).

22. C.J. Thomas and D.S. Barmby, J. Catal. 12, 341 (1968).

23. a. J.W. Ward, J. Catal. 9, 225 (1967).
    b. ibid 10, 34 (1968).
    c. ibid 13, 321 (1969).

24. J.A. Rabo, C.L. Angell and Schomaker, "Fourth Int. Congress on Catalysis", Moscow, Preprint 54 (1968).

25. P.E. Eberley, Jr., and C.N. Kimberlin, Jr., "Molecular Sieve Zeolites-II", Advan. Chem. Ser. 102 (Ed. E.M. Flanigen et al.), Am. Chem. Soc., Washington D.C., p.374 (1971).

26. Y.B. Taarit, M.V. Mathien, C. Naccache, in Adv. Chem. Series 102, "Molecular Sieve Zeolite-II", (Eds. E.M. Flanigen et al.), 362 (1971).

27. P.B. Venuto, L.A. Hamilton and P.S. Landis, J. Catal. 5, 484 (1966).

28. H. Pines, "Chemistry of Catalytic Hydrocarbon Conversions", (Academic Press, New York) 1981.

29. T. Kazuo and T. Hiroshi, J. Catal. 24, 1 (1972).

30. J.R. Anderson, T. Mole and V. Christov, J. Catal. 61, 477 (1980).

31. P.E. Keown, C.C. Meyers, R.G. Wetherold, U.S. Patent 3,751,504 (1973).

****

CHAPTER - 4

STUDIES ON ALKYLATION OF PHENOL WITH METHANOL

****

4.1 EXPERIMENTAL

(A) : Materials

A.R. grade phenol and methanol (GR) were used without further purification.

(B) : Catalysts

All the zeolite catalysts utilized in this study were prepared by a synthesis procedure described in Section 2.5. The HZSM-5 zeolites with varying SiO_2/Al_2O_3 ratio were characterised by XRD, sorption measurements, SEM and TPD of NH_3. The chemical composition of these zeolites is presented in Table 4.1.

(C) : Apparatus and Procedure

The apparatus and procedure followed for the reaction as well as the analysis of the products is described in Chapter 3. The liquid products were analysed by GC using a column of 3%OV 225 on chromosorb AW (6 feet x 1/8" i.d.) and another packed with 5% NPGSB + 1% H_3PO_4 on Anakrome A (6 feet x 1/8" i.d.). The gaseous products were analysed using a porapak-Q column (6 feet x 1/8" i.d.).

4.2 RESULTS AND DISCUSSION

The XRD, SEM and sorption data are presented in Fig. 2.19, 2.14b, and Table 4.2 respectively. These are in agreement with those reported for ZSM-5 zeolites[1,2].

(A) Influence of Temperature

The feed was prepared by dissolving AR grade phenol in methanol (GR) in the required mole ratio and was passed over the

TABLE : 4.1

CHEMICAL COMPOSITION OF HZSM-5 ZEOLITES (ANHYDROUS)

SAMPLE	CHEMICAL FORMULAE	SiO_2/Al_2O_3
HZSM-5	$Na_{0.02}H_{5.0}(AlO_2)_{5.02}(SiO_2)_{90.98}$	36
HZSM-5	$Na_{0.03}H_{2.25}(AlO_2)_{2.28}(SiO_2)_{93.72}$	86
HZSM-5	$Na_{0.07}H_{0.89}(AlO_2)_{0.96}(SiO_2)_{95.04}$	200

TABLE : 4.2

SORPTION OF WATER AND HYDROCARBON, SURFACE AREA AND VOID VOLUME OF HZSM-5 ZEOLITES

Zeolite[a]	n = Sorbate uptake(molecule u.c.$^{-1}$)[b]					Surface area	Pore vol.
	Water	CH	B	OX	TMB	M^2g^{-1}	ccg^{-1}
HZSM-5(36)	40.75	6.80	10.18	2.56	2.10	427.85	0.167
HZSM-5(86)	33.20	5.23	11.38	1.97	0.78	438.22	0.164
HZSM-5(200)	17.90	2.40	10.00	1.14	0.60	413.00	0.158

a : Figures in parenthesis indicate SiO_2/Al_2O_3 ratio

b : Sorption values at 25°C and P/P_o = 0.5

Abbreviations : CH = Cyclohexane
B = Benzene
OX = ortho-xylene
TMB = 1,2,4 trimethylbenzene

catalyst at the desired rate using the feed pump.

Table 4.3 lists the effect of temperature on the alkylation of phenol. Dimethyl ether (DME) is invariably one of the products. The analysis of gaseous products revealed the presence of CH_4 in large amounts (C_2 and C_3 hydrocarbons in traces) in addition to DME. The faster deactivation is attributed to the methanol reaction. Also, some unreacted methanol was noticed. Though all the hydroxylated products increased with increase in temperature, the increase in the yield of xylenols is more pronounced. Simultaneous and larger increase in the yield of xylenols indicates the ease of alkylation of cresols compared to phenol. At higher temperature (400°C), the yield of hydrocarbons by conversion of methanol becomes appreciable. Both aliphatic and aromatic hydrocarbons appear at 400°C. Among the cresols, o-cresol is predominant. Its yield is higher than the thermodynamic equilibrium value (32 %). m-Cresol, if formed, is present in small quantities and all that is happening is substitution of methyl group at the ortho and para position characteristics of electrophilic substitution. The observed yield of ortho-cresol > 60% (Table 4.3) is consistent with clean electrophilic substitution and evidence for total absence of steric hindrance to the entering CH_3^+, due to the OH-group. Further, absence of any higher yield of para-cresol shows that the higher para-selectivity observed in other reactions such as toluene alkylation with methanol or ethylbenzene alkylation with ethanol catalysed by modified ZSM-5 zeolites is absent here. The proportion of o-cresol in cresols decreases with temperature.

TABLE : 4.3

INFLUENCE OF TEMPERATURE ON PHENOL ALKYLATION OVER HZSM-5 ZEOLITE*

Activation Temp.^{o}C = 550; Methanol:Phenol (mole ratio) = 1

WHSV (h^{-1}) = 3

Product weight %	Temperature ^{o}C			
	250	300	350	400
Dimethyl ether	4.0	2.8	2.8	0.6
Aliphatics	4.3	4.1	5.2	21.4
Methanol	12.3	12.4	5.9	-
Anisole	4.5	4.6	8.3	12.7
Phenol	72.7	72.2	62.3	36.6
o-Cresol	1.2	1.8	7.1	8.6
(p+m) Cresol	0.5	1.2	4.1	9.8
Xylenols	0.3	0.1	1.6	6.5
Aromatics	0.2	0.8	2.6	3.8
Unidentified**				
% o-Cresol in total cresols	70.6	60.6	63.3	46.7
Thermodynamic value at 250^{o}C	32			

* SiO_2/Al_2O_3 mole ratio = 86

** Alkylated products plus methyl substituted anisoles.

Among the xylenols, 2,4 and 3,4 xylenols have been identified. 2,6 Xyleneol, if formed, is formed only in trace quantities. This is contrary to published literature[3], steric hindrance seems to become important at this stage of alkylation. 2,4 Xylenol is formed in larger amounts. The unidentified products may consist of isomers of methyl substituted anisoles.

(B) : Influence of reactant mole ratio

Table 4.4 presents data for the effect of mole ratio (methanol/phenol) on product distribution. The increase in the yield of xylenols and other alkylated products is as expected. For this reason, a lower mole ratio of alkylating agent to the substrate is preferred in alkylation reactions to inhibit multiple alkylations[4].

(C) : Influence of Space Velocity (WHSV)

Table 4.4 (column 3 and 4) also shows the effect of increasing WHSV on product distribution. It is seen that lower WHSV favours formation of cresols and xylenols.

(D) : Influence of SiO_2/Al_2O_3 molar ratio

The influence of increasing mole ratio (SiO_2/Al_2O_3) on the product distribution is shown in Table 4.5. The increae in DME and unconverted methanol is due to decrease in acidity of the zeolite with increase in the mole ratio[5]. Fig. 4.1 and Table 4.6 describe the acidity of HZSM-5 zeolites. An increase in the ratio of cresols to xylenols is also observed for the same reason. Higher alkylated products also show a marginal decrease. The proportion of 2,4 xylenol in xylenols is, however, found to

TABLE : 4.4

INFLUENCE OF METHANOL TO PHENOL MOLE RATIO IN PHENOL ALKYLATION OVER HZSM-5[a]

Activation temp. ^{o}C = 550: Reaction temp.^{o}C = 350, WHSV(h^{-1}) = 3

Product weight %	Methanol to phenol mole ratio			
	1	2	4	*
Dimethyl ether	2.8	6.1	5.8	7.0
Aliphatics	5.2	4.6	14.3	2.0
Methanol	5.9	12.3	23.1	24.7
Anisole	8.3	9.5	7.4	4.4
Phenol	62.3	46.7	30.3	54.5
o-Cresol	7.1	9.1	7.2	3.6
(p+m) Cresol	4.1	4.7	4.0	1.8
Xylenols	1.6	2.1	2.3	0.6
Aromatics	2.7	4.9	5.6	1.4
Uidentified**				
% o-cresol in total cresols	63.3	65.9	64.9	67.1
% 2,4 xylenol in total xylenols	76.4	96.0	94.6	-

* WHSV = 8, mole ratio 4.
** Alkylated products plus methyl substituted anisoles
a SiO_2/Al_2O_3 mole ratio = 86

TABLE : 4.5

INFLUENCE OF SiO_2/Al_2O_3 MOLE RATIO IN PHENOL ALKYLATION OVER HZSM-5

Activation temp.^oC = 550, Reaction temp.^oC = 350,

methanol :phenol (mole ratio) = 1, WHSV (h^{-1}) = 3

Product weight %	SiO_2/Al_2O_3 mole ratio		
	36	86	200
Dimethyl ether	1.4	2.8	3.5
Aliphatics	6.7	5.2	2.4
Methanol	3.3	5.9	10.7
Anisole	1.3	8.3	5.3
o-Cresol	9.7	7.1	6.6
(p+m) Cresols	6.3	4.1	3.9
Xylenols	3.4	1.6	1.7
Aromatics unidentified *	4.8	2.7	2.7
% o-Cresol in total cresols	60.6	63.3	62.8
% 2,4 Xylenol in total xylenols	85.0	76.4	70.9

* Alkylated products plus methyl substituted anisoles.

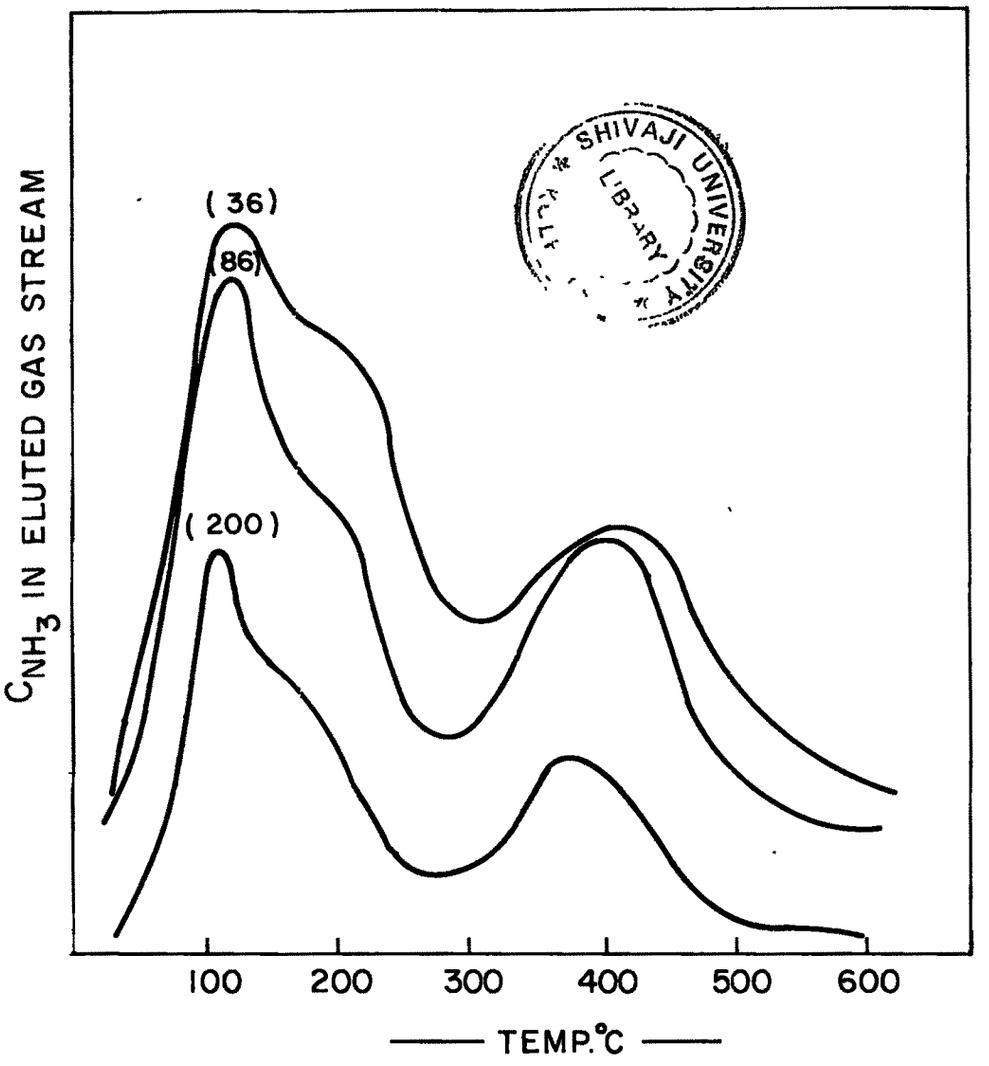

FIG.4-1-THE TEMPERATURE PROGRAMMED DESORPTION OF NH_3 FROM HZSM-5 ZEOLITES FIGURES IN PARENTHESIS INDICATE SiO_2/Al_2O_3 RATIO.

TABLE : 4.6

THE CONCENTRATION OF SURFACE ACID SITES

Sample	SiO_2/Al_2O_3 molar ratio	Al/uc	T_{max} (strong sites) ^oC	Acid sites/unit cell		
				Weak + medium	Strong	Total
HZSM-5	36	5.02	407	8.81	3.34	12.15
HZSM-5	86	2.28	400	6.68	1.60	8.28
HZSM-5	200	0.96	367.5	3.78	0.92	4.7

decrease.

4.3 ALKYLATION OF PHENOL OVER HFeZSM-5 ZEOLITE

The FeZSM-5 zeolite having SiO_2/Fe_2O_3 molar ratio of 200 was synthesised and modified as per procedure described[6]. This was studied for phenol alkylation. Table 4.7 shows the product distribution as a function of temperature. It is seen that with increase in temperature the yield of cresols and xylenols increased with simultaneous formation of impurities which could be isomers of methyl substituted anisoles. The decrease in the cresol to xylenol ratio shows the ease of alkylation of cresol compared to phenol. The ring alkylation is more favoured than the o-alkylation which is implied by the increase in the cresol to anisole molar ratio and is consistent with clean electrophilic substitution.

4.4. ALKYLATION OF PHENOL OVER Al-, Fe-, B-, and La-ZSM-5 ZEOLITES

The Al-, Fe-, B- and La-ZSM-5 zeolites were synthesised and converted to their protonic form as described earlier[6-8]. The data for alkylation of phenol over different isomorphously substituted zeolites and HLaZSM-5 in which La^{3+} can occupy only ion exchanged position or can be present only as a occluded phase are shown in Table 4.8. The data shows that the total conversion of phenol during alkylation over HAlZSM-5 is highest and over HLaZSM-5 the least. This is similar to the trend in acidity of zeolites which is Al > B > Fe > La. However, selectivity of o-cresol among cresols is the highest for HFeZSM-5. This may be due

TABLE : 4.7

ALKYLATION OF PHENOL WITH METHANOL OVER HFeZSM-5 ZEOLITE

Activation temp. 550°C, WHSV (h^{-1}) = 2.64,

Methanol:Phenol (mole ratio) = 4

Reaction temp.(°C)	250	300	350
Product weight %			
Dimethyl ether	4.23	3.28	4.97
Aliphatics	0.09	0.14	0.27
Methanol	17.69	34.32	26.05
Anisole	4.04	5.36	6.09
Phenol	69.47	43.92	33.73
o-Cresol	2.87	5.73	10.17
(p+m) Cresol	1.09	2.87	4.89
Xylenols	0.43	1.34	4.06
Aromatics - unidentified*	0.08	3.04	9.76
Cresol	3.96	8.60	15.06
Cresol/xylenol (mole)	10.35	7.21	4.18
Cresol/Anisole (mole)	0.98	1.59	2.47

* Alkylated products plus methyl substituted anisoles.

TABLE 4.8

ALKYLATION OF PHENOL WITH METHANOL OVER ZSM-5 ZEOLITES

Activation temp.^{o}C = 550, Reaction temp.^{o}C = 250

WHSV(h^{-1}) = 2.64, Methanol : Phenol (mole ratio) = 4

Catalyst	HAlZSM5(200)	HBZSM5(200)	HFeZSM5(200)	HLaZSM5(200)
Product Wt. %				
Dimethyl ether	3.30	2.19	3.42	1.35
Aliphatics	0.68	0.87	0.98	0.74
Methanol	39.68	33.88	30.51	32.79
Anisole	5.67	5.71	4.42	2.48
Phenol	44.87	52.0	54.22	60.00
o-Cresol	3.59	2.66	3.66	1.54
(p+m) Cresol	1.82	0.99	1.19	0.82
Xylenols	0.29	0.17	0.60	0.09
Aromatics - unidentified*	0.10	1.52	1.00	0.19
% O-Cresol in total cresols	66.35	72.87	75.46	65.25

* Alkylated products plus methyl substituted anisoles.

to largest pore size of HFeHZSM-5. In HFeZSM-5 the Fe-O (1.97A°) linkage is longer than Al-O linkage (1.75A°)[9] in HAlZSM-5 and can therefore have slightly larger pore size.

4.5. MECHANISM OF ALKYLATION

Two mechanisms have been proposed for methylation of pheno[3,10]. One of these follows the anisole route and the other the diphenyl ether route. Both these involve adsorption of the acidic phenol at the active site. It is probably better explained via formation of a labile methyl cation first suggested by Ono and Mori[4] for the conversion of methanol to hydrocarbons. This visualises formation of labile methyl cation as shown below:

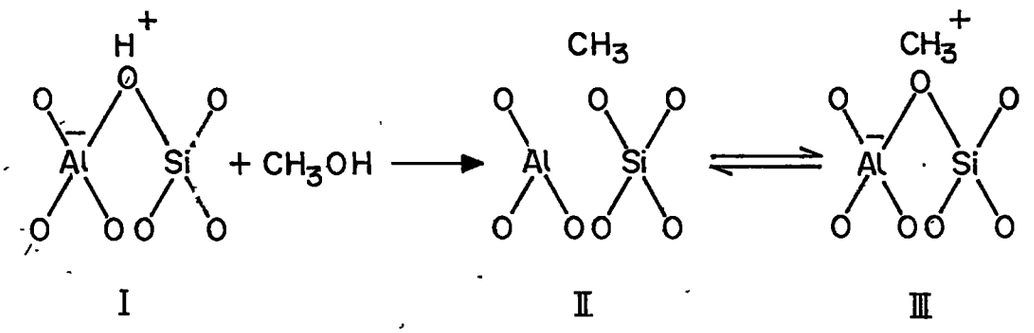

I II III

Brönsted acid site in the zeolite racts with methanol eliminating water and producing methoxy group on the surface structure II exists in equilibrium with the labile CH_3^+ ion (structure III). CH_3^+ reacts with phenol to produce either anisole or cresol depending upon whether it attacks oxygen or the ring. The former is favoured at higher temperature.

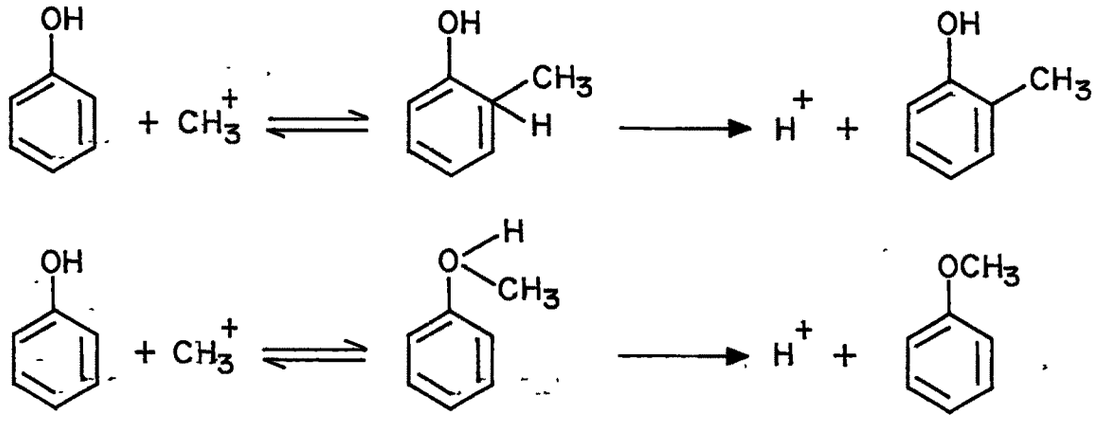

4.6. **CONCLUSIONS**

1. Study shows that alkylation of phenol over HSM-5 yields cresols in their equilibrium distribution.

2. Formation of 2,6 xylenol is negligible in this reaction, probably due to shape selective factors.

3. Unmodified ZSM-5 gives cresols in the thermodynamic equilibrium distribution. No p-selectivity is observed.

REFERENCES

1. J.R. Anderson, K. Foger, T. Mole, R.A. Rajadhyaksha and J.V. Sanders, J. Catal. 58, 114 (1979).
2. E.L. Wu, G.R. Landolt and A.W. Chester in New Developments in Zeolite Science and Technology, edited by Murakami, Iijima and Ward (Elsevier Amsterdam), 547 (1986).
3. P.D. Chantal, S. Kaliaguine and J.L. Grandmaison, Appl. Catal. 18, 133 (1985).
4. Y. Ono and T. Mori, J. Chem. Soc. Far. Tr. I, 77, 2209 (1981).
5. N. Topsøe, K. Pederson and E.G. Derouane, J. Catal. 70, 41 (1981).
6. A.N. Kotasthane, V.P. Shiralkar, S.G. Hegde and S.B. Kulkarni, Zeolites 6, 253 (1986).
7. P. Ratnasamy, A.N. Kotasthane, V.P. Shiralkar, S.B. Kulkarni and A.J. Chandwadkar, Indian Patent No.164416 (1988).
8. M. Taramaso, G. Perego and B. Notari, "Proc. 5th Intl. Conf. Zeolites, Naples" (Heydon, London), p. 40 (1980).
9. R.B. Borade, "Synthesis and Characterization of ZSM-5 Zeolites", Ph.D. Thesis, University of Poona (1983).
10. S. Balsama, P. Eeltrame, P.L. Carniti, L. Forni and G. Zuretti, Appl. Catal. 13, 161 (1984).

****

CHAPTER - *5*

SUMMARY

****

SUMMARY

The alkylation of benzene with ethylene and propylene to produce ethylbenzene and cumene, respectively, are major industrial processes in petrochemical industry. While pentasil zeolites have replaced the earlier $AlCl_3$ and BF_3^- based catalysts for production of ethylbenzene, cumene, the precursor for phenol, is still produced using solid phosphoric acid catalysts. There are also other limitations in the use of the latter catalysts for cumene process.

(1) The catalyst cannot be regenerated.
(2) The moisture content has to be regulated precisely to avoid leaching and deactivation of the catalyst.
(3) Transalkylation of diisopropylbenzene (formed to an extent of about 5% wt.) with benzene cannot be carried out.
(4) Environmental problems associated with the disposal of phosphoric acid sludge.

In view of the above limitations there are worldwide efforts to find an alternate catalyst system for this process.

The present studies aim at the selective synthesis of cumene (Isopropylbenzene) over mordenite and type Y zeolite catalysts. Some aspects of the applications of phosphorus and rare earth modified zeolite catalysts for this reaction are also outlined. The objective of this work is to study the influence of acid sites of varying acid strength of zeolite mordenite on their physico-chemical behaviour towards the selective formation of

cumene. The modificaticn in the acidity of mordenite catalysts has been achieved by (i) dealumination with the treatment of mineral acid (Hydrochloric acid), (ii) ion exchange with rare earth cations and by impregnation with phosphorus, (iii) degassing of zeolite at higher activation temperature, (iv) injecting poisons like pyridine or water, (v) surface silynation and (vi) deposition of coke. The activity of some of these modified zeolites are compared with those of ZSM-5 and ZSM-12 zeolites in propylation of benzene.

SYNTHESIS AND CHARACTERIZATION

Mordenite was synthesized under hydrothermal condition and at autogeneous pressure following the patented procedure. Na-mordenite was dealuminated with mineral acid to obtain aluminium deficient mordenite in the H-form. The phosphorus impregnated mordenites were prepared by impregnation of H-mordenite with o-phosphoric acid. Similarly rare earth Y and rare earth mordenite were prepared by exchanging these zeolites with appropriate amount of stock solution containing 3.03% RE_2O_3 by weight. The HZSM-5 and HZSM-12 zeolites were also synthesized following the patent literature.

The crystalline purity and the changes in the unit cell volume were ascertained with X-ray diffractometry. A reduction in unit cell volume upon dealumination was noticed. The stability of dealuminated mordenites was determined by thermogravimetric technique. Removal of aluminium atoms was explained on the basis of shifting of vibrational band of TO_4 tetrahedra to the higher

wave number and on the basis of intensity of band assigned to isolated AlO_4^- tetrahedra in the IR spectra. Dealumination was further confirmed by ^{29}Si MAS NMR. The surface acidity of Al-deficient mordenite was evaluated by temperature programmed desorption (t.p.d.) of NH_3. The total acidity estimated by the t.p.d. (NH_3 desorption) is related to the Al atoms/u.c. and is a direct measure of the number of acid sites present in the zeolite. X-ray photoelectron spectroscopy showed less aluminium concentration in the external layer than in the bulk of H-mordenite (HM). On dealumination, the aluminium concentration in the external layer decreased considerably.

The acidity of the rare earth exchanged Y zeolite was estimated by n-butylamine (nBA) titration using butter yellow as an indicator. The studies of sorption of water over dealuminated mordenites showed a decrease in the equilibrium capacity which is related to the hydrophobicity of the zeolite on dealumination. A marked increase in the equilibrium sorption capacities for benzene, cyclohexane, cumene and n-hexane is observed. This is attributable to increased Dubinin pore volume estimated by sorption of nitrogen at -195^{o}C. The zeolite incorporated with phosphorus showed a decrease in the uptake of solvents and a decrease in void volume. With the increase in the degree of exchange of the rare earth ion, the decrease in sorption capacity of type Y zeolite was observed. This has been ascribed to the unit cell contraction. The applicability of Dubinin equation of free energy of adsorption (ΔG^{o}) has been carried out for rare earth exchanged mordenites.

CATALYTIC REACTIONS

Catalytic reactions were carried out in a fixed bed down-flow integral silica reactor at atmospheric pressure. The high pressure study was carried out in a catatest unit (Geomechanique, France). The gaseous and liquid products were analysed by gas-chromatography.

SYNTHESIS OF IROPROPYLBENZENE (CUMENE)

The alkylation of benzene with isopropanol over pure and modified zeolites has been investigated under different process conditions such as reaction temperature, reactant mole ratio and space velocity. The major products were cumene, diisopropylbenzene along with small amounts of toluene, C_8, C_9-C_{11} aromatics. Tripropylbenzene and some unidentified higher boiling fractions (HBF) were formed in small amounts. The relative concentration of secondary products were found to depend on process conditions. The optimum process conditions were reaction temperature = 210^{o}C, reactant mole ratio = 8 and space velocity = 2.2 (h^{-1}). The long stable activity found in dealuminated mordenite was attributed to highly siliceous composition. The negligible oligomerisation, cracking reaction and coke formation is related to the highly hydrophobic nature and low acidity of dealuminated mordenite (R=147). This has resulted because the Brönsted acid sites associated with the frame work aluminium are widely spaced upon dealumination. A decrease in the yield of aromatics was noticed with the increase

of phosphorus impregnation which is attributed to a decrease in catalyst acid strength and/or the building of additional constraint on the formation of high molecular weight material due to binding of phosphorus compounds with zeolite frame work. The alkylating agents like isopropanol, propylene and n-propanol did not show any difference in the product pattern except the temperature condition. The rearrangement of isopropylbenzene (IPB) to n-propylbenzene (npB) was found to be dependent on temperature as well on the acidity of the zeolite. At a givan reaction temperature, the weaker acid sites favour the formation of only isopropylbenzene.

The deposition of coke is found to have a considerable influence on the product distribution in the mordenite based catalyst. It is found that conversion of propylene is decreased whereas selectivity to IPB is increased. The impurities are at the minimum level. Among the dialkylbenzenes p-isomer predominates over the m-isomer. The deposition of coke at the pore mouth and/or within the catalyst reduces the effective channel dimensions giving enhanced selectivity to p-diisopropylbenzene.

The silynation of H-mordenite catalyst showed lower propylene conversion and comparatively fast deactivation than unmodified H-mordenite. The deposition of silica blocks the pores of the zeolite which impose constraint on the accessibility of the reacting species to the active site resulting in lower activity.

With decreasing Na content in the sodium mordenite by exchange of rare earth cation, the propylene conversion was increased. The reduction in propylene conversion is as expected due to reduction in Brönsted acid centres which are needed for alkylation.

Poisoning of mordenite catalyst was studied by passing pyridine along with the feed over the catalyst bed and by passing moist propylene. The net decrease in the conversion of alcohol to total alkylbenzenes is correlated with the reaction of acidic sites with pyridine base. When moist propylene was passed over the catalyst, acid sites decreased due to the presence of water and caused higher concentration of diisopropylbenzene and reduction in impurities. The activity of the high temperature pretreated samples is much lower as compared to the samples activated at ordinary temperature.

Mordenite and ZSM-5 zeolites with comparable SiO_2/Al_2O_3 molar ratio were compared for their catalytic activity in isopropylation of benzene. The steric constraint imposed by the channel within the pores of ZSM-5 favours secondary reactions showing low selectivity for isopropylbenzene. When zeolites belonging to ZSM-12 and mordenite type were compared, ZSM-12 having comparable SiO_2/Al_2O_3 molar ratio was found to be superior than mordenite.

ISOPROPYLATION OF BENZENE OVER RARE EARTH EXCHANGED Y ZEOLITE

The prominent phenomenon of polarisation-dissociation of water molecule around the multivalent cations in the activation temperature range of 250-300(^{o}C) produces several framework OH groups which on dehydration give rise to protons responsible for catalytic activity. Hence, the maximum activity was observed in this range. Optimum reaction temperature was in the range of 175-200^{o}C. Higher temperature resulted in cracking reactions whereas at lower temperatures, yield of diisopropylbenzene due to successive alkylation affects selectivity to IPB. The optimum space velocity and reactant mole ratio are 2 h^{-1} and 8 respectively. Lower reactant mole ratio and higher space velocity liberated large amount of heat due to exothermicity of alkylation reaction. The maximum conversion of propylene observed at 80% rare earth exchange is in line with the acidity. At high pressure (25 Kg/cm^{2}) stable and extended activity was observed which is due to absence of oligomerisation reaction which results in the formation of coke responsible for deactivation of the catalyst.

PHENOL ALKYLATION OVER ZSM-5 ZEOLITES

The influence of temperature in the alkylation of phenol dictates that in addition to dimethylether (DME) there is simultaneous and larger increase in the yield of anisole indicating an ease of alkylation on the side chain. Higher temperature favours methanol reaction. The observed yield of O-cresol is consistent with clean electrophilic substitution and evidence of absence of steric hindrance to the entering CH_3^{+}, due

to OH-group. The observed increase in the yield of xylenols and other alkylated products with increase in mole ratio (Methanol to Phenol) is due to multiple alkylation. Increase of space velocity results in the lower yield of alkylated products and favours ether formation. The decrease of methanol conversion resulted in the smaller yield of cresols and xylenols with increase of the SiO_2/Al_2O_3 molar ratio of the zeolites. This is attributed to the decrease of acidity of zeolites.

Shape selective properties are not sufficient to cause higher para-selectivity in phenol alkylation. Formation of 2,6 xylenol, contrary to earlier studies over Y type is negligible in ZSM-5 catalysed alkylation, probably on account of shape selective factors.

The effect of temperature on HFeZSM-5 showed decrease in the Cresol/Xyenol molar ratio indicating ease of alkylation of cresol compared to phenol. The ring alkylation is more favoured than O-alkylation which is implied by the increase in the cresol to anisole molar ratio and is consistent with clean electrophilic substitution.

The alkylation of phenol over modified HZSM-5 zeolites showed the trend in activity in line with the acidity; which is Al > B > Fe > La. The formation of O-cresol is prominent in HFeZSm-5 due to its largest pore size.